Doctoral Dissertations   Graduate School

5-2023

Induction and Evasion of Neutrophil Extracellular Traps by Campylobacter jejuni and its Implication in Disease

Sean M. Callahan
University of Tennessee, Knoxville, scallah5@vols.utk.edu

To the Graduate Council:

I am submitting herewith a dissertation written by Sean M. Callahan entitled "Induction and Evasion of Neutrophil Extracellular Traps by Campylobacter jejuni and its Implication in Disease." I have examined the final electronic copy of this dissertation for form and content and recommend that it be accepted in partial fulfillment of the requirements for the degree of Doctor of Philosophy, with a major in Microbiology.

<div align="right">Jeremiah G. Johnson, Major Professor</div>

We have read this dissertation and recommend its acceptance:

Elizabeth Fozo, Tim Sparer, Heidi Goodrich-Blair, Gina Pighetti

<div align="right">Accepted for the Council:</div>

<div align="right">Dixie L. Thompson</div>

<div align="right">Vice Provost and Dean of the Graduate School</div>

(Original signatures are on file with official student records.)

Induction and Evasion of Neutrophil Extracellular Traps by *Campylobacter jejuni* and its Implication in Disease

A Dissertation Presented for the
Doctor of Philosophy
Degree
The University of Tennessee, Knoxville

Sean M. Callahan
May 2023

process; Bridget, Andy, David, Joseph, Trevor, Morgan, Jenny, Jemma, Paula, Keertana, Gina, and Olivia thank you for all the support and listening to my crazy ideas.

I would also like to thank my family for their constant support throughout this process. I could not have asked for a better support system, both in New York and in Knoxville. You all supported me in every stage of this program, even if it meant missing events going into lab on the weekends. You pushed me to my limits and taught me that if you truly want something, you do everything in your power to get it. I truly cannot put into words how grateful I am for your love and kindness.

Lastly, I would like to thank my amazing partner in crime, Clint. I do not think I could have finished graduate school without your love and support. Even if I promised you "I think I'll only be in lab for an hour" turning into a couple hours, you always understood. You have shown me how to be a good person, a good friend, and a good boyfriend, and I cannot thank you enough for it. I am so excited for what the future holds for us and all that comes along with it. Also, shout out to our dog, Graham, he's always excited to see me, even when experiments don't work. Thank you for getting me through the COVID-19 pandemic.

ABSTRACT

Campylobacteriosis, the foodborne disease caused by *Campylobacter* spp., infects one out of 10 individuals every year. *C. jejuni* accounts for 90% of these infections resulting in numerous postinfectious disorders including the development of colorectal cancer, Guillain-Barré syndrome, irritable bowel syndrome, and reactive arthritis. Despite its large impact on human health, the host immune response to the bacterium is largely uncharacterized. Chapter two of this dissertation addresses the development of neutrophil extracellular traps (NETs) within human and ferret campylobacteriosis. We observed NET-associated proteins increase in the feces of *C. jejuni*-infected patients and that *in vitro C. jejuni* induces NETs, which are cytotoxic to colonic epithelial cells. Furthermore, we observed NET-like structures within intestinal tissue of *C. jejuni*-infected ferrets where *C. jejuni* colonizes and causes tissue pathology. The work presented in chapter three of this dissertation characterizes a novel secreted *C. jejuni* effector, a sirtuin-like protein (SliP), which we found induces NETs. SliP is secreted into neutrophils, where it deacetylates proteins, specifically histone H3. As histone H3 acetylation plays a crucial role in chromatin structure and host transcription, activity of SliP could have immense impacts on the host cell physiology. Leveraging the murine model of campylobacteriosis, we determined a *C. jejuni sliP* mutant efficiently infects mice, but induction of proinflammatory cytokines and gastrointestinal pathology is decreased compared to wild-type *C. jejuni* infected mice demonstrating the importance of this protein in immune pathology *in vivo*.

Finally, the work done in chapter four of this dissertation sought to characterize a *C. jejuni* nuclease (MugA) and its ability to assist in NET evasion. In this work, we performed a transposon screen of *C. jejuni* for nuclease production. We discovered that a *mugA* mutant was sensitive to NET killing and lacked nuclease activity. Interestingly, MugA degraded NETs lead to inflammasome activation within macrophages, and subsequent host inflammation. In conclusion, this dissertation demonstrates the influence of NETs within campylobacteriosis and highlights a potential target for therapeutic strategies. By specifically targeting SliP and MugA in *C. jejuni* for their role in immune modulation, these could be attractive therapeutics to reduce host inflammation and potential post-infectious disorder onset.

TABLE OF CONTENTS

LIST OF TABLES

LIST OF FIGURES

CHAPTER ONE
INTRODUCTION

A portion of this chapter (Neutrophils during campylobacteriosis) is from a version of a manuscript originally published by Sean M. Callahan and Jeremiah G. Johnson:

Callahan, S. M., Dolislager, C. G., & Johnson, J. G. (2021). The Host Cellular Immune Response to Infection by *Campylobacter* Spp. And Its Role in Disease. *Infection and Immunity*, 89(8). https://doi.org/10.1128/IAI.00116-21

The portions of the review cited above were written by S.M.C. with edits from J.G.J. C.G.D. wrote the section regarding *C. jejuni* epithelial infection. The article was revised for this dissertation by only using the neutrophil section of the review manuscript, which was composed by S.M.C. These sections have also been shortened for clarity.

Campylobacter spp.

Campylobacter spp. are a leading cause of bacterial-derived gastroenteritis worldwide, causing approximately 400-500 million infections worldwide annually (1). While the bacteria are predominantly commensal in numerous species of livestock, including poultry and cattle, infection in humans and other hosts can lead to gastroenteritis (2–4). Interestingly, the infectious dose to cause human infection has been reported to be low, only requiring 100 cells (5). Once ingested, the bacterium infects the mucosal surface of intestinal crypts, where it can lead to pronounced inflammation and gastrointestinal pathology (Figure 1.1) (6,7). Clinical symptoms of acute gastrointestinal infection typically include bloody diarrhea, abdominal pain, fever, and weight loss, which last for an average of 6 days in immunocompetent individuals (8). In developing regions, *Campylobacter* infection is endemic; however, children are more likely to display symptoms than adults, possibly due to the protective immunity developing after early exposure to the bacterium (3,9). In contrast, in the developed world, campylobacteriosis is an acute, inflammatory illness with a greater incidence of postinfectious disorders. A potential dietary driver of these differences is the amount of fiber consumption.
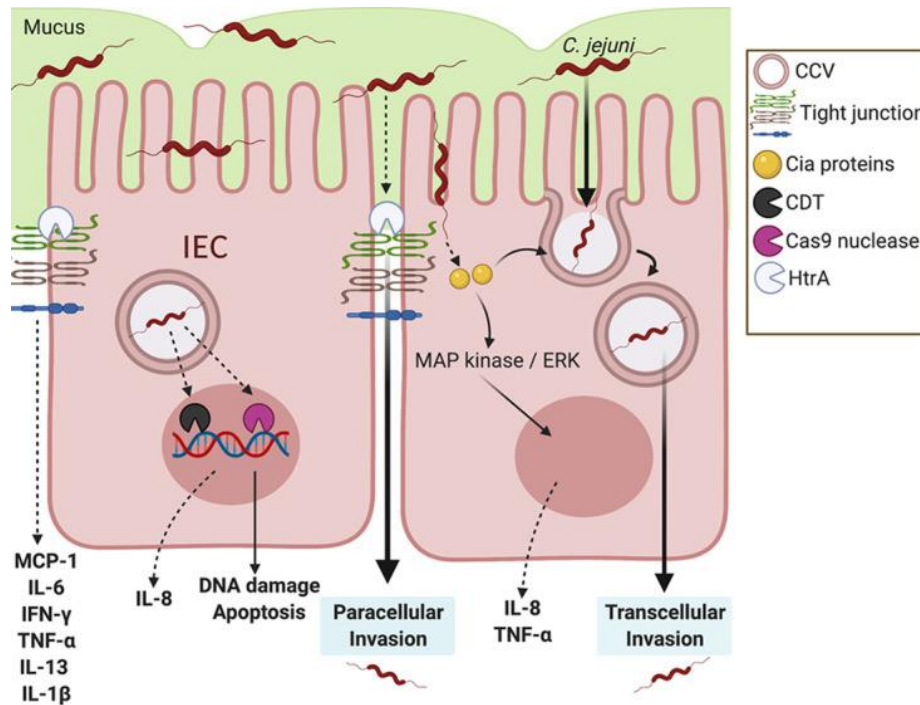
Figure 1.1. Influence of *C. jejuni* on intestinal epithelial cell (IEC) immune signaling.

After colonizing the mucus layer of intestinal crypts, *C. jejuni* can adhere and invade into IECs. For transcellular invasion: *C. jejuni* secretes *Campylobacter* invasion antigens (Cia proteins) possibly through a type III flagellar secretion system, in which it activates the MAPK/ERK pathway. *C. jejuni* enters the intestinal epithelial cell and is bound within a *Campylobacter*-containing vesicle (CCV) as it travels through the cell. Microtubules and actin are utilized by *C. jejuni* to travel from the apical side toward the nucleus and basolateral side of the cell. For paracellular invasion, *C. jejuni* can reach the basolateral side of the IECs by passing between cells through HtrA tight junction cleavage, rather than through the cell itself. This tight junction disruption results in the upregulation of proinflammatory cytokines. For DNA damage, instead of canonical gastrointestinal effector proteins, *C. jejuni* can secrete the CDT genotoxin and Cas9 nuclease. Both result in DNA damage, apoptosis, and potential upregulation of the neutrophil chemoattractant IL-8. Image created using BioRender.

3

Fiber-rich diets allow for heightened short-chain fatty acid (SCFA) production by microbial fermentation in the colon, and it has been shown that diets in developing countries are more fiber rich. As a result, patients in these regions may experience less inflammation but greater persistence because of the anti-inflammatory effects of SCFAs, most notably, butyrate (10–12). Beyond effects on the host, butyrate abundance may also promote colonization by *C. jejuni*, as the BumSR two-component system indirectly senses butyrate and upregulate genes essential for colonization of avian and human hosts (13). Based on these observations, there has been an emerging interest in developing dietary strategies that can promote an adequate immune response to eliminate the bacterium while at the same time preventing tissue damaging inflammation.

Unlike other gastrointestinal bacterial pathogens, *C. jejuni* lacks classically identified virulence factors often associated with disease, including canonical secretion systems and toxins (14). Hence, the clinical manifestations of human campylobacteriosis and its resulting gastrointestinal pathology are believed to be primarily due to the host immune response toward the bacterium. Further, while gastrointestinal infection is usually self-limiting, numerous post-infectious disorders can occur, including the development of Guillain-Barré syndrome (GBS), irritable bowel syndrome (IBS), and reactive arthritis (RA). Among patients that develop GBS, *C. jejuni* can be attributed to as many as 40% of all cases, with seropositivity toward *C. jejuni* occurring in up to 76% of patients (15). This results in total annual productivity losses and medical costs up to $1.8 billion per year (16,17). The outdated nature of these data, combined with observations that infections are increasing in prevalence, suggests that the current economic burden of this disease is currently far more than those previous estimates (18). Further, in the first year following *Campylobacter* infection, patients have a greater risk of developing IBS than uninfected individuals (19). Finally, it is estimated that 18% of infected individuals develop RA, which can result in potent joint inflammation and reduced range of motion (20). Because gastrointestinal disease likely results from the host immune response, the development of these post-infectious disorders

may be due to dysregulation or misdirection of the same inflammatory response (21). As a result, it is becoming increasingly important to the *Campylobacter* field, and human health, that the cellular immune responses toward *Campylobacter* be better understood, including which immunological events are critical to the development of disease and the post-infectious disorders mentioned above.

After being consumed in a relatively low infectious dose from contaminated food or drinking water, *C. jejuni* can penetrate the mucus layer of the distal intestine and proximal colon to reach the apical surface of the intestinal epithelial cells (IECs) (22,23). To reach the IECs, *C. jejuni* resists acidic stomach pH conditions through the upregulation of numerous acid stress responses and downregulation of protein synthesis (24). Mucus is crucial in the colonization of *C. jejuni*, as mucin is a chemoattractant and facilitates the increased flagellar gene expression and motility that is required to reach the underlying epithelium (25,26). Once *C. jejuni* has transited through the mucus layer, the bacterium is able to adhere to and invade into the IECs (27). To sense the bacterium, Toll-like receptor (TLR) reporters have been found to be stimulated by lysed *C. jejuni* through the sensing activities of various TLRs, including TLR1/2/6 and TLR4, which detect bacterial lipoproteins and lipopolysaccharides, respectively (28). Stimulation of these TLRs is transduced through the MyD88 signaling cascade and leads to activation of NF-κB, which drives the production and secretion of IL-8, tumor necrosis factor alpha (TNF-α), IL-1β, monocyte chemoattractant protein 1 (MCP-1), GRO-α, and IL-12p42 (29). Additionally, *C. jejuni* can activate ALPK1 in IECs through ADP-heptose production, resulting in heightened inflammation (30). Once *C. jejuni* is at the apical surface, the bacterium invades into IECs, a process dependent upon the secretion of *Campylobacter* invasion antigen (Cia) proteins, the translocation of which is believed to be through the flagellar type III secretion system (31–33). In addition to promoting cellular invasion, Cia proteins can stimulate p38 mitogen-activated protein (MAP) kinase and extracellular signal-regulated kinases (ERK) pathways to drive further IL-8 secretion from IECs, which results in potent neutrophil chemotaxis to the site of infection (34,35) Specifically, this increase in

5

IEC-dependent IL-8 causes neutrophil chemotaxis to the site of infection, where they are involved with proinflammatory signaling. However, the specific role of neutrophils during campylobacteriosis is poorly understood.

Neutrophils

Neutrophils are the most abundant circulatory leukocyte within the human immune system, with around 10^{11} cells produced daily, accounting for 50-70% of circulating leukocytes (36,37). Neutrophils are produced within the bone marrow in a process called granulopoiesis where hematopoietic stem cells differentiate into lymphoid-primed multipotent progenitors. Once lymphoid-primed multipotent progenitors are produced, they develop into granulocyte-monocyte progenitor cells due to the G-CSF produced by osteoclasts, resulting in proliferation of granulocyte progenitors. From this, progenitors go through numerous stages of cell differentiation, namely, myeloblast, pro-myelocyte, myelocyte, meta-myelocyte, and then band cell (38,39). During this differentiation, there is an increase in expression of CXCR2 and decrease in CXCR4 and VLA4 (40,41). This decrease in expression reduces binding capability of the developing neutrophil to the bone marrow endothelial cells, promoting neutrophil egress. Once egressed out of the bone marrow, neutrophils can chemotax to the site of high chemokine production through CXCR2, resulting in neutrophil trafficking to sites of infection or damage (42).

Neutrophils possess three main antibacterial mechanisms: phagocytosis of microbes, degranulation of antimicrobial proteins, and extrusion of neutrophil extracellular traps (NETs) (43,44). During phagocytosis, surface bound receptors bind to opsonized or non-opsonized microorganisms, leading to downstream signal transduction within the host cell and internalization of the microbe in a phagosome. Once the phagosome is initiated, it then develops into a mature phagosome through acquisition of antimicrobial machinery, including microbicidal enzymes, vacuolar ATPases, and the NADPH oxidase complex. Finally, the

6

phagosomes migrate to the lysosome-rich perinuclear region of the neutrophil characteristic of an alkaline pH in a microtubule-dependent manner (45–47). During degranulation, after surface bound receptors on the neutrophils recognize epitopes on the microorganism, granules translocate through actin polymerization to either the phagosomal or plasma membranes. Once docked, they then get translocated out of the cell through a process called exocytosis, where the granules can perform antimicrobial activities (48). Finally, neutrophils can undergo a unique form of cell death, termed a neutrophil extracellular trap (NET) which trap pathogens from disseminating throughout the host. In this process, myeloperoxidase (MPO), neutrophil elastase (Ela2), and protein arginine deaminase 4 (PAD4) translocate to the nucleus of the neutrophil, causing nuclear membrane disintegration (49). Once in the nucleus, PAD4 citrullinates arginine residues, specifically on histone H3, resulting in chromatin decondensation. As a result, chromatin DNA is extruded out into the extracellular environment, where it is studded with antimicrobial proteins (50). Recently, it has been shown there are multiple forms of NETosis: (1) suicidal NETosis, where the neutrophil loses cellular functions listed above and (2) vital NETosis, where the neutrophil preserves cellular functionality through blebbing of the nuclear envelope (51). However, the molecular mechanisms of NET induction in response to microorganisms are still poorly understood.

Interestingly, many microorganisms induce the formation of NETs despite their antimicrobial nature. These include *Staphylococcus aureus*, *Candida albicans*, *Pseudomonas aeruginosa*, *Toxoplasma gondii*, *Leishmania amazonensis*, Group B *Streptococcus*, *Shigella flexneri*, SARS-CoV-2, Influenza virus, HIV, Sendai virus, and *Salmonella* (44,52). In the early research of NETs, it was believed that NETs were solely cast in responses to large microbial aggregates, being able to clear a substantial portion of pathogens (53). However, it is now being appreciated that various forms of NETosis can occur and that microbial-induced NETosis can be pathogen-specific. Specifically, these differences have been linked to PAD4, ROS, calcium, and neutrophil elastase

7

requirements (54). Therefore, it is imperative to understand how individual pathogens induce NETs for targeted therapeutics to be developed.

Neutrophils during campylobacteriosis

After *Campylobacter* spp. successfully breaches the epithelial barrier, neutrophils are the first innate immune cells recruited to the site of infection (55). While these cells have long been noted as simple, transcriptionally inert phagocytes, current research demonstrated their multifunctionality and transcriptional diversity (56). Using human, ferret, cat, porcine ileal loop, and the IL-10$^{-/-}$ murine models of campylobacteriosis, neutrophils have been consistently shown to migrate and accumulate within the gastrointestinal tissue of infected hosts (Figure 1.2) (8,57–60). Furthermore, recent evidence has demonstrated that neutrophil-to-lymphocyte ratios of 3.05 correlate with GBS onset and hyperinflammation (normal ratio is 1.51), suggesting neutrophil abundance influences GBS onset and development in campylobacteriosis (61). As neutrophils are the most numerous leukocytes within colonic tissue during *C. jejuni* infection and possess proinflammatory activities, they need to be considered a potential source for acute and chronic campylobacteriosis and tissue pathology.

Within colonic crypts, neutrophils transmigrate from the basolateral to the apical side of the epithelium, in a process dependent on bacterially sourced n-formyl peptides and the host-derived enzyme, 12-lipoxygenase (12-LOX) (62). Furthermore, intestinal epithelial cell (IEC)-dependent secretion of IL-8 results in neutrophil chemotaxis and peak in abundance within the blood and colon at 3 days post-infection, which correlated with the height of *C. jejuni* fecal loads in the ferret model of campylobacteriosis (59). Using green fluorescent protein (GFP)-labeled *C. jejuni* in the IL-10$^{-/-}$ mouse model, 99.7% to 100% of CD11b^{+} Gr-1^{+} peritoneal neutrophils were found to have engulfed *C. jejuni* by four hours post-infection (63). During *Campylobacter* infection of cats, there appeared to be a close association

8
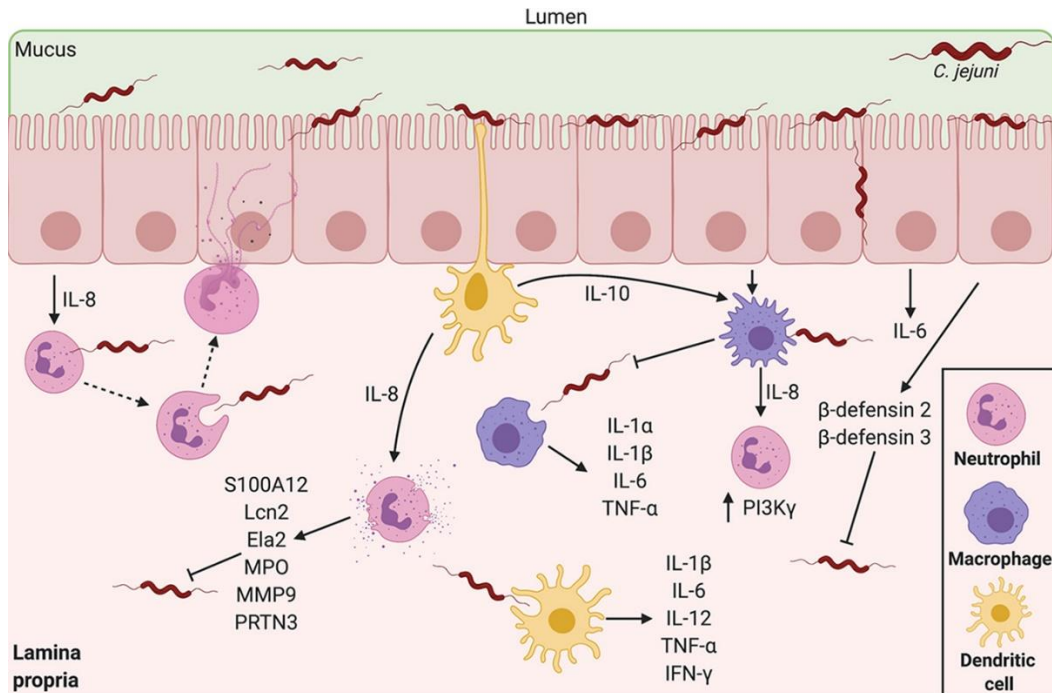
Figure 1.2. Innate leukocyte responses during initial stages of campylobacteriosis

During infection, neutrophils are recruited to the site of infection because of IEC IL-8 secretion, leading to elaboration of NETs and degranulation. Macrophages and dendritic cells are then recruited to the site of infection and perform both inflammatory and anti-inflammatory signaling. Within these first days of infection, macrophages, dendritic cells, neutrophils, and colonocyte antimicrobial proteins reduce *C. jejuni* levels within the infected host. These innate immune responses classically peak on day 3 post-infection, the heightened day of infection in hosts. Image created using BioRender.

with neutrophil elastase within the colon and the development of neutrophilic IBS (64).

At the molecular level, phosphatidylinositol 3-kinase-γ (PI3K-γ)-dependent signaling leads to the recruitment of neutrophils into colonic crypts during *C. jejuni* infection of IL-10$^{-/-}$ mice, which lead to the development of colitis (58). PI3K-γ is highly expressed in numerous immune cells and, via actin polymerization, mediates chemotaxis through G protein-coupled receptors (65,66). Inhibition of PI3K-γ activity by the pharmacological inhibitor AS252424 resulted in reduced inflammation, neutrophil accumulation, NF-κB activity, and transcript levels of IL-1β, CXCL2, and IL-17α during *C. jejuni* infection (58). This *C. jejuni*-induced inflammatory cascade was found to be dependent on mTOR activation, which is a signaling event downstream of PI3K-γ. Further, inactivation of mTOR signaling using rapamycin, a pharmacological inhibitor, led to attenuation of *C. jejuni*-induced inflammation (67).

Once neutrophils and *C. jejuni* interact, complement-opsonized cells are phagocytosed, which leads to reactive oxygen species (ROS) generation, resulting in direct bacterial killing and localized tissue damage (68). Interestingly, the ability of neutrophils to kill *C. jejuni* varies, as some bacteria can escape these bactericidal effects (68). In addition to phagocytosis and direct killing, a neutrophil-derived antimicrobial protein, S100A12, is released into the surrounding tissue and accumulates in the feces of *C. jejuni*-infected humans (59). Calgranulin, including S100A12, are a family of calcium-binding proteins that regulate cellular homeostasis and antimicrobial functions. Specifically, S100A12 can bind to numerous cofactors, including calcium, zinc, and copper. In addition to serving as a nutritional immunity protein to starve microbes of essential elements, it is also highly inflammatory by binding to the RAGE receptor on adjacent cells to induce proinflammatory signaling cascades (69). Within the *C. jejuni*-infected porcine ligated loop, numerous neutrophil-derived markers were shown to increase, including matrix metallopeptidase 9 (MMP9), Lcn2, Ela2, and proteinase 3 (PRTN3) (60). Based on the activities of these antimicrobial proteins, their release

during infection is likely to contribute to *C. jejuni* growth restriction (59). As the presence of Ela2 and MPO correlates with colonic tissue damage and IBS due to protease and ROS-generating activities, respectively, more research needs to be done on their roles during campylobacteriosis (70,71). While these proteins can be secreted out into the environment by the neutrophil through degranulation, many of these proteins are additionally embedded within NETs, however, this has yet to be explored within the *Campylobacter* community. Due to the cytotoxic nature of NETs, it has been hypothesized that NETs contribute to crypt abscess formation and intestinal pathology during campylobacteriosis. As NETs are also associated with numerous autoimmune diseases, these structures could have tremendous influence on the development of the post-infectious disorders mentioned above (72–75). Because of the association between neutrophil activity, inflammation, pathology, and autoimmune development, more research needs to be conducted on *C. jejuni*-neutrophil interactions.

Finally, it has been previously demonstrated that neutrophils play a key role in the onset and development of colorectal cancer (76,77). Interestingly, *Campylobacter* spp. have been repeatedly found within the microbiota of tumor sections in patients with colorectal cancer (78–80). However, whether *C. jejuni* – neutrophil interactions shape the development of colorectal cancer is poorly understood. To better understand if *C. jejuni* can promote colorectal cancer, a mouse model of spontaneous colorectal cancer (germ-free *Apc^{Min/+}*) was used to determine if *C. jejuni* accelerates this development. In this, the study found *C. jejuni* induces DNA damage and promotes colorectal tumorigenesis through the action of *cdtB*. some *C. jejuni* strains produce a genotoxin called cytolethal distending toxin (CDT) which can cause cell cycle arrest, cell distension, and cell swelling (81). To determine if neutrophils can promote this colorectal tumorigenesis phenotype, our group has shown that *C. jejuni* causes neutrophils to become hypersegmented in their nuclei with cancer-promoting activities. Specifically, we found that *C. jejuni* infected neutrophils causes T cells to decrease the ζ-chain of the T cell receptor (TCR) and generates a hypoxic environment and HIF-1α

stabilization in IECs (82). Whether *C. jejuni* secreted CDT causes neutrophil hypersegmentation activities remains unclear, it appears that *Campylobacter* spp. has evolved numerous ways to promote colorectal tumorigenesis. Hence, while understanding *C. jejuni* – neutrophil interactions are critical for understanding inflammatory innate immune responses during campylobacteriosis, they are also needed for understanding post-infectious disorder onset and progression.

Flagellar type III secretion systems

Type III secretion systems (T3SSs) are protein complexes present in gram-negative pathogens to secrete bacterial effector proteins directly into the host cytosol (83). For effector proteins to be secreted through the T3SS, chaperons must present effector proteins to a cytoplasmic sorting platform complex. These complex sorts and loads effector proteins onto the membrane-bound basal body export apparatus subcomplex. The export apparatus contains a helical needle complex containing tip complex, which is responsible for creating a translocon pore in the host cell membrane. With this complex, bacterial effector proteins can exit the bacterial cytoplasm and transport into the host cell cytosol (84,85).

Interestingly, structural information and bioinformatic analyses determined shared ancestral features between T3SS and flagellar T3SS (fT3SS) (86,87). In the fT3SS, the bacterial flagellum, rod, hook, and filament are unfolded and transported through the cell membrane, leading to the complete formation of the bacterial flagella. Similar to the T3SS, the fT3SS contains an export gate comprised of FliPQR, FlhA, and FlhB located within the flagellar basal body and an adjacent soluble cytoplasmic ATPase complex, FliHIJ (88). Intriguingly, numerous pathogenic bacteria, including *Campylobacter jejuni*, enteropathogenic *Escherichia coli* (EPEC) *Salmonella enterica*, *Shigella* spp., and *Yersinia* spp. contain structural and functional homologs between T3SS and components of the flagellum (89,90).

12

In *C. jejuni*, the fT3SS serves as the primary export machinery within the bacterium (91). Here, the core of the fT3SS is in the inner membrane, where it is surrounded by a multimer of flagellar motor switch protein, FliF, which is referred to as the MS ring. Additionally, it is also surrounded by multimers of the FliG rotor and flagellar motor switch proteins, referred to as the cytoplasmic C ring. Once the MS and C rings surround the core of the fT3SS, it triggers the FlgRS two-component system (TCS), resulting in flagellar biogenesis and assembly (92). However, there is a lack of information on the molecular mechanism for *C. jejuni* fT3SS effector secretion and the identity of these effectors. Interestingly, it is known that an intestinal signal, deoxycholate (DOC) has been shown to induce fT3SS secretion of *Campylobacter* invasion antigens (Cia). These proteins have been found to be necessary for *C. jejuni* epithelial invasion capability, therefore, the fT3SS could play a significant role in the pathogenesis of *C. jejuni* (93,94). DOC is a secondary bile acid produced by the gut microbiome as metabolic byproducts (95). Interestingly, DOC can regulate T3SS in a few organisms, leading to upregulation or downregulation of virulence components. In *Shigella flexneri*, DOC has been shown to bind to the T3SS tip protein, IpaD, resulting in conformational changes to IpaD to recruit the first hydrophobic translocator, IpaB. Once in contact with the host cell membrane, the second hydrophobic transporter, IpaC then binds to the T3SS tip, resulting in formation of the translocon pore in the host cell membrane (96). Additionally, in *Salmonella*, deoxycholate has been shown to bind to its tip protein, SipD. Interestingly, deoxycholate in *Salmonella* appears to hinder T3SS activity, with differential binding compared to *S. flexneri* (97). However, in *C. jejuni*, how DOC induces fT3SS secretion is poorly understood. In chickens, it has been shown that the *Campylobacter* multidrug efflux pump (Cme) and the transcriptional regulator, CbrR, play significant roles in the resistance to bile salts in the intestinal tract (98). While DOC could promote secretion of effectors in *C. jejuni*, the molecular mechanism for this phenomenon could be more thoroughly investigated.

13

Sirtuins and post translational modifications

Acetylation is a key post-translational modification on protein lysine residues, which critically influence the protein conformation or ability to bind cofactors and substrates (99). To acetylate proteins, lysine acetyltransferases utilize acetyl coenzyme A (acetyl-CoA) as the primary substrate (100). Acetyl-CoA is a molecule produced through glucose, fatty acid, and amino acid catabolism (101). Due to the high abundance of lysine and arginine residues, histones have been extensively investigated for their role in epigenetics and post-translational modifications during chromatin remodeling. When histones are acetylated, the chromatin bound by these histones are within topologically associating domain (TAD) boundaries in the A compartment (102). The A compartment is in the nuclear interior of host cell nuclei, where active transcription of euchromatin by RNA polymerase is capable (103–105). However, when histones are deacetylated, primarily through histone deacetylases (HDACs), the heterochromatin is more compact and bound to nuclear lamina, resulting in B compartment switching and RNA repression due to the unavailability of space for RNA polymerase (106). Interestingly, HDAC inhibitors have been shown to resolve numerous inflammatory and autoimmune diseases, namely cancer, Alzheimer's disease, Parkinson's disease, interstitial fibrosis, cardiovascular diseases, and diabetes (107–110). Interestingly, HDACs are now being investigated for their role in microbial infections (111).

Sirtuins are a class of histone deacetylases proteins that are crucial for linking cellular metabolism and signaling (112,113). By utilizing NAD+, an essential cofactor within metabolic redox, sirtuins have been hypothesized to be metabolic sensors and transcriptional regulators through their ability to deacetylate histones. Because the host uses acetylation to control these cellular processes, pathogens, including *Listeria monocytogenes*, *Salmonella typhimurium*, *Shigella flexneri*, and *Mycobacterium tuberculosis*, can manipulate and utilize host proteins HDACs and HATs to promote infection, especially sirtuin-2 (SIRT2) (114–118). Furthermore,

while bacteria do contain sirtuins (often named *cobB*), often involved with metabolism, stress resistance, and transcriptional regulation, they are less abundant than eukaryotic sirtuins (119). Interestingly, *C. jejuni* encodes a *cobB* enzyme, in which it deacetylates AMP-forming acetyl coenzyme A (acetyl-CoA) synthetase (Acs) enzyme, resulting in the conversion of acetate to acetyl-CoA. This would then allow lysine acetyltransferases to acetylate proteins within the bacterium, regulating acetylation status within the bacterial cell (120). Importantly, bacterial effectors that are translocated and directly bind host proteins to differentially acetylate them remain to be identified.

Nucleases

Nucleases are ubiquitous in pathogens and allow bacteria to acquire nucleotide nutrients, uptake foreign DNA, induce tissue damage, degrade neutrophil extracellular traps, and modulate the host inflammatory response. In the environment, numerous bacteria have acquired the ability to utilize extracellular DNA as a carbon, nitrogen, and phosphorus source, especially in marine systems (121–123). This phenomenon is additionally seen in pathogenic bacteria during infections, with pathogens including *Pseudomonas aeruginosa*, *Staphylococcus aureus*, and *Vibrio cholerae* utilizing extracellular DNA to promote infection (124–127). Often, these bacterial nucleases require cofactors, including calcium, magnesium, and manganese. In *Shewanella oneidensis*, ExeM, an extracellular nuclease, requires all three cofactors (128). While nucleases can be secreted out into the environment to degrade DNA, they can be surface bound. In *S. aureus*, while they produce an extracellular nuclease, termed Nuc, they additionally produce a second nuclease, Nuc2, which is surface bound, with identical enzymatic activities as Nuc (129). Hence, bacterial nucleases play a key and regulatory role in numerous bacterial physiological responses.

In addition to assisting bacteria to acquire nutrients in the environment and host, nucleases also play a significant role in innate immune evasion and

inflammatory cascade induction. Specifically, since the discovery of NETs, researchers have investigated the role of bacterial nucleases in the evasion of these antimicrobial structures. Interestingly, numerous bacterial pathogens have acquired the ability to degrade NETs, including *S. aureus*, *Streptococcus mutans, Prevotella intermedia, Vibrio cholerae, Yersinia enterocolitica, and Neisseria gonorrhoeae* (130–135). Interestingly, in *S. aureus*, nuclease deficient bacteria are more sensitive to NET-mediated killing, but when cocultured with macrophages, the antimicrobial activity between NETs and macrophages synergize (136).

In addition to modulating antimicrobial function, degraded NETs can drastically alter macrophage functionality. Within hosts, once a neutrophil undergoes NETosis, resident macrophages engulf and breakdown NETs intracellularly, which is dependent on active endocytosis. Interestingly degraded NETs before engulfment of the NET can lead to rapid clearance of these structures (137). However, NETs can often serve as damage-associated molecular patterns (DAMPs) to monocytes and macrophages, resulting in the production of IL-1β (138). IL-1β is a proinflammatory cytokine produced through an inflammasome-dependent manner, primarily through a nucleotide-binding domain, leucine-rich repeat-containing family, CARD domain-containing protein 4 (NLRC4) or NOD-, LRR- and pyrin domain-containing protein 3 (NLRP3) dependent manner (139). Interestingly, macrophage IL-1β appears to be driven through mononucleosomal-associated citrullinated histone H3 binding to TLR4 on macrophages (140). Extracellular histones are also classified as DAMPs, where they can often lead to oxidative stress and inflammasome activation in an NLRP3-dependent manner (141). However, the molecular mechanism underlying degraded NET inflammasome activation has yet to be investigated.

Conclusions

As described in the above sections, the innate immune responses during campylobacteriosis are poorly understood. As *C. jejuni* lacks numerous classical

virulence factors, our field has hypothesized the inflammation, tissue pathology, and onset of often autoimmune diseases are due to the misdirection and over stimulation of the host immune response. Previously, the Johnson Lab determined that neutrophils accumulate during the ferret model of campylobacteriosis, especially during heightened bacterial burden and inflammation. In this, they determined that S100A12, a neutrophil antimicrobial protein increases within *C. jejuni* infected humans and ferrets. This production of S100A12 nutritionally starves *C. jejuni* of essential nutrients, specifically zinc, resulting in lowered bacterial burden (59). However, there are few studies which seek to investigate the *C. jejuni* – neutrophil interface.

To understand what occurs at the *C. jejuni* – neutrophil interface, this dissertation investigated whether *C. jejuni* can induce a proinflammatory form of cell death, termed a NET. In this, using both primary human neutrophils and the ferret model of campylobacteriosis, we determined that *C. jejuni* is a potent inducer of NETs and that these structures can be seen in regions where *C. jejuni* colonizes the colonic tissue. Logically, we next sought to determine any factors *C. jejuni* may utilize to induce NETs. In the next chapter of my thesis, we identify and characterize a secreted effector protein, termed SliP. We found SliP functions as a sirtuin, where it deacetylates neutrophil proteins, resulting in the elaboration of NETs. Interestingly, using the murine model of infection, we found a *sliP* mutant was unable to cause clinical signs within infected mice. Finally, the last chapter utilized a transposon library to identify *C. jejuni* proteins necessary for NET-evasion strategies. In this, we identified *mugA*, which promotes NET degradation, resulting in inflammasome activation in adjacent macrophages. Fascinatingly, this mutant is unable to colonize mice as readily as wild-type *C. jejuni* and is sensitive to NET killing. Altogether, this dissertation highlights the importance of investigating NETs within infectious diseases so that novel therapeutics can be developed targeting these structures.

CHAPTER TWO
INDUCTION OF NEUTROPHIL EXTRACELLULAR TRAPS IN RESPONSE TO
CAMPYLOBACTER JEJUNI

This chapter is a version of a manuscript originally published by Sean M. Callahan and Jeremiah G. Johnson in *Cellular Microbiology* (2020).

Sean M. Callahan, Ryan S. Doster, Joseph W. Jackson, Brittni R. Kelley, Jennifer A. Gaddy, Jeremiah G. Johnson. "Induction of neutrophil extracellular traps in response to *Campylobacter jejuni*." *Cellular Microbiology* (2020).

The work described in this study was conducted by the following individuals: ELISAs, growth and viability assays, NET flow cytometry, Western blots, *in vitro* confocal microscopy, NETosis assays, H&E microscopy, and NET cytotoxicity assays were all conducted by S.M.C. *In vivo* confocal microscopy was conducted by R.S.D. Ferret flow cytometry and initial flow cytometry were conducted by J.W.J. Ferret fecal *C. jejuni* viability assays were conducted by B.R.K and J.G.J.

Abstract

Campylobacter jejuni is the leading cause of bacterial-derived gastroenteritis worldwide and can lead to several post-infectious inflammatory disorders. Despite the prevalence and health impacts of the bacterium, interactions between the host innate immune system and *C. jejuni* remain poorly understood. To expand on earlier work demonstrating that neutrophils traffic to the site of infection in an animal model of campylobacteriosis, we identified significant increases in several predominantly neutrophil-derived proteins in the feces of *C. jejuni*-infected patients, including lipocalin-2, myeloperoxidase, and neutrophil elastase. In addition to demonstrating that these proteins significantly inhibited *C. jejuni* growth, we determined they are released during formation of *C. jejuni*-induced neutrophil extracellular traps (NETs). Using quantitative and qualitative methods, we found that purified human neutrophils are activated by *C. jejuni* and exhibit signatures of NET generation, including presence of protein arginine deiminase-4, histone citrullination, myeloperoxidase, neutrophil elastase release

and DNA extrusion. Production of NETs correlated with *C. jejuni* phagocytosis/endocytosis and invasion of neutrophils suggesting that host- and bacterial-mediated activities are responsible for NET induction. Further, NET-like structures were observed within intestinal tissue of *C. jejuni*-infected ferrets. Finally, induction of NETs significantly increased human colonocyte cytotoxicity, indicating that NET formation during *C. jejuni* infection may contribute to observed tissue pathology. These findings provide further understanding of *C. jejuni*–neutrophil interactions and inflammatory responses during campylobacteriosis.

Introduction

Campylobacter species are a leading cause of bacterial-derived gastroenteritis worldwide, impacting 90–96 million people annually (142,143). Following consumption of contaminated food or water, *Campylobacter jejuni* adheres to the intestinal mucosa, causing inflammation and tissue pathology (6,144). Symptoms of acute campylobacteriosis typically include inflammatory, bloody diarrhea, abdominal cramps, fever, and vomiting (8). While infection is often self-limiting and resolves after several days, numerous post-infectious disorders have been observed, including Guillan-Barré syndrome (GBS), irritable bowel syndrome (IBS) and reactive arthritis (145). Furthermore, the rise of antibiotic-resistant strains has led the Centers for Disease Control and the World Health Organization to classify *Campylobacter* as a serious threat to public health (146,147).

Despite the global prevalence and consequences of campylobacteriosis on human health, the innate immune response to this bacterium is poorly understood when compared with other less prevalent gastrointestinal pathogens such as *Escherichia*, *Listeria*, *Shigella*, and *Vibrio* genera (147). In both ferret and murine models of campylobacteriosis, neutrophils are recruited to infected intestinal tissue, leading to accumulation of neutrophil-derived antimicrobial proteins in the feces and tissue (57,59). Additionally, recruited neutrophils promote development

20

of crypt abscesses in hyperinflammatory IL-10$^{-/-}$ mice infected with *C. jejuni* (58). Taken together, these observations suggest that neutrophils are particularly important to the development of disease and resolution of infection, but the neutrophil responses to *C. jejuni* remain uninvestigated.

Neutrophils are the most abundant leucocytes in humans and have three main antibacterial functions: (a) phagocytosis of microbes, (b) degranulation of antimicrobial proteins and (c) extrusion of neutrophil extracellular traps (NETs) (55). After engulfment of the microbe during phagocytosis, neutrophils utilize bactericidal proteins and enzymes found within lysosomes to degrade the pathogen (148). While phagocytosis is an effective method for bacterial clearance, pathogens have developed mechanisms to invade and/or survive within neutrophils (149,150). Invasion of phagocytes by bacterial pathogens is typically induced through bacterial secretion systems. This activity has been observed for *C. jejuni* during invasion of host colonic epithelial cells where the bacterium utilizes a flagellar secretion system to invade and form *Campylobacter*-containing vacuoles (35,83). While this work has been done on epithelial cells, the ability of *C. jejuni* to invade and persist in leucocytes remains uncharacterized. During neutrophil degranulation, antimicrobial peptides are released into the external environment to limit growth and/or kill microbes localized to that region of tissue (55). Similar to degranulation, NETs are composed of extracellular DNA bound by numerous antimicrobial granule components that function to both prevent pathogen dissemination throughout the host while also restricting their growth and viability at the site of induction (44,55). Bacteria have evolved strategies to specifically counteract NETs through the production of pathogen-derived DNases, which can degrade the NET and limit contact with the antimicrobial molecules present within the structure (151).

While NETosis benefits the host by restricting growth and facilitating clearance of pathogenic microbes, there is increasing evidence that NET components are cytotoxic to host cells and stimulate inflammation (152). As a result, NETs have been linked to numerous inflammatory disorders in humans,

including rheumatoid arthritis (RA), IBS, systemic lupus erythematosus and tumor metastasis (72,153,154). Since several of the post-infectious disorders that occur following *Campylobacter* infection resemble these, we hypothesized that NETs are induced within the intestinal tissue during infection and may play a role in disease induction and progression.

While the neutrophil response to *C. jejuni* remains mostly uncharacterized, work has been done to understand how other immune cells recognize and respond to the pathogen. Previous work demonstrated that *C. jejuni* activates dendritic cells (DCs) through toll-like receptor 4 (TLR4), which led to B-cell proliferation and antibody secretion (155). This finding was supported by *in vitro* experiments utilizing HEK293 TLR4-expressing reporter cells (156). Toll-like receptor 4 mediates multiple activities in innate immune cells, including recognition of lipopolysaccharides (LPS) from Gram-negative bacteria. This recognition initiates a proinflammatory cascade that includes NF-κB expression and subsequent proinflammatory cytokine secretion. *C. jejuni* expresses lipooligosaccharides (LOS), which are recognized and bound by the cluster of differentiation 14 (CD14)/MD2/TLR4 complex on immune cells (155). Interestingly, the LOS structure of *C. jejuni* is hypothesized to be a molecular mimic of human gangliosides and has been implicated in the development of GBS. To date, it is unknown whether *C. jejuni* LOS is immunogenic to neutrophils during infection. In addition to binding LPS/LOS via Lymphocyte antigen 96 MD2, TLR4 also co-ordinates production of immune cell endocytosis, facilitating internalization of microbes into phagocytes (157).

In this work, we expand upon earlier observations and demonstrate that neutrophil-derived proteins are readily detectable in the feces of *Campylobacter*-infected patients and that these proteins inhibit *C. jejuni* growth in vitro. We also found that *C. jejuni* induces NET production in primary human neutrophils and that *C. jejuni* stimulates NET production at a level like that of the well-characterized NET inducer, *Salmonella enterica* serovar Typhimurium. Further, we observed that *Campylobacter* invades and/or is endocytosed by human neutrophils and that,

22

using non-invasive flagellar mutants or blocking TLR4-mediated endocytosis, we could successfully reduce NET induction. This indicates that host-mediated phagocytosis/endocytosis and bacterial-driven invasion may promote the release of NETs during infection. To determine whether this response occurs in vivo, we visualized NETs within weaning-aged ferret colon tissue during *C. jejuni* infection. Finally, we demonstrate that NETs induced by *C. jejuni* significantly increase colonocyte cytotoxicity, indicating that the production of NETs during infection may contribute to the pathology of colon tissue.

Results

Using fecal samples from *C. jejuni*-infected individuals, concentrations of lipocalin-2 (Lcn2) (Fig. 2.1A), myeloperoxidase (MPO) (Fig. 2.1B), and neutrophil elastase (Ela2) (Fig. 2.1C) were measured using protein-specific ELISAs. In uninfected individuals, the mean Lcn2 concentration was determined to be $3.82 \times 10^5 \pm 3.63 \times 10^5$ pg/mL, while infected individuals exhibited a significant increase with a mean concentration of $1.51 \times 10^6 \pm 3.15 \times 10^5$ pg/mL. MPO concentration of uninfected individuals was observed at a mean concentration of $1.29 \times 10^3 \pm 1.30 \times 10^3$ pg/mL and infected individuals exhibited a significant increase with a mean concentration of $3.94 \times 10^4 \pm 2.86 \times 10^3$ pg/mL. Lastly, Ela2 in uninfected fecal samples was detected at a mean concentration of $5.88 \times 10^2 \pm 8.61 \times 10^1$ pg/mL while infected samples demonstrated significant increases with a mean concentration of $1.67 \times 10^3 \pm 6.93 \times 10^2$ pg/mL. These represent approximate fold increases of 3.97, 30.47, and 2.85 for Lcn2, MPO, and Ela2, respectively. Increases in these proteins led us to hypothesize that neutrophil degranulation and/or NET production are occurring at the host-pathogen interface during human infection. In summary, we have shown that *C. jejuni* infected individuals' stool samples contain higher levels of proteins Lcn2, MPO, and Ela2.

Since Lcn2, MPO, and Ela2 were elevated in infected stool samples, we examined whether these proteins could inhibit *C. jejuni* growth *in vitro.* When
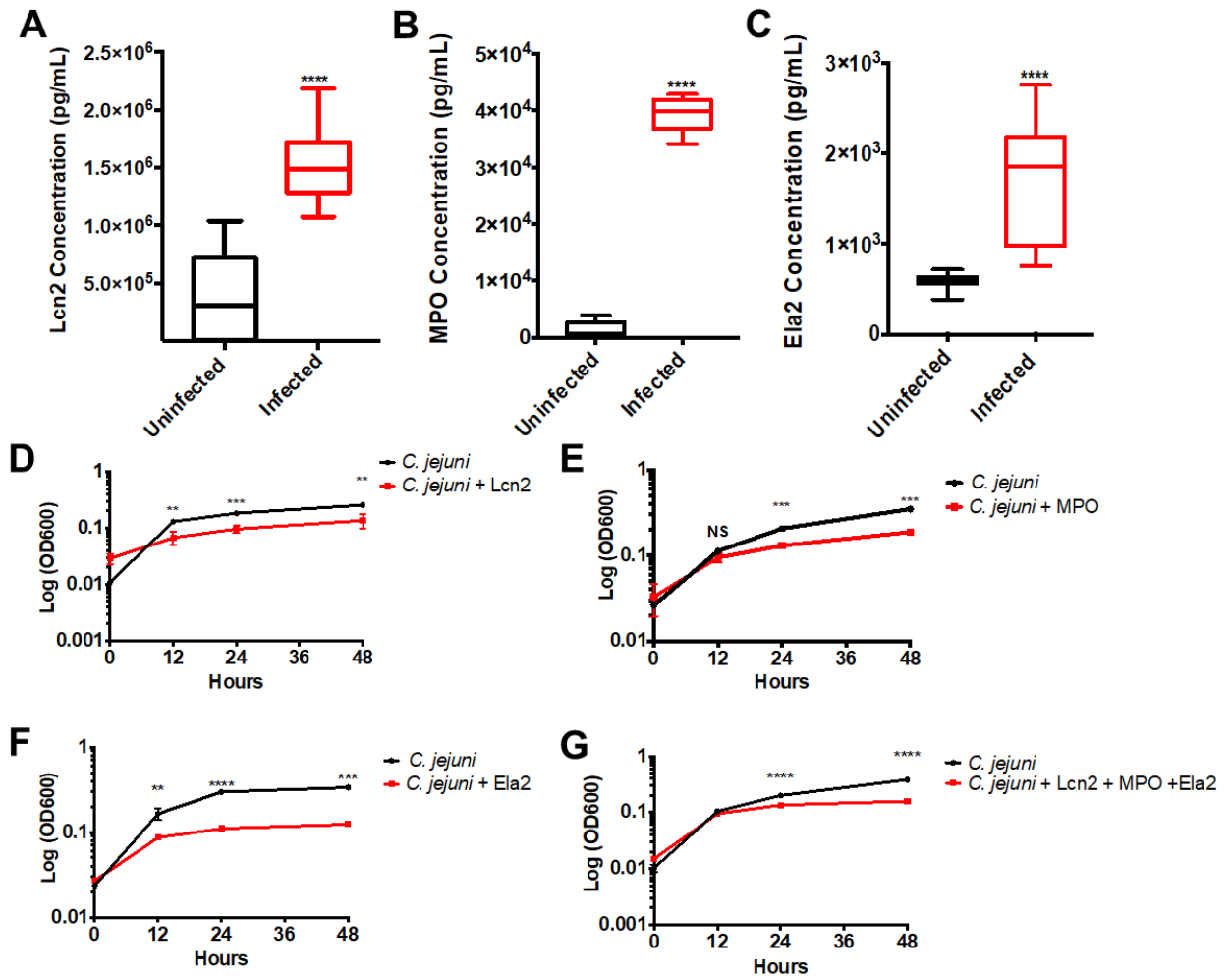
Figure 2.1. Neutrophil-derived antimicrobial proteins and NET components accumulate in *C. jejuni*-infected patient fecal samples.

(A-C) Lipocalin-2 (Lcn2), myeloperoxidase (MPO), and neutrophil elastase (Ela2) protein levels significantly increases in infected individuals. (D-F) Neutrophil-derived proteins decrease *C. jejuni* growth for up to 48 hours. (G) Granule proteins synergistically decrease *C. jejuni* growth *in vitro*. Statistical analyses of representative fecal samples were performed using a nonparametric Mann-Whitney U test between uninfected and infected groups. Statistical analysis of growth curves performed using an unpaired t test between *C. jejuni* and *C. jejuni* - antimicrobial groups. **p < 0.01; ***p < 0.001; ****p < 0.0001.

purified components (Lcn2, MPO, and Ela2) were incubated with *C. jejuni*, bacterial growth was significantly reduced, especially during the exponential phase. When cultures were grown in iron-restricted media supplemented with 3.125 mM ferric-enterobactin and 42.375 µg/mL Lcn2, mean *C. jejuni* growth (OD600) significantly decreased from 0.13 ± 0.014 to 0.068 ± 0.018, 0.183 ± 0.008 to 0.096 ± 0.015, and 0.26 ± 0.01 to 0.14 ± 0.04 at 12, 24, and 48 hours when compared to iron-restricted cultures containing ferric-enterobactin (Fig. 2.1D). When incubated in the presence of MPO at a concentration of 73 µg/mL, *C. jejuni* growth (OD600) significantly decreased from 0.11 ± 0.01 to 0.094 ± 0.011, 0.21 ± 0.008 to 0.13 ± 0.008, and 0.35 ± 0.03 to 0.19 ± 0.003 at 12, 24, and 48 hours, respectively (Fig. 2.1E). Finally, when incubated with Ela2 at a concentration of 25 µg/mL, the *C. jejuni* mean growth (OD600) significantly decreased from 0.17 ± 0.026 to 0.086 ± 0.0015, 0.29 ± 0.018 to 0.11 ± 0.0006, and 0.34 ± 0.026 to 0.12 ± 0.007 at 12, 24, and 48 hours respectively (Fig. 2.1F). These represent approximately 2-3-fold reductions in growth at each time point tested for all antimicrobial proteins. Finally, these granule proteins work in concert to synergistically decrease *C. jejuni* growth (Fig. 2.1G). Consequently, we hypothesize that the increase of these antimicrobial proteins during human infection may aid in *C. jejuni* clearance by inhibiting *C. jejuni* growth at or within the gastrointestinal tissue.

To understand neutrophil responses to *C. jejuni*, flow cytometry was utilized to determine neutrophil activation and response. When neutrophils were incubated with varying multiplicities of infection (MOIs) of *C. jejuni*, neutrophil activation and response was determined to be population density dependent. The highest activated population (SSC^{hi}CD11b$^+$MPO$^+$) was observed at an MOI of 1:50 (neutrophil:*C. jejuni*) with a mean MFI of $1.76 \times 10^5 \pm 2.74 \times 10^3$ using the flow cytometry analysis described below (Fig. 2.2A). Further, when this MOI was incubated with neutrophils for varying amounts of time, the highest activated population was observed at three hours using the same flow cytometry analysis
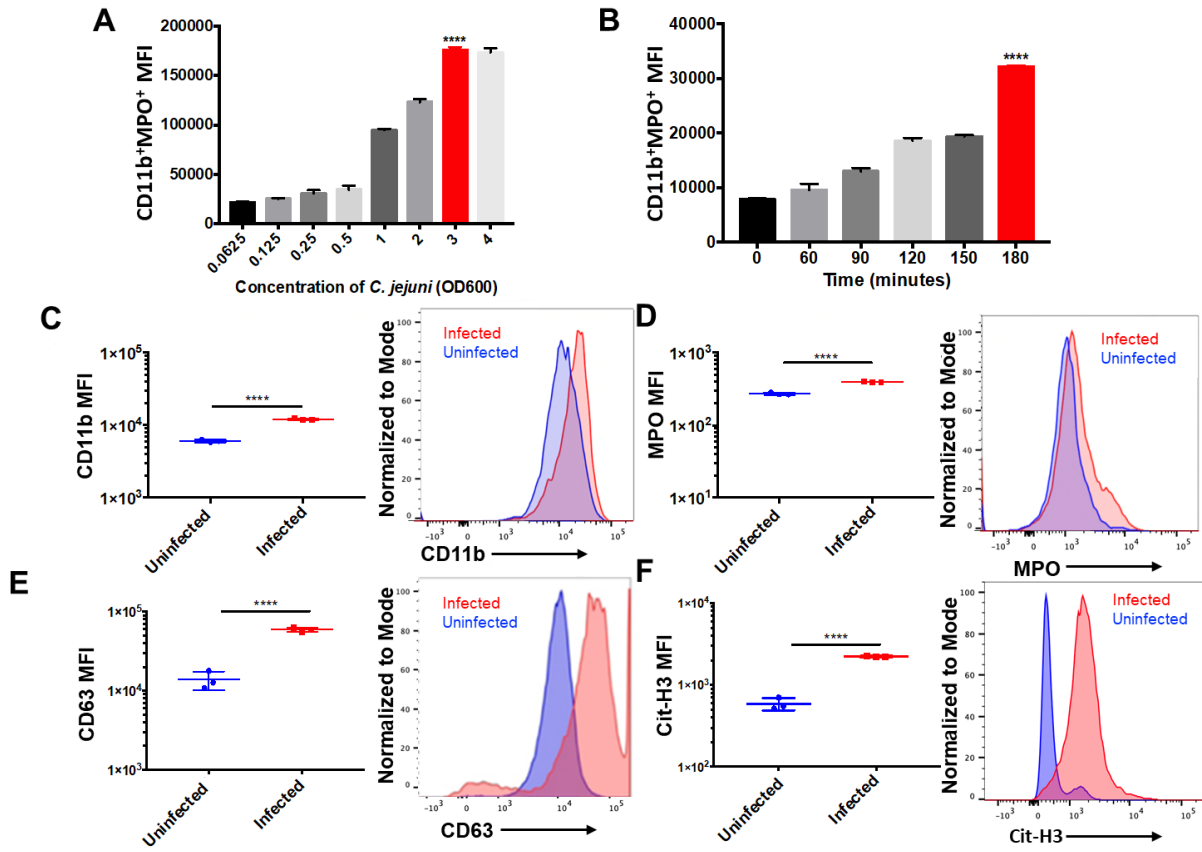
Figure 2.2. Flow cytometry analysis of *C. jejuni* induced NETs.

(A) Neutrophils exhibited increased NET production up until an OD600 of 3.0 (B) Neutrophils exhibited increased NET production when incubated with *C. jejuni* up to three hours. Flow cytometry analysis of human neutrophil activation using CD11b (C), extracellular expression of MPO (D), CD63 (E), and citrullinated histone 3 (Cit-H3) (F) Expression of each marker was normalized to the mode of the population. Results are expressed as representative data of biological and technical triplicates. Statistical analysis was performed using an unpaired t test between uninfected and infected groups. ***p* < 0.01; ****p* < 0.001; *****p* < 0.0001.

with a mean MFI of $3.21 \times 10^4 \pm 2.97 \times 10^2$ (Fig. 2.2B). These results indicate that neutrophils are activated in response to *C. jejuni* in a dose and time dependent manner. To assess the cellular response of activated human neutrophils to *C. jejuni*, flow cytometry was similarly performed on purified human neutrophils that were incubated with *C. jejuni* and analyzed using SSC^{hi}, CD11b, MPO, CD63, and citrullinated histone 3 (Cit-H3) as markers of NET formation. After incubation with *C. jejuni*, there was a significant increase in the population of mean fluorescence intensity (MFI) of $CD11b^+$ neutrophils from uninfected human neutrophils ($6.06 \times 10^3 \pm 2.78 \times 10^2$) to infected human neutrophils ($1.21 \times 10^4 \pm 3.06 \times 10^2$) (Fig. 2.2C). There was a subpopulation of $CD11b^+$ neutrophils that also stained as MPO^+ in the absence of permeabilization and this population significantly increased when neutrophils were uninfected ($2.73 \times 10^2 \pm 11.55$) and then infected with *C. jejuni* ($3.96 \times 10^2 \pm 1.53$) (Fig. 2.2D). Additionally, there was a significant increase in $CD63^+$ neutrophils ($1.38 \times 10^4 \pm 3.6 \times 10^3$) when infected with *C. jejuni* ($5.92 \times 10^4 \pm 3.41 \times 10^3$) (Fig. 2.2E). Similarly, neutrophils exposed to *C. jejuni* were more frequently Cit-H3 ($2.22 \times 10^3 \pm 43.7$) positive when compared to uninfected neutrophils ($5.88 \times 10^2 \pm 99.0$) (Fig. 2.2F). These data suggest that upon activation, neutrophils were increasingly decorated with extracellular MPO, CD63, and Cit-H3. When subpopulations of $CD11b^+MPO^+$ and $CD63^+Cit-H3^+$ cells were analyzed using LIVE/DEAD™ Fixable Near-IR (NIR) stain, cells in these populations were found to be more frequently positive, indicating that neutrophils stimulated by *C. jejuni* undergo 'suicidal' NETosis.

To further determine whether neutrophils form extracellular traps in response to *C. jejuni*, NET components were quantitatively analyzed by western blot. Neutrophils isolated from three healthy volunteers were infected with wild-type *C. jejuni* and whole cell lysates were examined for the presence of lipocalin-2 (Lcn2), myeloperoxidase (MPO), neutrophil elastase (Ela2), peptidylarginine deiminases 4 (PAD4), and citrullinated histone 3 (Cit-H3) (Fig. 2.3A). Using β-actin abundance as an internal control, mean relative abundances for each protein in unstimulated neutrophils were determined by densitometry: Lcn2 (0.23 ± 0.23),
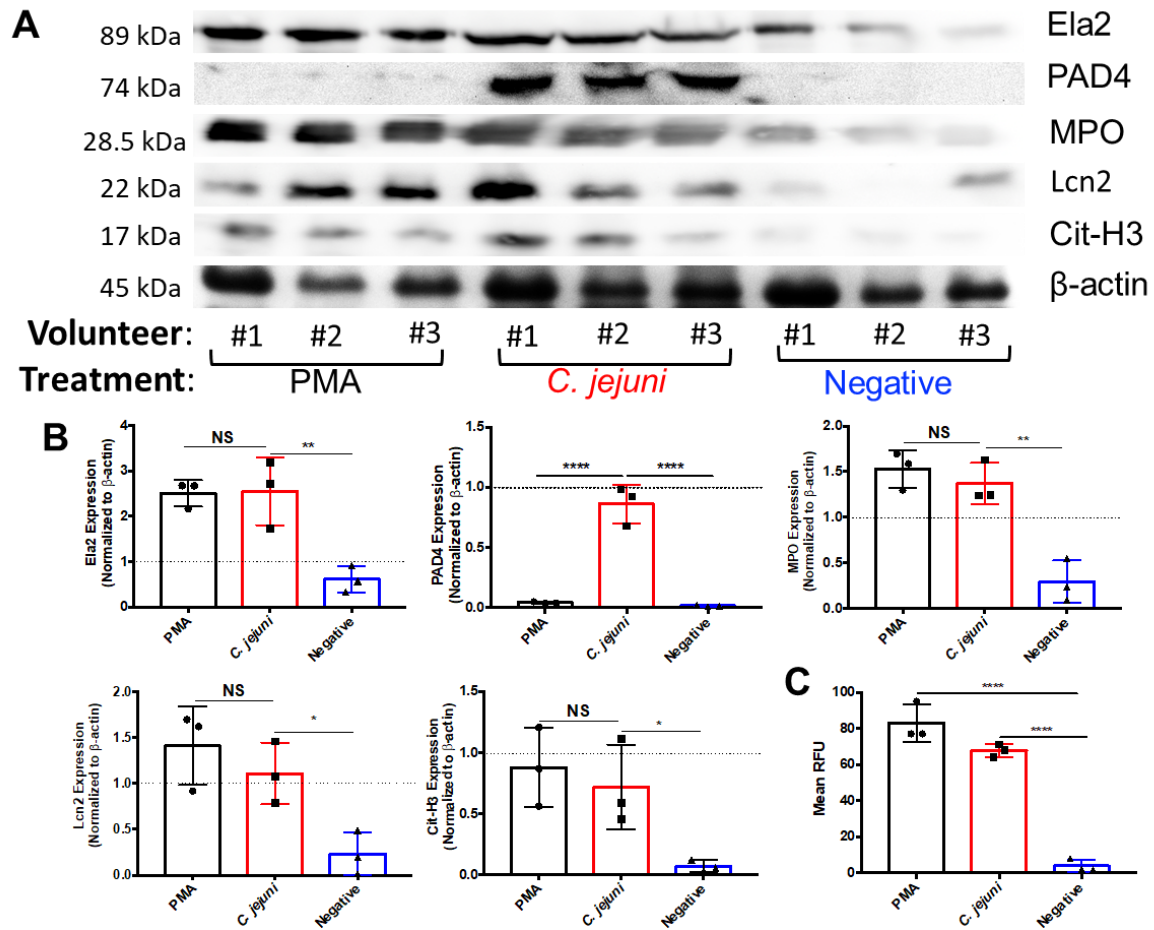
Figure 2.3. Western blot analysis of essential NET components.

Volunteer neutrophils were incubated with PMA, wild-type *C. jejuni*, or media. (A) Western blot detection of neutrophil elastase (Ela2), PAD4, myeloperoxidase (MPO), lipocalin-2 (Lcn2), citrullinated histone H3 (Cit-H3), and β-actin as a loading control. (B) Densitometry quantification of NET components relative to beta actin density. (C) SYTOX assay to detect extracellular DNA. Results are expressed as representative data of biological and technical triplicates. Statistical analysis was performed using an unpaired t test between PMA, *C. jejuni*, and negative treated neutrophils. Multiple comparison testing was performed using ANOVA with post hoc test. *$p < 0.05$; **$p < 0.01$; ***$p < 0.001$; ****$p < 0.0001$.

MPO (0.29 ± 0.23), Ela2 (0.61 ± 0.29), PAD4 (0.016 ± 0.007), and Cit-H3 (0.071 ± 0.048). Using PMA stimulated neutrophils as a positive control for NET production, mean relative protein levels were: Lcn2 (1.41 ± 0.43), MPO (1.53 ± 0.21), Ela2 (2.51 ± 0.29), PAD4 (0.043 ± 0.006), and Cit-H3 (0.88 ± 0.32). These represent significant increases in all proteins examined except for PAD4. *C. jejuni*-stimulated neutrophils exhibited increased mean relative protein levels of Lcn2 (1.11 ± 0.34), MPO (1.37 ± 0.22), Ela2 (2.55 ± 0.75), PAD4 (0.86 ± 0.16), and Cit-H3 (0.72 ± 0.35) (Fig. 2.3B). These abundances represent significant increases when compared to unstimulated neutrophils, with most increases between 4.1 to 4.8-fold and an increase of 10.1-fold for PAD4 expression. These increases were similar for PMA-induced neutrophils, except for PAD4 abundance. Finally, to quantify extracellular DNA extruded during *C. jejuni*-induced NETosis, a SYTOX Green assay was performed to quantify extracellular DNA and dead cells. When incubated with *C. jejuni*, a significant increase in extracellular DNA was observed as the mean relative fluorescence units (RFUs) for unstimulated neutrophils (7.43 ± 4.32) increased to 61.57 ± 9.07 when stimulated with *C. jejuni*. The amount of extruded DNA in response to *C. jejuni* stimulation was not significantly different when compared to PMA-induced neutrophils (71.14 ± 13.28) (Fig. 2.3C). As an additional control, we confirmed that *C. jejuni* lysates did not cross-react with any of the above antibodies (Lcn2, MPO, Ela2, PAD4, and Cit-H3) nor did it exhibit significant fluorescence when stained with SYTOX (data not shown). Therefore, these indicate that human neutrophils exhibit numerous markers of NETosis following interaction with *C. jejuni*.

To further confirm that NET production occurs during the neutrophil response to *C. jejuni*, immunofluorescence microscopy was performed using antibodies directed against human NET components as well as SYTOX Green to stain extruded DNA. Following examination of 100 fields of view, unstimulated neutrophils were found to possess intact, multi-lobed nuclei, punctate MPO staining (presumed MPO contained within granules), and low levels of Ela2 that were contained within the neutrophil border. After stimulating with *C. jejuni*, a

proportion of neutrophils exhibited fewer compact nuclei with some extruding extracellular DNA that co-localized with MPO and Ela2 (Fig. 2.4A). Using this morphology to designate a NETosing cell, examination of 100 fields indicated that approximately 17% of neutrophils formed NET structures at 3h post challenge (Fig. 2.4B). This result supported our flow cytometry-based analysis above, causing us to conclude that human neutrophils produce NETs in response to *C. jejuni* and that they contain antimicrobial proteins that can inhibit *C. jejuni* growth.

To compare the *C. jejuni*-induced NET response to other gastrointestinal pathogens, NET induction was quantitatively compared between *E. coli* O157:H7, *Salmonella* SL1344, and *C. jejuni* 81-176 at the same MOI of 1:50 (neutrophil:bacteria) for three hours. *E. coli* O157:H7 has been found to not induce NETs while *Salmonella* has been shown to be a potent NET inducer (44). Using flow cytometry and SYTOX assays described above, we confirmed previous results and found that *E. coli* O157:H7 incubation with purified human neutrophils resulted in only slight increases in the CD11b$^+$MPO$^+$ neutrophil population MFI ($1.17 \times 10^4 \pm 2.08 \times 10^3$) while *Salmonella* SL1344 induced significant increases in the CD11b$^+$MPO$^+$ neutrophil population MFI ($1.67 \times 10^4 \pm 3.05 \times 10^3$). Similarly, incubation with *C. jejuni* increased the CD11b$^+$MPO$^+$ neutrophil population MFI to one comparable to what was observed for *Salmonella* (Fig. 2.5A) ($2.13 \times 10^4 \pm 3.21 \times 10^3$). These results were further supported by assaying DNA extrusion using SYTOX Green with mean RFUs of: *E. coli* O157:H7 (7 ± 1), *Salmonella* SL1344 (18.33 ± 1.15), and *C. jejuni* 81-176 (23.33 ± 3.22) (Fig. 2.5B). These results support our conclusions that *C. jejuni* induces NETs and that the magnitude of induction is at least comparable to *Salmonella* if not higher.

One notable difference between *E. coli* O157:H7 and *Salmonella* is that *E. coli* O157:H7 is largely regarded as non-invasive while *Salmonella* is understood to be a highly invasive pathogen. To assess whether *C. jejuni* can be efficiently internalized into human neutrophils, and whether this may be a mechanism for NET induction, we leveraged gentamicin protection assays. In a control
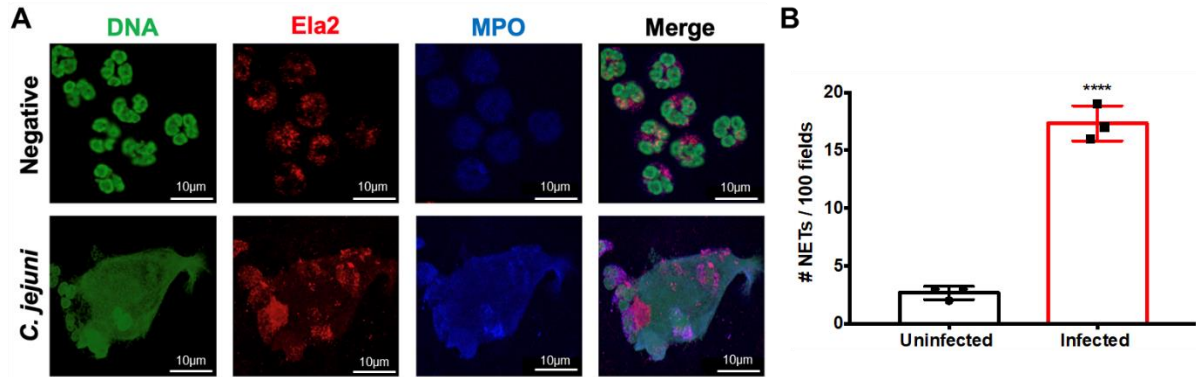
Figure 2.4. Visualization of *C. jejuni*-induced NETs using fluorescent microscopy.

(A) Images were individually taken at the appropriate wavelength for each fluorescent antibody following incubation with wild-type *C. jejuni* or media alone (negative). Representative images for each marker were then merged to visualize NET components, including extracellular DNA. (B) NET production was assessed for 100 fields from three separate neutrophil purifications. Scale bars are 10 μm. Results are expressed as representative data of biological and technical triplicates. Statistical analysis was performed using an unpaired t test between uninfected and infected groups. ****$p < 0.0001$.
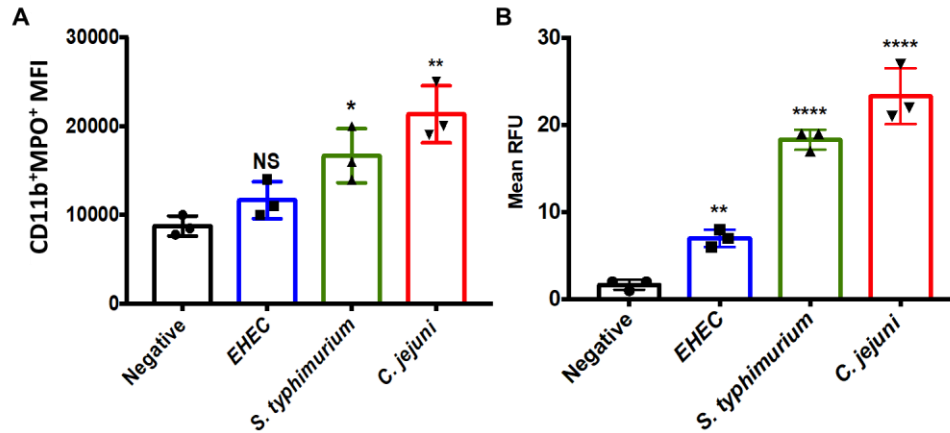
Figure 2.5. Comparison of NET production by other gastrointestinal pathogens.

(A) Flow cytometry analysis of CD11b and myeloperoxidase (MPO) markers accumulating on human neutrophils following incubation with either media alone (negative), *E. coli* O157:H7, *Salmonella* SL1344, or wild-type *C. jejuni* for three hours. (B) SYTOX assay detecting extracellular DNA from neutrophils incubated from three separate volunteers. Results are expressed as representative data of biological and technical triplicates. Statistical analysis was performed using an unpaired t test between negative, *EHEC*, *Salmonella*, and *C. jejuni* stimulated neutrophil groups. Multiple comparison testing was performed using ANOVA with post hoc test. $^*p < 0.05$; $^{**}p < 0.01$; $^{****}p < 0.0001$.

experiment, human neutrophils were incubated with *C. jejuni* at an MOI of 1:10 (neutrophil:*C. jejuni*), a concentration shown to not induce NET formation (Fig. 2.2A), for varying time points. *C. jejuni* was efficiently internalized into neutrophils within one hour with a mean CFU/mL of $6.67 \times 10^6 \pm 5.77 \times 10^5$, representing an approximately 4-log10 increase when compared to the zero-hour time point (Fig. 2.6A). Similar results have been observed in other studies using human-derived epithelial cell lines (158). Interestingly, once internalized, the number of viable *C. jejuni* cells remains constant with $5.33 \times 10^6 \pm 5.77 \times 10^5$ CFU/mL at three hours of infection, suggesting that *C. jejuni* can counteract the bactericidal effects of the neutrophil phagosome (Fig. 2.6A). Lastly, to determine whether neutrophil internalization was dependent on actin polymerization, we incubated human neutrophils with the actin polymerization inhibitor, cytochalasin-D. The incorporation of this inhibitor significantly reduced the number of internalized bacteria from $6.67 \times 10^6 \pm 5.77 \times 10^5$ to $9.33 \times 10^3 \pm 1.53 \times 10^3$ CFU/mL at hour one (Fig. 2.6B). Since actin polymerization-dependent internalization may be mediated by the host cell through phagocytosis/endocytosis or the bacterium through invasion, we examined the effects of each on *C. jejuni* numbers within neutrophils. Previous work demonstrated that endocytosis of bacteria by neutrophils is dependent on interaction with TLR4 (159). Using a commercially available TLR4-blocking antibody, internalized wild-type *C. jejuni* CFUs/mL significantly decreased from $1.12 \times 10^7 \pm 3.52 \times 10^6$ to $1.63 \times 10^5 \pm 2.08 \times 10^4$, indicating that host-directed endocytosis may contribute to bacterial entry (Fig. 2.6B). In addition, we incubated human neutrophils with the invasion-deficient *C. jejuni* Δ*flgE* mutant, finding that mean viable CFUs/mL significantly decreased to $2.57 \times 10^5 \pm 2.52 \times 10^4$ (Fig. 2.6B). As a result of these data, we concluded that *C. jejuni* internalization by human neutrophils is both dependent on TLR4-mediated phagocytosis/endocytosis and flagella-mediated bacterial invasion.

To determine whether internalization is responsible for NET induction, we used the combination of reagents above to examine whether production of NETs was negatively impacted. Using DNA extrusion as an output of NETosis, TLR4

33
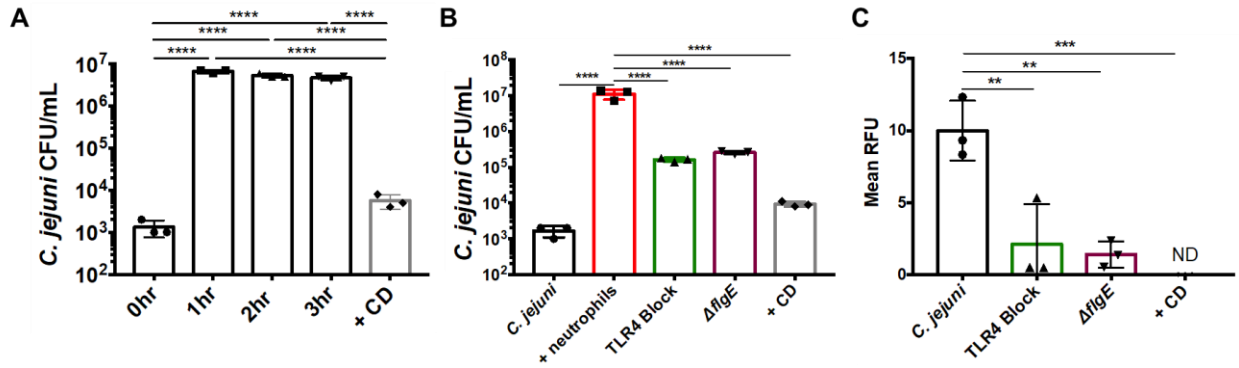
Figure 2.6. Neutrophil phagocytosis and internalization of *C. jejuni*.

(A) Gentamicin protection assay of *C. jejuni* within neutrophils for varying amounts of time and cytochalasin D (CD). (B) Gentamicin protection assay of neutrophils lacking functional TLR4 and neutrophils incubated with flagellar mutants. (C) SYTOX assay to detect extracellular nucleic acids of neutrophils lacking functional TLR4 and neutrophils incubated with flagellar mutants. Results are expressed as representative data of biological and technical triplicates. Statistical analysis was performed using an unpaired t test between *C. jejuni* stimulated neutrophil groups. Multiple comparison testing was performed using ANOVA with post hoc test. *$p <$ 0.05; **$p <$ 0.01; ***$p <$ 0.001; ****$p <$ 0.0001.

blocking significantly decreased from 10 ± 2.08 to 2.11 ± 2.79 RFUs, representing an approximately 5-fold decrease in extracellular DNA. Further, when neutrophils were incubated with *C. jejuni* Δ*flgE*, DNA extrusion significantly decreased to 1.39 ± 0.92 RFUs (Fig. 2.6C). This data suggests that inhibiting TLR4-mediated endocytosis or flagella-directed *C. jejuni* invasion may reduce NET production during *C. jejuni* infection.

In previous work, we demonstrated that granulocytes (presumed neutrophils) and monocytes (presumed macrophages) accumulate in *C. jejuni*-infected ferret colons (59). Neutrophils from uninfected ferrets were incubated with *C. jejuni*, similar to above. There was a significant increase in the population of CD11b$^+$ neutrophils ($3.16 \times 10^4 \pm 8.86 \times 10^2$) when compared to those incubated with *C. jejuni* ($9.69 \times 104 \pm 1.36 \times 10^4$) (Fig. 2.7A). Further, CD11b$^+$ neutrophils stained as MPO$^+$ in the absence of permeabilization significantly increased from 2.43×10^2 ± 1.22×10^2 for uninfected neutrophils to $8.06 \times 10^2 \pm 18.5$ for infected ferret neutrophils (Fig. 2.7B). This demonstrated that ferret neutrophils become similarly activated in response to *C. jejuni* when compared to human neutrophils. As a result, ferrets were infected with 1.5×10^9 CFU orally and sacrificed at day three post infection, the day at which our previous studies indicated peak infection and inflammation. Infected ferrets exhibited mean *C. jejuni* loads of $1.26 \times 10^5 \pm 2.17 \times 10^4$ CFU/g of feces, while mock-infected ferrets did not yield detectable colonies (limit-of-detection: 2,000 CFU/g) (Fig. 2.7C). To expand upon those findings, we evaluated H&E-stained colonic tissue from these animals for signs of inflammation, including edema, presence of blood, hyperplasia, loss of goblet cells, epithelia raggedness, and neutrophil infiltration (Fig. 2.7D). Using double blind inflammation scoring, all categories were increased in infected ferret colons when compared to the mock-infected controls (Figure 2.8-appendix). Based on these observations, increases in neutrophil abundance correlated with increased inflammation and histopathology.

Since H&E staining is unable to detect *in vivo* NETs, we sought to determine if NETs released by neutrophils in response to *C. jejuni* infection could be

Figure 2.7. Histopathology of ferret tissues and cytotoxicity of *C. jejuni* induced NETs.

Flow cytometry analysis of ferret neutrophil activation using CD11b (A) and extracellular expression of MPO (B). (C) Fecal loads of *C. jejuni* infected ferrets day three post infection. (D) H&E stained *C. jejuni* infected ferret colon exhibiting signs of pathology. (E) Immunofluorescent analysis of ferret colon tissue for NETs. Ferret colon tissues were stained using anti-Ela2 antibodies (green) or Hoechst for DNA (blue) and were examined by confocal microscopy. In *C. jejuni* infected colonic tissues several collections of Ela2 staining projections were noted just below the colonic crypts but were not seen in uninfected tissues (red boxes) Higher magnification of these collections (orange box) demonstrated extended Ela2 projections that colocalized with DNA staining, suggestive of NET structures. In the villi of infected animals and in the mucosa of uninfected animals, Ela2 positive cells were noted with intact nuclei and punctate Ela2 staining (green boxes). (F) LDH assay of colonic HCT116 cells incubated with *C. jejuni* induced NETs. Results are expressed as representative data of biological and technical triplicates. Statistical analysis was performed using an unpaired t test between uninfected and infected groups. *$p < 0.05$; **$p < 0.01$; ***$p < 0.001$.
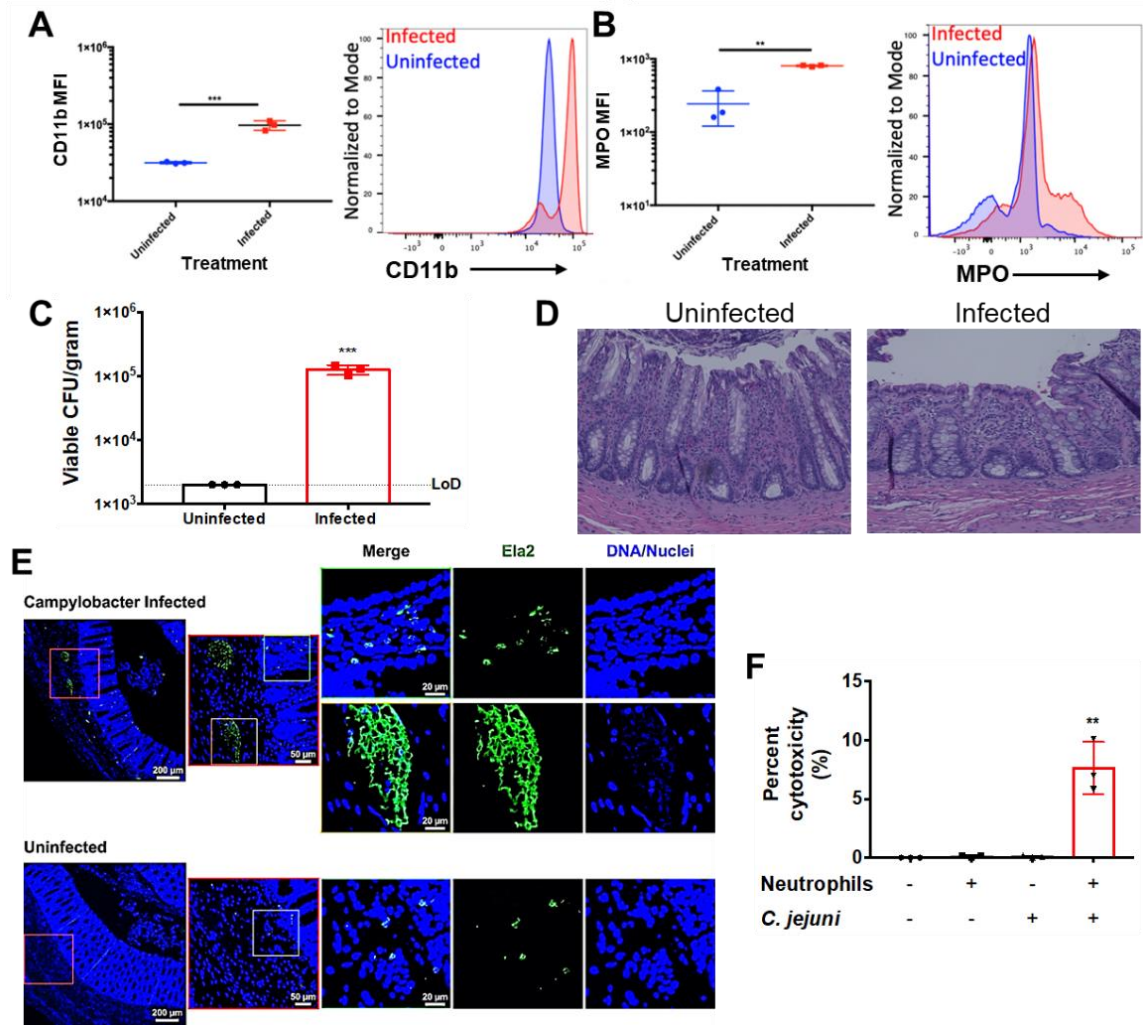
visualized *in vivo*. We interrogated ferret colon tissues with immunofluorescence staining for Ela2 and DNA. At low power, collections of Ela2 staining were seen just below the crypts in the colonic mucosa of infected animals. Higher magnification imaging of these collections demonstrated elongated structures with co-localized staining for both Ela2 and DNA, suggesting these structures are NETs, potentially within a crypt abscess (Fig. 2.7E, orange box). This contrasted with Ela2 positive cells seen within the villi in infected tissues and throughout uninfected tissues that had well-defined nuclei and punctate Ela2 staining (Fig. 2.7E, green boxes).

One common histologic characteristic of *C. jejuni*-infected individuals is disruption of the intestinal epithelial barrier, including the neutrophil-dependent formation of intestinal crypt abscesses (58). To determine whether *C. jejuni*-induced NETs may be responsible for epithelial barrier disruption and crypt abscess formation, we sought to quantify the cytotoxic potential of these NETs on human colonocytes. Using an LDH assay, *C. jejuni* was incubated with neutrophils to induce NET formation prior to the products being incubated for 24h with human colonocytes (HCT116). When compared to *C. jejuni*-only (0.08 ± 0.79%) or neutrophil-only controls (0.1% ± 0.09%), there was a significant increase in mean LDH release from the human colonocytes (7.64% ± 2.21%) (Fig. 2.7F). This release of LDH was determined to be from HCT116 cells, as a neutrophil only control resulted in minimal LDH release. Therefore, the production of NETs in response to *C. jejuni* infection may lead to colonocyte cytotoxicity and contribute to the tissue damage observed in *C. jejuni*-infected patients.

Discussion

Campylobacter jejuni has been recognized as the most common cause of bacterial-mediated diarrheal disease in the world (142). Following ingestion of contaminated food or water, it is suspected that the bacterium adheres to the intestinal epithelium at the mucosal surface to induce a mild to severe inflammatory response. Surprisingly, compared to less prevalent gastrointestinal pathogens, the

inflammatory process during campylobacteriosis is not well understood. Using the ferret model of campylobacteriosis, our group recently demonstrated that innate immune cells are recruited to intestinal tissue during infection and that a single neutrophil-derived protein (S100A12) could be detected in ferret feces (59). Since these results indicate that neutrophils may be important during acute disease, we sought to further characterize the response of neutrophils during *C. jejuni* infection using both *ex vivo* and *in vivo* models.

We initially observed increases in multiple, predominantly neutrophil-derived antimicrobial proteins (Lcn2, MPO, and Ela2) in the feces of infected patients (55). While many of these proteins are not exclusive to neutrophils, the repeated abundance of these proteins - in addition to our earlier results with S100A12 - supports the conclusion that neutrophils are present at relatively high abundance at the host-pathogen interface (59). Some variability was noted among infected patient samples, which may have arisen due differences in time from when symptoms initiated to when samples were collected. Of the proteins assayed, Lcn2 has been shown to bind ferric-enterobactin and may serve to restrict iron acquisition by the bacterium (160). Recent data from a *C. jejuni* human feeding study indicated that several iron acquisition systems are upregulated during infection, suggesting that iron may be limited within infected intestines (161). Whether iron restriction is mediated solely through Lcn2 remains to be investigated. MPO is antimicrobial as it produces compounds, including hypochlorous acid, which are highly toxic to bacteria, virus-infected cells, and fungi (162). Ela2 is a serine protease that can directly kill bacteria, generate antimicrobial peptides, and inactivate virulence factors (163). The presence of these proteins indicated that the environment surrounding the neutrophils may be inhospitable to *C. jejuni* and limit its growth, which we demonstrated using *in vitro* experiments with purified Lcn2 (with addition of ferric-enterobactin as an iron source), MPO, and Ela2. To further understand how these proteins may be released from neutrophils into gastrointestinal tissues, we first determined the

ability of *C. jejuni* to induce neutrophil extracellular traps (NETs) using human and ferret cells.

While many of the above proteins serve as antimicrobials, MPO and Ela2 are also essential for development of NETs (44). Using purified human and ferret neutrophils, we observed *C. jejuni* inducing molecular events that precede NETosis, including activation of neutrophils. Upon further investigation of human neutrophils, increased PAD4 expression, histone citrullination, and extrusion of MPO, Ela2, and extracellular DNA was additionally observed. We were able to demonstrate these cellular changes quantitatively and qualitatively, as neutrophils incubated with *C. jejuni* lead to the extrusion of NET-like structures and increases in necessary NET proteins. This provided evidence for NETosis, as these structures do not occur in apoptosis or necrosis. One reason for the decreased expression of PAD4 for PMA induced neutrophils is that these NETs could be produced independent of PAD4 activity. During early research, neutrophils were viewed as terminally differentiated and transcriptionally inert; however, recent research has shown gene regulation and molecular plasticity of neutrophils. In fact, *Helicobacter pylori*, a close relative to *C. jejuni*, causes neutrophil hypersegmentation and subtype differentiation (164,165). These results could support the notion of neutrophil plasticity, as *C. jejuni* could cause neutrophils to enter a proinflammatory phenotype. Neutrophil subtype differentiation within the intestinal tissue during campylobacteriosis has yet to be investigated. Further, we demonstrated *C. jejuni* elicits a NET response similar to another well characterized NET inducer, *Salmonella*. Curiously, *C. jejuni* and *Salmonella*, two bacteria noted for their invasiveness, induced a NET response, while non-invasive *E. coli* O157:H7 did not. As a result, NETs may arise due to bacterial internalization and subsequent intracellular signaling.

Previous research demonstrated that dendritic cell TLR4 recognizes *C. jejuni* LOS and elicits a potent proinflammatory immune response (155). In addition, TLR4 has been shown to be required for phagocytosis of bacteria by neutrophils (159). Based on these observations, we initially demonstrated that

blocking TLR4 on primary human neutrophils decreased *C. jejuni* internalization, which was accompanied by a reduction in the number of neutrophils undergoing NETosis. Since NETosis was also previously shown to be dependent on TLR4 stimulation independent of internalization, we examined whether *C. jejuni* invasion occurred in neutrophils and impacted NET production. *C. jejuni* invasion into epithelial cells has been studied extensively and found to require the delivery of bacterial effectors like CiaC into the host cell cytosol using the flagellar secretion apparatus (158). During this process, actin polymerization produces actin-rich cell surface projections which envelop and internalize the bacterium (166). The Δ*flgE* mutant of *C. jejuni* does not encode a flagellar hook and is non-flagellated as a result, which leads to defective effector secretion and epithelial cell invasion (158). Using this strain, we found that internalization into neutrophils was significantly reduced and that the number of NET releasing cells decreased. While *C. jejuni* LOS synthesis is not influenced by deletion of *flgE*, these systems share modification enzymes, including a phosphoethanolamine (pEtN) transferase, which has been shown to protect against cationic antimicrobial peptides and assist in innate immune evasion (167). Future studies will investigate the role of LOS modifications in strains with flagellar defects since these strains may be able to synthesize LOS. This reduction supports the conclusion that bacterial internalization, potentially independent of proinflammatory signaling, drives NET production during *C. jejuni* infection. Additionally, *C. jejuni* possesses numerous DNases, encoded by the *cdt* and *dns* genes, that are secreted into the environment (81,168). These factors are notably absent in *Salmonella*, which appears to only possess intracellular DNases, and could be the basis for the bactericidal nature of NETs to *Salmonella* (44). Further studies will be required to more thoroughly investigate links between neutrophil phagocytosis, *C. jejuni* invasion into neutrophils, and the implications these have on NET production.

Due to the lack of a small animal model that exhibits clinical signs and responses like that of humans, knowledge is limited regarding the host response to *C. jejuni* infection. In addition to previous studies demonstrating that ferrets

develop disease similar to humans, we have shown that ferret neutrophils exhibit markers of NETosis when incubated with *C. jejuni*. Limited ferret specific antibodies are available to evaluate all the cellular changes that occur during NETosis; however, immunofluorescence staining of ferret colonic tissues demonstrated Ela2 positive staining that colocalized with DNA. This staining pattern differed from that of other Ela2 positive cells in uninfected tissues, suggesting that NET responses do occur within colonic tissue during infection. These observations are supported by previous work, which demonstrated neutrophils induce intestinal crypt abscesses in a hyperinflammatory IL-10$^{-/-}$ mouse model of campylobacteriosis (58). Using purified human neutrophils and NET inducing conditions, we demonstrated that the combination of *C. jejuni* and neutrophils leads to increased colonocyte cytotoxicity. This cytotoxicity could explain the hallmark histopathology seen within intestinal tissue during campylobacteriosis. As a result, further work is being conducted to determine whether damage to the epithelial cells during *C. jejuni* infection could be due to neutrophil transmigration and subsequent NET induction.

In summary, diarrheal diseases resulting from enteric pathogens are a leading cause of morbidity and mortality in the world, with *Campylobacter* as the leading cause for bacterially induced gastroenteritis (169). While several of these pathogens have been identified as potent inducers of NETs, there is a gap in knowledge as to the role of NETs in infectious gastroenteritis. This study highlights the importance of neutrophils in the host response to *C. jejuni* infection and how unique activities during infection may drive neutrophil responses that ultimately harm host tissues. Numerous studies have demonstrated that neutrophil accumulation in various inflammatory diseases is accompanied by increased pathology (170). In addition, the induction of NET formation has been correlated with poorer disease outcomes, including several postinfectious disorders associated with *C. jejuni* infection, such as irritable bowel syndrome (IBS) and rheumatoid arthritis (RA). As a result, further work will be conducted to determine the contribution of *C. jejuni*-induced NET formation on the manifestation of these

post-infectious disorders. In addition, leveraging of anti-NET therapeutics may hold potential for resolving acute inflammation during *C. jejuni* infection and/or ameliorating chronic or post-infectious outcomes.

Materials and Methods

Human fecal ELISA assays for neutrophil-derived proteins. Residual human fecal samples from standard-of-care testing were obtained from the University of Nebraska Medical Center's Department of Pathology and Microbiology (approval UTK IRB-17-03795-XM). Fecal specimens were evaluated for the presence of gastrointestinal pathogens using a BioFire FilmArray Gastrointestinal Panel. Samples that did not contain detectable gastrointestinal pathogens ("uninfected") and those that tested positive for only *C. jejuni* ("infected") were used for subsequent analyses. Approximately 100 µl of liquid or 100 µg of solid feces were aliquoted into 1.5 mL microcentrifuge tubes along with 1 mL of diluent (0.1% Tween 20 solution in sterile 1X phosphate-buffered saline (PBS)). Samples were vortexed for 20 minutes then centrifuged at 12,000 rpm to isolate the supernatants (171). From these supernatants, 100 µl was used for lipocalin-2 (Lcn2) (R&D Cat. DY1757-05) myeloperoxidase (MPO) (Cayman Cat. 501410), and neutrophil elastase (Ela2) (R&D Cat. DY9167-05) detection ELISAs. Absorbance values (450 nm) were determined following the manufacturer's protocol and concentrations were calculated using a standard curve of known protein concentrations. Statistical analysis was performed using a Mann-Whitney t-test with Welch's correction.

Bacterial cultures and culture conditions. *Campylobacter* jejuni 81-176, enterohemorrhagic Escherichia coli (EHEC) 0157:H7, and Salmonella typhimurium SL1344 were stored at -80℃ in MH broth supplemented with 20% glycerol. *C. jejuni* was routinely grown on Mueller-Hinton agar containing 10% sheep's blood and 10 ug/ml trimethoprim (TMP) at 37°C under microaerobic

conditions (85% N2, 10% CO2, and 5% O2) for 48 hours. Where indicated, *C. jejuni* was also grown on Mueller-Hinton agar containing 10% sheep's blood, 40 µg/ml cefoperazone, 100 µg/ml cycloheximide, 10 µg/ml trimethoprim, and 100 µg/ml vancomycin (*Campylobacter*-selective). EHEC and *Salmonella* were grown on LB agar under similar microaerobic conditions for 24 hours.

Analysis of *C. jejuni* growth in the presence of neutrophil-derived antimicrobial proteins. Using the neutrophil-derived antimicrobial proteins, *C. jejuni* growth was monitored when incubated with purified human Lcn2 (R&D, Cat. 1757-LC-050), MPO (R&D, Cat. 3174-MP-250), and Ela2 (Millipore, Cat. 324681-50UG). To examine for Lcn2-dependent growth inhibition, the minimum inhibitory concentration (MIC) of deferoxamine mesylate (DFOM) was first determined by adding linearly increasing concentrations from 1 µg/mL to 100 µg/mL to MH broth containing *C. jejuni* 81-176 at an optical density at 600 nm (OD600) of 0.025. Cultures were grown for 12, 24, and 48 hours under microaerobic conditions at 37°C. Next, linear concentrations of ferric enterobactin from 1 µg/mL to 10 µg/mL were added to cultures containing DFOM at the MIC until growth was fully restored for 48 hours under microaerobic conditions at 37°C. Finally, cultures containing both DFOM at the MIC and ferric enterobactin at a concentration that restored growth, were incubated with linearly increasing concentrations of Lcn2 from 1 µg/mL to 100 µg/mL added until growth decreased under microaerobic conditions at 37°C. To examine for the effects of MPO and Ela2 on *C. jejuni* growth, MH broth cultures containing *C. jejuni* 81-176 at an OD600 of 0.025 were grown in the presence of linearly increasing concentrations of these proteins from 1 µg/mL to 100 µg/mL for 12, 24, and 48 hours under microaerobic conditions at 37°C.

Isolation of primary human neutrophils. To obtain human neutrophils, 10 mL of blood was drawn from healthy donors into heparinized Vacutainer tubes and mixed 1:1 with sterile 1X phosphate buffered saline (PBS) (approval UTK IRB-18-04604-XP) (172). After mixing, 10 mL of lymphocyte separation medium (Corning, Cat.

25-072-CV) was underlaid. Following centrifugation at 1400 rpm for 30 minutes, the top layers were aspirated off, leaving the red blood cell and neutrophil pellet. Pellets were resuspended in 20 mL Hanks' Balanced Salt Solution 1x (Gibco, Cat. 14025076) and 20 mL 3% dextran in 0.9% NaCl. After incubating at room temperature for 20 minutes, the upper layer was transferred to a new tube. Following centrifugation at 400 x g for 5 minutes and aspiration of the supernatant, the pellet was washed with 20 mL ice-cold 0.2% NaCl and 20 mL ice-cold 1.6% NaCl two times. Following the final aspiration, the neutrophil pellet was resuspended in 10 mL RPMI 1640 1x (Corning, Cat. 10-040-CV). Neutrophil viability and counts were performed through Trypan blue stain (Lonza, Cat. 17-942E). Neutrophil purity was determined to be approximately 95% by flow cytometry analysis of CD11b^{hi} (Biolegend, Cat. 101212) and CD66b$^+$ (Biolegend, Cat. 305104).

Analysis of *C. jejuni* NET induction by flow cytometry. To examine for NET induction, *C. jejuni*, EHEC, and *Salmonella* were grown microaerobically at 37°C for 24 to 48 hours on MH media. Bacteria were resuspended in RPMI 1640 and incubated with neutrophils for three hours under microaerophilic conditions at an equal MOI of 1:50 (neutrophil:bacteria). Following incubation, these reactions were aliquoted into wells of a 96-well plate and centrifuged at 400 x g. Pelleted cells were washed three times with sterile 1x PBS cells before incubation with Live/Dead NIR stain (Thermo, Cat. L10119) for 25 minutes at room temperature. After incubation, cells were blocked with 1% goat serum for 10 minutes, then incubated with CD11b (Biolegend, Cat. 101212) myeloperoxidase (Biolegend, Cat. 347201), CD63 (Biolegend, Cat. 353007), and Cit-H3 (Novus, Cat. NB100-57135SS and Biolegend, Cat. 406403) antibodies for 30 minutes (173). Cells were subsequently fixed in fixation buffer (Biolegend, Cat. 420801) for 10 minutes at room temperature and stored at 4°C until flow cytometry analysis. TLR4 was blocked with 50 µl of TLR4 neutralizing antibody (InvivoGen, Cat. pab-hstlr4) and incubated for one hour. Flow cytometry preparation was performed as stated above. Samples were

analyzed using an LSR II flow cytometer and data was processed using FlowJo software. Statistical analysis was performed using unpaired t tests and significance inferred at $p < 0.05$.

Western blot analysis of NET products. After the NET induction protocol described above, cells from three healthy volunteers were lysed with Laemmli buffer with beta-mercaptoethanol and boiled for 10 minutes. 10 µl whole cell lysate samples were loaded onto a 12.5% SDS-PAGE gel and run for 1.25 hours at 140V at room temperature. Separated proteins were transferred to nitrocellulose membranes (GE Healthcare, Cat. 10600011) for 1.5 hours at 0.25A using a semi-dry transfer apparatus. Membranes were blocked in 5% milk in TBS-T for 60 minutes shaking. To probe for proteins of interest, 1:5000 dilution rabbit anti-human Lcn2 (Invitrogen, Cat. 702248), 1:5000 dilution mouse anti-human Ela2 (R&D, Cat. MAB91671), 1:5000 dilution goat anti-human MPO (R&D, Cat. AF3174), 1:1000 dilution rabbit anti-human PAD4 (Thermo, Cat. PA5-12236), 1:5000 dilution rabbit anti-human Cit-H3 (Novus, Cat. NB100-57135SS) and 1:500 dilution mouse anti-human β-actin (Biolegend, Cat. 643801) were incubated on individual membranes for 1 hour at room temperature with shaking. Membranes were subsequently washed three times with filtered TBS-T for 5 minutes each. Proteins of interest were detected using a 1:2000 dilution of appropriate horseradish peroxidase conjugated secondary antibodies in 15 mL 5% milk in TBS-T and incubated for 45 minutes at room temperature with shaking. Membranes were then washed three times with filtered TBS-T, shaking for 5 minutes each. After the final wash, membranes were developed with a solution containing 5 mL peroxide and 5 mL luminol/enhancer solution (Thermo, Cat. 34580) and incubated for 5 minutes at room temperature with shaking. A *C. jejuni* negative control was also performed to ensure there was no cross-reactivity and no detection of proteins was noted. Chemiluminescent bands were imaged using the ChemiDoc-It Imager and densitometry measurements were made using

46

ImageJ software. Statistical analysis was performed using unpaired t tests and significance inferred at $p < 0.05$.

Analysis of *C. jejuni* NET induction by SYTOX assay. Following the *C. jejuni* NET induction described above, cells were added to wells of black 96-well plates (Invitrogen, Cat. 655077-25) and centrifuged at 400 x g. Supernatants were discarded and 1.0 µM SYTOX Green (Invitrogen, Cat. S7020) was added to each sample and incubated under microaerobic conditions at 37°C for one hour (174). After incubation, cells were centrifuged at 400 x g and the supernatant was discarded. The cells were washed once with 1x PBS and then resuspended in 100 µl 1x PBS. SYTOX fluorescence was measured at 504/523 nm using a BioTek plate reader. Statistical analysis was performed using unpaired t tests and significance inferred at $p < 0.05$.

Visualization of *C. jejuni* NET induction by fluorescence microscopy. *C. jejuni* NET induction described above occurred on poly-l-lysine coated glass coverslips (Corning, Cat. 354085) for three hours at 37°C under microaerobic conditions (174). Following three 1x PBS washes, coverslips were incubated with a goat anti-myeloperoxidase (R&D, Cat. AF3174) and donkey anti-goat Alexa Fluor 405 (AbCam, Cat. Ab175664). Coverslips were also incubated with a mouse anti-neutrophil elastase (R&D, Cat. MAB91671) and goat anti-mouse Alexa Fluor 594 (Biolegend, Cat. 405326). After three 1x PBS washes, coverslips were incubated with 1.0 µM SYTOX Green (Invitrogen, Cat. S7020). Finally, after three 1x PBS washes, coverslips were placed on glass slides with a drop of Mowiol mounting medium (Sigma, Cat. 81381-50G) and kept in the dark at 4 °C until fluorescent microscopy was performed. Ten fields of each sample condition were visualized using a Nikon E600 Eclipse at the Advanced Microscopy and Imaging Center at the University of Tennessee. For statistical analysis, three individual neutrophil isolations were performed and stained as described above. Of those,

100 fields were observed for the presence of fluorescent NETs. Statistical analysis was performed using unpaired t tests and significance inferred at $p < 0.05$.

Analysis of *C. jejuni* internalization by neutrophils. *C. jejuni* and neutrophils were incubated at an MOI of 10:1 for 1, 2, and 3 hours at 37°C under microaerobic conditions. Additionally, neutrophils where indicated were incubated with 2µM cytochalasin-D (CD) (Sigma, Cat. C8273-1MG) or 50 µl of TLR4 neutralizing antibody (Invivogen, Cat. pab-hstlr4). Following incubation, cells were incubated in 100 µl RPMI 1640 containing 10% FBS and 100 µg/mL gentamicin sulfate (Negretti & Konkel, 2017). This concentration of gentamicin was determined as the highest concentration that killed extracellular bacteria but did not kill internal bacteria or negatively impact neutrophil viability. After treatment, neutrophils were washed three times with 1x PBS to remove remaining antibiotic and neutrophils were lysed with 0.1% Triton X-100 for 5 minutes to release intracellular bacteria. Three 1x PBS washes were then performed to remove excess Triton X-100. Cell pellets were resuspended in MH broth and serial dilutions were plated on *Campylobacter*-selective media. Cultures were grown for two days at 37°C under microaerobic conditions and CFUs were counted. Statistical analysis was performed using unpaired t tests and significance inferred at $p < 0.05$.

Infection of ferrets with *C. jejuni*. As previously described, *C. jejuni* 81-176 was grown on MH + TMP and Gram strained to ensure culture purity prior to inoculation (59). This culture was streaked on *Campylobacter*-selective media and incubated at 37°C under microaerophilic conditions for 48 hours. Suspensions of *C. jejuni* 81-176 were made in sterile PBS and diluted to an OD600 of 2.0. Three male ferrets were anesthetized with isoflurane and inoculated via orogastric tube with 5 mL of *C. jejuni* 81-176 inoculum - an infectious dose of 1.5×10^9 CFU - which was combined with 5 mL of 5% sodium bicarbonate buffer prior to administration (UTK IACUC protocol #2519). Additionally, three male ferrets were mock infected with 5 mL of sterile 1X PBS which was combined with 5 mL of 5% sodium bicarbonate

buffer prior to inoculation. Morphine was administered intraperitoneally to each ferret one-hour following inoculation and ferret blood was collected from the vena cava into EDTA-treated vacutainers at three days post infection. Neutrophils were isolated by density gradient centrifugation and ACK osmotic red blood cell lysis (172). Ferrets were subsequently sacrificed by cardiac puncture of barbiturate.

Histologic analysis of ferret intestinal tissue during _C. jejuni_ infection. The terminal 1 cm of the ferret colon was removed following sacrifice, and the lumen was washed five times with 1 mL of sterile, cold 1X PBS. Tissue was placed in 10% buffered formalin and fixed for 4 hours at room temperature. Fixed tissue was embedded in formalin, and 4 μm sections were stained with hematoxylin and eosin (H&E). Stained slides were visualized through bright-field microscopy, and representative images are presented. Inflammation scoring was performed as described in a blind manner, noting edema, presence of blood, hyperplasia, loss of goblet cells, epithelia raggedness, and neutrophil infiltration (175). Statistical analysis was performed using unpaired t tests and significance inferred at $p < 0.05$.

Immunofluorescence staining of ferret colonic tissue for NETs. Ferret colon tissues were stained for the presence of NETs as previously described (176,177). Tissues were deparaffinized and incubated in R universal Epitope Recovery Buffer (Electron Microscopy Sciences) at 50°C for 90 minutes. Samples were then rinsed in deionized water three times followed by washing with TRIS-buffered saline (TBS, pH 7.4). Samples were permeabilized for 5 minutes with 0.5% Triton X100 in TBS at room temperature followed by 3 washes with TBS. Samples were then blocked with TBS with 10% BSA for 30 minutes prior to incubation with 1:50 dilutions of rabbit poly-clonal anti-neutrophil elastase antibodies (MilliporeSigma, Cat. 481001). The following day, samples were washed in TBS followed by repeat blocking with blocking buffer for 30 minutes at room temperature before incubation with 1/00 dilution of Alexa Fluor® 488 conjugated donkey anti-rabbit IgG (Invitrogen) for 4 hours at room temperature. Samples were then washed and

incubated with 5 µM Hoechst 33342 for 30 minutes to stain DNA/nuclei. After final washes, slides were dried and cover slipped. Tissues were visualized with a Zeiss LSM 710 META Inverted Laser Scanning Confocal Microscope. Images presented are composites of z-stacked images.

HCT116 Cytotoxicity in response to *C. jejuni* induced NETs. HCT116 cells were routinely cultured in 75 cm2 flasks in 10 mL of DMEM supplemented with 10% FBS, 100 U/mL Pen-Strep antibiotics, and 2 mM L-glutamate at 37°C and 5% CO_2. $6x10^4$ cells were then seeded in 96 well plates to adhere overnight. After neutrophils were incubated with *C. jejuni* to allow NETosis as previously described, *C. jejuni*-neutrophil pellets were incubated with HCT116 cells for 24 hours at 37°C and 5% CO_2. Following incubation, the plate was centrifuged at 250 x g for three minutes. 50 µL of culture supernatant was then plated on another 96 well plate and an LDH assay was performed as described by the Pierce™ LDH Cytotoxicity Assay Kit protocol (Thermo, Cat. 88954). In brief, supernatant of the cell incubation was taken off and added to a new well. To the well, reaction mixture was added and incubated at room temperature for thirty minutes. Following incubation, stop solution was added to the well to stop the reaction from proceeding. The 96 well plate was read at the absorbances 490 nm and 680 nm. Percent cytotoxicity was calculated through the equation: [(Experimental value – Effector Cells Spontaneous Control – Target Cells Spontaneous Control) / (Target Cell Maximum Control – Target Cells Spontaneous Control)] * 100. Statistical analysis was performed using unpaired t tests and significance inferred at $p < 0.05$.

Figure 2.8. Inflammation scoring of uninfected and infected ferret colon tissue sections.

H&E slides were observed for one hundred fields of visions for multiple signs of histopathology. Statistical analysis was performed using an unpaired t test between uninfected and infected groups. *$p \leq 0.05$; **$p \leq 0.01$

CHAPTER THREE

A SECRETED SIRTUIN FROM *CAMPYLOBACTER JEJUNI* CONTRIBUTES TO NEUTROPHIL ACTIVATION AND INTESTINAL INFLAMMATION DURING INFECTION

This chapter is a version of a manuscript originally published by Sean M. Callahan and Jeremiah G. Johnson currently in revisions at *Science Advances*.

Sean M. Callahan, Trevor J. Hancock, Ryan S. Doster, Caroline B. Parker, Mary E. Wakim, Jennifer A. Gaddy, Jeremiah G. Johnson. "A secreted bacterial sirtuin from *Campylobacter jejuni* activates neutrophils and induces inflammation during infection."

The work described in this study was conducted by the following individuals: purification of murine leukocytes were conducted by T.J.H. *In vitro* confocal microscopy was conducted by R.S.D. Cloning reporter strains was conducted by C.B.P. Cloning for protein production and bioinformatic analysis of clinical *sliP* presence were conducted by M.E.W. All other experiments were conducted by S.M.C.

Abstract

Histone modifications control numerous processes in eukaryotes, including inflammation. Some bacterial pathogens alter the activity or expression of host-derived factors, including sirtuins, to modify histones and induce responses that promote infection. In this study, we identified a deacetylase encoded by *Campylobacter jejuni* which possesses sirtuin activities and contributes to activation of human neutrophils by the pathogen. Importantly, this sirtuin is secreted from the bacterium into neutrophils, where it associates with and deacetylates host histones, which correlated with neutrophil activation and extracellular trap production. Using the murine model of campylobacteriosis, we found that a mutant of this bacterial sirtuin efficiently colonized the gastrointestinal tract, but was unable to induce cytokine production, gastrointestinal inflammation, and tissue pathology. In conclusion, these results suggest that secreted bacterial sirtuins represent a new class of bacterial effector and that bacterial-mediated modification of host histones is responsible for the inflammation and pathology that occurs during campylobacteriosis.

Introduction

Campylobacter species are a leading cause of bacterial-derived gastroenteritis worldwide, infecting a projected four hundred million individuals (1,178). While infection is often self-limiting in immunocompetent individuals, numerous post-infectious disorders can develop, including Guillain-Barré syndrome (GBS), irritable bowel syndrome (IBS), and reactive arthritis (ReA) (179–181). In addition to the prevalence of infection and these various outcomes, the high incidence of antibiotic resistance has led both the Centers for Disease Control and World Health Organization to classify *Campylobacter* spp. as serious threats to public health (143,146,147). Despite these impacts, little is known about the bacterial and host factors responsible for the inflammation which occurs during human campylobacteriosis and how that might be responsible for intestinal disease. In our previous work, we found neutrophils are recruited to the site of infection and that predominantly neutrophil-derived proteins are present in fecal samples of *C. jejuni*-infected patients. In addition, we found *C. jejuni* is a potent activator of human neutrophils and that stimulation leads to the production of neutrophil extracellular traps (NETs), which appear to localize to abscesses within colonic crypts (59,182). Because neutrophil activation during campylobacteriosis has been associated with inflammation and tissue pathology (58,67,183), understanding the microbial factors which drive this could lead to the development of therapeutics. To identify bacterial factors which promote neutrophil activation by *C. jejuni*, including the production of NETs, we screened a transposon library of *C. jejuni* for mutants unable to degrade neutrophil DNA (unpublished results) and activate primary human neutrophils. As a result, we identified a locus (Cjj81176_0779) that encodes a putative bacterial sirtuin, which we found was unable to activate and NETose neutrophils.

Post-translational modifications (PTMs) in eukaryotes play a vital role in orchestrating host-microbe interactions. Differential acetylation of host proteins is accomplished using numerous enzymes, including histone acetyltransferases

55

(HATs), histone deacetylases (HDACs). The outcomes of altering host protein acetylation are varied and include impacts to processes involved in autoimmunity, inflammation, and tumorigenesis (184–186). Because the host uses acetylation to control these cellular processes, pathogens, including *Listeria monocytogenes*, *Salmonella typhimurium*, and *Mycobacterium tuberculosis*, can manipulate and utilize host HDACs and HATs to promote infection, especially sirtuin-2 (SIRT2) (114,115,117,187–190). However, recent research has found that bacterial-derived effectors can directly modify host proteins PTMs. While some pathogens have acquired and incorporated host enzymes into their virulence factor repertoire, others have convergently evolved to mimic the activity of host enzymes (191–193). Importantly, bacterial effectors that are translocated and directly bind host proteins to differentially acetylate them remain to be identified.

In eukaryotes, a common target of PTMs are histones, which play a critical role in the structure and function of chromatin, having profound effects on gene expression. Core histones are characterized by a histone folding domain and N-terminal tails accessible to enzymes involved in PTMs (194). For example, HATs acetylate the ε-amino group of lysine residues on histones, which results in a neutral charge and opening of chromatin for RNA polymerase (195). In contrast, during histone deacetylation, the acetyl group is removed from lysine residues, which causes the chromatin to close and prevent RNA polymerase binding (196). Beyond reducing gene transcription, other research found HDACs can induce gene expression by limiting acetylation near gene bodies and intergenic regions, which allows RNA elongation factors to bind more readily (197–199). As a result, numerous pro-inflammatory genes are upregulated in response to HDAC activity, including IL-8, CSF-1, and TNF-α (200–202).

In addition to impacting gene expression, differential acetylation of proteins, including histones, can alter other cellular responses. In neutrophils, for example, increased HDAC activity promotes citrullination of histone H3 by protein arginine deiminase 4 (PAD4), which results in the elaboration of neutrophil extracellular traps (NETs) and the associated inflammation (203–205). This post-translational

56

conversion of arginine to citrulline on histone H3 through PAD4 replaces the primary ketamide with a ketone group and is indispensable in the production of NETs (206). Further, PAD4 promotes decondensation of heterochromatin to facilitate NET release into the extracellular milieu (207). Despite the apparent relation between histone acetylation and neutrophil physiology, the role of sirtuins in these responses is not well defined.

Importantly, because histone acetylation plays a role in proinflammatory gene expression and cellular outcomes, investigators have sought to characterize their effects in various diseases and whether altering these responses can improve health. For example, in the gastrointestinal tract, deacetylation inhibition is a naturally occurring phenomenon. Sodium butyrate is a short-chain fatty acid (SCFA) produced by the human gut microbiota as a byproduct of anaerobic fermentation of dietary fibers (208). By binding to and inhibiting the enzymatic activity of various HDACs and sirtuins, butyrate has been shown to reduce inflammation within the gastrointestinal tract, specifically through suppressing neutrophil activity and inhibiting nuclear factor κB (NF-κB)-dependent proinflammatory gene expression in colonocytes (12,209,210). Similarly, trichostatin A (TSA) is a potent HDAC inhibitor and was recently found to interact with mammalian sirtuins, suppressing cellular inflammatory responses and promotes neutrophil apoptosis (211–214). Because of these results, HDACs and sirtuins are emerging therapeutic targets for the development of treatments for inflammatory disorders of the gastrointestinal tract.

In the present study, we characterize a unique bacterial effector protein in *C. jejuni*, which we have termed SliP, that we determined is involved in the activation of human neutrophils and the production of NETs. We show SliP functions as an NAD$^+$-dependent sirtuin, that zinc is involved with SliP's ability to deacetylate acetylated peptides, and that it is secreted into neutrophils using the flagellar secretion apparatus. Following secretion, SliP associates with neutrophil histones, which correlates with a reduction in the acetylation of these structures. Finally, we demonstrate inflammation and intestinal pathology is promoted by SliP

57

despite the mutant being able to efficiently colonize and disseminate within the host. These findings suggest histone deacetylation mediated by SliP is a unique mechanism by which a pathogen induces an inflammatory response and tissue pathology during infection. With these findings, we expect therapeutic strategies can be developed to mitigate SliP-dependent inflammation and pathology during acute and chronic human disease.

Results

C. jejuni **encodes a sirtuin-like deacetylase more frequently present in clinical isolates than agricultural or environmental isolates.** The DUF4917 family of proteins are ubiquitous in microorganisms, with many representatives found in *Burkholderia* and *Brucella* species, but little is known about the function of these proteins (EMBL-EFI). The Cjj81176_0779 locus we identified in *C. jejuni* is predicted to contain a DUF4917 domain with shared amino acid homology with other human bacterial pathogen-derived DUF4917 family proteins, including those from *Yersinia enterocolitica* and *Legionella pneumophila* (Figure 3.1A) (215,216). We also determined Cjj81176_0779 is downstream of *dnaK* and *grpE*, both of which are chaperones involved in flagellar biogenesis and chaperoning T3SS effectors (Figure 3.1B) (217,218). As this family of proteins has yet to be investigated for function, secondary structure prediction was performed using Phyre2 and iTASSER (219,220). In both analyses, the protein encoded by Cjj81176_0779 appears to share secondary structure homology with bacterial sirtuins, specifically sirtuin-2, hence, this protein has been termed SliP for s̲irtuin-l̲ike p̲rotein (Figure 3.1B). Interestingly, there is little known about the domain architecture of DUF4917 family proteins, with SliP only containing identifiable Rossmann folds and a coil domain (Figure 3.1C, D). Important to our homolog analysis, sirtuins also contain a Rossmann fold comprised of a Gly-X-Gly motif that is responsible for binding the phosphate group of NAD^+ and a small pocket of charged amino acids that bind the two ribose molecules of NAD^+ (221). SliP
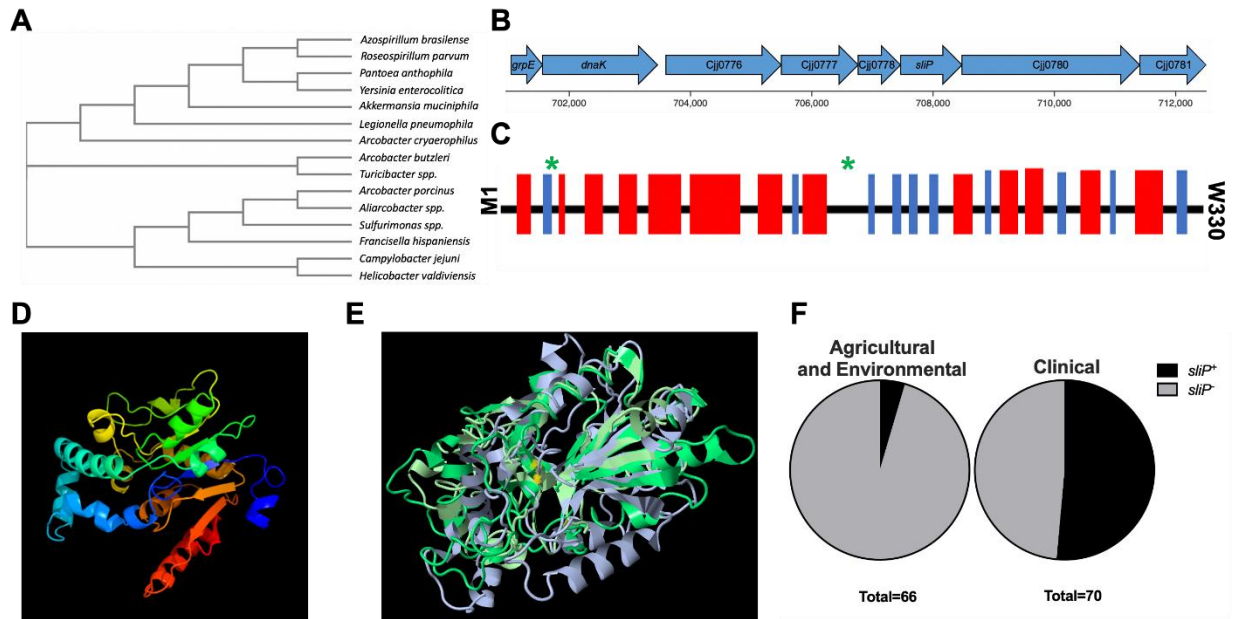
Figure 3.1. Identification of the predicted sirtuin, SliP, in *C. jejuni*.

(A) Phylogenetic analysis of the DUF4917 family proteins in relation to *C. jejuni*. A BLAST analysis was performed for proteins homologous to the *C. jejuni* DUF4917 family protein. (B) Gene neighborhood of *sliP* within the *C. jejuni* genome. Predicted operons were done through Microbial Signal Transduction Database (MiST) analysis. (C) Predicted protein scheme of SliP secondary structure through iTASSER analysis. Black bars designate coils, blue bars represent strands, and red bars represent helices. Green stars designate predicted Rossman fold domains within SliP. (D) Prediction of the secondary structure of SliP using Phyre2 threaded through the *B. subtilis* ThsA, the highest amino acid similarity protein to SliP. (E) Overlapped secondary structure models of DUF4917 family proteins using Jmol software. Yellow dots indicate position of the G26 residue within the structural model for the representative *C. jejuni* SliP shown. (F) Percentage of *sliP* containing environmental and clinical *C. jejuni* genomes from a previous study. Whole genomes were uploaded to KBase, where the homology threshold was set to 75%. Chi-square contingency testing was performed, $\chi^2 = 36.51$, $z = 6.042$, p = < 0.0001.

59

possesses a Gly-Asn-Gly sequence and the second glycine residue, at position 26 (G26) was predicted to be an NAD$^+$ binding residue through iTASSER (Figure 3.1E). To determine the potential role of this protein in the pathogenesis of *C. jejuni*, we examined *sliP* presence in the genomes of agricultural and environmental isolates of *C. jejuni* and compared that incidence to human clinical isolates collected and sequenced in a previous study (222). We found *sliP* is more frequently present in clinical isolates, with 36 of 70 isolates encoding *sliP* (Figure 3.1F) and only 3 of 66 agricultural and environmental *C. jejuni* possessing the gene (χ = 36.51, z = 6.042, p = < 0.0001).

SliP functions as a canonical sirtuin by deacetylating lysines in an NAD$^+$ and zinc-dependent manner. To investigate the function of SliP, His-tagged protein was purified by Ni-NTA chromatography (Figure 3.8.A, B, D-appendix). Because NAD$^+$ and zinc are often required for sirtuin activity (223), the deacetylase activity of purified SliP was determined for acetyl-lysine peptides with or without those cofactors. As expected, when either 5 mM NAD$^+$ or 20 µM zinc chloride were individually added to deacetylase reactions, there was a 1.92 and 3.11-fold increase in lysine deacetylation after one hour relative to reactions without the cofactors, respectively. When both NAD$^+$ and zinc chloride were added, we observed a 3.76-fold increase in lysine deacetylation when compared to reactions without the cofactors (Figure 3.2A). As sirtuins classically hydrolyze NAD$^+$ during lysine deacetylation (224), we sought to determine whether SliP-mediated deacetylation leads to NAD$^+$ hydrolysis. Using purified SliP, NAD$^+$ concentrations were monitored over time during lysine deacetylation using a commercially available kit. Purified sirtuin-2 (SIRT2) was used as a positive control for both NAD$^+$ hydrolysis and lysine deacetylation. As expected, NAD$^+$ concentrations decreased 1.94-fold and 2.06-fold during deacetylation of acetyl-lysine peptides by purified N- and C- terminal His tagged SliP, respectively, while similarly purified lysates without recombinant SliP (empty vector) were unable to significantly decrease NAD$^+$ concentrations (1.07-fold and 1.06-fold reduction for N-and C- terminal His
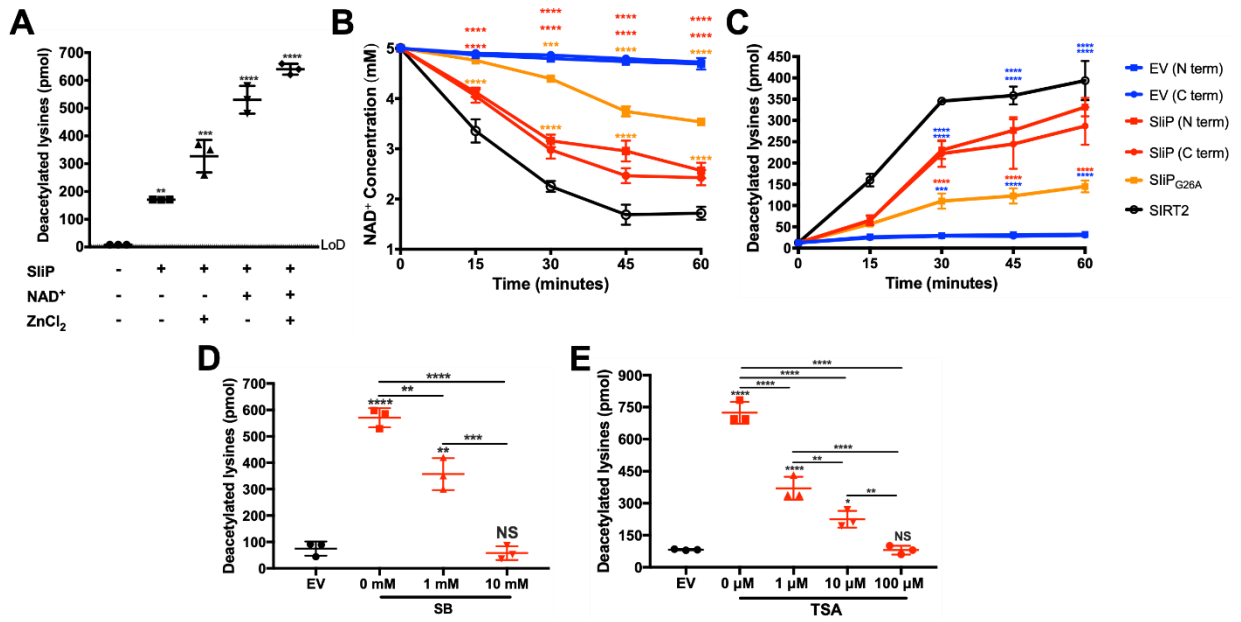
Figure 3.2. SliP is an NAD$^+$-dependent sirtuin and requires zinc for maximal activity.

(A) Lysine deacetylation was performed for SliP with common sirtuin cofactors, NAD$^+$ and zinc chloride, and assayed after one-hour post incubation at 37°C. For statistical analysis, each treatment group was compared to the empty vector (EV) control. (B) NAD$^+$ hydrolysis assay and (C) lysine deacetylation during a one-hour time course at 37°C. Blue bars represent the EV controls, whereby the N-and C-terminally 6X His tagged SliP are represented in red and SliP$_{G26A}$ incubated reactions are represented in orange. Pure sirtuin-2 (SIRT2) is represented in black lines (D) Sodium butyrate (SB) and (E) trichostatin-A (TSA) dose-response analysis of SliP inhibition after one-hour post incubation at 37°C. Multiple comparison testing was performed using ANOVA with Tukey's *post-hoc* test. *$p < .05$; **$p < .01$; ***$p < .001$; ****$p < .0001$

tagged vectors, respectively) (Figure 3.2B). Importantly, deacetylase reactions containing SliP or empty vector lysates did not result in significant hydrolysis of NADH (Figure 3.9-appendix). To determine whether the conserved glycine residue in SliP (Figure 3.1C, E) is required for full sirtuin activity, a single point mutation was introduced into SliP (SliP$_{G26A}$) (Figure 3.8C-appendix). Compared to wild-type SliP, SliP$_{G26A}$ was unable to deacetylate lysine residues and hydrolyze NAD$^+$ as readily, exhibiting 2.28 -fold decrease and 1.38 -fold increase, respectively compared to wild-type SliP (Figure 3.2B, C). Pure SIRT2 was able to perform lysine deacetylation with NAD$^+$ hydrolysis, with 31.5-fold increase in lysine deacetylation and 2.91-fold decrease in NAD$^+$ concentration. As such, we hypothesize SliP functions as a canonical sirtuin, and the glycine residue within the predicted Rossman fold is involved in NAD$^+$ binding and hydrolysis during lysine deacetylation.

Because SliP functions as a sirtuin, we further sought to determine if characterized deacetylase inhibitors can reduce SliP activity. To accomplish this, we used conditions where maximum lysine deacetylation was observed and titrated in either media alone, sodium butyrate (SB), or trichostatin A (TSA) and assayed for lysine deacetylation as above. We observed a dose-dependent inhibition of deacetylation for both SB and TSA to where at 10 mM (for SB) and 100 μM (for TSA), the presence of SliP did not lead to significantly more deacetylation than when eluates lacking a deacetylase were used. For example, there was a 9.85-fold reduction in lysine deacetylation at 10 mM SB (Figure 3.2D) and a 9.01-fold reduction in lysine deacetylation at 100 μM TSA (Figure 3.2E). These results demonstrate SB and TSA can chemically inhibit SliP-dependent lysine deacetylation, which supports the conclusion that SliP functions as a canonical sirtuin.

SliP is a secreted bacterial sirtuin which requires the flagellar secretion apparatus. To determine whether host proteins can be targeted by SliP during infection, we first established whether SliP was secreted from *C. jejuni*. To examine

SliP secretion, polyclonal antibodies were raised against purified His-tagged *C. jejuni* SliP and cell-free supernatants were assayed for the presence of the protein by western blot. In addition, because deoxycholate (DOC) has been shown to promote secretion by *C. jejuni* through the flagellar secretion system (31,90), we investigated whether SliP translocation into culture supernatants increased in response to sodium deoxycholate and whether SliP secretion was absent in a non-flagellar mutant of *C. jejuni* (Δ*flgE*). Regardless of whether strains were grown with or without DOC, SliP was detected in whole cell lysates of each strain except for Δ*sliP* (Figure 3.3A). When we examined for translocation of SliP into media lacking sodium deoxycholate, we did not detect SliP in those cell-free supernatants. In contrast, when strains were grown in media containing sodium deoxycholate, SliP was detected in the cell-free supernatants of all strains except the Δ*sliP* and Δ*flgE* mutants (Figure 3.3A). Furthermore, when we probed for a known intracellular protein, RpoA, we only observed protein within cell pellets and not within supernatant regardless of media condition (Figure 3.3A) (225). To eliminate the possibility that SliP was present in the supernatant due to sodium deoxycholate-induced cell lysis, we quantified the amount of *C. jejuni* genomic DNA in supernatants with or without sodium deoxycholate by qPCR and observed no significant differences across strains or growth conditions. However, genomic DNA was readily amplified once cells were incubated in the presence of SDS (Figure 3.10-appendix). This result supports our observation that SliP is specifically translocated through the flagellar secretion apparatus in response to an intestinal signal, such as deoxycholate.

To determine whether secreted SliP is functional, cell-free supernatants of cultures grown in media supplemented with sodium deoxycholate were investigated for sirtuin activities, including lysine deacetylation and NAD^+ hydrolysis. We observed significant NAD^+ hydrolysis in supernatants from both wild-type and *sliP* complemented strains, with 1.41-fold and 1.42-fold decreases in NAD^+ concentrations relative to the starting concentration respectively (Figure 3.3B). Additionally, the complemented strain harboring the G26A mutation, there

Figure 3.3. SliP is translocated into host neutrophils through the flagellar secretion system.

(A) Deoxycholate (DOC) induces SliP translocation through the flagella into the supernatant. Cultures were grown in Mueller-Hinton (MH) broth alone (MH) or supplemented with deoxycholate (MH + DOC) for 48 hours under microaerobic conditions. Whole cell lysates (CP) and supernatants (sup.) were analyzed for SliP abundance by western blot. Cell pellets and supernatants were also analyzed for RpoA, serving as a negative control. (B) NAD^+ hydrolysis during (C) Lysine deacetylation using supernatants over a one-hour incubation period at 37°C. Pure sirtuin-2 (SIRT2) was used as a positive control for both NAD^+ hydrolysis and lysine deacetylation (black lines). (D) Schematic for the calmodulin-dependent *B. pertussis* adenylate cyclase (CyaA) bacterial secretion assay for *C. jejuni* within neutrophils. (E) CyaA translocation assay performed in wild-type and the flagella mutant ($\Delta flgE$) infected neutrophils. The *ciaB-cyaA* and *heuR-cyaA* translational fusions served as positive and negative controls, respectively. The data is representative of biological triplicate. Multiple comparison testing was performed using ANOVA with Tukey's *post-hoc* test. *$p < .05$; **$p < .01$; ***$p < .001$; ****$p < .0001$.
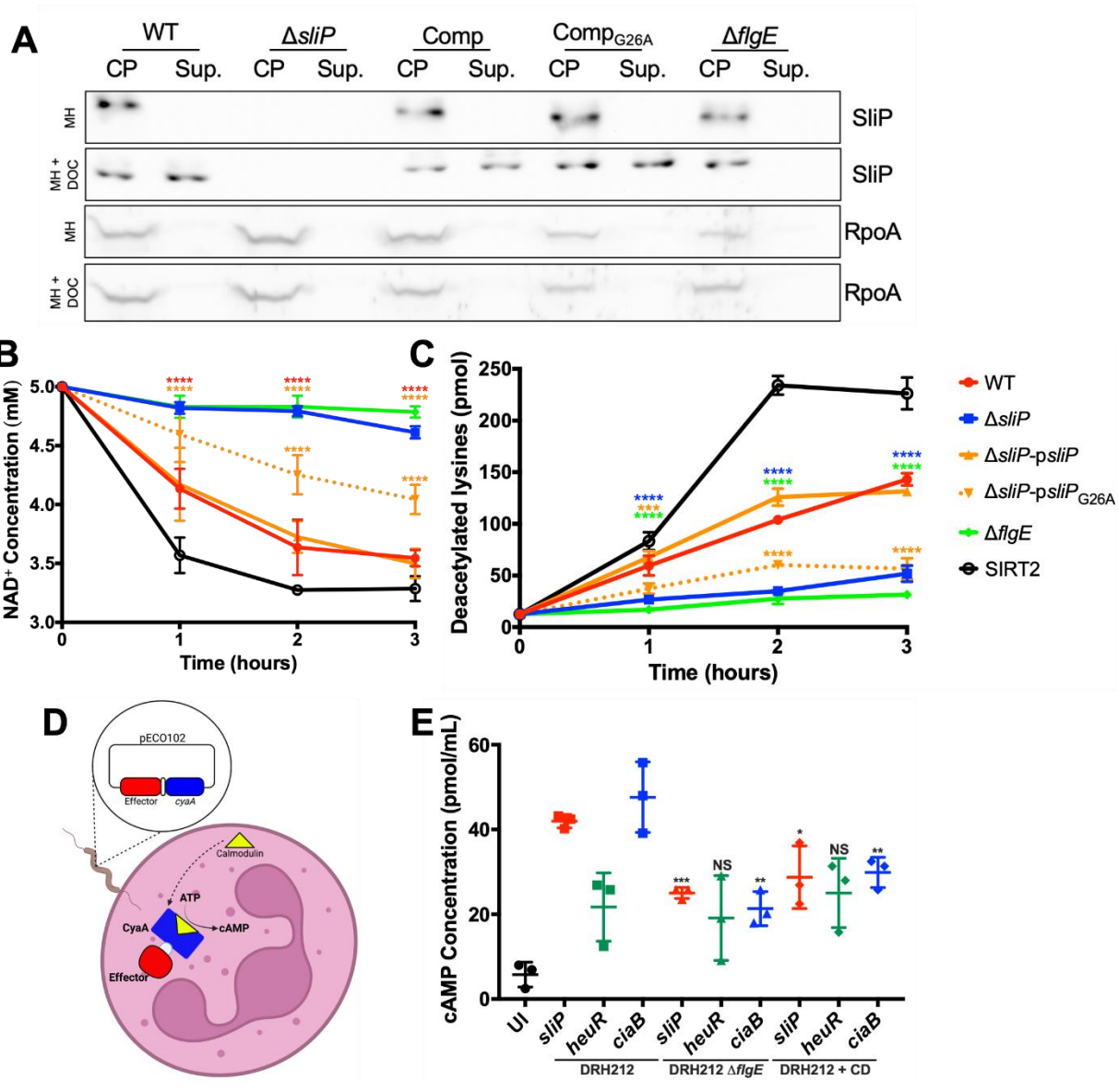
was a 1.16-fold increase in NAD^+ concentration relative to wild-type *sliP* complemented strain (Figure 3.3B). In contrast, supernatants from both Δ*sliP* and a flagellar hook mutant (Δ*flgE*) did not produce significant NAD^+ hydrolysis with only 1.08-fold and 1.04-fold decrease relative to the initial concentrations following one-hour incubation, respectively (Figure 3.3B). Furthermore, we observed deacetylase activity within the supernatants of wild-type and *sliP* complemented strains, with the amount of lysines deacetylated increasing by 11.45 and 10.52-fold when compared to the zero-hour time point, respectively (Figure 3.3C). As expected, supernatants from the Δ*sliP* and Δ*flgE* mutants were unable to significantly deacetylate lysine residues, exhibiting 4.14 and 2.52-fold increases when compared to the zero-hour time point, respectively. Finally, the complemented strain harboring the G26A mutation, there was a 2.32-fold decrease in lysine deacetylation concentration relative to wild-type *sliP* complemented strain (Figure 3.3C). For SIRT2, there was an 18.1-fold increase in lysine deacetylation compared to the zero-hour time point (Figure 3.3C). This observation not only confirms the presence of SliP in *C. jejuni* supernatants, but also suggests it is enzymatically active as a deacetylase and requires the flagellar secretion apparatus for translocation. As such, we show SliP is a secreted bacterial effector which deacetylates lysine residues.

SliP is secreted into human neutrophils and promotes elevated deacetylase activity. To investigate whether SliP is secreted into human neutrophils, we constructed plasmids containing translational fusions of proteins of interest to the *Bordetella pertussis* adenylate cyclase (CyaA) domain (Figure 3.3D) (226). In addition to the SliP-CyaA reporter, we also constructed HeuR-CyaA and CiaB-CyaA reporters as negative and positive secretion controls, respectively (90,227,228). For HeuR, it is a well-characterized intracellular *C. jejuni* transcription factor unable to be secreted out into the extracellular environment, while CiaB is a secreted flagellar protein delivered to the cytosol of host cells. These plasmids were introduced into wild-type and Δ*flgE* strains as the flagellar

T3SS serves as the major secretion system in *C. jejuni* (158,229). Three hours post-infection, cAMP levels were measured as a proxy for effector secretion into host cells using an enzyme-linked immunosorbent assay (ELISA). In wild-type strains, cAMP levels increased by 7.26, 3.76, and 8.24-fold when they possessed the SliP-CyaA, HeuR-CyaA, and CiaB-CyaA plasmids, respectively, when compared to uninfected neutrophils (Figure 3.3E). In contrast, when $\Delta flgE$ containing the same constructs were used to infect neutrophils, cAMP levels decreased by 1.68, 1.13, and 2.23-fold when compared to their wild-type SliP-CyaA, HeuR-CyaA, and CiaB-CyaA counterpart, respectively (Figure 3.3E). Furthermore, wild-type strains encoding the various CyaA reporters were able to internalize at similar rates and produced similar intracellular CyaA despite the fusion (Figure 3.11-appendix). Because decreased translocation of bacterial-derived proteins in $\Delta flgE$ could be due to reduced secretion or endocytosis, actin rearrangement was blocked using cytochalasin D (CD). Treatment with CD resulted in reduced cAMP by 1.46, 0.87, and 1.6-fold when compared to untreated infections with wild-type SliP-CyaA, HeuR-CyaA, and CiaB-CyaA strains, respectively (Figure 3.3E). As actin polymerization has been implicated in *C. jejuni* invasion, neutrophil phagocytosis, and T3SS-dependent effector secretion in various organisms, SliP could require actin polymerization to translocate to the host cytosol (230).

Based on this data, we next sought to establish whether translocation of SliP is associated with intracellular environments which exhibit elevated lysine deacetylase activity. To accomplish this, human neutrophils were infected with wild-type *C. jejuni*, *sliP* deletion mutant ($\Delta sliP$), $\Delta sliP$ complemented with the wild-type *sliP* allele ($\Delta sliP$-p*sliP*), or $\Delta sliP$ complemented with the G26A substitution ($\Delta sliP$-p*sliP*$_{G26A}$). As predicted, intracellular lysine deacetylation was elevated in neutrophils infected with wild-type *C. jejuni* and $\Delta sliP$-p*sliP*; however, neutrophils infected with $\Delta sliP$ possessed intracellular environments that exhibited significantly reduced lysine deacetylase activity despite increased uptake of the $\Delta sliP$ strain into neutrophils (Figure 3.4A; Figure 3.12-appendix). Furthermore, $\Delta sliP$

Figure 3.4. *C. jejuni* neutrophil activation and NET extrusion is dependent SliP binding and deacetylating histone H3.

(A) Intracellular lysine deacetylation of neutrophils infected with *C. jejuni* and incubated under microaerobic conditions for up to three hours at 37°C. (B) Corresponding intracellular NAD^+ and NADH concentrations within *C. jejuni* infected neutrophils after three hours at 37°C. (C) Colocalization of SliP with histones during neutrophil infection. Uninfected (UI), wild-type (WT), Δ*sliP*, and *sliP* complement (Δ*sliP*-p*sliP*) infected neutrophils were stained for nuclei/DNA (blue), histone H3 (green), and SliP (red) and imaged two hours post-infection. Scale bars are 20 μm for zoomed out images and 5 μm for zoomed in images. Images presented are composites of 3D reconstructions of z-stacked images. (D) Histone H3 was immunoprecipitated from *C. jejuni* wild-type, Δ*sliP*, and *sliP* complement infected neutrophils. After three hours under microaerobic conditions, cells were fixed and then histone H3 was pulled down using an anti-histone H3 antibody. Presence of SliP within the histone H3 complex was determined through immunoblotting. Controls included media alone (-), wild-type bacteria alone (WT), Δ*sliP* bacteria alone (Δ*sliP*), and *sliP* complemented bacteria alone (Δ*sliP*-p*sliP*). (E) Immunoblot of SliP-dependent neutrophil histone H3 deacetylation after bacterial infection. (F) SliP-dependent *C. jejuni* induction of neutrophil activation through flow cytometry analysis of CD11b expression. (G) SliP-dependent *C. jejuni* induction of NETs through an extracellular DNA SYTOX assay and (H) PAD4 expression in neutrophils infected with *C. jejuni* expressing *sliP* for three hours under microaerobic conditions. (I) Inhibition of SliP-dependent neutrophil activation and (J) NET generation using sodium butyrate (SB) and trichostatin A (TSA). The data is representative of technical triplicates from a single donor. Multiple comparison testing was performed using ANOVA with Tukey's *post-hoc* test. *$p < .05$; **$p < .01$; ***$p < .001$; ****$p < .0001$

68
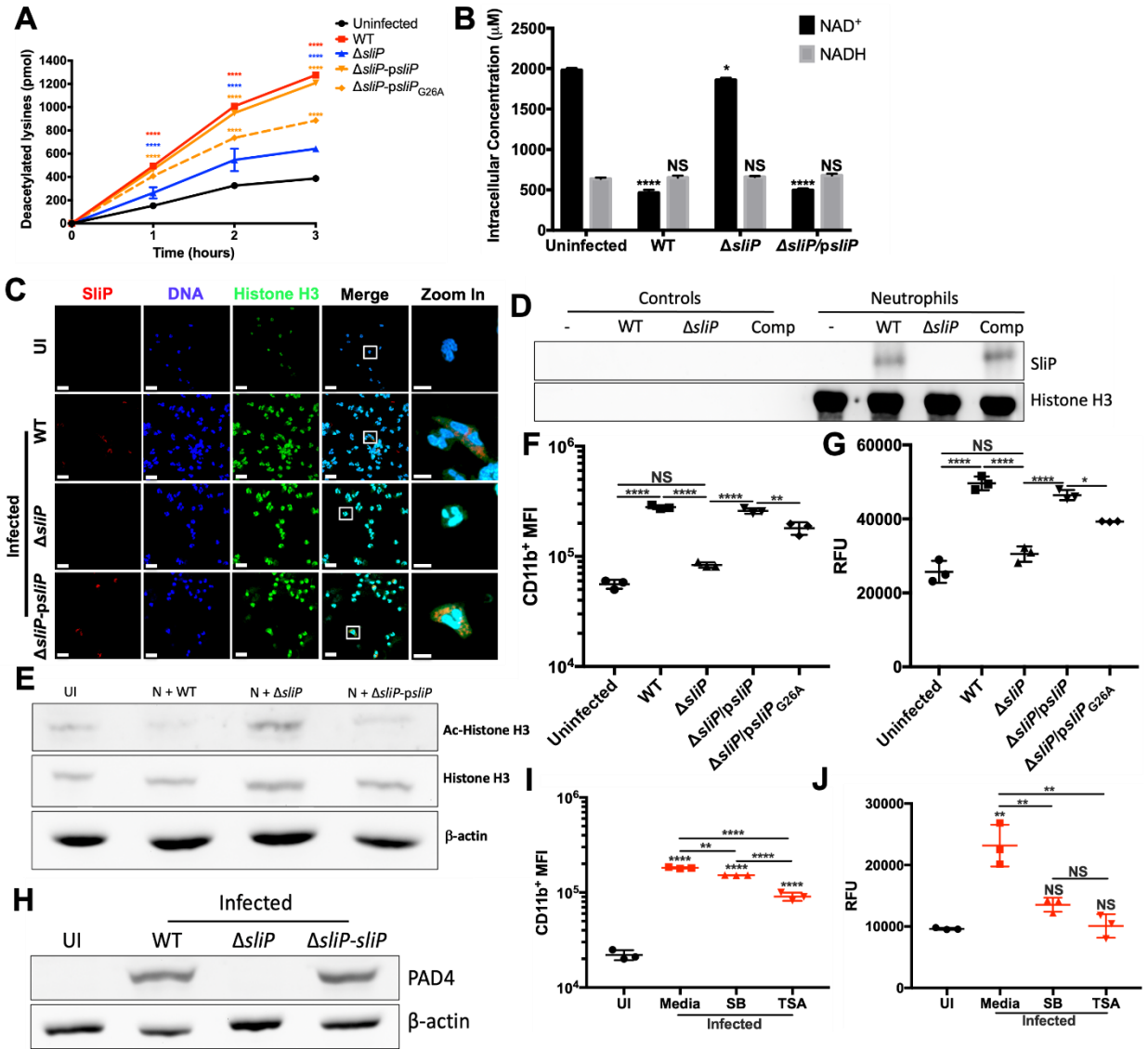
expressing the *sliP*G26A variant resulted in neutrophil infections with significantly less deacetylase activity was detected than when the strain possessed wild-type *sliP* (Figure 3.4A). To support these results, we also quantified NAD$^+$ levels in similarly infected neutrophils. As expected, infected neutrophils possessing higher deacetylase activity due to the presence of wild-type SliP also exhibited significantly lower NAD$^+$ levels (Figure 3.4B). In contrast, neutrophils infected with Δ*sliP,* or the mutant complemented with the G26A variant exhibited significantly higher levels of intracellular NAD$^+$ when compared to wild-type infected neutrophils (Figure 3.4B). No changes to NADH levels occurred under any condition tested (Figure 3.4B). These findings indicate SliP is translocated into neutrophils and the enzymatic activity of SliP promotes deacetylase activity in neutrophils, resulting in the deacetylation of numerous neutrophil proteins.

SliP translocates to the cytoplasm during infection of neutrophils by *C. jejuni* and directly associates with histone H3. Following intracellular translocation, we hypothesized a likely target of SliP-dependent deacetylation were neutrophil histones. This rationale was based on observations that histone H3 is a frequent target of post-translational regulation and histone H3 is involved in several neutrophil behaviors, including PAD4-dependent hypercitrullination of deacetylated histone H3 prior to NET production (231). In line with the CyaA reporter, we observed cytosolic SliP within wild-type and complemented infected neutrophils only (Figure 3.4C). Additionally, we observed colocalization of SliP with histone H3 under non-NETosing conditions. Interestingly, we observe this localization outside the nucleus of infected neutrophils, potentially due to the *de novo* synthesis of histone H3 within the cytoplasm in approximately 13% of neutrophils (Figure 3.4C; Figure 3.13-appendix).

Because we were able to demonstrate localization of SliP within the cytoplasm and histone H3 during infection, we next sought to determine whether SliP binds neutrophil histone H3 during *C. jejuni* infection and promotes its deacetylation. To accomplish this, we immunoprecipitated histone H3 from primary

human neutrophils that were formalin-fixed following infection with either wild-type *C. jejuni,* Δ*sliP*, or Δ*sliP*-p*sliP*. In our media and bacteria alone controls, we did not observe any histone H3 nor SliP, indicating the specificity of our immunoprecipitation. After purification infected neutrophils, we found SliP was present in protein complexes containing histone H3 during neutrophil infection with either wild-type *C. jejuni* or Δ*sliP*-p*sliP* (Figure 3.4D). As expected, we did not detect SliP associating with histone H3 in Δ*sliP*-infected neutrophils (Figure 3.4D). To eliminate non-specific protein crosslinking as a potential explanation, we probed for cytoplasmic lipocalin-2 (Lcn2) in those same immunoprecipitated histone H3 complexes but were unable to detect Lcn2 (Figure 3.14A-appendix). This suggests SliP association with histone H3 was not due to non-specific crosslinking of proteins to neutrophil histones. As we observed SliP association with histone H3, we next sought to investigate whether SliP affects the acetylation of histone H3 during infection. In neutrophils infected with wild-type *C. jejuni*, histone H3 acetylation was significantly reduced by 9.57-fold when compared to the amount of histone acetylation present in uninfected neutrophils. Similar results were also observed for neutrophils infected with the complemented mutant (8.45-fold reduction of uninfected neutrophil levels). In contrast, Δ*sliP*-infected neutrophils displayed histone H3 acetylation intensities similar to those of uninfected neutrophils (1.12-fold reduction of uninfected result) (Figure 3.4E; Figure 3.13C-appendix). To determine whether these deacetylation results may be due to the SliP-dependent recruitment of host sirtuins, we examined for the predominant human sirtuin within infectious disease, SIRT2, in immunoprecipitated histone H3 complexes. Human SIRT2 was not detected in these complexes, which is a notable difference from other intracellular pathogens where the bacteria promote the recruitment of host SIRT2 to induce histone deacetylation (Figure 3.14A-appendix). To eliminate other host-derived factors that post-translationally modify histones, we examined the expression of all known histone H3-targeting HDACs and HATs during infection with *C. jejuni* and found none of these genes were significantly impacted (Figure 3.14B-appendix). While

some HDACs and HATs appears up and down regulated, there were no differences in expression between WT and Δ*sliP* infected neutrophils. Regardless, there could be additional host HDACs performing deacetylation within the neutrophil, however, we hypothesize SliP plays a more significant role. Furthermore, we did not observe significant increases in SIRT2 abundance in infected neutrophils (Figure 3.14C). We therefore concluded SliP translocates to the cytoplasm of infected neutrophils and binds to histone H3 to directly deacetylate the protein rather than affecting the production or localization of a host-derived enzyme.

SliP promotes neutrophil activation and extracellular trap formation by *C. jejuni* through its deacetylase activity. As host HDACs and sirtuins are necessary for neutrophil activation, NET production, and intracellular infection by other bacteria, we hypothesized the SliP may impact neutrophil behaviors through the above effects through histone deacetylation. To assess this, we used wild-type *C. jejuni*, Δ*sliP*, Δ*sliP*-p*sliP*, and Δ*sliP*-p*sliP*$_{G26A}$ to infect primary human neutrophils. Using CD11b$^+$ as an output of neutrophil activation, wild-type infected neutrophils expressed 5-fold more CD11b protein as previously described (232), while Δ*sliP*-infected neutrophils exhibited only a 1.49-fold increase when compared to uninfected neutrophils (Figure 3.4F). Infection of neutrophils with Δ*sliP*-p*sliP* resulted in a 4.61-fold increase in the number of CD11b$^+$ neutrophils while infection with Δ*sliP*-p*sliP*$_{G26A}$ led to an intermediate 3.22-fold increase when compared to the uninfected neutrophils (Figure 3.4F). Furthermore, when NET production was evaluated, infection with wild-type *C. jejuni* led to a 1.93-fold increase in NET-associated DNA when compared to uninfected neutrophils using fluorescent staining of extracellular DNA (Figure 3,4G) (232). Similar to our activation results, Δ*sliP*-infected neutrophils exhibited a 1.19-fold increase in extracellular DNA when compared to uninfected neutrophils. When *sliP* was complemented, extracellular DNA increased by 1.81-fold while infection with *sliP*$_{G26A}$ variant-infected neutrophils exhibited a 1.53-fold increase in extracellular

DNA when compared to uninfected neutrophils (Figure 3.4G). To support these observations, we also examined for SliP-dependent accumulation of PAD4 in *C. jejuni*-infected human neutrophils and obtained fold-changes relative to uninfected neutrophils of 12.95, 1.03, and 12.23 for wild-type, Δ*sliP*, and Δ*sliP*-p*sliP*, respectively (Figure 3.4H). To determine whether other bacterial deacetylases may be involved in neutrophil activation and NETosis, we examined the above phenotypes in a transposon mutant of the predicted intracellular sirtuin, *cobB*. In contrast to Δ*sliP* responses, all neutrophil activities elicited by *cobB*::*hawkeye* resembled those of wild-type infected neutrophils (Figure 3.15-appendix). As the presence of *sliP* is necessary for neutrophil activation and NETosis in response to *C. jejuni* infection, we concluded SliP plays a crucial role in modulating neutrophil responses to *C. jejuni* through its deacetylation of host proteins.

To determine if chemical inhibition of SliP deacetylase activity reduces neutrophil activation and NETosis, we preincubated neutrophils with SB and TSA at the concentrations that inhibited SliP dependent deacetylation from above. When neutrophils were pre-incubated with these inhibitors and then infected with wild-type *C. jejuni*, we observed a significant 1.2 and 2.0-fold reduction in CD11b$^+$ neutrophil populations when SB and TSA were added, respectively (Figure 3.4I). This reduced activation also resulted in a significant decrease in NETosis, with SB and TSA treatment leading to a 1.71-fold reduction and a 2.30-fold reduction in extracellular DNA, respectively (Figure 3.4J). Supporting this result, PAD4 levels were also significantly reduced in SB and TSA treated neutrophils during infection with wild-type *C. jejuni* (Figure 3.16-appendix). Furthermore, when SB and TSA treated neutrophils were infected with wild-type *C. jejuni*, histone H3 acetylation significantly increased (Figure 3.16-appendix). These results indicate SliP promotes neutrophil activation and NET induction through deacetylation of histone H3.

SliP promotes inflammation and gastrointestinal disease during murine campylobacteriosis. To determine whether these SliP-dependent impacts on

neutrophil activities affect host inflammation and gastrointestinal tissue damage during infection, we orally infected IL-10$^{-/-}$ mice with either wild-type *C. jejuni* or Δ*sliP* and examined for systemic and tissue-level impacts on the host. Prior to orally infecting mice, we determined murine neutrophils behave similarly to human neutrophils when infected with *C. jejuni*, including activating similar numbers of neutrophils and inducing NETosis in those neutrophil populations (Figure 3.17-appendix). When IL-10$^{-/-}$ mice were orally infected with wild-type *C. jejuni*, they exhibited significantly reduced percent weight change at days 7, 9, and 10 post-infection when compared to uninfected mice (Figure 3.5A). In contrast, Δ*sliP*-infected mice gained weight similar to uninfected mice, which led to significantly higher weights when compared to wild-type infected mice at days 7 through 10 post-infection (Figure 3.5A). Importantly, Δ*sliP* was able to colonize mice, with fecal, colonic, and cecal loads similar to wild-type-infected mice (Figure 3.5B, C; Figure 3.18A,B-appendix). In addition, we examined for bacterial dissemination from the gastrointestinal tract by determining the bacterial burden within the spleens of infected mice, finding Δ*sliP*-infected mice harbored 3.06-fold more bacteria than wild-type infected mice (Figure 3.5D). These results indicate SliP does not affect colonization of susceptible hosts and instead suggests neutrophil activation and NET induction could aid in restricting *C. jejuni* to the colon.

To determine whether SliP promotes inflammation and disease during infection, we first quantified the levels of several proinflammatory chemokines and cytokines within the serum of wild-type and Δ*sliP*-infected IL-10$^{-/-}$ mice, including IL-1β, IL-6, IFN-γ, KC, and TNF-α. For IL-1β concentrations, uninfected mice were observed at 83.86 ± 60.63 pg/mL, while wild-type and Δ*sliP*-infected mice were at 332 ± 138 pg/mL and 122.3 ± 41.81 pg/mL, respectively (Figure 3.5E). Finally, for IL-6 concentrations, uninfected mice were observed at 8.617 ± 1.535 pg/mL, while wild-type and Δ*sliP*-infected mice were at 26.33 ± 14 pg/mL and the limit of detection, respectively (Figure 3.5E). Similarly, the concentration of IFN-γ in uninfected mice was determined to be 16.95 ± 13.33 pg/mL, with wild-type and Δ*sliP*-infected mice exhibiting concentrations at 127.3 ± 70.49 pg/mL and 23.92 ±

Figure 3.5. SliP promotes inflammation within the IL-10$^{-/-}$ C57BL/6 mouse model of campylobacteriosis.

(A) Percent body weight changes of mice uninfected or infected with wild-type (red) or Δ*sliP* (blue) *C. jejuni* over the ten-day infection study. Percent body weight changes were normalized to the weights of each mouse before savage treatment. (B) Fecal viable CFUs of each mouse over the ten-day infection study. Feces were collected each day and plated on *Campylobacter* specific media and incubated for two days under microaerobic conditions. (C) Viable CFUs from the colon and (D) spleen in *C. jejuni* infected mice ten days post-infection. (E) Serum cytokine expression levels for each mouse per treatment group. Levels of cytokines IFN-γ, KC, IL-1β, IL-6, and TNF-α were analyzed through flow cytometry-based beads and concentrations were determined through a standard curve for each protein. Multiple comparison testing was performed using ANOVA with Tukey's *post-hoc* test. (F) H&E-stained murine colons for each representative treatment group. Scale bars are 100 μm for zoomed out and in images for each treatment mouse group. (G) Inflammation scoring from the H&E-stained colons per colon section. Analysis of inflammation scoring was performed using a nonparametric Mann-Whitney U test. Two rounds of mouse infections were performed on separate days, with five mice per condition each time. *p < .05; **p < .01; ***p < .001; ****p < .0001
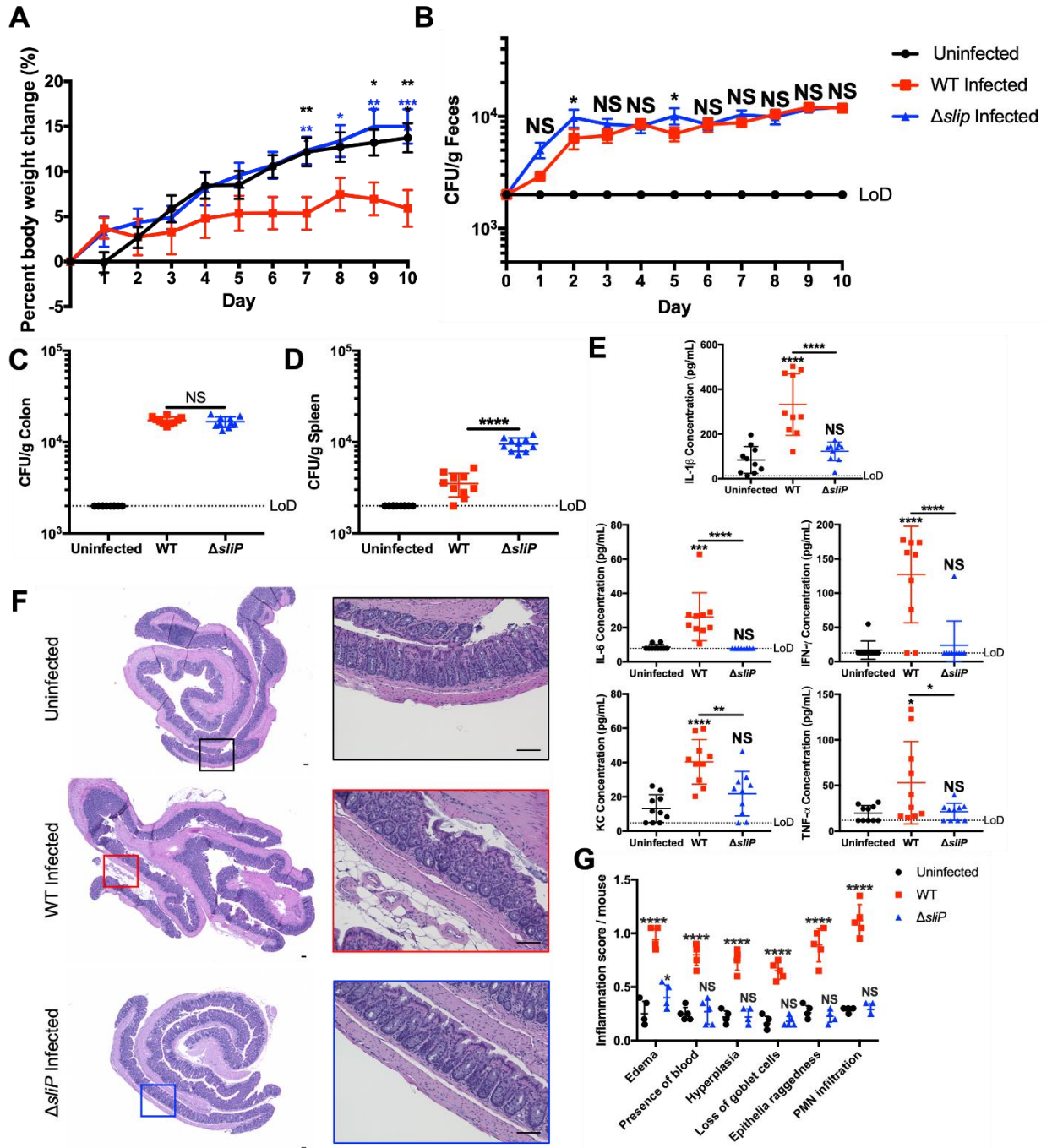
35.55 pg/mL, respectively (Figure 3.5E). In uninfected mice, the concentration of KC was 13.13 ± 8.041 pg/mL, while concentrations in wild-type and Δ*sliP*-infected mice were 40.35 ± 12.99 pg/mL and 21.85 ± 12.99 pg/mL, respectively (Figure 3.5E). For TNF-α, uninfected mice concentrations were observed at 19.66 ± 8.53 pg/mL, while wild-type and Δ*sliP*-infected mice were at 53.13 ± 45.17 pg/mL and 21.31 ± 9.36 pg/mL, respectively (Figure 3.5E). In addition to promoting an immune response, we analyzed and scored colon pathology from wild-type and Δ*sliP*-infected mice, including the development of edema, blood in the tissue, epithelial raggedness, and hyperplasia (175). Importantly, when mice were infected with the Δ*sliP*, histopathological scores for the previously mentioned features were not significantly different from uninfected mice, aside from edema (Figure 3.5F, G; Figure 3.18C-appendix). In support of this, we observed significant increases in neutrophil abundance (CD11b$^+$Ly6G$^+$) within wild-type infected mice, but lowered concentrations in uninfected and Δ*sliP*-infected mice (Figure 3.18D-appendix). These results suggest despite colonizing mice at levels similar to wild-type and disseminating to extraintestinal sites, the absence of SliP leaves the bacterium less immunogenic and able to cause disease in a susceptible host.

SliP associates with and promotes histone H3 deacetylation during murine infection. To connect the SliP-dependent activities we observed in primary human neutrophils to the pathological effects we observed in mice, we sought to demonstrate SliP association with histone H3 during infection. To initially examine this, colon sections from the above cohorts were analyzed by immunofluorescence microscopy. As expected, *C. jejuni* clusters were detected within the colons of wild-type and Δ*sliP* infected mice, but not within uninfected mice (Figure 3.6A). When histone H3 was examined within these clusters, increased histone acetylation co-localized in Δ*sliP* infected mice, however, this was absent in wild-type infected mice where histone acetylation was markedly reduced (Figure 3.6A). Further, myeloperoxidase (MPO), a leukocyte-derived antimicrobial protein, was also more abundant in wild-type-infected mice than uninfected and Δ*sliP*-infected mice

Figure 3.6. *In vivo* detection of SliP binding to and deacetylating immune cell histone H3.

(A) *In vivo* fluorescent microscopy to determine the abundance of DNA/nuclei (blue), *C. jejuni* (green), acetylated histone H3 (red), and myeloperoxidase (MPO, purple) within uninfected, wild-type, and Δ*sliP* infected mouse colons. For each tissue section, the exposure for each channel remained constant. Images presented are individual channels and composites of z-stacked images. Scale bars are 100 µm for zoomed out images and 10 µm for zoomed in WT (red) and Δ*sliP* (blue) images. (B) Histone H3 co-immunoprecipitation from CD45$^+$ immune cells purified from uninfected, wild-type, and Δ*sliP* infected mouse colons. Presence of SliP and the acetylation of histone H3 within the histone H3 complex was determined through immunoblotting. (C) Densitometry analysis of SliP abundance normalized to the abundance of histone H3 precipitated. (D) Densitometry analysis of histone H3 acetylation normalized to the abundance of histone H3 precipitated. Two rounds of mouse infections were performed on separate days, with five mice per condition each time. Multiple comparison testing was performed using ANOVA with Tukey's *post-hoc* test. *$p < .05$; **$p < .01$; ***$p < .001$; ****$p < .0001$

A

	DNA/nuclei	*C. jejuni*	Ac-histone H3	MPO	Merged
Uninfected					
WT Infected					
Δ*sliP* Infected					

B
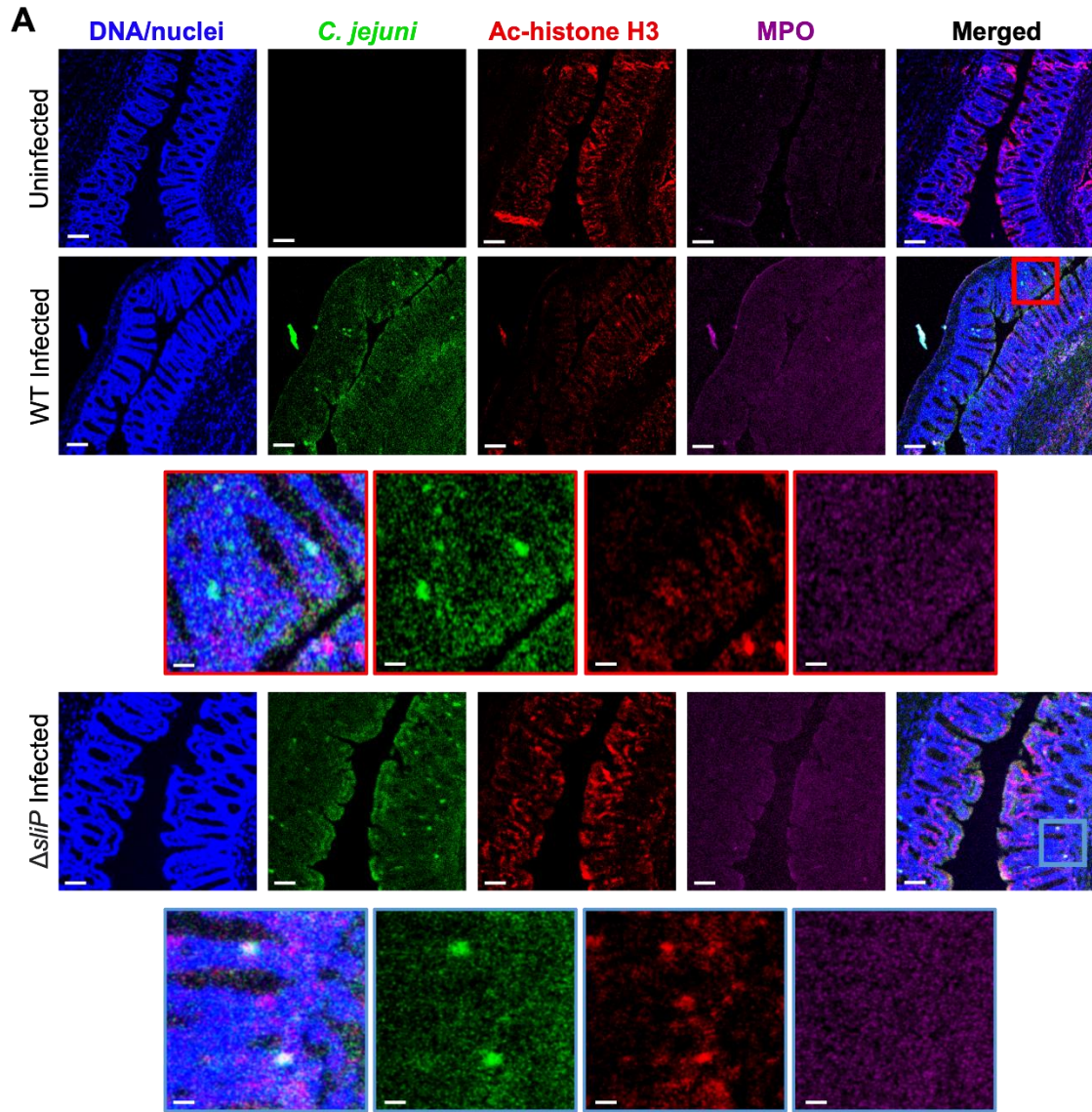
	UI	Infected WT	Δ*sliP*	
				SliP
				Ac-histone H3
				Histone H3

C SliP Abundance (Normalized to histone H3)

D Acetylated histone H3 Abundance (Normalized to histone H3)
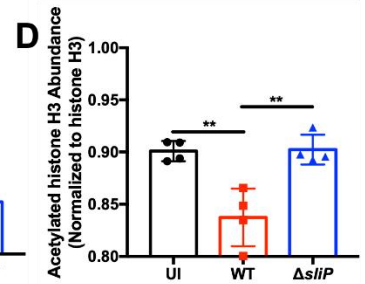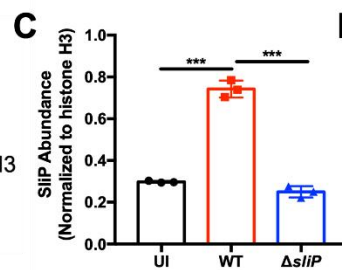
(Figure 3.6A). To more specifically address whether SliP directly impacts the acetylation status of leukocyte histones during infection, colons from uninfected, wild-type, and Δ*sliP*-infected mice were harvested and CD45$^+$ immune cells were purified. After purification, cellular proteins were cross-linked and histone H3 was immunoprecipitated as above. After purifying histone H3 complexes, we observed SliP was present in histone H3 complexes in only wild-type infected mice (Figure 3.6B, C). Furthermore, when the acetylation status of these complexes was examined, histone H3 acetylation was found to be reduced in wild-type-infected mice when compared to uninfected and Δ*sliP*-infected mice, both of which exhibited similar levels of acetylation (Figure 3.6D). As such, we have concluded SliP binds to histone H3 in murine immune cells and the resulting activation of those leukocytes is in part responsible for gastrointestinal disease. In the future, we will expand on these experiments to examine for SliP-dependent impacts to the acetylome of other cell types, including colonocytes and macrophages, and whether chemical inhibition of this activity reduces disease severity.

SliP deacetylates both neutrophil and *C. jejuni* proteins. As we observed in the present study that SliP appears to bind to and deacetylate neutrophil histone H3, we wanted to further understand which proteins SliP could be additionally targeting. To achieve this, we utilized mass spectrometry for differential acetylation patterns between wild-type and Δ*sliP*-infected neutrophils along with wild-type and Δ*sliP* bacteria alone. Additionally, we could then understand which lysine residues on the proteins SliP deacetylates. In this, we determined SliP presence leads to the deacetylation of numerous neutrophil proteins, namely annexin A1, bactericidal/permeability-increasing protein, beta actin, bromodomain-containing protein 8, cytochrome p450, enolase 1, eukaryotic translation elongation factor 1 alpha, glyceraldehyde 3-phosphate dehydrogenase, HIRA, histone H1, histone H2B, histone H3, histone H4, lactoferrin, myeloperoxidase, pyruvate kinase, serum albumin, S100A8, S100A9, S100A11, and S100A12. In agreement with our previous data, we observed significant enrichment of acetylation in Δ*sliP*-infected

neutrophil histone H3, specifically on lysine (K) 9 and 79 (Figure 3.7A,B). Furthermore, when gene ontology (GO) for biological enrichment is performed on the proteins deacetylated in the presence of *sliP*, numerous categories stood out, including humoral immune response, chromatin organization, defense response to bacterium, and glycolytic process (Figure 3.7C). When cellular enrichment was performed on differentially acetylated proteins, the two categories with the most enrichment were extracellular exosomes and nucleosome (Figure 3.7D). Finally, when molecular enrichment was performed, structural constituent of chromatin, calcium-dependent protein binding, RAGE receptor binding, TLR4 binding, and nucleosomal DNA binding were all enriched (Figure 3.7E). Additionally, the presence of *sliP* appeared to increase lysine acetylation in numerous *C. jejuni* proteins, including ATP synthase subunit alpha, class I SAM-dependent methyltransferase, delta-aminolevulinic acid dehydratase, elongation factor Tu, ferritin, FtsY, GroEL, Methyl-accepting transducer domain-containing protein, PAS domain-containing protein, Phage integrase, SPOR domain-containing protein, succinate--CoA ligase subunit beta, YajC, and 4-hydroxy-tetrahydrodipicolinate synthase. As such, while we have shown SliP is translocated into host cells, it is capable of deacetylating bacterial targets as well.

Discussion

Campylobacter species are the leading cause of bacterial-derived gastroenteritis worldwide and have broad impacts on human health which range from acute intestinal inflammation to pediatric stunting (233). Despite these effects, knowledge relating to how infection with *Campylobacter* species results in these outcomes is limited. For example, because whole-genome analysis of *C. jejuni* isolates suggests the pathogen lacks many of the prototypical secretion systems and virulence factors often associated with pathogenesis, gastrointestinal disease is hypothesized to be due to dysregulated activation of the host immune response through a factor or process unique to *C. jejuni* (234). Since little work has been done to understand the host response to *C. jejuni* and its consequence on
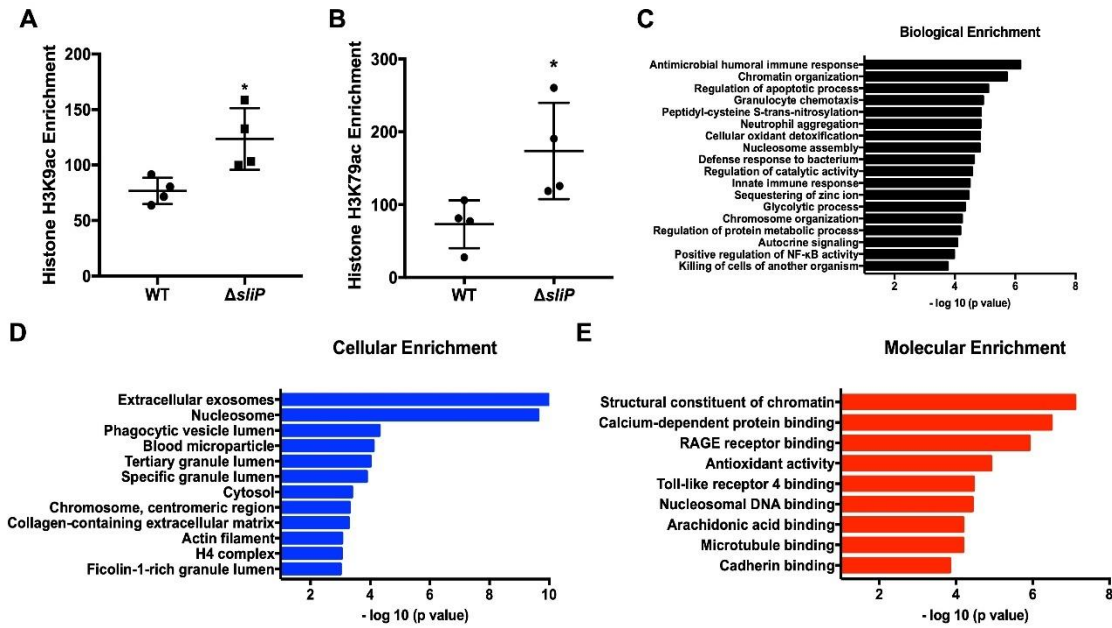
Figure 3.7. SliP promotes the deacetylation of numerous host proteins.

(A) Histone H3 lysine (K)9 acetylation enrichment in wild-type (WT) and Δ*sliP C. jejuni* infected neutrophils. (B) Histone H3 K79 acetylation enrichment in wild-type (WT) and Δ*sliP C. jejuni* infected neutrophils. Individual data points represent averaged technical triplicates from biological replicates. (C) Gene ontology (GO) analysis for biological enrichment of proteins significantly deacetylated in the presence of *sliP*. (D) GO analysis for cellular enrichment of proteins significantly deacetylated in the presence of *sliP*. (D) GO analysis for molecular enrichment of proteins significantly deacetylated in the presence of *sliP*. Multiple comparison testing was performed using ANOVA with Tukey's *post-hoc* test. *$p < .05$

gastrointestinal health, our group previously examined and observed neutrophils are recruited to the colon of infected animals and that predominantly neutrophil-derived proteins are elevated in the feces of *C. jejuni*-infected patients. Because neutrophils play a key role in the development of several inflammatory diseases, some of which are related to the post-infectious disorders which potentially occur following *C. jejuni* infection, we worked to further characterize the neutrophil response to *C. jejuni*. For example, we recently demonstrated that *C. jejuni* is a potent activator of human neutrophils and stimulation leads to the production of NETs. Since neutrophil activities, including NETosis, can damage adjacent colonocytes and has been associated with numerous inflammatory disorders, we sought to identify unique factors of *C. jejuni* which promote neutrophil activation and NET extrusion.

In this work, we identified a unique *C. jejuni* effector which functions as a bacterial sirtuin and is released into neutrophils during intracellular infection. This protein, which we call SliP, is responsible for full neutrophil activation and NET production in response to *C. jejuni* infection. While several bacterial pathogens have been found to hijack host sirtuins to create an intracellular environment that promotes infection, an example of a bacterial-derived sirtuin being translocated into host cells to directly alter host responses has yet to be described. In addition to the enzymatic activity and proinflammatory functions of SliP, the gene is more frequently present in the genomes of human clinical isolates of *C. jejuni*. While the evolutionary rationale for this incidence is unknown, one explanation is that the role of SliP in neutrophil activation would lead strains which possess SliP to be more inflammatory, which would result in a detection bias since patients with severe disease are more likely to seek medical care where those strains are more likely to be isolated and sequenced. While about half of our sequenced clinical isolates lack SliP, we hypothesize this could be due to the bacterium's ability to colonize, even when it lacks *sliP*, however, these infections may not be as inflammatory. Therefore, we hypothesize SliP drives hyperinflammation within infected hosts, however, it is not necessary for host colonization, therefore, still

resulting in infection. Beyond its role in *C. jejuni,* we found other bacterial pathogens encode DUF4917 family proteins; however, they have yet to be investigated. For example, the human pathogens *Legionella pneumophila* and *Yersinia enterocolitica* encode DUF4917 proteins with shared amino acid homology to *C. jejuni* SliP in addition to the multitude of other effector proteins these two pathogens possess. This observation suggests infection or disease caused by these pathogens may be similarly facilitated by the production of a bacterial-derived sirtuin.

Because we determined SliP acts as a canonical sirtuin *in vitro* and *in vivo*, we examined whether SliP inhibition could be achieved using the known deacetylase inhibitors, sodium butyrate and trichostatin A. Interestingly, sodium butyrate has been found to abrogate colonization of numerous gastrointestinal pathogens and reduce host inflammation, including those caused by *Salmonella* Typhimurium (235,236), *Escherichia coli* (237), *Citrobacter rodentium* (238,239), and *Staphylococcus aureus* (240,241). While the underlying molecular mechanism of this attenuation remains unclear, it may occur through inhibition of host-derived histone deacetylases (HDACs), which has been shown to have anti-inflammatory effects in other disorders, including inflammatory bowel disease. In addition, our results suggest sodium butyrate may reduce inflammation during infection by inhibiting the activities of bacterial-derived sirtuins that would otherwise alter the intracellular environment of the host to a more proinflammatory state.

Prior to identifying targets of SliP, we first examined whether SliP is secreted both *in vitro* and *in vivo*. As we found lysine deacetylation and NAD^+ levels during *C. jejuni* infection of neutrophils were SliP dependent and that SliP is actively secreted into host cells, we hypothesized SliP targets host proteins to promote disease. Because HDAC upregulation and the resulting histone deacetylation promote NETosis and host inflammation, we initially focused on SliP-dependent impacts to the acetylation status of host histones. As predicted, we found SliP colocalizes and binds to histone H3 during neutrophil infection and that the presence of SliP leads to decreased histone acetylation. As we observed

colocalization of SliP and histone H3 occurring outside the neutrophil nucleus, we hypothesize SliP could be binding to histone H3 synthesized within the cytoplasm before shuttling into the nucleus for chromatin binding. Interestingly, it has been previously demonstrated that other effectors in *C. jejuni* (Cia proteins) are injected into the host cells through the flagellum after binding to host cells mediated by CadF, CapA, and FlpA (158). Due to SliP's presence in the host cell cytosol, we hypothesize after secretion through the flagellum, it diffuses either from the phagosome or *Campylobacter* containing vacuole (CCV) into the host cytosol. We further demonstrated *C. jejuni*-induced neutrophil activation and NETosis is SliP-dependent, which suggests direct bacterial-mediated modification of host histones affect inflammatory responses and cell death. While we showed histone H3 becomes deacetylated in a SliP-dependent manner, other PTMs could occur after deacetylation, including lysine methylation, ubiquitination, and SUMOylation (242–245). Further supporting the role of SliP-dependent deacetylation in neutrophil activation, we found inhibition of SliP using the HDAC inhibitors discussed above reduced neutrophil activation and NET formation during *C. jejuni* infection of neutrophils. While it has been shown that *C. jejuni* can sense sodium butyrate through sensor phosphatase activity (13), no research has been conducted on the ability of butyrate to influence host responses or pathogenesis during campylobacteriosis. Supporting the hypothesis that butyrate might reduce disease severity by affecting the host during infection, previous work found butyrate inhibits proinflammatory responses from neutrophils through downregulation of numerous antimicrobial proteins during mucosal inflammation models (246). Similarly, TSA has been shown to inhibit neutrophil proinflammatory responses; however, like butyrate, no research has been conducted to investigate the ability of TSA to reduce inflammation or disease during *C. jejuni* infection. As a result, the *C. jejuni* field is well-positioned to investigate the role of these inhibitors on campylobacteriosis disease severity and whether their abundance affects either bacterial and/or host-derived factors and processes.

85

Despite the ability of the *sliP* mutant to colonize and be shed in the feces similar to mice infected with wild-type bacteria, the bacterial burden within the spleen of *sliP* mutant-infected mice was significantly increased. We hypothesize this observation is similar to what was observed in a previous study where NET production was shown to be involved in limiting bacterial dissemination to the spleen during *Citrobacter rodentium* infection of mice (247). Furthermore, we observed *sliP* mutant infected mice have reduced levels of proinflammatory cytokines IL-1β, IL-6, IFN-γ, KC, and TNF-α compared to wild-type infected mice. We postulate either i) proinflammatory cytokines could be released by activated neutrophils during infection (248,249), ii) tissue resident macrophages could detect citrullinated histone H3, resulting in upregulation of proinflammatory cytokines (136,140,250), or iii) influx of other leukocytes could be responsible for the increases in proinflammatory cytokines (251,252). Finally, we found murine inflammation and tissue pathology is dependent on the presence of SliP in *C. jejuni*. In this we observed SliP binding to histone H3 *in vivo* and acetylation status decreases in the presence of SliP. While FACS sorting neutrophils in vivo would allow this to be more clearly visualized, there are numerous technical issues with FACS sorting neutrophils (253,254). As neutrophil activation and NETosis has been implicated in numerous inflammatory diseases, whether autoimmune or microbially driven, we hypothesize SliP-dependent neutrophil responses drive campylobacteriosis disease manifestation.

Finally, within this chapter, we were able to utilize mass spectrometry to determine the lysine residues deacetylated on histone H3 by SliP, along with other host and bacterial targets of SliP for deacetylation. Interestingly, the two lysines on histone H3 were lysines 9 and 79, are both on the tails of histone H3, being able to bind DNA wrapped around the histone octamer, linker DNA, and acidic patches of neighboring nucleosomes (255). Furthermore, when other host proteins were analyzed, many of the enrichments for biological, cellular, and molecular functions belonged to structure and organization of the host chromatin, highlighting SliP's ability to alter the host chromatin structure. Within the GO biological enrichment,

additional categories which had significance was antimicrobial humoral immune response, defense response to bacterium, innate immune response, and glycolytic process. As glycolytic processes lead to antimicrobial functionality of neutrophils, it would be interesting to investigate the potential immune evasion strategies of SliP by altering the neutrophil metabolism and production of antimicrobial proteins (256). Additionally in the GO cellular enrichment, along with nucleosome enrichment, we additionally saw significant enrichment for deacetylated proteins associated with extracellular exosomes. As extracellular exosomes have been implicated in regulating inflammation within the host and autoimmune onset, this could be an interesting research avenue to investigate within the *Campylobacter* field (257,258). Lastly, when we investigated molecular enrichment, while we again saw categories associated with chromatin, we additionally observed significant enrichment of calcium-dependent protein binding, RAGE receptor binding, antioxidant activity, and TLR4 binding. Interestingly, calcium-dependent signaling plays a significant role in activation of neutrophils, along with RAGE and TLR4 signaling. While we observe neutrophil activation in a *sliP* dependent manner, deacetylation of these host proteins could underly the molecular mechanism for this inflammatory phenotype (259–261).

With the characterization of a new class of bacterial effectors, sirtuins, the role of deacetylation on the host-microbe paradigm can be further understood. While microbial short-chain fatty acids have been implicated to abrogate bacterial-mediated gastroenteritis, future research can be focused on the ability of these molecules to mitigate clinical signs of campylobacteriosis. By further understanding the unique mechanisms *C. jejuni* employs to promote infection and inflammation, therapeutics can be developed for treating acute and chronic outcomes of infection.

Materials and Methods

Abundance of SliP within environmental and clinical isolates. Environmental and clinical isolates of *C. jejuni* were isolated from a previous study (222). Whole genomes were uploaded to Kbase, and their genomes were annotated to the 81-176 wild-type genome. After the genomes were annotated, amino acid homology was performed, with the minimum homology set to 75%. For statistical analysis, a two-sided Chi-square test was performed.

Phylogenetic analysis of DUF4917 family proteins. To understand the homology of SliP with other members of the DUF4917 family, an amino acid BLAST was performed, excluding *Campylobacter* spp. DUF4917 proteins. From this BLAST search, amino acids were pulled from the top 14 percent homology organisms. The annotated amino acids were then aligned using multiple sequence alignment using T-Coffee (EMBL-EFI) with a ClustalW output. From this, a neighbor-joining tree without distance correction cladogram was produced.

Bacterial cultures and culture conditions. *Campylobacter jejuni* 81-176 strain DRH212 was stored at −80°C in MH broth supplemented with 20% glycerol. In this study, non-polar deletions and plasmid-borne strains of *sliP* were constructed in wild-type *C. jejuni* DRH212 as previously described (262). All strains were routinely grown for 24 hours on selective media (10% sheep's blood, 40 µg/ml cefoperazone, 100 µg/ml cycloheximide, 10 µg/ml TMP and 100 µg/ml vancomycin) before passing onto Mueller-Hinton agar containing 10% sheep's blood and 10 ug/ml trimethoprim (TMP) at 37°C under microaerobic conditions (85% N2, 10% CO2 and 5% O2) for an additional 24 hours. *E. coli* expression strain C3013 containing pQE30-*sliP* and pQE-30-*sliP*$_{G26A}$ were constructed as previously described (263). *E. coli* strains were stored in Luria-Bertani (LB) broth supplemented with 20% glycerol at −80°C and grown shaking at 37°C in LB broth supplemented with ampicillin for purification as described below.

Isolation of primary human neutrophils. Neutrophils were isolated as previously described (232,264). Briefly, 10 ml of blood was drawn from healthy donors into heparinized Vacutainer tubes and mixed 1:1 with sterile 1× PBS (approval UTK IRB-18-04604-XP) (172). After mixing, 10 ml of lymphocyte separation medium was underlaid. Following centrifugation at 1,400 rpm for 30 min, the top layers were aspirated off, leaving the red blood cell and neutrophil pellet. Pellets were resuspended in 20 ml Hanks' balanced salt solution and 20 ml 3% dextran in 0.9% NaCl. After incubating at room temperature for 20 min, the upper layer was transferred to a new tube. Following centrifugation at 400g for 5 min and aspiration of the supernatant, the pellet was washed with 20 ml ice-cold 0.2% NaCl and 20 ml ice-cold 1.6% NaCl two times. Following the final aspiration, the neutrophil pellet was resuspended in 10 ml RPMI 1640. Neutrophil viability and counts were performed through Trypan blue stain.

Protein induction and native purification of SliP. Protein induction and purification was performed as previously described (227,263). Briefly, *E. coli* strains C3013 encoding SliP, SliP$_{G26A}$, or empty pQE-30 vector were grown overnight in LB broth containing 100 µg/ml ampicillin at 37°C shaking. Cultures were then back-diluted by adding 1 mL overnight culture in 100 mL LB broth containing 100 µg/ml ampicillin. Culture was grown at 37°C shaking for two hours before spiking in 100 µM isopropyl-β-d-thiogalactopyranoside (IPTG) to induce protein expression. Cultures were allowed to incubate for an additional two hours at 37°C shaking. After incubation, cells were pelleted at 2,147 rcf for 10 min. After centrifugation, the pellets were resuspended in lysis buffer (50 mM NaH$_2$PO$_4$, 300 mM NaCl, 10 mM imidazole, pH 8.0) before sonication on ice (6 rounds of 15 s each at 45 A). Cell lysates were then pelleted at 2,147 rcf for 10 min before incubating the resultant supernatant with washed Ni-nitrilotriacetic acid (Ni-NTA) for one hour at 4°C rocking. After the incubation, the SliP resin was packed in a 20-ml chromatography column before it was washed three times with 4 ml wash buffer (50 mM NaH$_2$PO$_4$, 300 mM NaCl, 20 mM imidazole, pH 8.0) and eluted in

three 750-µl fractions of elution buffer (50 mM NaH_2PO_4, 300 mM NaCl, 250 mM imidazole, pH 8.0). Each wash and elution fraction were diluted 1:1 with a Laemmli buffer containing β-mercaptoethanol and boiled for 10 minutes. Ten microliters of lysate samples were loaded onto a 12.5% SDS-PAGE gel and run for 1 hour at 150 V at room temperature and stained with Coomassie to ensure protein purification (37 kDa). Elution fractions were then pooled and dialyzed using a dialysis buffer (200mM NaCl, 2mM DTT, and 20mM HEPES buffer (pH 7.5) three times at 4°C spinning. After dialysis, protein was collected from the dialysis cassette using a syringe and stored at 4°C until future use.

To generate C terminally 6x His tagged SliP, a 6x His tag was incorporated onto the primers to amplify *sliP*. The amplified *sliP* was put into pGemT plasmid and then sequenced through Sanger sequencing. Once sequenced, pGemT-*sliP* was electroporated into C3013. C terminal 6x His tagged SliP was purified as previously described.

Site-directed mutagenesis to create *sliP*G26A. To create *sliP*G26A for complementation and protein purification, the SNP was generated using primer-derived SNP. To do this, the SNP was generated in the forward primer and then used stitching overlapping extensions to generate the full-length sliP encoding the G26A mutation. The mutation was confirmed through PCR and Sanger sequencing technology.

Detection of *in vitro* and *in vivo* lysine deacetylation. Quantification of *in vitro* and *in vivo* lysine deacetylation was performed using the BioVision InSitu HDAC Activity Fluorometric Assay kit (Cat. No. K339-100). For *in vitro* quantification, 10 ng purified SliP was incubated in the presence of HDAC substrate (acetylated lysine side chain) with 5 mM NAD^+ and 20 µM $ZnCl_2$ at 37°C. For *in vivo* quantification, 10^5 neutrophils were incubated with 10^6 *C. jejuni* to a final volume of 150 µl containing the HDAC substrate and the cells were infected as previously described[7]. After the allotted amount of time, developer and HDAC assay buffer

was added to 100 µl reaction mixture (with the other 50 µl being used for the NAD^+ hydrolysis assay described below) and was incubated for 30 minutes at 37°C. After incubation, fluorescence was read using a BioTek Synergy microplate reader at 368/442 nm wavelength. A deacetylated substrate standard curve was additionally run and plotted with fluorescence. Once plotted, the amount of deacetylated lysine residues were calculated.

Quantification of NAD^+ and NADH within neutrophils and supernatants. The abundance of NAD+ and NADH *in vitro* and *in vivo* were performed using the Promega NAD/NADH-Glo^{TM} Assay. All reagents used for this assay were brought to room temperature before use. For the *in vitro* NAD^+ hydrolysis assay, 5 mM of pure NAD^+ was added to the reaction as described above in the lysine deacetylation assay. After deacetylation, the NAD/NADH-Glo^{TM} detection reagent was made as described by the manufacturer. In a white welled plate, 50 µl from the lysine deacetylation reaction mixture was combined with 50 µl detection reagent. The plate was incubated at 37°C for 30 minutes while shaking. After incubation, luminescence was read using a BioTek Synergy microplate reader. For quantification of intracellular NAD^+ and NADH, neutrophils were infected with their respective strain for the allotted amount of time under microaerobic conditions at 37°C to a final volume of 50 µl. Neutrophils were then lysed by adding 50 µl RPMI 1640 containing 1% dodecyltrimethylammonium bromide (DTAB). To measure NAD^+, 50 µl of the reaction mixture was allotted and mixed with 25 µl 0.4N hydrochloric acid and incubated at 60°C for 15 minutes. After the incubation, the samples were cooled at room temperature for 10 minutes. Then, 25 µl Trizma base was added to the reaction mixture. Finally, 100 µl of detection reagent was added, incubated as previously described and luminescence was read as previously described. For NADH quantification, 50 µl of the cell lysis solution was incubated at 60°C for 15 minutes. The samples were cooled at room temperature for 10 minutes. Then, 50 µl HCl/Trizma base solution was added to the reaction mixture. Finally, 100 µl of detection reagent was added, incubated as previously described

and luminescence was read as previously described. Along with each experiment, a known concentration standard curve for NAD^{+} and NADH were constructed to calculate the concentration of each small molecule.

SliP-CyaA neutrophil translocation assay. To determine if SliP is translocated into neutrophils, adenylate cyclase translational fusions were produced at the C terminus of *sliP*, *heuR*, and *ciaB* (265). For each infection, 10^6 neutrophils were incubated with wild-type or Δ*flgE C. jejuni* strains harboring pECO102 encoding *sliP-cyaA*, *heuR-cyaA*, or *ciaB-cyaA* at an MOI of 10 for three hours under microaerobic conditions at 37°C. Additionally, actin polymerization was chemically blocked with 2 μM cytochalasin D (CD) for one hour before bacterial infection under microaerobic conditions at 37°C. Cells were lysed with 0.1M HCl and the direct ELISA was performed as according to the manufacturer protocol (Enzo). All experiments were additionally done with wild-type and Δ*flgE C. jejuni* and CD incubated neutrophils without the addition of *cyaA*. These values can be taken out of the respective treatment groups.

Analysis of *C. jejuni* NET induction by flow cytometry. Flow cytometry detection of *C. jejuni* induced NETs was performed as previously described (232,264). Briefly, *C. jejuni* strains were resuspended in RPMI 1640 and incubated with neutrophils for 3 hours under microaerophilic conditions at an equal multiplicity of infection (MOI) of 50:1 (bacteria:neutrophil). Following incubation, these reactions were aliquoted into wells of a 96-well plate and centrifuged at 400 x *g*. Pelleted cells were washed three times with sterile 1x PBS cells before incubation with Live/Dead Near-IR (NIR) stain for 25 min at room temperature. After incubation, cells were blocked with 1% goat serum for 10 min, then incubated with CD11b and MPO antibodies for 30 min (173). Cells were subsequently fixed in the fixation buffer for 10 min at room temperature and stored at 4°C until flow cytometry analysis. Samples were analyzed using an LSR II flow cytometer and data were processed using BD FlowJo software. Statistical analysis was performed using unpaired *t* tests and significance inferred at *p* < .05.

Analysis of *C. jejuni* NET induction by SYTOX assay. SYTOX NET quantification was performed as previously described (232,264). Briefly, Following the *C. jejuni* NET induction described above, cells were added to wells of black 96-well plates and centrifuged at 400 x *g*. Supernatants were discarded and 1.0 µM SYTOX Green was added to each sample and incubated under microaerobic conditions at 37°C for 1 hr (174). After incubation, cells were centrifuged at 400 x *g* and the supernatant was discarded. The cells were washed once with 1× PBS and then resuspended in 100 µl 1× PBS. SYTOX fluorescence was measured at 504/523 nm using a BioTek Synergy microplate reader. Statistical analysis was performed using unpaired *t* tests and significance inferred at $p < .05$.

Western blot analysis of NET products. Detection of NET components via western blot was performed as previously described (232). Briefly, NETs were induced as described above, cells from healthy volunteers were lysed with Laemmli buffer with β-mercaptoethanol and boiled for 10 min. Ten microlitres of whole-cell lysate samples were loaded onto a 12.5% SDS-PAGE gel and run for 1.25 hr at 140 V at room temperature. Separated proteins were transferred to nitrocellulose membranes (GE Healthcare, Cat. 10600011) for 1.5 hr at 0.25 A using a semi-dry transfer apparatus. Membranes were blocked in 5% milk in Tris-buffered saline (TBS)-T for 60 min shaking. To probe proteins of interest, 1:500 dilution rabbit anti-*C. jejuni* SliP (Cocalico Biologicals), 1:5000 dilution rabbit anti-human Lcn2 (Invitrogen, Cat. 702248), 1:1000 dilution rabbit anti-human peptidylarginine deiminases 4 (PAD4; Thermo, Cat. PA5-12236), 1:1000 dilution rabbit anti-human histone H3 (Active Motif, Cat. 61799), 1:1000 dilution rabbit anti-human acetyl histone H3 (Active Motif, Cat. 39040), and 1:500 dilution mouse anti-human β-actin (Cell Signaling, Cat. 4970) were incubated on individual membranes for 1 hr at room temperature with shaking. Membranes were subsequently washed three times with filtered TBS-T for 5 min each. Proteins of interest were detected using a 1:2000 dilution of appropriate horseradish peroxidase-conjugated secondary antibodies in 15 ml 5% milk in TBS-T and

incubated for 45 min at room temperature with shaking. Membranes were then washed three times with filtered TBS-T, shaking for 5 min each. After the final wash, membranes were developed with a solution containing 5 ml peroxide and 5 ml luminol/enhancer solution (Thermo, Cat. 34580) and incubated for 5 min at room temperature with shaking. A *C. jejuni* negative control was also performed to ensure there was no cross-reactivity and no detection of proteins was noted. Chemiluminescent bands were imaged using the ChemiDoc-It Imager and densitometry measurements were made using NIH ImageJ software. Statistical analysis was performed using unpaired *t* tests and significance inferred at $p < .05$.

Production of rabbit anti-SliP antibodies. To generate anti-SliP antibodies, SliP was purified as previously described. Then, 500 µg of SliP were run on an SDS-PAGE gel and allowed to run to separate out whole cell *E. coli* lysates. After the gel ran, the gel was stained with Coomassie blue and then de-stained to view protein on the gel. After the gel was de-stained, the bands containing SliP were excised and placed in sterile water and shipped to Cocalico Biologicals, Inc. Two rabbits were initially inoculated with a minimum of 50 µg SliP in Incomplete Freund's via subcutaneous injection. After two- and three-weeks post-inoculation, the rabbits were boosted with a minimum of 50 µg SliP in Incomplete Freund's via subcutaneous injection or intramuscular injection at multiple sites. After two weeks following the three-weeks post-inoculation booster, rabbits were bled, and serum was saved for laboratory use. Two weeks following the test bleed, the rabbits were boosted with a minimum of 50 µg SliP in Incomplete Freund's via subcutaneous injection or intramuscular injection at multiple sites. One week following the last booster, rabbits were bled, and serum was saved for laboratory use. Rabbit sera was aliquoted in 1 mL aliquots and frozen at -20°C until western blot or co-immunoprecipitation was performed.

Neutrophil acetone protein powder for antibody cleaning. To clean the sera for nonspecific binding, Δ*sliP* infected neutrophils were incubated as previously described in this manuscript. After incubation, cells were washed three times with

1x PBS. After washes, cells were resuspended in 0.9% NaCl to a ratio of 1 mL salt solution for one gram of cells. Next, the cells were incubated on ice for 5 minutes. After incubation, -20°C chilled 100% acetone was added to the cells at a 4:1 ratio and incubated at 0°C rocking for 30 minutes. After rocking incubation, tubes were centrifuged at 10,000 X g for ten minutes at 4°C, where supernatant was discarded. The pellet was then resuspended in -20°C chilled 100% acetone, mixed vigorously, and then incubated at 0°C for ten minutes. Tubes were then centrifuged at 10,000 X g for ten minutes at 4°C, where supernatant was discarded. Once the supernatant was discarded, the pellet was transferred to a clean piece of filter paper and allowed to airdry. Once dried, the acetone protein powder was stored in an airtight container at 4°C until use (266). To use, powder was incubated with anti-SliP sera at a concentration of 1%. Sera was then incubated for 30 minutes at 4°C. After incubation, the sera was centrifuged at 10,000 X g for ten minutes at 4°C. After centrifugation, the supernatant was saved and stored at -20°C until usage.

RT-qPCR analysis of gene expression. For extracting neutrophil RNA, RNA was extracted using a Qiagen Rneasy Kit per the manufacturer protocol. RNA samples were eluted from the kit columns using nuclease-free water and stored at -20°C. All RNA samples were then Dnase treated, and pure RNA was clean and concentrated using a kit (Zymo). Each sample was tested for DNA contamination through standard PCR. cDNA was then produced from DNA-clear RNA using the BioRad iScript kit using the manufacturer protocol. Primers specific to *sliP*, *HDAC1*, *HDAC2*, *HDAC3*, *SIRT1*, *SIRT2*, *SIRT6*, *SIRT7*, *GCN5*, *PCAF*, *P300*, *CBP*, *SRC1*, *ACTR*, *TAF11250*, *TFIIIC90*, *GAPDH*, *and rpoA* were designed using PrimerQuest (IDT) (Table S1). The abundance of each gene expression was determined using the iTaq Universal SYBR green master mix (BioRad). Threshold values (C_T) were used to calculate the $\Delta\Delta C_T$ using *GAPDH* as the internal control for human genes. For neutrophil gene expression, abundance was normalized to neutrophils in media alone (uninfected).

***In vitro* immunofluorescence microscopy.** Cocultures were completed in wells containing sterile 12 mm poly-L-lysine coated coverslip (Corning, Corning NY) and cells were fixed in a solution of 2% paraformaldehyde, 2.5% glutaraldehyde in 0.1M sodium cacodylate buffer (pH 7.4) (Electron Microscopy Sciences, Hatfield, PA). Coverslips were washed thrice with tris buffered saline (TBS, pH 7.4) before permeabilizing with 0.25% Triton-X 100. Samples were then incubated in blocking buffer (TBS with 10% bovine serum albumin) for 120 minutes followed by overnight incubation at 4°C with a 1/200 dilution of the poly-clonal rabbit sera and antibodies for histone H3 (final concentration 2.5 µg/mL, Sigma SAB4200651) in blocking buffer. Samples were washed in blocking buffer thrice and stained with 1:1000 dilution of Alpaca anti-Rabbit IgG Nano (VHH) Recombinant Secondary Antibody conjugated with Alexa Fluor™ 647 (Invitrogen SA5-10327), Goat anti-Mouse IgG conjugated with Alexa Fluor™ Plus 488 (5 µg/mL final concentration, Invitrogen A32723), and 10 µM Hoechst 33342 for 120 minutes at room temperature. Coverslips were washed twice in blocking buffer and twice in TBS before mounting with ProLong™ Glass Antifade Mountant (Invitrogen P36982). Samples were visualized with a Zeiss LSM 710 META inverted laser scanning confocal microscope in part using the Vanderbilt Cell Imaging Shared Resource. Presented images are 3D reconstructions of z-stacked images.

Co-immunoprecipitation of histone H3 and SliP. Neutrophils were purified and infected with *C. jejuni* wild-type, Δ*sliP*, and complement strains as previously described. After non-NETosing condition incubation, cells were fixed and cross-linked by the addition of paraformaldehyde to a final concentration of 4% and incubated for 10 minutes at room temperature. After cross-linking, glycine was added to a final concentration of 125 mM and incubated for 5 minutes, shaking. The cells were then washed three times with ice cold 1x PBS. After the final wash, the cells were lysed using 750 µl RIPA buffer (150 mM NaCl, 1% Nonidet P-40, 0.5% deoxycholate, 0.1% sodium dodecyl sulfate, and 50 mM Tris (pH 7.4)). After lysis of the cells, the samples were centrifuged for 10 min at 4°C, 14,000 x g. After

centrifugation, the supernatant was pulled off and placed in a sterile 1.5 mL Eppendorf tube. Next, the histone H3 antibody was added to the supernatant at a dilution of 1:1000. The supernatant-antibody solution was incubated overnight at 4°C rocking. After the incubation, 10 µl protein A beads were added to each sample and incubated at 4°C for 3 hours rocking. After incubation, the tubes were placed on a magnet to pull down beads conjugated to the antibody-protein complexes. The conjugated beads were washed three times with RIPA buffer, using a magnet at 4°C each time. After the last wash, the proteins were eluted by adding Laemmli buffer with β-mercaptoethanol and boiled for 10 minutes. After the boiling, the tubes were placed on a magnet to discard the protein A agarose beads. Eluted proteins in Laemmli buffer were stored at -20°C until western blot analysis as previously described.

Infection of IL-10$^{-/-}$ mice with *C. jejuni*. All animal protocols were approved by the Institutional Animal Care and Use Committee at the University of Tennessee – Knoxville (UTK IACUC protocol #2885). As previously described, *C. jejuni* DRH212 and Δ*sliP* were grown on *Campylobacter*-specific medium and Gram stained to ensure culture purity prior to inoculation (59). This culture was streaked on *Campylobacter*-selective media and incubated at 37°C under microaerophilic conditions for 48 hr. Suspensions of *C. jejuni* 81–176 were made in sterile PBS and diluted to an OD600 of 10. Five female specific pathogen free 8- to 12- week old IL-10$^{-/-}$ C57BL/6 mice were gavaged with a single dose of 10^{10} CFUs per mouse of *C. jejuni* wild-type strain 81-176 or the Δ*sliP* mutant. Additionally, five female mice were mock infected with sterile 1× PBS. Each day for 10 days, approximately 20 mg of feces from one sample from each animal was immediately weighed out and diluted 1:100 in PBS. The remaining samples were immediately frozen at −80°C. Diluted samples were further serially diluted in PBS to 10^{-8}, and 100 µl of each dilution was plated on *Campylobacter*-specific medium. The plates were then incubated at 37°C under microaerophilic conditions for 48 hours before *Campylobacter* loads were determined. After 10 days post-infection, blood was

collected by cardiac puncture and mice were euthanized as previously described. From the blood, serum was collected and frozen at −20°C for further analyses. Ceca, colons, and spleens were excised from each mouse and placed in sterile 1X PBS. Colons were additionally rolled in Swiss Rolls and placed in formalin solution before being fixed in paraffin. To determine bacterial load in these tissues, ground tissue was weighed and diluted 1:100 in PBS. Diluted samples were further serially diluted in PBS to 10^{-8}, and 100 µl of each dilution was plated on *Campylobacter*-specific medium.

Histological analysis of murine intestinal tissue during *C. jejuni* infection. Pathology scoring for intestinal tissue was performed as previously described (232). The terminal 1 cm of the murine colon was removed following sacrifice, and the lumen was washed five times with 1 ml of sterile, cold 1× PBS. Tissue was placed in 10% buffered formalin and fixed for 4 hours at room temperature. Fixed tissue was embedded in formalin, and 4 µm sections were stained with haematoxylin and eosin (H&E). Stained slides were visualized through bright-field microscopy, and representative images were presented. Inflammation scoring was performed as described in a blind manner, noting oedema, presence of blood, hyperplasia, loss of goblet cells, epithelia raggedness and neutrophil infiltration (175). Statistical analysis was performed using a nonparametric Mann-Whitney U test.

Quantification of proinflammatory cytokines from murine sera. Murine cytokines from sera were quantified using the BioLegend LEGENDplex Anti-Virus response panel in a V-bottom plate per the manufacturer guidelines (267). Briefly, sera was plated, alongside a standard curve of known concentrations for various cytokines. Assay buffers were added to each well, along with mixed beads that had been sonicated in water baths and vortexed to ensure homogeneity. The plate was sealed, wrapped in aluminum foil, and shook on a plate shaker at 800 rpm for two hours at room temperature. After incubation, the plate was centrifuged at 250 X G for 5 minutes using a swinging basket. After centrifugation, the plate seal was

removed, and the supernatant was immediately flicked off into a bucket. The wells were then washed using the manufacturer wash buffer twice before the detection antibody was added to each well. The plate was sealed and covered in aluminum foil and shook on a plate shaker at 800 rpm for one hour at room temperature. After incubation, a streptavidin-phycoerythrin solution was added to the wells and the plate was sealed and wrapped in aluminum foil, where it incubated on a plate shaker at 800 rpm for 30 minutes at room temperature. After incubation, the plate was centrifuged and washed as previously described. Once the preparation was complete, the samples were resuspended in wash buffer until flow cytometry analysis. Samples were analyzed using an LSR II flow cytometer and data were processed using the BioLegend LEGENDplex data analysis software. Cytokine concentrations were determined due to the standard curve generated by standard bead concentrations.

***In vivo* fluorescence microscopy of mouse tissue samples.** Parrafin embedded mouse tissues were stained for fluorescence microscopy as previously described (176,177,232). Briefly, slides containing slices of paraffin embedded tissues were digested in three rounds of xylene washes for five minutes, followed by a final wash in xylene for 10 minutes at room temperature. Afterwards, slides were washed with two rounds of 5-minute washes with 100%, 95%, 70%, 50% ethanol each at room temperature. After the final ethanol wash, slides were rehydrated in deionized water by incubating for 5 minutes twice at room temperature. After rehydration, slides were incubated in R universal Epitope Recovery Buffer (Electron Microscopy Sciences) at 50°C for 90 minutes. After incubation, slides were then washed with deionized water three times for 5 minutes each. The slides were then washed with TRIS-buffered saline (TBS, pH 7.4) three times for 5 minutes each at room temperature. Samples were then permeabilized for 5 minutes with 0.5% Triton X100 in TBS at room temperature followed by three washes with TBS for 5 minutes each at room temperature. Samples were then blocked with TBS with 10% BSA for 30 minutes at room temperature. After

blocking, samples were then incubated with 1:20 dilution of histone H3, 1:20 acetyl-histone H3, 1:50 *Campylobacter*, and 1:100 MPO antibodies overnight at room temperature covered in the dark. After overnight incubation, slides were washed three times with TBS for 5 minutes each at room temperature. After the final wash, the samples were stained with 5 µM Hoechst 33342 for 30 minutes at room temperature. After the incubation, slides were washed three times with TBS for 5 minutes each at room temperature. After the final wash, the slides were air dried and coverslipped using Mowiol. Tissues were visualized with a Nikon E600 Eclipse at the Advanced Microscopy and Imaging Center at the University of Tennessee. Images presented are composites of z-stacked images.

Purification of immune cells from murine colon tissues for co-immunoprecipitation. CD45$^+$ immune cells were purified from the colons of uninfected, wild-type, and Δ*sliP* infected mice per manufacturer guidelines (MojoSort Biolegend). After purification of CD45$^+$ cells, cells were incubated in formalin to cross-link protein complexes at 4°C. The histone H3 co-immunoprecipitation was performed as previously described, with samples stored at -20°C until western blot analysis was performed.

Cell lysis dependent genomic DNA quantification. To determine if SliP presence in the supernatant of *C. jejuni* grown in the presence of deoxycholate, concentration of genomic DNA was determined as a proxy for cell lysis. After 48 hours of incubation in Mueller–Hinton (MH) with or without deoxycholate (DOC), supernatant was pulled off for DNA extraction. Before extraction, human DNA was spiked in to account for loss of DNA during the extraction process. For the DNA extraction, one-tenth volume of ice-cold 3M sodium acetate was added to each tube on ice. Next, three volumes of 95% ethanol were added to the tubes on ice. The tubes were then incubated at -20°C for 30 minutes. After incubation, the tubes were centrifuged at 15,000 rpm for 15 minutes at 4°C. After centrifugation, the supernatant was aspirated off, whereby the pellets were washed with 70% ethanol. The tubes were then centrifuged at 15,000 rpm for 5 minutes at 4°C. The

supernatant was aspirated off and the DNA pellet were air-dried before resuspension in nuclease-free water. *C. jejuni* genomic DNA was amplified using *mapA*-specific primers, while human DNA was amplified using GAPDH-specific primers. Concentrations of each were determined using known DNA concentrations of each alongside the qPCR amplifications.

Gentamicin protection assay. A gentamicin protection assay was performed as previously described (232). Briefly, 10^6 neutrophils were infected with *C. jejuni* at an MOI of 10 and incubated under microaerobic conditions at 37°C for one hour. After incubation, cells were treated with 100 µl RPMI 1640 containing 10% FBS and gentamicin sulfate for one hour at 37°C under microaerobic conditions. After gentamicin treatment, neutrophils were washed three times with 1x PBS before being lysed with 0.1% Triton X-100 for 5 minutes. Cell pellets were resuspended in 1x PBS and serially diluted before being plated on *Campylobacter*-selective media. Cultures were grown for 2 days at 37°C under microaerobic conditions and CFUs were counted. Statistical analysis was performed using unpaired *t* tests and significance inferred at $p < .05$.

C. jejuni **growth curve.** To determine if the *sliP* mutant has a growth defect, bacteria were grown up on *Campylobacter*-specific media for 48 hours under microaerobic conditions. After 48 hours, cells were resuspended in MH broth and normalized to an optical density (OD) of 0.05. After normalization, cells were plated in 96 well plates and incubated under microaerobic conditions at 37°C. Bacterial growth was checked at 24- and 48-hours post-inoculation to determine the growth kinetics. OD readings were performed through a BioTek Synergy microplate reader.

C. jejuni **motility assay.** To determine if the *sliP* mutant has a motility defect, bacteria were grown up on *Campylobacter*-specific media for 48 hours under microaerobic conditions. After 48 hours, cells were resuspended in MH broth and then normalized to an OD of 1 and a final volume of 1 mL. After normalization of

all strains, the blunt ends of inoculation loops were dipped into the bacterial culture before being stabbed into low agar MH media. After puncturing the bacterial culture into the media, the inoculation site was indicated. At 24- and 48-hours post-inoculation, the diameter of the zone of motility was determined.

Purification of mouse leukocytes. To obtain murine leukocytes, blood was drawn by cardiac puncture. Neutrophils were isolated by density gradient centrifugation and ammonium-chloride-potassium (ACK) osmotic red blood cell lysis (172). Briefly, clotted blood was added to 1 mL 1x PBS and centrifuged at 400 x G for 5 minutes. After centrifugation, pellets were resuspended in 500 µl ACK buffer and incubated for 30 seconds before 500 µl 1X PBS was added. Cells were centrifuged at 400 x G for 5 minutes. Cells underwent further ACK lysis treatment until solely leukocytes were obtained. Once isolated, leukocytes were resuspended in RPMI 1640 containing 10% FBS.

Immunofluorescence to image *C. jejuni* induced murine NETs. To determine if murine neutrophils were able to induce NETs, we purified leukocytes as previously described. After isolation, murine leukocytes were incubated with *C. jejuni* at an MOI of 10:1 for three hours under microaerobic conditions on poly-l-lysine coated coverslips. After incubation, coverslips were washed thrice with tris buffered saline (TBS, pH 7.4) before permeabilizing with 0.25% Triton-X 100. Samples were then incubated in blocking buffer (TBS with 10% bovine serum albumin) for 60 minutes minutes followed by overnight incubation at 4°C with a 1/1000 dilution of the antibody for citrullinated histone H3 (Cayman, 17855) in blocking buffer. Samples were washed in blocking buffer thrice and stained with 1:1000 dilution of donkey anti-rabbit secondary antibody conjugated with Alexa Fluor™ 647 (Biolegend, 406414) and 1.0 µM SYTOX Green for 120 minutes at room temperature. Coverslips were washed twice in blocking buffer and twice in TBS before mounting with Mowiol mounting medium. NETs were visualized with a Nikon E600 Eclipse at the Advanced Microscopy and Imaging Center at the

University of Tennessee. Presented images are 3D reconstructions of z-stacked images.

Flow cytometry preparation of mouse colon leukocytes. To determine the number of neutrophils traffic to the colon of uninfected, WT, or Δ*sliP C. jejuni* infected mice, mice were infected or uninfected via oral gavage. Mice were infected for ten days, and infection was confirmed through viable CFU plating from mouse feces. After ten days, mice were sacrificed, and colons were isolated. Colons were washed three times with 1x PBS and then fixed in formalin. After fixation, colons were cut into 1 mm sections and then digested with collagenase for two hours at 37°C. After digestion, colons were pushed through a 40 µm filter to isolate colonic cells. Cells were then prepared for flow cytometry as previously described, however, with the staining of CD11b and Ly6G antibodies. Samples were analyzed using an LSR II flow cytometer and data were processed using BD FlowJo software. Statistical analysis was performed using unpaired *t* tests and significance inferred at $p < .05$.

SliP-dependent acetylome of host and bacterial proteins. To determine the acetylome of host and bacterial proteins influenced by the deacetylase activity of SliP, PTMScan® Acetyl-Lysine Motif (Cell Signaling Technology) kit was used for immunoaffinity of differentially acetylated peptides. Briefly, either bacterium alone (wild-type or Δ*sliP C. jejuni*) or uninfected (media alone), wild-type infected or ΔsliP *C. jejuni* infected neutrophils were incubated in their respective conditions for two hours at 37°C at an MOI of 5:1 under microaerobic conditions (bacteria:neutrophil). After incubation, cells were washed, put in a urea lysis buffer (20mM HEPES pH 8.0, 9M urea, 1mM sodium orthovanadate, 2.5mM sodium pyrophosphate, 1mM β-glycerophosphate), and then sonicated at 15 W in triplicate on ice. After sonication, cell-free supernatant was isolated through centrifugation and reduced using DTT. After reduction, reduced supernatant was then alkylated using iodoacetamide. After alkylation, supernatants were then digested with Trypsin-TPCK overnight to generate peptides. The next day, peptides were purified using

C_{18} reversed-phase columns (Cell Signaling Technology – 35741). After purification, samples were frozen at -80°C and then lyophilized. After samples were lyophilized, peptides were dissolved in immunoaffinity purification (IAP) buffer (50 mM MOPS/NaOH pH 7.2, 10 mM Na_2HPO_4, 50 mM NaCl) and added to anti acetyl-lysine antibody beads and incubated rotating for two hours at 4°C. After incubation, samples were washed using IAP buffer and then acetylated peptides were eluted from the antibody-bead complex using 0.15% TFA. After elution, peptides were quantified and analyzed through 60-minute separation LC-gradient Thermo Orbitrap Fusion Lumos mass spectrometer.

Acknowledgments

Appendix

Table 3.1. Primers used in the *sliP* study

Primers used for making the bacterial strains (5'-3'):

sliP F	GTATATTCGCGTATGGAGTGG
sliP R	GGATTACCTGCTCCATTTGCT
SOE *sliP* F	ATGGAAAATAAACTATTAGAAGGATCCAAAAGTGTAAAAATTTGGTAA
SOE *sliP* R	TTACCAAATTTTTACACTTTTGGATCCTTCAAATAGTTTATTTTCCAT
sliP complement F	GGATCCATGGAAAATAAACTATTTGA
sliP complement R	GGATCCTCCTTGTTTTTTACCAAATT
JJ13	TGCTCTAGATTTATGATATAGTCGATA
sliP G26A F	GACACCTTCTTTTAGGAAATGCTTTTAGTATGGCTTATGAT
sliP G26A R	ATCATAAGCCATACTAAAAGCATTTCCTAAAAGAAGGTG
sliP-cyaA SOE F	TATAAAAGTGTAAAAATTTGGGCTGCTCAGCAATCGCATCAG
sliP-cyaA SOE R	GCTGAGCAGCCCAAATTTTTACACTTTTATA
heuR-cyaA SOE F	TATCTGAAGAAATTTAAAAAAGCTGCTCAGCAATCGCATCAGGC
heuR-cyaA SOE R	CGATTGCTGAGCAGCTTTTTTAAATTTCTTCAGATA

Table 3.1 Continued:

heuR complement F	GGATCCATGGATGAGGGACAAAA ACAA
ciaB-cyaA SOE F	TTTGAAAGATATAAGAAAAAAGCT GCTCAGCAATCGCATCAGGC
ciaB-cyaA SOE R	GCTGAGCAGCTTTTTTCTTATATC TTTCAAA
ciaB complement F	GGATCCATGAATAATTTTAAAGAA ATAGCTAAATTGG
cyaA complement R	GGATCCTGTCATAGCCGGAATCC TGGC
sliP qPCR F	TGGTGGTAATGATGGAGAATATG T
sliP qPCR R	TTCTGATGTGCGTTCCGATAC
HDAC1 F	GGAAGAGGAGTGAGCATTAGAG
HDAC1 R	CTACCTTGGGATTGGGTTAGAG
HDAC2 F	GGAGGGTCTCTTGTCTGTATTG
HDAC2 R	TGGGTCATGCGGATTCTATG
HDAC3 F	TGCATTGTGCTCCAGGTAATA
HDAC3 R	CCTTCCACCACCAACCTAAA
SIRT1 F	GCCCGGTCAGGTTTCTTATT

Table 3.1 Continued:

SIRT1 R	CCTCCCAAAGTGCTAGGATTAC
SIRT2 F	GAAAGGACCCTGGCTACTAAAG
SIRT2 R	TCCCAATGTGCTGGGATTAC
SIRT6 F	GTGGACATCGCCTTCTCTAATC
SIRT6 R	GACCAGGAGAAACAGGAACAA
SIRT7 F	CTGTTACTCTCACTCGGCTTTC
SIRT7 R	CGTCATCACACTTCCCATGTAG
Gcn5 F	CTAAAGGAGGGTGTGAGTGAAG
Gcn5 R	AGTAGCTAGAGAGAAGAGGAAGG
PCAF F	GTGGGACATCCTTGACACTAAT
PCAF R	CATCCAGAGGAACAGGAGAAAG
P300 F	CGGCCAGAGGTACCATTATATC
P300 R	GAGGTGATGTGCCTCCAATAA
CBP F	CTCCCAGGTTCAAGCTATTCTC
CBP R	CGAAACCCTGTCTCCACTAAA
SRC-1 F	GGAGGACGAAGACTGAACATAAA

Table 3.1 Continued:

SRC-1 R	CCTCATCCATAAAGCTGTCTCC
ACTR F	GGGTAAGAGACCGAGGATAGAA
ACTR R	CAGAGTGGTGGGTATGGAATG
TAFII250 F	GTTCTGAGCTGCCAAGAGATA G
TAFII250 R	CTTCCTCCAGGTTGAGCATAAA
TFIIIC90 F	CATCCTCCTTCCTTGCGTTAT
TFIIIC90 R	CCTGTCCTCATACAGCTTTCC

Table 3.2. Bacterial strains used in the *sliP* study

Genus and Species	Strain	Description	Source
Campylobacter jejuni	DRH212	Wild-type *C. jejuni*	This study
Campylobacter jejuni	DRH212-pECO102	*C. jejuni* harboring empty plasmid pECO102	This study
Campylobacter jejuni	DRH212 Δ*sliP*	*sliP* deletion strain of *C. jejuni*	This study
Campylobacter jejuni	DRH212 Δ*sliP*-p*sliP*	*sliP* deletion strain of *C. jejuni* complemented with pECO102-*sliP*	This study

Table 3.2 Continued:

Campylobacter jejuni	DRH212 Δ*sliP*-p*sliP*G26A	*sliP* deletion strain of *C. jejuni* complemented with pECO102-*sliP*G26A	This study
Campylobacter jejuni	DRH212 ΔflgE	*flgE deletion strain of C. jejuni*	(225)
Escherichia coli	C3013-pQE30	*Empty vector expression E. coli strain*	This study
Escherichia coli	C3013-pQE30-sliP	*His tagged sliP expression E. coli strain*	This study
Escherichia coli	C3013-pQE30-sliPG26A	*His tagged sliPG26A expression E. coli strain*	This study
Escherichia coli	DH5α-pCYA-ankB	*E. coli strain expressing a Legionella pneumophila ankB gene fused with an N-terminal adenylate cyclase cyaA*	(268)
Campylobacter jejuni	DRH212-psliP-cyaA	*C. jejuni strain harboring pECO102 encoding sliP-cyaA fusion*	This study
Campylobacter jejuni	DRH212-pciaB-cyaA	*C. jejuni strain harboring pECO102 encoding ciaB-cyaA fusion*	This study
Campylobacter jejuni	DRH212-pheuR-cyaA	*C. jejuni strain harboring pECO102 encoding sliP-cyaA fusion*	This study

Table 3.2 Continued:

Campylobacter jejuni	DRH212-cobB::hawkeye	*C. jejuni strain harboring a transposon insertion in cobB*	This study
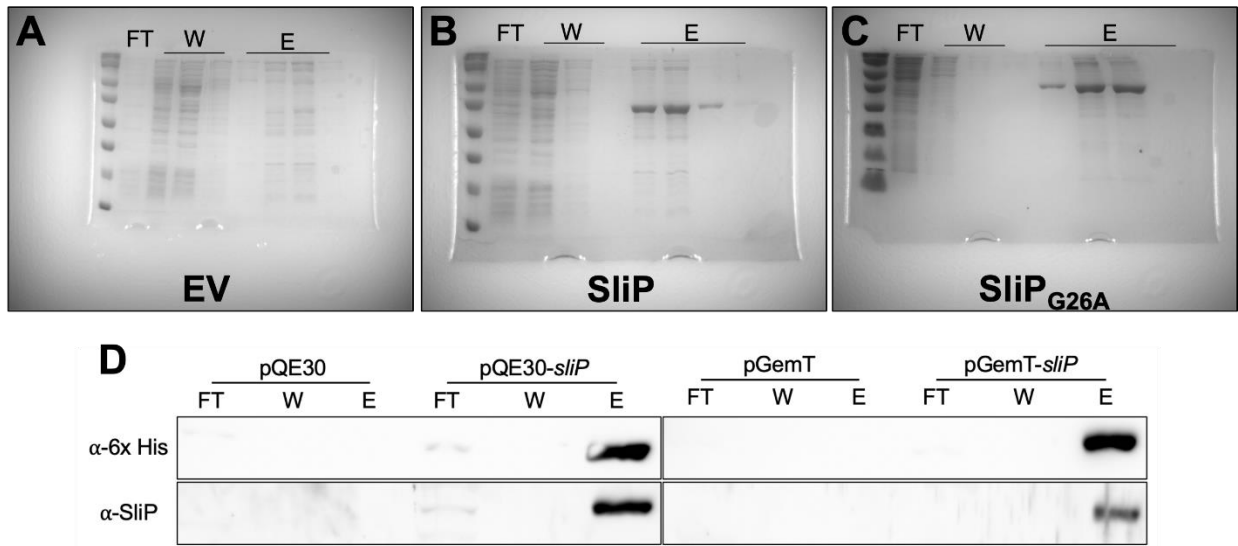
Figure 3.8. Production and specificity of SliP and SliP anti-sera.

Gels of the elutions for the (A) pQE-30 empty vector (EV), (B) SliP, and (C) SliP$_{G26A}$. After packing the Ni-NTA column with lysed *E. coli* supernatant, proteins were eluted from the column. SliP and SliP$_{G26A}$ can be visualized as the predicted molecular weight is 37 kDa. (D) Specificity of the SliP antibody along with immunodetection for anti-6x His. SliP and 6x His were probed for abundance in protein preparation flow through (FT), wash (W), and elution (E) steps of the protein purification process. pQE-30 served as the empty vector control for the N terminal 6x His SliP and pGemT served as the empty vector control for the C terminal 6x His SliP.
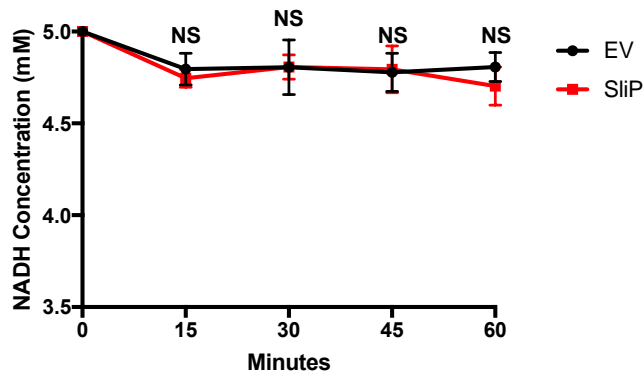
Figure 3.9. Inability of SliP to hydrolyze NADH.

To determine if SliP could hydrolyze NADH during deacetylation, 5mM NADH was added to lysine deacetylation assays as previously described. Every 15 minutes, reactions were measured for the abundance of NADH. Multiple comparison testing was performed using ANOVA with a *post-hoc* test.
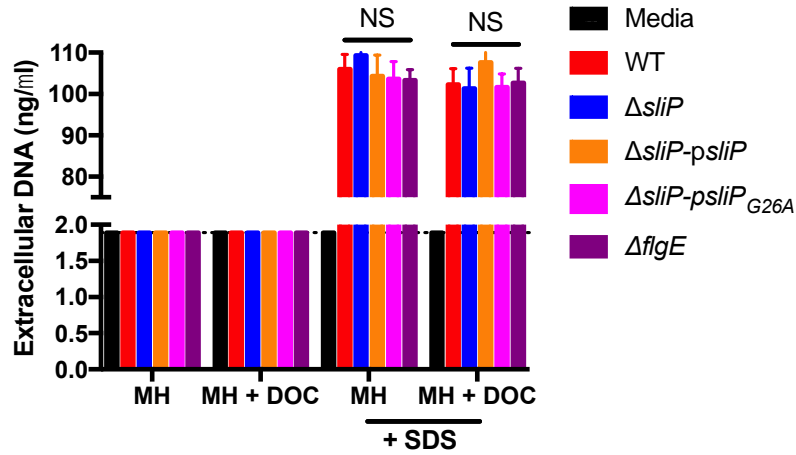
Figure 3.10. Abundance of *C. jejuni* gDNA within MH and MH supplemented with deoxycholate (DOC).

After 48 hours of growth in the respective media, the supernatant was isolated, and the DNA was extracted as a proxy for cell lysis. Additionally, one set of replicates was additionally incubated with SDS to a final concentration of 1% and incubated to lyse *C. jejuni*. Abundance of gDNA was determined using primers specific for *mapA* through qPCR, with most concentrations solely detected at the limit of detection.
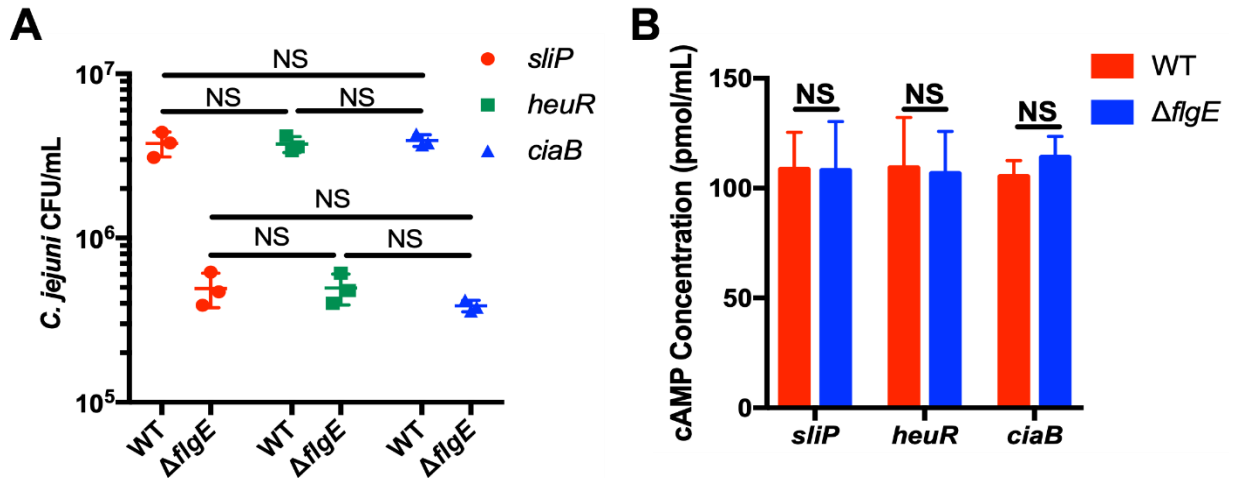
Figure 3.11. CyaA reporter assays do not influence *C. jejuni* internalization within neutrophils.

(A) Gentamicin protection assay of *C. jejuni* wild-type and Δ*flgE* harboring the various *cyaA* reporters for *sliP*, *heuR*, and *ciaB*. (B) *In vitro* CyaA cAMP assay determined that the various strains of reports produce similar levels of functional CyaA. Cell lysates of the various reporter strains were produced and incubated with ATP and recombinant human calmodulin for one hour at 37°C. After incubation, cAMP levels were measured as previously described. Levels of cAMP were not statistically significantly different across the reporters, indicating all strains produce similar levels of functional intracellular CyaA. Multiple comparison testing was performed using ANOVA with a *post-hoc* test.
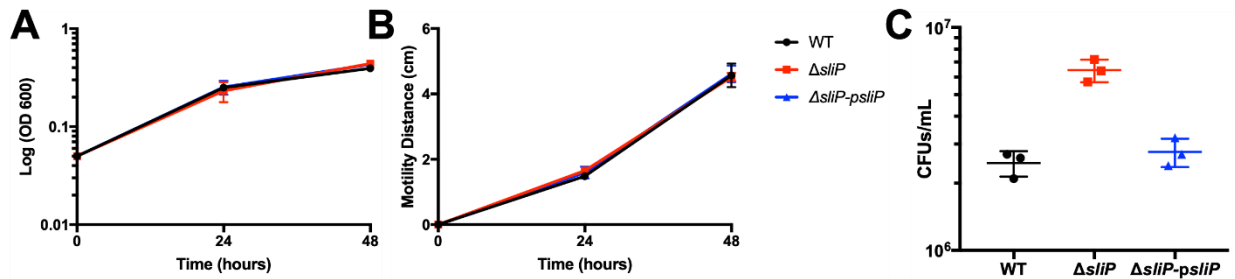
Figure 3.12. Key phenotypes of *C. jejuni* are maintained in the Δ*sliP* mutant.

(A) Growth of both strains in MH broth are not significantly different for up to 48 hours. (B) Flagellar motility of both strains in low agar media are not significantly different after 48 hours post inoculation. After 48 hours, the diameter of motility was measured. (C) Intracellular levels of *C. jejuni* within neutrophils are maintained after three hours post-infection. After three hours of incubation, a gentamicin protection assay was performed to determine the abundance of intracellular bacteria. Multiple comparison testing was performed using ANOVA with a *post-hoc* test. ***$p < .001$
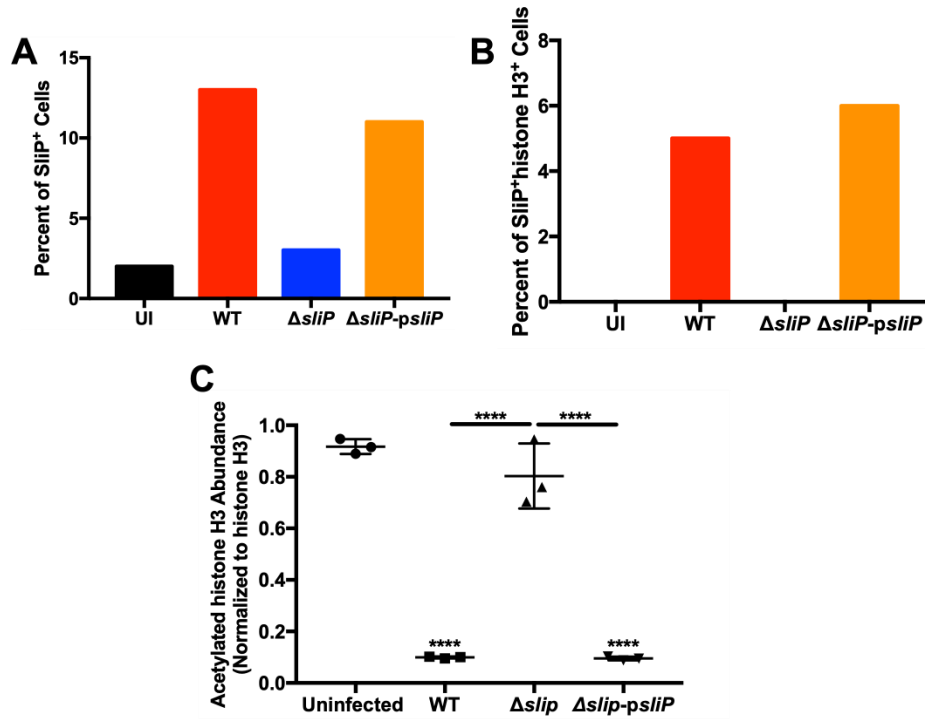
Figure 3.13. Quantification of SliP⁺ neutrophils and SliP-dependent neutrophil histone H3 deacetylation.

(A) Incidence of SliP within uninfected, WT, Δ*sliP*, and *sliP* complement infected neutrophils. (B) Incidence of SliP colocalizing with histone H3 within uninfected, WT, Δ*sliP*, and *sliP* complement infected neutrophils. Intracellular abundances was determined using 100 randomly selected cells from each treatment. (C) Densitometry quantification of acetylated histone H3 is SliP dependent. Western blot (Figure 3.8E) was performed, and densitometry quantification was performed using ImageJ.

115
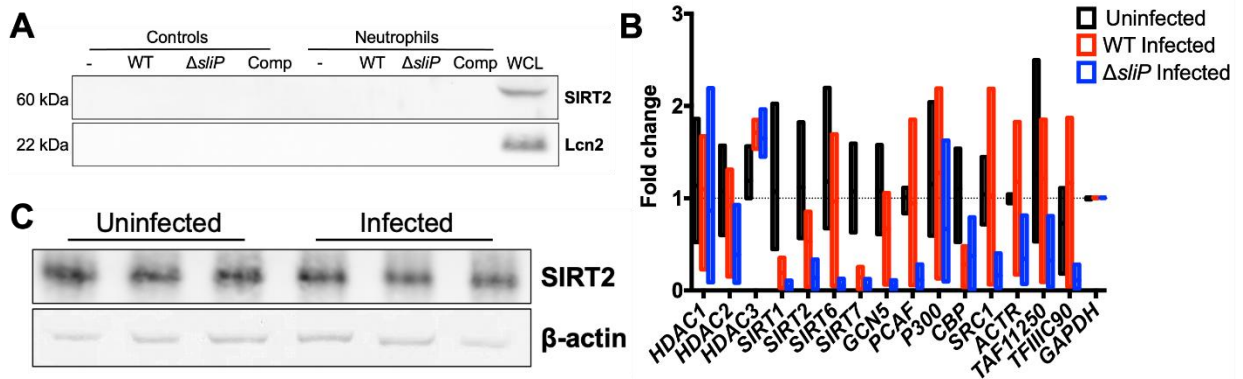
Figure 3.14. Abundance of host sirtuins and histone deacetylases are not upregulated during *C. jejuni* neutrophil infections.

(A) Host sirtuin-2 does not translocate and bind to histone H3 during *C. jejuni* infection of neutrophils. Samples from the neutrophil co-immunoprecipitation were probed for the abundance of Sirt-2 as this is a common feature during other bacterial infections. Samples were further analyzed for non-specific cytoplasmic contamination through probing for lipocalin-2 (Lcn2). Whole cell lysates for each protein were included in the blots to ensure the immunoblotting was performed correctly. (B) To determine if histone deacetylation was due to upregulation of a host protein that deacetylates host histones, transcript abundance was determined by RT-qPCR for proteins that classically target histone H3. Transcript abundance for each gene was normalized to GAPDH abundance. (C) Protein abundance of host sirtuin-2 is not significantly different between uninfected and *C. jejuni* infected neutrophils. Densitometry of Sirt-2 was normalized to the abundance of β-actin.
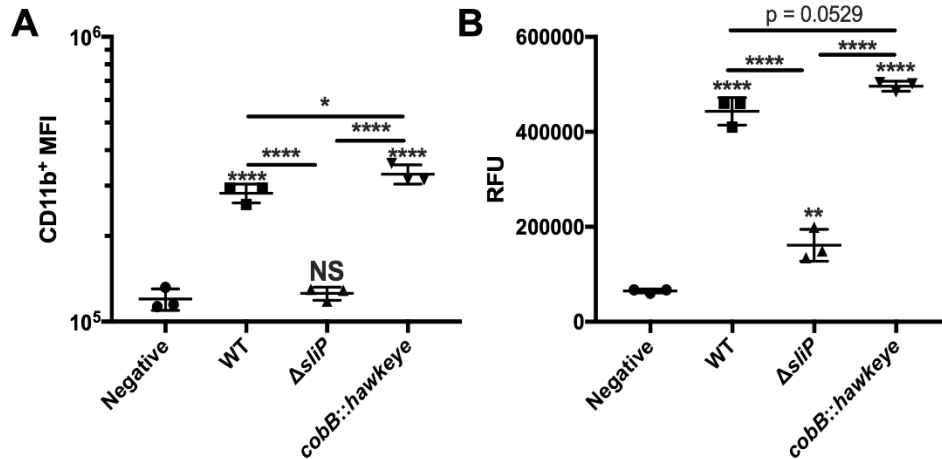
Figure 3.15. The intracellular sirtuin, _cobB_, in _C. jejuni_ is not involved in neutrophil activation or NETosis.

(A) Neutrophil activation through CD11b expression was significantly increased in the transposon mutant of _cobB_ (_cobB_::_hawkeye_) compared to wild-type infected neutrophils. (B) NET abundance through SYTOX staining in the _cobB_ mutant was not significantly different from wild-type infected neutrophils. Multiple comparison testing was performed using ANOVA with a _post-hoc_ test. *$p < .05$; **$p < .01$; ***$p < .001$; ****$p < .0001$
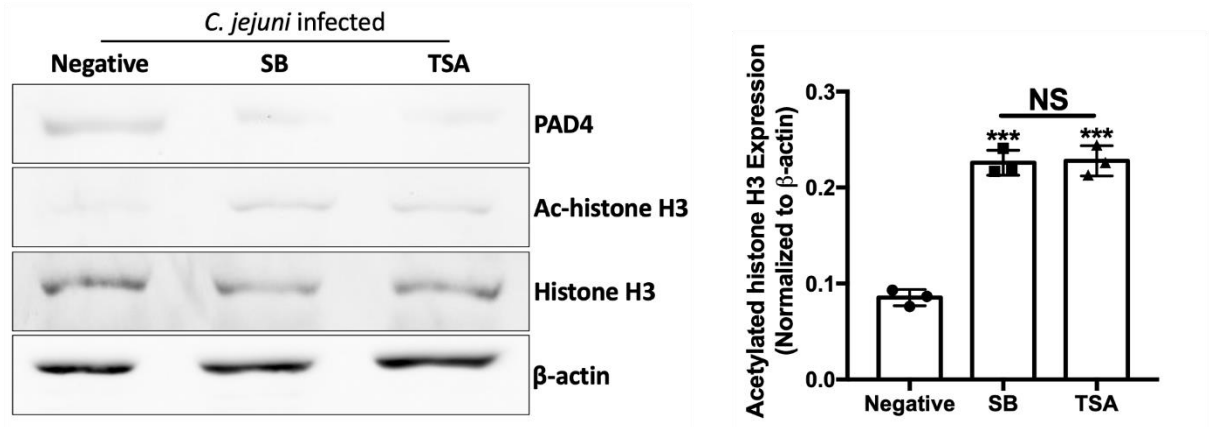
Figure 3.16. Sodium butyrate (SB) and trichostatin-A (TSA) reverse SliP-dependent changes in PAD4 and histone acetylation.

Prior to *C. jejuni* infection, neutrophils were pre-incubated with 10mM SB, 100 µM TSA, or media alone (negative) as these concentrations chemically inhibit SliP-dependent lysine deacetylation. SB and SB both significantly reduce the abundance of PAD4 in neutrophils, while additionally increasing the abundance of histone H3 acetylation. PAD4 and histone H3 acetylation abundance was normalized to β-actin and histone H3, respectively. Quantification was performed through densitometry.
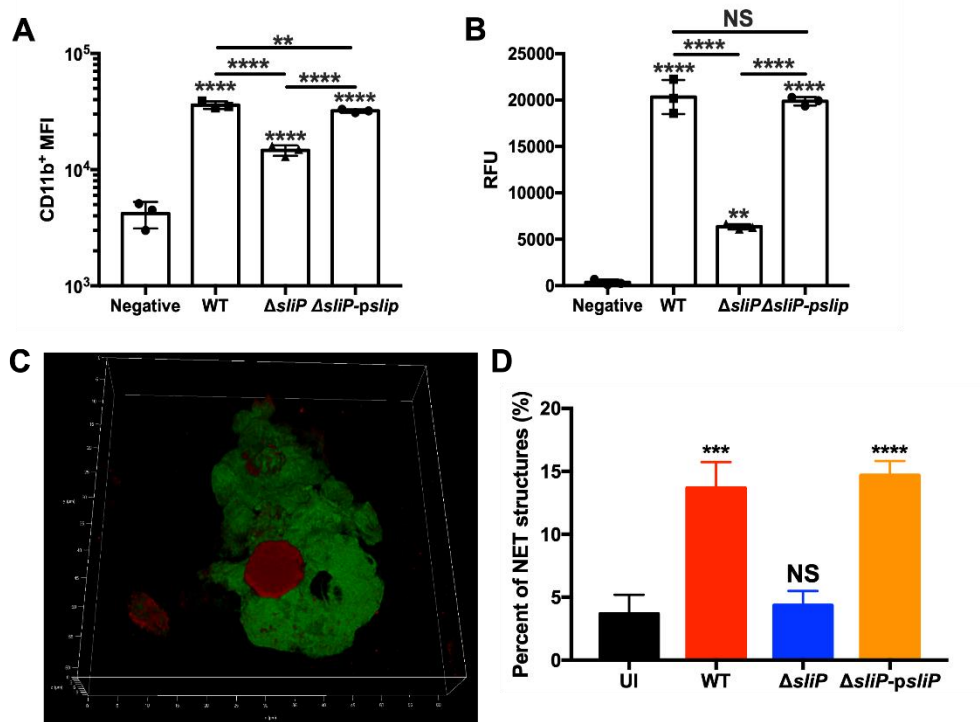
Figure 3.17. *In vitro* **murine neutrophil activation and NETosis are SliP-dependent.**

(A) Neutrophils from C57BL/6 mice were potently activated by wild-type *C. jejuni*, with a significant reduction in CD11b expression compared to wild-type infected neutrophils. Neutrophil activation was restored with the complementation of plasmid-borne *sliP*. (B) NET induction through SYTOX staining was robustly produced, with a reduction in the amount produced by Δ*sliP* infected neutrophils. Complementation through plasmid-borne sliP restored the NET phenotype. (C) Immunofluorescence showing *C. jejuni*-induced murine NETs. DNA (green) and citrullinated histone H3 (red) can be seen both in the nucleus and studded in the extracellular DNA, demonstrating NETosis. Multiple comparison testing was performed using ANOVA with a *post-hoc* test. ***p* < .01; ****p* < .001; *****p* < .0001
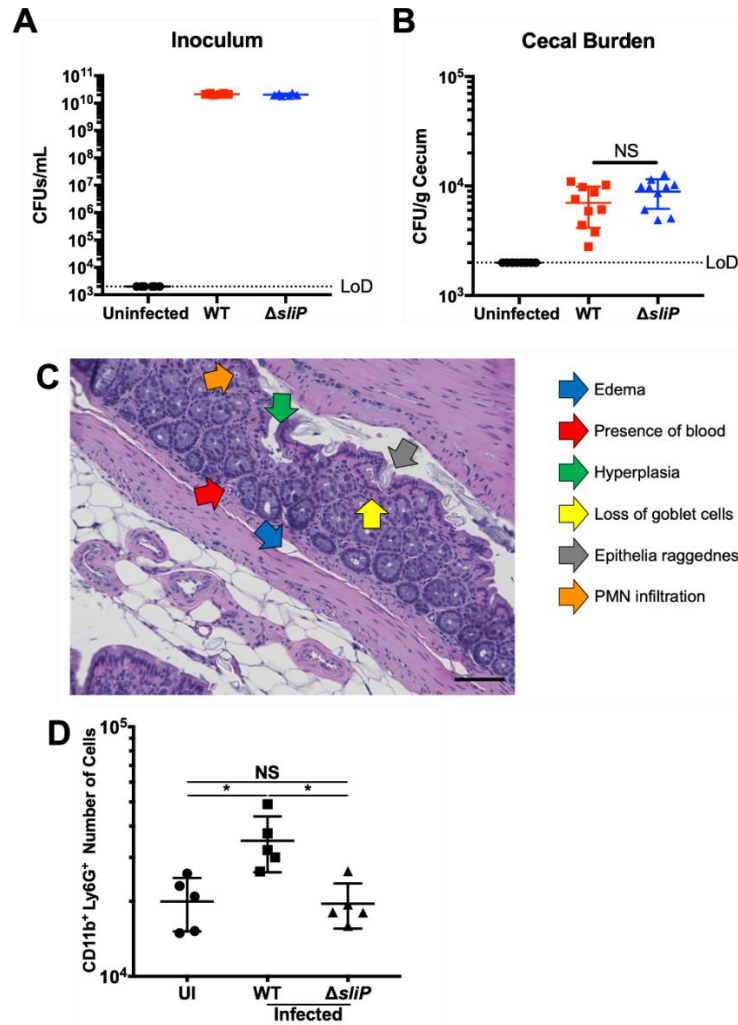
Figure 3.18. Colonization of *C. jejuni* and the Δ*sliP* mutant within the ceca of infected IL-10⁻/⁻ C57BL/6 mice ten days post-infection.

(A) Inoculation control for two separate experiments to ensure mice were inoculated with the correct amount of *C. jejuni*. (B) Cecal burden of *C. jejuni* within uninfected, wild-type, and Δ*sliP* infected mice. Multiple comparison testing was performed using ANOVA with a *post-hoc* test. (C) H&E colonic tissue pathology scoring scheme used for this study. (D) Quantification of neutrophils (CD11b⁺Ly6G⁺) within the colons of uninfected, wildtype, and Δ*sliP* infected mice. Multiple comparison testing was performed using ANOVA with a *post-hoc* test. *p < .05

CHAPTER FOUR
A SECRETED NUCLEASE IN *CAMPYLOBACTER JEJUNI* LEADS TO NEUTROPHIL EXTRACELLULAR TRAP EVASION AND INFLAMMASOME ACTIVATION

This chapter is a version of a manuscript in preparation for journal submission.

Sean M. Callahan, Madison L. Bunch, Eleanor G. Mancini, Tiara D. Ashurst, Jeremiah G. Johnson. "A secreted nuclease in *Campylobacter jejuni* leads to neutrophil extracellular trap evasion and inflammasome activation."

The work described in this study was conducted by the following individuals: cloning of the bacterial mutants and protein purification were conducted by E.G.M. and T.D.A. Biofilm assays, natural competence, and confocal microscopy were conducted by M.L.B. All remaining experiments were conducted by S.M.C. Writing and editing of the manuscript has been conducted by S.M.C., M.L.B., E.G.M., and J.G.J.

Abstract

Campylobacter jejuni is the leading cause of bacterial-derived gastroenteritis worldwide and we previously determined *C. jejuni* induces neutrophil extracellular traps (NETs), which are structures that prevent pathogens from disseminating throughout a host. While NETs are efficient at reducing bacterial burden at the site of various infections, numerous pathogens encode nucleases that can degrade the DNA that makes up the NET to evade their effects. Previous research found that some *C. jejuni* strains encode nucleases to promote dispersal of biofilms, but we further hypothesize that these factors may be used to evade NETs during infection. Because the determinants required for nuclease production are poorly understood, we conducted a mutant screen to identify genes necessary for extracellular DNA degradation. In this work, we identified *mugA*, which allows the bacterium to evade entrapment of NETs. We demonstrate pure MugA can degrade NET-associated DNA and a mutant of *C. jejuni* lacking *mugA* is sensitive to NET antimicrobial activity. In addition to evading antimicrobial activity of NETs, the products of NET degradation additionally result in host inflammation. Specifically, we demonstrate that degraded NETs lead to NLRP3-

dependent inflammasome activation in macrophages. As such, while MugA assists the bacterium in evading NET killing mechanisms, it still promotes host inflammation. This was correlated in the murine model of campylobacteriosis, as *C. jejuni* deficient in *mugA* are unable to colonize or cause inflammation to wild-type levels. In conclusion, MugA-dependent NET degradation allows for *C. jejuni* to elude NET killing mechanisms while promoting host inflammation. Such results could allow for targeted therapeutics to be developed to reduce pathogen burden within infected hosts.

Introduction

Pathogenic bacteria produce extracellular nucleases that are either anchored to the cell wall or secreted into the extracellular environment, where they can promote DNA hydrolysis during biofilm dispersal, nutrient acquisition, or innate immune evasion (128,269). For example, extracellular nucleases can act upon DNA within the biofilm matrix and thereby regulate biomass and dispersal (129,270–273). Further, bacteria can produce nucleases so that exogenous DNA can be used as a source of phosphorus, carbon, and nitrogen (122,274–276). Beyond using DNA as a nutrient source, naturally competent bacteria can use similar factors to promote the acquisition of genetic elements during adaptation or developing antibiotic resistance (277–279). Finally, extracellular nucleases can degrade neutrophil extracellular traps (NETs), which is where the neutrophil extrudes its DNA into the extracellular environment to ensnare pathogens and prevent them from disseminating throughout the host (72,280). In addition, NETs decorate this extracellular DNA with various antimicrobial proteins, which allows NETs to possess bactericidal activity against numerous pathogens including, *Burkholderia pseudomallei*, *Escherichia coli*, and *Salmonella* Typhimurium (44,281). To counteract these effects, some pathogens that induce NETs evade NET-dependent killing through the production and secretion of nucleases (282).

Because these nucleases likely assist in promoting infection, they are a promising target for anti-infective therapies.

The inflammatory response to *C. jejuni* includes upregulation of IL-1β (59,182,283–286), which is an anti-inflammatory cytokine involved in autoimmunity and host defense during infection (287). At elevated concentrations, IL-1β is a proinflammatory cytokine involved in the development of numerous autoimmune diseases (288,289). For IL-1β to be secreted out of host cells, inflammasome-dependent signaling along with pyroptotic cell death must occur (290,291). In this signaling pathway, the NLR family of apoptosis inhibitory proteins (NAIPs) assemble with the adaptor protein NLRC4 (underline nucleotide-binding domain, leucine-rich repeat-containing family, CARD domain-containing protein 4) upon ligand sensing. This protein complex activates caspase-1 which proteolytically cleaves pro-IL-1β, pro-IL-18, and gasdermin D (GSDMD) into their respective, active proteins. Cleaved GSDMD then forms pores within the host cell, resulting in cytokine secretion and pyroptotic host cell death (292,293). In addition to the NAIP/NLRC4-dependent inflammasome, IL-1β can be secreted in an NLRP3 (NOD-, LRR- and pyrin domain-containing protein 3) dependent manner. NLRP3 forms a complex with ASC (apoptosis-associated speck-like protein containing a CARD) to recruit and activate caspase-1, resulting in IL-1β secretion and host cell death (294–296). Hence, inflammasomes are crucial immunological structures to produce IL-1β and regulate host inflammation.

C. jejuni induces inflammasome activation within murine and human macrophages in an NLRP3-dependent manner (297). When neutrophil chemotaxis was blocked during campylobacteriosis, IL-1β was significantly decreased (58, 298). Additionally, nuclease-dependent NET degradation can activate inflammasome signaling within monocytes and tissue resident macrophages (140). Specifically, extracellular histones can induce NLRP3-dependent inflammasome activation within endothelial cells and Kuppfer cells (141,299–301). However, the molecular mechanism underlying macrophage inflammasome activation in response to degraded NET components remains unclear.

124

Additionally, how neutrophils contribute to macrophage inflammasome activation during campylobacteriosis has yet to be investigated. Therefore, we hypothesize that NLRP3-dependent inflammasome activation could drastically shape the inflammatory immune response during campylobacteriosis.

In this study, we sought to determine the molecular mechanisms underlying *C. jejuni* nuclease production. We describe a previously hypothetical nuclease, mismatch T:U/G glycosylase (MugA). We demonstrate that a *C. jejuni mugA* mutant is sensitive to NET antimicrobial activities, and that purified MugA protein degrades NETs. Consequently, MugA-degraded NETs lead to macrophage inflammasome activation, resulting in increased IL-1β production dependent on NLRP3. Finally, we demonstrate that *C. jejuni* deficient in *mugA* are not able to colonize nor grow within the host to the same degree as wild-type bacterium. By highlighting how NET degradation can be beneficial to the bacterium while promoting inflammation through IL-1β, inhibitors can start to be developed to limit MugA-dependent evasion strategies.

Results

Evaluation of a *C. jejuni* transposon library identifies a mismatch repair protein, MugA, involved with NET evasion. To determine if *C. jejuni* evades NET-mediated killing, *C. jejuni* or *Salmonella enterica* serovar Typhimurium were incubated with phorbol 12-myristate 13-acetate (PMA)-induced NETs. As expected, we observed a significant 1.33-fold decrease in *S*. Typhimurium CFUs after incubation with NETs, since this bacterium has been shown to be sensitive to NET killing (Figure 4.1A). In contrast, we observed a significant 1.52-fold increase in viable *C. jejuni* CFUs following incubation with NETs. This result suggests that *C. jejuni* is resistant to the antimicrobial activity of NETs (Figure 4.1A). Because *C. jejuni* induces NET formation yet is resistant to these structures, we hypothesized that *C. jejuni* could produce extracellular nucleases to evade NET killing by hydrolyzing the DNA that is associated with NETs. To identify these

125

Figure 4.1. Identification of a potential nuclease, MugA, through screening of a *C. jejuni* transposon library.

(A) NETs are not inhibitory to *C. jejuni* growth. *Salmonella* Typhimurium (ST - blue/light blue) and *C. jejuni* (CJ - red/pink) were incubated with NETs for three hours and then plated for viability. After incubation with PMA-induced NETs, percent growth was determined normalizing to bacteria along control. (B) Diagram demonstrating the transposon screen for *C. jejuni* nuclease production. A total of 8,640 transposon isolates were analyzed in the primary DNase agar screen. After the primary screen, 130 isolates remained which lacked nuclease production. After the secondary qPCR screen, 12 transposon isolates remained did not produce nuclease activity. (C) A *mugA*::hawkeye transposon isolate identified through the screen was sensitive to NET antimicrobial activity. Wild-type *C. jejuni*, *mugA*::hawkeye, and *Salmonella* Typhimurium were incubated with NETs and then plated on media for viability. (D) Gene neighborhood analysis of *mugA* within the *C. jejuni* genome and predicted operon was performed through Microbial Signal Transduction Database (MiST) analysis. (E) Prediction of the secondary structure of MugA using Phyre2. (F) Predicted protein scheme of MugA secondary structure through iTASSER analysis. Black bars designate coils, blue bars represent strands, and red bars represent helices. Multiple comparison testing was performed using ANOVA with Tukey's post-hoc test. $**p < .01$; $***p < .001$; $****p < .0001$
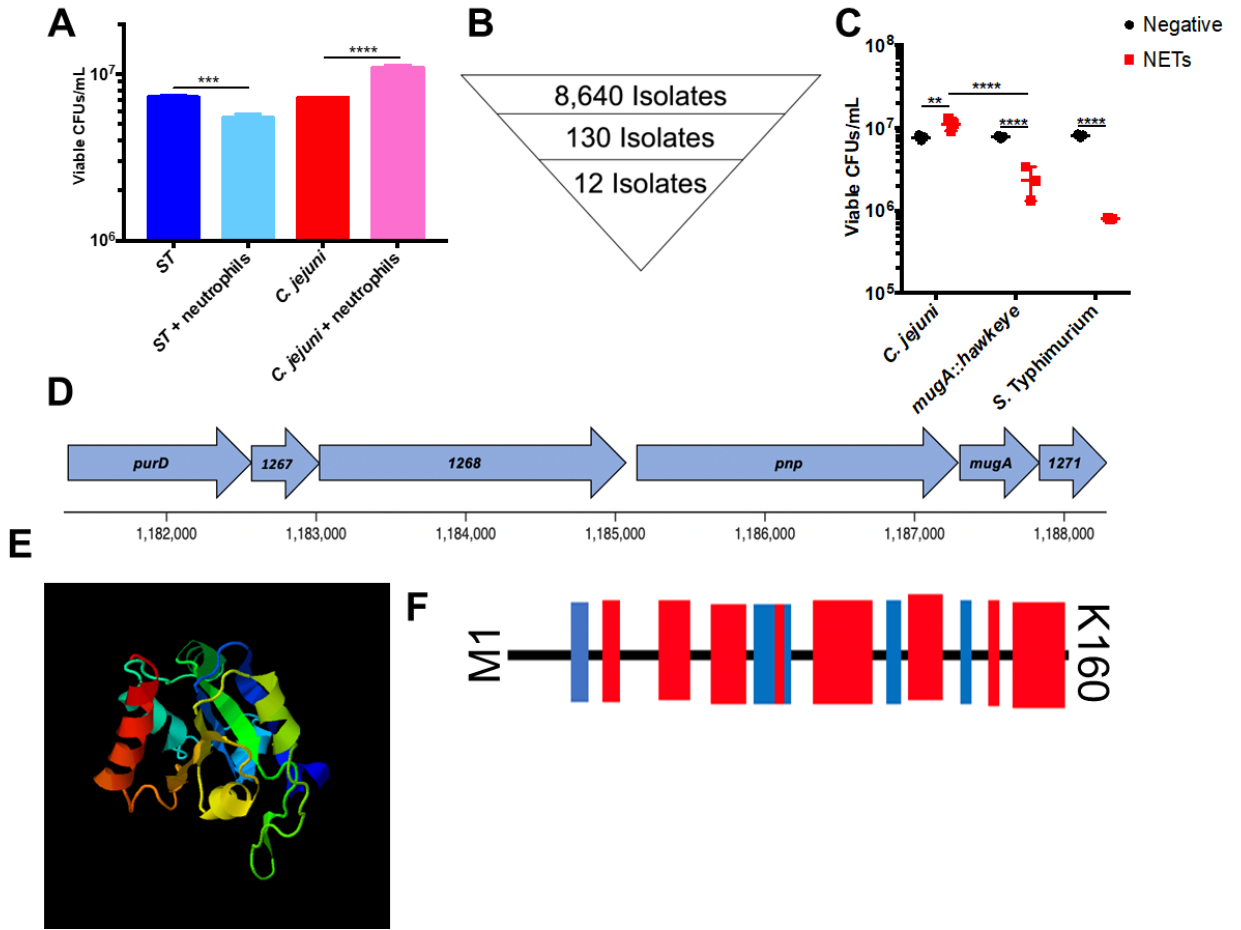
extracellular nucleases, we used a *C. jejuni* transposon mutant library (227,302) and screened 8,640 individual mutants for their ability to degrade DNA using a commercially available DNase agar. One hundred-and-thirty transposon mutants were found to lack a zone of clearing and selected for the secondary screen. (Figure 4.1B).

As nucleases associated with NET degradation are often secreted, we sought to specifically investigate cell-free supernatant associated nucleases. These 130 mutants were grown in Muller-Hinton broth with deoxycholate to induce protein secretion, as previously demonstrated (93). After growing to stationary phase, we collected the supernatants and incubated them with neutrophil DNA. After incubation, *C. jejuni* DNA was spiked in as a DNA extraction control. The abundance of intact neutrophil DNA was quantified using quantitative PCR on both human (*GAPDH*) and *C. jejuni* (*mapA*) DNA. Mutants lacking statistically significant changes in C_T values from DNA incubated with media alone were deemed lacking nuclease activity. After the secondary screen, twelve isolates without nuclease activity remained: *Cjj81176_0025* (*flgE*); *Cjj81176_0252* (*argD*); *Cjj81176_0580* (*citT*); *Cjj81176_0644* (*pstA*); *Cjj81176_0780* (type I site-specific deoxyribonuclease chain R); *Cjj81176_0803* (*napH*); *Cjj81176_0936* (cytosol aminopeptidase); *Cjj81176_1243* (*dnaJ-1*); *Cjj81176_1270* (*mugA*); *Cjj81176_1353* (*ceuD*); *Cjj81176_1425* (HrEpiB); and *Cjj81176_1585* (*hisD*) (Figure 4.1B; Table 4.1). As *Cjj81176_1270* (*mugA*) has been previously identified as a secreted protein in *C. jejuni*, we assayed this strain for NET antimicrobial activity. The *mugA* transposon isolate (*mugA*::hawkeye) was the only isolate sensitive to NET killing (Figure 4.1C), with a 3.33-fold decrease in viable CFUs/mL compared to wild-type which exhibited a 1.45-fold increase after incubation with NETs. The *mugA*::hawkeye NET killing activity resembled that of *Salmonella*, which had a 10.08-fold decrease in viable CFUs/mL when cultured with NETs (Figure 4.1C). Therefore, we hypothesized MugA assists *C. jejuni* in evading NET-mediated antimicrobial activity.

MugA is involved with *C. jejuni* evading NET entrapment and integrity of NETs. Using Phyre2 and iTASSER (219,220), MugA was predicted to encode numerous nucleotide binding residues (Figure 4.1D, E, F). We hypothesized that MugA functions as an extracellular nuclease. To test if MugA modulates *C. jejuni* - neutrophil interactions, we assayed for neutrophil activation and measured NETosis in infected neutrophils. To examine neutrophil activation, primary human neutrophils were infected with wild-type *C. jejuni* (WT), a non-polar deletion mutant of *mugA* (Δ*mugA*), or Δ*mugA* complemented with the plasmid-borne *mugA* (Δ*mugA*-p*mugA*). Utilizing CD11b$^+$ mean fluorescence intensity (MFI) as an output of neutrophil activation, wild-type, Δ*mugA*, and Δ*mugA*-p*mugA* infected neutrophils all displayed significantly higher activation marker than uninfected neutrophils, with 4.16-, 4.15-, and 4.46-fold increases, respectively (Figure 4.2A). This demonstrated that *mugA* is not involved in neutrophil activation. However, when extracellular DNA was measured as a proxy for intact NETs using SYTOX, we observed a significant increase in extracellular DNA staining from Δ*mugA* infected neutrophils when compared to wild-type infected neutrophils, indicative of higher NETosis (1.32-fold increase) (Figure 4.2B). To determine if MugA was involved with *C. jejuni* NET entrapment through DNA binding to the bacterium, we incubated PMA-induced NETs with wild-type, Δ*mugA*, or Δ*mugA*-p*mugA C. jejuni* and assayed for viable CFUs. In wild-type *C. jejuni*, there was a 2.89-fold increase in viable *C. jejuni* after incubation with NETs compared to bacteria treated with media (Figure 4.2C). However, when *C. jejuni* Δ*mugA* was incubated with NETs, we observed a statistically significant 3.15-fold decrease in viable CFUs when compared to bacteria incubated with media (Figure 4.2C). This phenomenon was also observed for *S. typhimurium* during incubation with NETs with a 5.51-fold decrease in viable CFUs when compared to bacteria treated with media alone (Figure 4.2C). In contrast, when Δ*mugA*-p*mugA* was similarly incubated with NETs and assayed for viable CFUs, we did not observe a statistically significant difference compared to wild-type bacterium (3.56-fold increase compared to bacteria treated with media) (Figure 4.2C). As entrapment facilitates the

Figure 4.2. MugA contributes to *C. jejuni* NET evasion.

(A) Neutrophil activation is maintained in a *C. jejuni mugA* deletion mutant. Neutrophils were either uninfected or infected with wild-type, Δ*mugA*, or *mugA* complement (Δ*mugA*-p*mugA*) for three hours under microaerobic conditions and then analyzed for neutrophil activation through CD11b. (B) MugA influences the magnitude of intact NET structures. Neutrophils were either uninfected or infected with wild-type, Δ*mugA*, or *mugA* complement (Δ*mugA*-p*mugA*) and stained with SYTOX green to measure extracellular DNA extrusion. (C) MugA leads to the evasion of NET antimicrobial activity of *C. jejuni*. Wild-type *C. jejuni*, Δ*mugA*, Δ*mugA*-p*mugA*, or *Salmonella* Typhimurium were incubated with PMA induced NETs and then plated on media for viable CFUs. (D) NETs entrap Δ*mugA C. jejuni* than wild-type *C. jejuni*. Wild-type or Δ*mugA C. jejuni* were incubated either with media alone or PMA induced NETs for one hour. After one hour, samples were loaded on a transwell apparatus with a known *C. jejuni* chemoattractant molecule, L-serine, in the bottom well. Chemotaxed bacteria were plated every fifteen minutes from the bottom well as a proxy for NET entrapment. Data were normalized to bacteria alone without NETs. (E) Δ*mugA* infected neutrophils result in more intact NETs compared to wild-type infected neutrophils. Neutrophils were incubated with wild-type, Δ*mugA*, or Δ*mugA*-p*mugA C. jejuni* and then stained for DNA (green) and citrullinated histone H3 (red). NETs could be seen with extracellular DNA studded with citrullinated histone H3. Scale bars are 10 μm. Multiple comparison testing was performed using ANOVA with Tukey's *post-hoc* test. *$p < .05$; **$p < .01$; ***$p < .001$; ****$p < .0001$
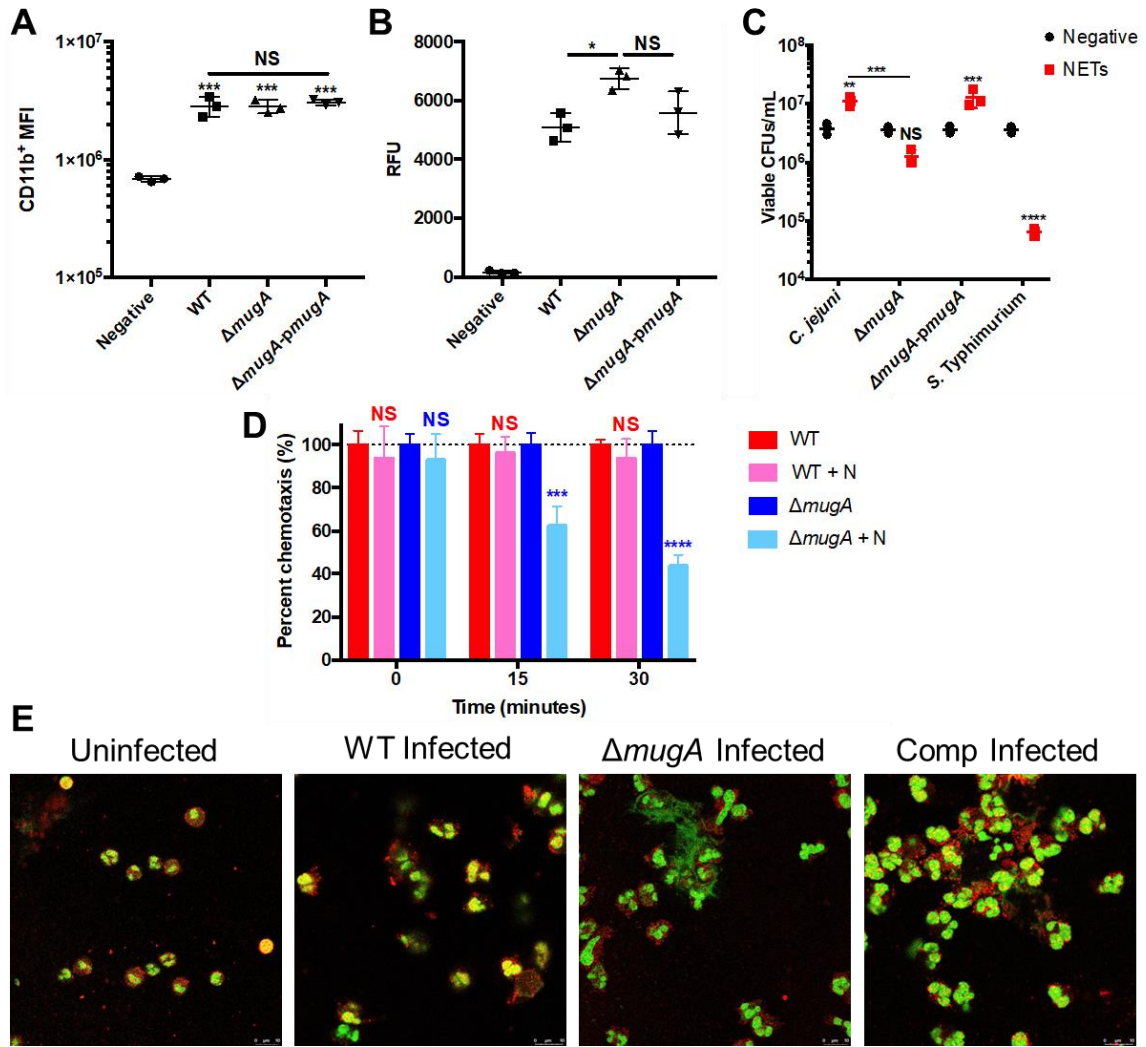
antimicrobial activity of NETs, we next sought to determine whether Δ*mugA* was differentially entrapped by NETs. To quantify entrapment, wild-type, Δ*mugA*, or Δ*mugA*-p*mugA* were incubated with PMA-induced NETs and placed in a transwell system where L-serine was added to the bottom chamber as a known chemotactic molecule. If *C. jejuni* degrades NETs, we predicted that the bacterium would chemotax into the L-serine containing chamber; however, if the bacterium is entrapped within the NETs, they would be less able to chemotax toward the L-serine, which would result in fewer CFUs in the bottom chamber. As predicted, we observed that approximately 38% and 56% of Δ*mugA* bacteria were unable to chemotax toward L-serine at fifteen and thirty minutes, respectively, while wild-type *C. jejuni* was unaffected (4% and 7% of bacteria unable to chemotax at fifteen and thirty minutes, respectively) (Figure 4.2D). Accordingly, when NETs were imaged, Δ*mugA* induced NETs appeared more intact, whereas wild-type infected neutrophils were degraded (Figure 4.2E). As entrapment of a pathogen is required for NET-associated antimicrobial proteins to function efficiently, we hypothesize that MugA degrades these structures to escape those activities, disperse into the extracellular environment, and facilitate *C. jejuni* growth.

To determine if MugA exhibits nuclease activity, we purified MugA containing a His tag (Figure 4.6-appendix). Nuclease activity was analyzed by incubating purified neutrophil genomic DNA with either purified MugA, control eluates from cultures containing the empty expression vector (EV), or purchased DNase as a positive control. Using SYTOX, extracellular DNA was quantified every five minutes over an hour-long time course. We observed significant decreases in SYTOX staining over the hour time course which also occurred for the DNase positive control. For example, DNA incubated with purchased DNase resulted in a 3.04-fold reduction in relative fluorescence units (RFU) at one hour, whereas MugA led to a 1.81-fold decline in RFUs, and the EV negative control led to a 1.36-fold decrease in RFU values (Figure 4.3A). To determine if MugA can also degrade NET DNA, NETs were induced from primary human neutrophils using PMA treatment for three hours and either purified MugA, EV eluates, or purchased

132
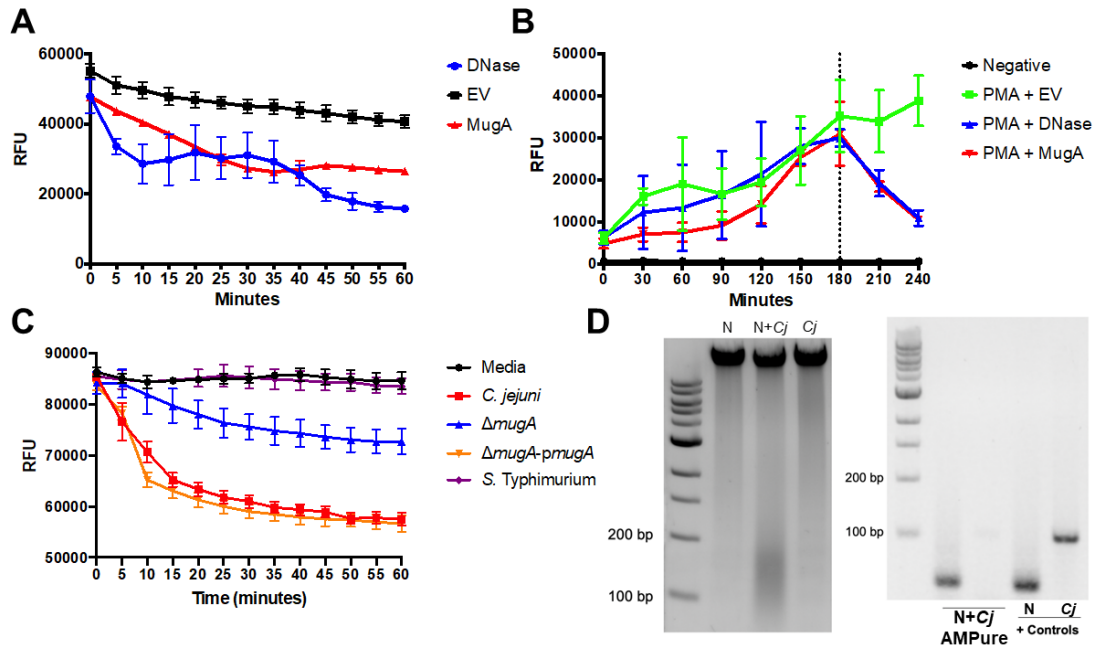
Figure 4.3. Pure MugA degrades neutrophil and NET-associated DNA.

(A) MugA can promote the degradation of neutrophil DNA as readily as pure DNase I. MugA (red), equal volume of empty vector (EV) (black), or DNase I (blue) was incubated with neutrophil DNA stained with SYTOX green (B) NETs can be degraded by the presence of MugA and DNase I. In the presence of SYTOX green, neutrophils were induced for NETs for three hours. After three hours, MugA (red), EV (green), or DNase I (blue) and measured for DNA hydrolysis through loss of SYTOX RFU. (C) Supernatant of wild-type and *mugA* complement lead to DNA degradation. Strains were grown in rich medium broth for 48 hours, whereby supernatants were isolated. After, NETs were incubated with cell-free supernatants and SYTOX green to measure DNA hydrolysis over an hour time course at 37°C. (D) Neutrophil-derived degraded DNA is formed when neutrophils are incubated with *C. jejuni*. To determine if degraded DNA was present under *C. jejuni* NETosing conditions, DNA was isolated from uninfected neutrophils (N), *C. jejuni* infected neutrophils (C+N), or *C. jejuni* alone (C). After imaging degraded DNA on a gel, DNA between 100-200 base pairs was extracted through AMPure bead size selection. The eluted DNA analyzed for human or *C. jejuni* origin.

DNase were added to the NETs. Using SYTOX to measure intact extracellular DNA, we observed increased RFUs over the three-hour PMA treatment, which suggests NETs were being produced. Following addition of the above nucleases, we observed significant decreases in RFUs for MugA and DNase-treated NETs, with decreases of 2.91 and 2.81-fold, respectively, when compared to the EV control (Figure 4.3B). As we observed NETs being degraded by MugA, we therefore hypothesized that MugA is a secreted nuclease. To examine this, *C. jejuni* was cultured with deoxycholate to induce flagellar type III secretion system effector secretion. When cell-free supernatants were extracted, we observed significant NET hydrolysis over an hour time course in wild-type and *mugA* complemented strains (Figure 4.3C). Additionally, we observed less NET hydrolysis in the Δ*mugA C. jejuni* strain and *S.* Typhimurium cultured in deoxycholate (Figure 4.3C). As *Salmonella* has been shown to not produce an extracellular nuclease, this verifies that a secreted nuclease, specifically MugA facilitates NET degradation and evasion. To confirm that *C. jejuni*-induced NETs are cleaved after induction, DNA was extracted from neutrophils (N), neutrophils incubated with *C. jejuni* (N+*Cj*), or *C. jejuni* (*Cj*) alone. In this, we observed degraded DNA products around 150 base pairs (Figure 4.3D). When the degraded product was extracted through AMPure size selection and amplified to determine if it was neutrophil or *C. jejuni* derived, the product amplified for human DNA, indicating the presence of degraded NET DNA (Figure 4.3D). Nucleosomes, which are the structural components of eukaryotic chromatin, contain approximately 147 base pairs of DNA wrapped around a central histone octamer (303). It has been previously demonstrated that degraded NETs are comprised of predominantly mononucleosomes, which are chromatin structures consisting of the histone octamer complex bound to 147 basepairs of DNA (140). Hence, we hypothesize *C. jejuni* induces NETs and that extracellular MugA degrades these NETs into mononucleosome structures.

MugA degraded NETs lead to inflammasome activation in macrophages through a TLR4- and NLRP3-dependent manner. During campylobacteriosis, IL-1β highly upregulated (58,59,283,284,304,305). As neutrophil chemotaxis to the site of infection can lead to increased IL-1β during murine campylobacteriosis (283), we hypothesized that degraded NETs promote macrophage-dependent inflammasome activation and IL-1β secretion. Specifically, NET degradation into mononucleosomes and extracellular histones leads to inflammasome-dependent IL-1β production, however, whether this is occurring during campylobacteriosis was unknown (140,301,306,307). To determine if *C. jejuni* induced NETs can lead to macrophage inflammasome activation, wild-type infected neutrophils were incubated with THP-1 differentiated macrophages after removal of extracellular bacteria. There was a significant 13.2-fold increase in IL-1β in wild-type infected neutrophils incubated with macrophages compared to uninfected neutrophils incubated with macrophages (Figure 4.4A). However, when Δ*mugA* infected neutrophils were incubated with macrophages, there was a significant 1.59-fold decrease in IL-1β (Figure 4.4A). When plasmid-borne *mugA* was complemented in a Δ*mugA* background, there was a 1.06-fold increase compared to wild-type infected (Figure 4.4A). Because NETS are not generated in Δ*sliP* infected neutrophils, we measured IL-1β in Δ*sliP* infected neutrophils incubated with macrophages to see if NETs regulate this process (Figure 4.4A). As a result, there was a 1.33-fold reduction in IL-1β from macrophages incubated with Δ*sliP*-infected neutrophils when compared to those incubated with wild-type infected neutrophils (Figure 4.4A). Hence, we hypothesize that *C. jejuni* induced NETs lead to inflammasome activation in adjacent macrophages via sensing of degraded NET components by an unknown mechanism.

To investigate whether sensing of MugA degraded NETs are a cause of inflammasome activation, MugA was incubated with PMA induced NETs and cell-free supernatants were incubated with either wild-type (WT), NAIP$^{-/-}$, NLRC4$^{-/-}$, or MCC950 (chemical inhibitor of NLRP3) treated differentiated THP-1 cells (293). After one hour, supernatants were collected from macrophages and IL-1β

135

Figure 4.4. MugA-dependent NET degradation leads to macrophage NLRP3 inflammasome activation in a TLR4-dependent manner.

(A) *C. jejuni*-induced NETs and degraded NETs lead to THP-1 macrophage inflammasome activation and resultant IL-1β production. Neutrophils (N) were incubated with wild-type (WT), Δ*mugA* (unable to degrade NETs), *mugA* complemented with plasmid-borne mugA (Δ*mugA*-p*mugA*), or Δ*sliP* (unable to induce NETs) *C. jejuni* and then incubated with wild-type primed THP-1 cells for one hour. After incubation, cell-free supernatant was isolated and analyzed for IL-1β production. (B) MugA-degraded NETs lead to NLRP3-dependent inflammasome activation. PMA induced NETs were incubated with 10 μM MugA or protein eluents from *E. coli* harboring empty vector (EV) and then incubated with primed wild-type (red), NAIP deficient (NAIP$^{-/-}$, pink), NLRC4 deficient (NLCR4$^{-/-}$, green), or NLRP3 chemically blocked (MCC950, blue) THP-1 macrophages. After incubation, cell-free supernatant was isolated and analyzed for IL-1β production. (C) MugA-dependent NET degradation NLRP3 inflammasome activation is through TLR4 signaling. Before incubation of wild-type or NLRP3 blocked macrophages, cells were incubated with a TLR4 neutralizing antibody. After incubation, cell-free supernatant was isolated and analyzed for IL-1β production. (D) Clinical fecal samples of campylobacteriosis had significantly higher IL-1β production than uninfected hosts. Statistical analyses of representative fecal samples were performed using a nonparametric Mann-Whitney U test between uninfected and infected groups. Multiple comparison testing was performed using ANOVA with Tukey's *post-hoc* test. $^*p < .05$; $^{**}p < .01$; $^{***}p < .001$; $^{****}p < .0001$
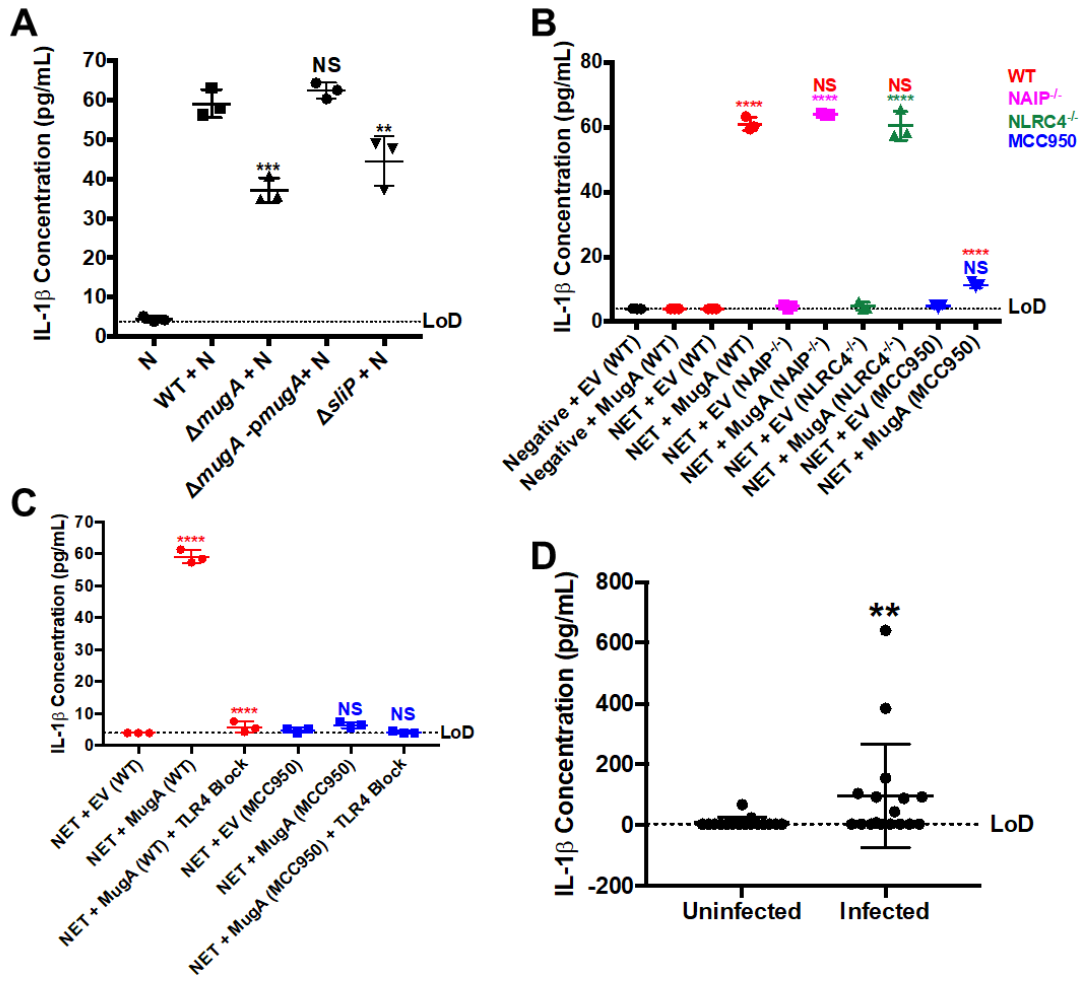
concentrations quantified. We observed robust IL-1β production in wild-type macrophages incubated with MugA-degraded NETs with a 15.61-fold increase in IL-1β concentration when compared to NETs incubated with the EV control (Figure 4.4B). In MugA degraded NETs incubated with NAIP$^{-/-}$ THP-1 macrophages, we observed a 13.62-fold increase in IL-1β concentration compared to NETs incubated with EV (1.05-fold increase compared to WT THP-1 macrophages) (Figure 4.4B). Additionally, we observed a similar response in NLRC4$^{-/-}$ macrophages with a 12.69-fold increase in IL-1β concentration when incubated with MugA degraded NETs compared to NETs incubated with EV (1.01-fold decrease compared to WT THP-1 macrophages) (Figure 4.4B). However, we observed significantly lower IL-1β in NLRP3 blocked macrophages. For example, in MCC950 pretreated WT THP-1 macrophages, there was only a 2.37-fold increase in IL-1β abundance compared to EV treated NETs, along with a 5.37-fold decrease compared to WT THP-1 macrophages (Figure 4.4B). Hence, we conclude that MugA degraded NETs lead to macrophage inflammasome activation in an NLRP3-dependent manner.

TLR4 has been shown to bind and be stimulated by DNA associated with histones, resulting in NLRP3 priming (140,308,309). We sought to determine if NLRP3 becomes activated in response to TLR4 binding to degraded NET DNA-histone complex. To determine if TLR4 is responsible for NLRP3 inflammasome activation, wild-type and MCC950 incubated wild-type THP-1 cells were pre-treated with a TLR4 neutralizing antibody before incubation with either NETs incubated with EV or MugA. In wild-type THP-1 cells treated with TLR4 blocking antibody, MugA-induced IL-1β secretion was significantly decreased when compared to isotype control treated THP-1 cells incubated with MugA degraded NETs (Figure 4.4C). In addition, when NLRP3 and TLR4 were blocked and macrophages treated with MugA degraded NETs, no detectable IL-1β was produced (Figure 4.4C). As such, we conclude that MugA degraded NETs bind to and stimulate TLR4, which results in downstream signaling and NLRP3-dependent inflammasome activation.

While IL-1β has been investigated heavily within animal models of campylobacteriosis, little research has investigated this cytokine during human infection. As we hypothesize that IL-1β is relevant during human campylobacteriosis, we sought to quantify this cytokine in human fecal samples from patients infected with *C. jejuni*. Interestingly, infected patients exhibited significantly increased concentrations of IL-1β when compared to uninfected patients (10.32-fold increase) (Figure 4.4D). Hence, *C. jejuni* induced NETs and subsequent MugA-dependent degradation of those structures could promote clinical manifestation of campylobacteriosis.

MugA is necessary to induce persistent, long-term infection and inflammation in the murine model of campylobacteriosis. As MugA appeared to be facilitating *C. jejuni* NET survival and inflammation through NET degradation, we sought to determine whether MugA impacts disease in an animal model. IL-10$^{-/-}$ mice were orally infected with wild-type or Δ*mugA* and weighed throughout infection. From this, we determined that mice infected with wild-type *C. jejuni* gradually lost weight, while uninfected and Δ*mugA* infected mice either maintained or gained weight (Figure 4.5A). When the feces from these mice were plated for viable CFUs to quantify colonization, Δ*mugA C. jejuni* was found to be significantly reduced in its ability to colonize, with 785.37-fold decrease compared to wild-type infected mice at ten days post-infection within the feces (Figure 4.5B). While the bacterial burden in mice infected with wild-type *C. jejuni* increased during the study, individual mice were able to clear Δ*mugA*, but could begin shedding bacteria again later in the study (Figure 4.5C). As mice are coprophagic, we hypothesize this could be the result of mice consuming Δ*mugA* contaminated feces from cage mates. After ten days post-infection, we sought to determine the bacterial burden in the ceca, colon, and spleen to determine if colonization could occur within the tissues. In the cecal content, we observed an average 7.69-fold decrease in viable CFUs/mL in Δ*mugA* infected mice when compared to wild-type infected mice. Within these groups, it appeared that 100% of wild-type infected mice harbored

Figure 4.5. MugA is necessary for colonization, persistence, and inflammation in the murine model of campylobacteriosis.

(A) Percent body weight changes of mice uninfected (black) or infected with wild-type (red) or Δ*mugA* (blue) *C. jejuni* over the ten-day infection study. Percent body weight changes were normalized to the weights of each mouse before savage treatment. (B) Fecal viable CFUs of each mouse over the ten-day infection study. Feces were collected each day and plated on *Campylobacter* specific media and incubated for three days under microaerobic conditions. (C) Monitoring of individual mice fecal viable CFUs/mL in wild-type (red) and Δ*mugA* (blue) infected mice. (D) Viable CFUs from the cecal content, (E) colon, and (F) spleen in *C. jejuni* infected mice ten days post-infection. (G) Serum cytokine expression levels for each mouse per treatment group. Levels of cytokines IFN-γ, KC, IL-1β, IL-6, and TNF-α were analyzed through flow cytometry-based beads and concentrations were determined through a standard curve for each protein. Multiple comparison testing was performed using ANOVA with Tukey's *post-hoc* test. $**p < .01$; $***p < .001$; $****p < .0001$
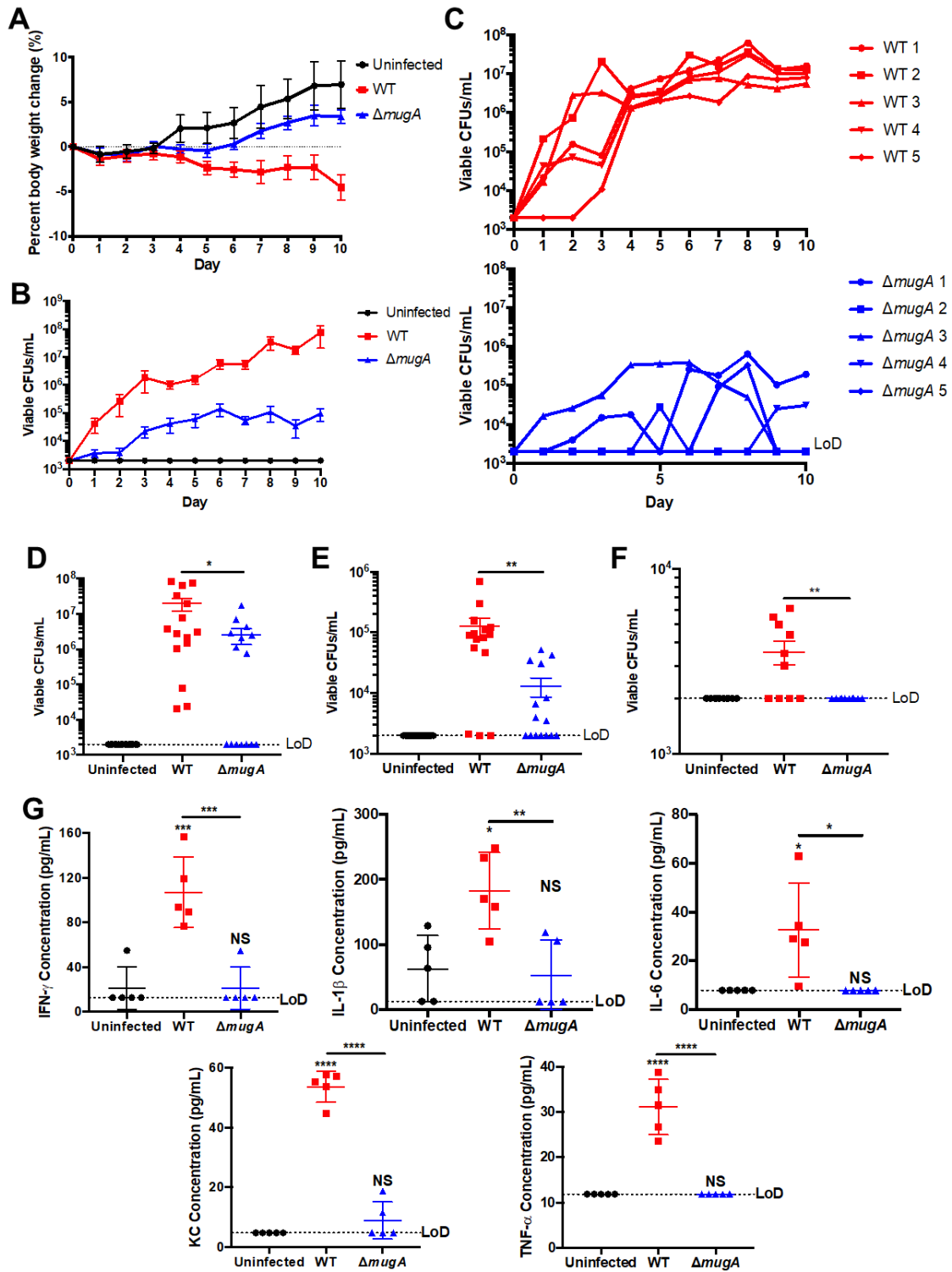
viable cecal *C. jejuni*, while only 53% of Δ*mugA* were colonized (7.69-fold decrease in viable CFUs) (Figure 4.5D). Furthermore, within colonic tissue, we observed a decrease in viable CFUs in Δ*mugA* infected mice, with a 9.73-fold decrease when compared to wild-type infected mice. Within these groups, it appeared that 87% of wild-type infected mice harbored viable colonic *C. jejuni*, while only 60% of Δ*mugA* infected mice were colonized (9.74-fold decrease in viable CFUs) (Figure 4.5E). When we examined the spleen for extraintestinal bacterial dissemination, we observed a significant 1.78-fold decrease in viable splenic *C. jejuni* in Δ*mugA* infected mice compared to wild-type infected mice (Figure 4.5F). As a Δ*mugA* mutant is sensitive to NET killing, we hypothesize that *C. jejuni* induced NETs constrain the bacterium to the colon. By NETs entrapping the bacterium with antimicrobial activity, a *mugA* mutant would not be able to propagate within the host and disseminate to an extraintestinal site.

To understand if MugA is involved with host inflammation, we sought to characterize immune signaling during infection. When cytokine profiles were compared between uninfected, wild-type, and Δ*mugA* infected mice, proinflammatory cytokines, including IL-1β, IL-6, IFN-γ, KC, and TNF-α were all decreased in Δ*mugA* infected mice compared to wild-type infected mice (Figure 4.5G). Specifically, IL-1β, IL-6, IFN-γ, KC, and TNF-α were significantly decreased 3.48-, 4.14-, 5.06-, 6.03-, and 2.62-fold in Δ*mugA* infected mice when compared to wild-type infected mice, respectively (Figure 4.5G). Hence, we hypothesize that a Δ*mugA* mutant is unable to colonize to the same extent as wild-type bacterium, nor produce inflammatory mononucleosomes from NET degradation, resulting in blunted inflammatory signaling and cytokine expression.

Discussion

Campylobacter spp. are the leading cause of bacterial-derived gastroenteritis in both developed and developing countries with *C. jejuni* being the species that most often causes these infections. The molecular mechanisms of disease, including colonization and inflammatory responses, are understudied

compared to less-prevalent gastrointestinal pathogens. *C. jejuni* lacks numerous virulence factors classically associated with gastrointestinal pathogens, including the production of various toxins and canonical secretion systems. Hence, we hypothesize that colonization and the subsequent inflammatory response to the pathogen is derived from using unique factors and misdirection from the host immune response. Neutrophils play a significant role during the inflammatory response during campylobacteriosis. Our group and others have shown neutrophils to play an important role not only in inflammation, but also tissue pathology through numerous cellular processes (58). In this, we have previously reported *C. jejuni* as a potent inducer of NETs, which are cytotoxic structures released by neutrophils which damage neighboring cells and possess antimicrobial properties (232). As we do not observe significant antimicrobial activity of NETs to *C. jejuni*, we sought to perform a genome-wide screen for extracellular nucleases, which may facilitate NET evasion.

To assay for extracellular nucleases, an arrayed transposon *C. jejuni* library (227) (8,640 individual mutants) was analyzed with DNase agar media to visualize loss of DNA clearance phenotypes. After screening the transposon library, twelve isolates did not possess extracellular nuclease activity. These isolates included *flgE*, *argD*, *citT*, *pstA*, type I site-specific deoxyribonuclease chain R, *napH*, a cytosol aminopeptidase, *dnaJ*, a DNA glycohydrolase (*mugA*), *ceuD*, HrEpiB, and *hisD*. As many of the transposon hits belonged to *C. jejuni* metabolism, there could be a crucial link between metabolism and nuclease production. As another group observed the secretion of MugA from another strain of *C. jejuni*, we sought to further investigate this protein.

When we analyzed NET-dependent killing in a non-polar deletion mutant of *mugA*, we observed that this mutant still induced NETosis, but exhibited a significant decrease in viable CFUs when co-cultured with these structures. While the field has believed that NETs are solely antimicrobial due to NETs being studded with numerous antimicrobial proteins such as neutrophil elastase, myeloperoxidase, and cathepsin G, it is now being appreciated that NET DNA and

associated histones possess antimicrobial activity (310–312). As we observed significant entrapment of *C. jejuni* in our Δ*mugA* strain, we hypothesize that NET entrapment allows for higher antimicrobial activity within this complex, due to the inability of the bacterium to degrade NET associated DNA. Hence, we believe that MugA plays a significant role in NET evasion strategies in *C. jejuni* through its capability to degrade NET DNA.

During campylobacteriosis, IL-1β is one of the most upregulated cytokines. As such, understanding the induction of this proinflammatory cytokine may be crucial to developing anti-inflammatory therapeutics for chronic and persistent *C. jejuni* infections. Previously, it was shown by other groups that *C. jejuni* stimulates inflammasome activation through NLRP3, which can sense a wide array of ligands, including extracellular ATP, toxins, along with bacterial, viral, and fungal substrates (313). Furthermore, recent research determined that NETs can also stimulate macrophage and endothelial NLRP3 inflammasomes, especially the products of degraded NETs (140,141,307,314). In the present study, we determined that MugA-dependent NET degradation leads to NLRP3-dependent macrophage inflammasome activation, which results in the secretion of IL-1β into the environment. Hence, we hypothesize that there are multiple ways for NLRP3 to be stimulated during campylobacteriosis, resulting in the potent upregulation of IL-1β. While IL-1β has been extensively investigated in campylobacteriosis, the cognate receptor, IL-1R, has not been investigated for modulating infection to amplify the innate immune response. These could be promising targets during campylobacteriosis for therapeutics, as this would drastically improve tissue repair.

Because we observed that MugA functions as an extracellular nuclease and degrades NETs to promote evasion and inflammatory signaling, we sought to determine whether this protein promotes disease in a murine model of campylobacteriosis. After mice were orally inoculated with either wild-type or Δ*mugA,* we found that Δ*mugA* was unable to colonize mice to the level of wild-type. In fact, in wild-type infected mice, where bacterial burden in the feces has a positive correlation with time, individual mice infected with Δ*mugA* would clear the

144

infection, but then get re-infected during the infection time course. We hypothesize the clearance of Δ*mugA* during infection is at least partially due to NET-entrapment and the antimicrobial activity of the associated proteins. Additionally, we hypothesize the reinfections which occurred during the experiment were due to the coprophagic nature of the mice, whereby their immune system would clear the infection. Finally, when inflammatory cytokine expression, namely IL-1β, IL-6, IFN-γ, KC, and TNF-α, was analyzed in these mice, uninfected and Δ*mugA* mice had no significant upregulations in inflammatory cytokine abundance compared to wild-type infected mice. Hence, *mugA* is crucial for *C. jejuni* to colonize within an infected host, resulting in the upregulation of inflammatory cytokine expression.

In the future, we could use our knowledge about MugA to develop nuclease-targeted therapeutics that can mitigate campylobacteriosis. Specifically, since Δ*mugA* was unable to colonize mice, this could be an attractive alternative to antibiotics to lower bacterial burden during long-term *C. jejuni* infections.

Materials and Methods

Bacterial cultures and culture conditions. *Campylobacter jejuni* 81-176 strain DRH212 was stored at −80°C in MH broth supplemented with 20% glycerol. In this study, non-polar deletions and plasmid-borne strains of *mugA* were constructed in wild-type *C. jejuni* DRH212 as previously described (262). Plasmid-borne *mugA* was done through insertion of *mugA* into pECO102. All strains were routinely grown for 24 hours on selective media (10% sheep's blood, 40 μg/ml cefoperazone, 100 μg/ml cycloheximide, 10 μg/ml TMP and 100 μg/ml vancomycin) before passing onto Mueller-Hinton agar containing 10% sheep's blood and 10 ug/ml trimethoprim (TMP) at 37°C under microaerobic conditions (85% N2, 10% CO2 and 5% O2) for an additional 24 hours. *E. coli* expression strain C3013 containing pQE30-*mugA* were constructed as previously described (263). Briefly, *mugA* was inserted into pQE30 to generate N terminal His tagged MugA. *E. coli* strains were stored in Luria-Bertani (LB) broth supplemented with

20% glycerol at −80°C and grown shaking at 37°C in LB broth supplemented with ampicillin for purification as described below.

Isolation of primary human neutrophils. Neutrophils were isolated as previously described (232,264). Briefly, 10 ml of blood was drawn from healthy donors into heparinized Vacutainer tubes and mixed 1:1 with sterile 1× PBS (approval UTK IRB-18-04604-XP) (172). After mixing, 10 ml of lymphocyte separation medium was underlaid. Following centrifugation at 1,400 rpm for 30 min, the top layers were aspirated off, leaving the red blood cell and neutrophil pellet. Pellets were resuspended in 20 ml Hanks' balanced salt solution and 20 ml 3% dextran in 0.9% NaCl. After incubating at room temperature for 20 min, the upper layer was transferred to a new tube. Following centrifugation at 400 x *g* for 5 min and aspiration of the supernatant, the pellet was washed with 20 ml ice-cold 0.2% NaCl and 20 ml ice-cold 1.6% NaCl two times. Following the final aspiration, the neutrophil pellet was resuspended in 10 ml RPMI 1640. Neutrophil viability and counts were performed through Trypan blue stain.

Cell culture of THP-1s. Wild-type, NAIP^{-/-}, and NLRC4^{-/-} THP-1 cells were propagated with RPMI 1640 supplemented with 10% (volume/volume) heat-inactivated FBS, 0.05 nM β-mercaptoethanol, 100 IU/mL penicillin, and 100 ug/mL streptomycin at 37°C in an aerobic, humidified cell culture incubator. From -140°C stock, cells were propagated in non-tissue culture treated 6 well plates. After approximately a week of propagation, cells were allowed to propagate in 10 cm Petri dishes for experimentation. Two days before experimentation, cells were plated without antibiotics in a 48 well plate at a concentration of 10^5 cells per well and incubated with 400 ug/mL phorbol 12-myristate 12-acetate (PMA) for 24 hours for differentiation of monocytes into macrophages. After 24 hours, adherent macrophages were primed with 100 ng/mL Pam3CSK4 (Invivogen) for 16 hours. For experiments involving the chemical inhibition of NLRP3, adherent macrophages were incubated with 1 µM MCC950 (Sigma Aldrich) one hour before

experimentation (293). For blocking TLR4 on wild-type and MCC950 THP-1 cells, 50 µl of TLR4-neutralising antibody (InvivoGen, Cat. pab-hstlr4) was added to each well and incubated for one hour.

NET Entrapment Transwell Assay. Bacteria were grown as previously described (59). After purification of neutrophils, as previously described, NETs were induced by the addition of 100 µM phorbol 12-myristate 12-acetate (PMA) at 37°C for three hours under aerobic conditions. After induction of NETs, 10^6 CFUs of wild-type or $\Delta mugA$ *C. jejuni* were incubated with the NETs under microaerobic conditions for one hour at 37°C. After NET entrapment, samples were placed in the top well of a transwell system, where the bottom well contained RPMI 1640 containing 100 mM L-serine. Samples were taken every fifteen minutes for viable CFU plating to measure bacterial chemotaxis. Data was normalized to bacteria alone with media to account for chemotaxis deficiencies.

Protein induction and native purification of MugA. Protein induction and purification was performed as previously described (227,263). Briefly, *E. coli* strains C3013 encoding *mugA* or empty pQE-30 vector were grown overnight in LB broth containing 100 µg/ml ampicillin at 37°C shaking. Cultures were then back-diluted by adding 1 mL overnight culture in 100 mL LB broth containing 100 µg/ml ampicillin. Culture was grown at 37°C shaking for two hours before spiking in 100 µM isopropyl-β-d-thiogalactopyranoside (IPTG) to induce protein expression. Cultures were allowed to incubate for an additional two hours at 37°C shaking. After incubation, cells were pelleted at 2,147 RCF for 10 min. After centrifugation, the pellets were resuspended in lysis buffer (50 mM NaH_2PO_4, 300 mM NaCl, 10 mM imidazole, pH 8.0) before sonication on ice (6 rounds of 15 s each at 45 A). Cell lysates were then pelleted at 2,147 RCF for 10 min before incubating the resultant supernatant with washed Ni-nitrilotriacetic acid (Ni-NTA) for one hour at 4°C rocking. After the incubation, the MugA resin was packed in a 20-ml chromatography column before it was washed three times with 4 ml wash buffer

(50 mM NaH$_2$PO$_4$, 300 mM NaCl, 20 mM imidazole, pH 8.0) and eluted in three 750-µl fractions of elution buffer (50 mM NaH$_2$PO$_4$, 300 mM NaCl, 250 mM imidazole, pH 8.0). Each wash and elution fraction were diluted 1:1 with a Laemmli buffer containing β-mercaptoethanol and boiled for 10 minutes. Ten microliters of lysate samples were loaded onto a 12.5% SDS-PAGE gel and run for 1 hour at 150 V at room temperature and stained with Coomassie to ensure protein purification (18 kDa). Elution fractions were then pooled and dialyzed using a dialysis buffer (200mM NaCl, 2mM DTT, and 20mM HEPES buffer (pH 7.5) three times at 4°C spinning. After dialysis, protein was collected from the dialysis cassette using a syringe and stored at 4°C until future use.

Nuclease Activity of MugA. To test if MugA can degrade neutrophil DNA, 10 ng of purified MugA or equal volume of empty vector (EV) eluate were combined with 100 ug DNA along with 1.0 µM SYTOX Green and DNase buffer (Promega) in a black 96 well plate. As a positive control, pure RNase-free 1U DNase I was incubated with DNA. The plate was incubated in a plate reader, where it was incubated at 37°C. Every 5 minutes, fluorescence was measured in a plate spectrophotometer. Degraded DNA was compared to the EV control and pure DNase positive control.

Analysis of *C. jejuni* NET induction by flow cytometry. Flow cytometry detection of *C. jejuni* induced NETs was performed as previously described (232,264). Briefly, *C. jejuni* strains were resuspended in RPMI 1640 and incubated with neutrophils for 3 hours under microaerophilic conditions at an equal multiplicity of infection (MOI) of 50:1 (bacteria: neutrophil). Following incubation, these reactions were aliquoted into wells of a 96-well plate and centrifuged at 400 x g. Pelleted cells were washed three times with sterile 1x PBS cells before incubation with Live/Dead Near-IR (NIR) stain for 25 min at room temperature. After incubation, cells were blocked with 1% goat serum for 10 min, then incubated with CD11b and MPO antibodies for 30 min (173). Cells were subsequently fixed in the

fixation buffer for 10 min at room temperature and stored at 4°C until flow cytometry analysis. Samples were analyzed using an LSR II flow cytometer and data were processed using BD FlowJo software. Statistical analysis was performed using unpaired t tests and significance inferred at p < .05.

Analysis of *C. jejuni* NET induction by SYTOX assay. SYTOX NET quantification was performed as previously described (232,264). Briefly, Following the *C. jejuni* NET induction described above, cells were added to wells of black 96-well plates and centrifuged at 400 x *g*. Supernatants were discarded and 1.0 µM SYTOX Green was added to each sample and incubated under microaerobic conditions at 37°C for one hour (174). After incubation, cells were centrifuged at 400 x *g* and the supernatant was discarded. The cells were washed once with 1× PBS and then resuspended in 100 µl 1× PBS. SYTOX fluorescence was measured at 504/523 nm using a BioTek Synergy microplate reader. Statistical analysis was performed using unpaired *t* tests and significance inferred at *p* < .05.

Inflammasome Activation assay in THP-1 cells. To determine if MugA-degraded NETs lead to inflammasome activation in macrophages, 10^6 purified neutrophils were incubated with 300 mg/mL PMA for three hours at 37°C to induce NETosis. After three hours, 10 ng of MugA or equal volume of EV were incubated with the induced NETs and incubated for one hour at 37°C to allow nuclease activity. After one hour, cells were spun at 400 X G for 5 minutes, and the supernatant was saved as the degraded DNA fragment. Once THP-1 cells were primed as previously described, the supernatant containing the degraded DNA fragments were added to the differentiated, primed THP-1 cells. The supernatant was allowed to incubate with the THP-1 cells for three hours 37°C under aerobic conditions to allow for inflammasome activation. After three hours, the supernatant was pulled off, which contained IL-1β. The supernatant was spun at 1000 X G for 30 minutes to ensure there were no cellular components present in the

supernatant. The cleared supernatant was saved and used for an IL-1β ELISA per manufacturer recommendations (R&D).

Infection of IL-10$^{-/-}$ mice with *C. jejuni*. All animal protocols were approved by the Institutional Animal Care and Use Committee at the University of Tennessee - Knoxville (UTK IACUC protocol #2885). As previously described, *C. jejuni* wild-type DRH212 and Δ*mugA* were grown on *Campylobacter*-specific medium and Gram stained to ensure culture purity prior to inoculation (59). This culture was streaked on *Campylobacter*-selective media and incubated at 37°C under microaerophilic conditions for 48 hr. Suspensions of *C. jejuni* were made in sterile PBS and diluted to an OD600 of 10. Five female specific pathogen free 8- to 12-week-old IL-10$^{-/-}$ C57BL/6 mice were gavaged with a single dose of 10^{10} CFUs per mouse of *C. jejuni* wild-type strain DRH212 or the Δ*mugA* mutant. Additionally, five female mice were mock infected with sterile 1× PBS. Each day for 10 days, approximately 20 mg of feces from one sample from each animal was immediately weighed out and diluted 1:10 in PBS. The remaining samples were immediately frozen at −80°C. Diluted samples were further serially diluted in PBS to 10^{-8}, and 100 µl of each dilution was plated on *Campylobacter*-specific medium. The plates were then incubated at 37°C under microaerophilic conditions for 48 hours before *Campylobacter* loads were determined. After 10 days post-infection, blood was collected by cardiac puncture and mice were euthanized as previously described. From the blood, serum was collected and frozen at −20°C for further analyses. Ceca, colons, and spleens were excised from each mouse and placed in sterile 1X PBS. Colons were additionally rolled in Swiss Rolls and placed in formalin solution before being fixed in paraffin. To determine bacterial load in these tissues, ground tissue was weighed and diluted 1:10 in PBS. Diluted samples were further serially diluted in PBS to 10^{-8}, and 100 µl of each dilution was plated on *Campylobacter*-specific medium.

Quantification of proinflammatory cytokines from murine sera. Murine cytokines from sera were quantified using the BioLegend LEGENDplex Anti-Virus response panel in a V-bottom plate per the manufacturer guidelines. Briefly, sera were plated, alongside a standard curve of known concentrations for various cytokines. Assay buffers were added to each well, along with mixed beads that had been sonicated in water baths and vortexed to ensure homogeneity. The plate was sealed, wrapped in aluminum foil, and shook on a plate shaker at 800 rpm for two hours at room temperature. After incubation, the plate was centrifuged at 250 X G for 5 minutes using a swinging basket. After centrifugation, the plate seal was removed, and the supernatant was immediately flicked off into a bucket. The wells were then washed using the manufacturer wash buffer twice before the detection antibody was added to each well. The plate was sealed and covered in aluminum foil and shook on a plate shaker at 800 rpm for one hour at room temperature. After incubation, a streptavidin-phycoerythrin solution was added to the wells and the plate was sealed and wrapped in aluminum foil, where it incubated on a plate shaker at 800 rpm for 30 minutes at room temperature. After incubation, the plate was centrifuged and washed as previously described. Once the preparation was complete, the samples were resuspended in wash buffer until flow cytometry analysis. Samples were analyzed using an LSR II flow cytometer and data were processed using the BioLegend LEGENDplex data analysis software. Cytokine concentrations were determined due to the standard curve generated by standard bead concentrations.

Acknowledgments

Table 4.1. Twelve *C. jejuni* transposon isolates identified as nuclease deficient:

Locus	Gene Name
CJJ81176_0025	Flagellar hook protein (*flgE*)
CJJ81176_0252	Acetylornithine aminotransferase (*argD*)
CJJ81176_0580	Membrane protein (*citT*)
CJJ81176_0644	Phosphate ABC transporter, permease protein (*pstA*)
CJJ81176_0780	Type I site-specific deoxyribonuclease chain R
CJJ81176_0803	Ferredoxin-type protein (*napH*)
CJJ81176_0936	Cytosol aminopeptidase
CJJ81176_1243	Chaperone protein (*dnaJ-1*)
CJJ81176_0779	DNA glycohydrolase (*mugA*)
CJJ81176_1353	Enterochelin ABC transporter, ATP-binding protein (*ceuD*)
CJJ81176_1425	HrEpiB
CJJ81176_1585	Histidinol dehydrogenase (*hisD*)

Table 4.2. Primers used for *mugA* (5'-3')

mugA F	CATGGAAGAAGCTGCAAAAG
mugA R	ATCATCATGCCAGAGTGTAG

Table 4.2 Continued:

SOE *mugA* F	GTGAGTGAATTTCTAACTCAGGATCCTCAAAAAATTTACA AAATAA
SOE *mugA* R	TTATTTTGTAAATTTTTTGAGGATCCTGAGTTAGAAATTCA CTCAC
mugA complement F	GGATCCGTGAGTGAATTTCTAA
mugA complement R	GGATCCTTATTTTGTAAATTTTTTGATT
JJ13	TGCTCTAGATTTATGATATAGTCGATA

Table 4.3. Strains used in the *mugA* study

Genus and Species	Strain	Description	Source
Campylobacter jejuni	DRH212	Wild-type *C. jejuni*	This study
Campylobacter jejuni	DRH212-pECO102	*C. jejuni* harboring empty plasmid pECO102	This study
Campylobacter jejuni	DRH212 Δ*mugA*	*mugA* deletion strain of *C. jejuni*	This study
Campylobacter jejuni	DRH212 ΔmugA-pmugA	*sliP deletion strain of C. jejuni complemented with pECO102-sliP*	This study

154

Table 4.3 Continued:

Campylobacter jejuni	DRH212 ΔflgE	*flgE deletion strain of C. jejuni*	(225)
Escherichia coli	C3013-pQE30	*Empty vector expression E. coli strain*	This study
Escherichia coli	C3013-pQE30-mugA	*His tagged mugA expression E. coli strain*	This study
Campylobacter jejuni	DRH212-mugA::hawkeye	*C. jejuni strain harboring a transposon insertion in mugA*	This study
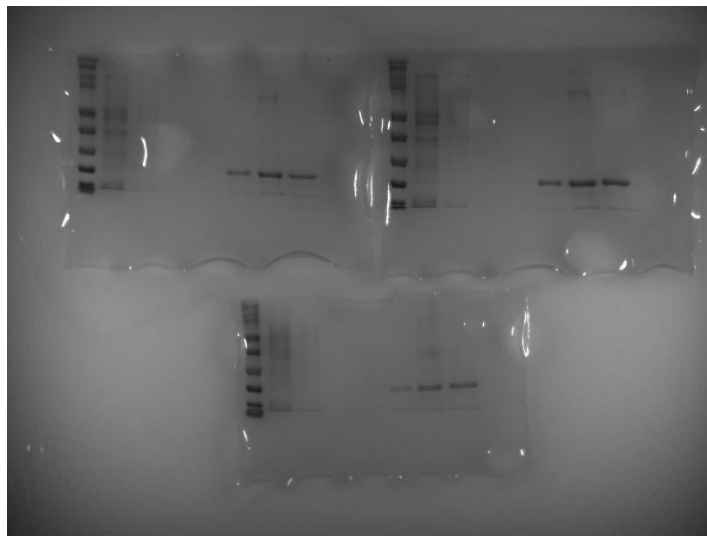
Figure 4.6. Production of His Tagged MugA.

Gels for the purification of MugA from C3013 *E. coli* strains harboring pQE-30-*mugA*. MugA is predicted to be approximately 18 kDa with a pI of around 9.3. Gels can be seen with one lane of ladder, one lane of flow through, three lanes of washes, and then three lanes of protein elutions.

CHAPTER FIVE
DISCUSSION

Discussion

Innate immune responses during campylobacteriosis have been understudied. To characterize the innate immune responses that occur during campylobacteriosis, this dissertation examined the molecular events that occur in host neutrophils during infection with *C. jejuni*. The work presented in Chapter Two established that *C. jejuni* induces a proinflammatory cell death in neutrophils, called a NET (232). In Chapter Three, I identified and characterized a *C. jejuni* secreted effector protein, which I termed SliP, that is necessary for NET induction, inflammation, and pathology during murine campylobacteriosis (283). Chapter Four described the identification and characterization of a *C. jejuni* nuclease, MugA, which appears to be necessary for evading the antimicrobial activities of NETs, which promotes colonization and inflammasome activation in macrophages.

Neutrophils accumulate within the colonic tissue of *C. jejuni* infected susceptible hosts and neutrophil-derived S100A12 nutritionally starves *C. jejuni* of essential zinc (58,59). Expanding on this foundation, I sought to elucidate the molecular interactions between *C. jejuni* and host neutrophils. Specifically, NETs are inflammatory and are implicated in numerous autoimmune diseases complications following campylobacteriosis. Therefore, I hypothesized that NETs play a crucial role in the initiation of host inflammation and onset of post-infectious disorders. Using fecal samples from patients infected with *C. jejuni*, I found numerous NET-associated proteins, including lipocalin-2, neutrophil elastase, and myeloperoxidase, accumulate in the feces of these patients. Additionally, purified lipocalin-2, neutrophil elastase, and myeloperoxidase exhibited antimicrobial activities against *C. jejuni*. Furthermore, primary human neutrophils infected with *C. jejuni* had higher abundance of all NET associated proteins compared to uninfected neutrophils. Upon microscopic examination, seventeen percent of neutrophils undergo NETosis in response to *C. jejuni*. While we are unsure if the increased NET associated proteins in the fecal samples were associated with NETs, this provided crucial insight into clinical manifestations of

157

campylobacteriosis through an immunological lens, which had not been thoroughly investigated.

To begin to understand *C. jejuni* induction of NETs, I explored the intracellular lifestyle of *C. jejuni* within neutrophils, as numerous intracellular pathogens induce NETs. I demonstrated *C. jejuni* retains viability within neutrophils, relying on TLR4, actin polymerization, and a functional flagellum. Accordingly, I demonstrated *C. jejuni* induced NETs were dependent on TLR4, actin polymerization, and a functional flagellum. Therefore, we hypothesize that *C. jejuni* induced NETs are due to intracellular bacterium, dependent on TLR4, actin polymerization, and a functional flagellum. As *C. jejuni* has been shown to evade phagolysosomal fusion within epithelial cells (35), we hypothesize that *C. jejuni* survives within the phagosome of neutrophils. Furthermore, as TLR4 plays a vital role in phagocytosis of Gram-negative bacteria (315), we hypothesize that this receptor either is involved with *C. jejuni* invasion into neutrophils or phagocytosis of the bacterium.

Using the ferret model of campylobacteriosis, I demonstrated ferret neutrophils become activated and undergo NETosis at similar rates as human neutrophils. Using confocal microscopy, we detected NET-like structures within the colon section where *C. jejuni* colonizes, yet these structures were absent in uninfected ferrets. This infection site has been characterized with tissue pathology, specifically crypt abscesses; therefore, I investigated if *C. jejuni* induced NETs cause epithelial cell death. When *C. jejuni* and neutrophils interact under NETosing conditions, colonic epithelial cells underwent cell death, suggesting that NETs during campylobacteriosis could be a source of cytotoxicity. As crypt abscess formation through neutrophil activation results in electrogenic chloride secretion, and subsequent diarrheal episodes, this could be a mechanism for campylobacteriosis clinical signs within infected hosts (170). As crypt abscess formation has only been investigated in ferret IBS (316), neutrophils could play a significant role in this tissue pathology and should be investigated further.

158

The work highlighted in chapter two of this dissertation demonstrated that *C. jejuni* is a potent inducer of NETs and that these structures can be visualized in an animal disease model of campylobacteriosis. While the *Campylobacter* field has hypothesized that neutrophils play a key role in the onset and duration of inflammation during campylobacteriosis (58), this study is the first to investigate the events at the *C. jejuni* – neutrophil interface. A long-standing belief in the field of immunology is that neutrophils are terminally differentiated cell types, lacking either transcriptional plasticity or protein synthesis (317). In this study, we observed that *C. jejuni* caused increased abundance of NET associated antimicrobial proteins, demonstrating that neutrophils are in fact not transcriptionally and translationally inert. Additionally, we demonstrated *C. jejuni* can persist within neutrophils, though it remains unclear if this is due to *C. jejuni* invasion or evasion of phagolysosome fusion killing mechanisms within neutrophils. As this phenotype has been demonstrated in epithelial cells infected with *C. jejuni* (35), more research needs to be conducted on the mechanism of this evasion. Therefore, this could be a unique future research question, potentially allowing *C. jejuni* as a model organism to study bacterial persistence in neutrophils (318). Furthermore, ferrets are being used as model organisms to study SARS-CoV-2 NET formation *in vivo* (319). Hence, NET inhibitors should be investigated for potential therapeutic strategies to abrogate host inflammation and tissue damage.

In chapter three of this dissertation, I described a secreted *C. jejuni* effector protein, SliP, responsible for NET induction and host inflammation. I demonstrated that *sliP* was present in over half of clinical strains of *C. jejuni* but absent in agricultural and environmental strains. While this phenotype can be a result of detection bias in inflammatory infections, abundance of *sliP* within clinical isolates could originate through horizontal gene transfer (320). Through secondary structure homology, I determined SliP shared homology with other bacterial sirtuins, a family of lysine deacetylases. I was able to demonstrate SliP functions as a sirtuin, being able to deacetylate lysine residues in a zinc and NAD$^+$

dependent manner. Additionally, I identified a residue within SliP, G26, which I hypothesized to be within a Rossmann fold, which sirtuins often use to bind NAD$^+$ (321). Using a single amino acid substitution of glycine to alanine within SliP, I determined this glycine residue was crucial for maximal NAD$^+$ hydrolysis and lysine deacetylation. Using known HDAC inhibitors, trichostatin A and sodium butyrate, I demonstrated inhibition of SliP sirtuin activity using the HDAC inhibitors in a dose-dependent manner. While trichostatin A and sodium butyrate inhibit class I and II HDACs, we hypothesize that SliP has broad HDAC activity, spanning multiple families of HDACs.

As deacetylated host proteins often result in inflammation (324), I sought to determine if SliP could be a secreted effector protein, being able to deacetylate neutrophil proteins. Using a secretion reporter assay along with confocal microscopy, I demonstrated SliP was secreted into host neutrophils. This secretion was dependent both on a functional flagella and actin polymerization, both of which *C. jejuni* utilizes to secrete effector proteins in colonic epithelial cells. I additionally used molecular tools, including a co-immunoprecipitation and western blotting to demonstrate that SliP binds to and deacetylates histone H3. Interestingly, multiple bacteria hijack host sirtuins to deacetylate histone H3 to promote cellular infection (114,117). As deacetylated histones result in heterochromatin (325), whereby host transcription cannot occur, this could be a conserved immunosuppressive strategy to dampen the host response to the invading pathogen. Furthermore, when I quantified the amount of NAD$^+$ and NADH within *C. jejuni* infected neutrophils, I observed a *sliP*-dependent depletion of NAD$^+$, but not NADH, within neutrophils. While this phenomenon could have drastic influences on the neutrophil metabolic capabilities, especially regarding mitochondrial dysfunction, we have not yet explored this.

As host HDACs are necessary for inducing NETs, I sought to identify if *C. jejuni*-induced NETs are due to the presence of SliP. Using a non-polar deletion mutant of *sliP*, I determined that SliP is necessary for neutrophil activation and NETosis. As PAD4 is required for induction of NETs and this enzyme often forms

160

complexes with histone deacetylases (326) , it has been hypothesized there is a connection between histone deamination and deacetylation in NETosis. As such, we hypothesize that SliP works in conjugation with PAD4 to initiate the induction of NETs. Additionally, like HDACs and PAD4 forming protein complexes, SliP could oligomerize with PAD4 to synergize NET formation, however, this has yet to be determined. Furthermore, when neutrophils were preincubated with SliP inhibitors, TSA and butyrate, *C. jejuni*-induced neutrophil activation and NETosis were significantly decreased. As TSA is a natural byproduct produced by *Streptomyces* (327) and butyrate is a short-chain fatty acid produced by the gut microbiota, specifically within the genus *Ruminococcus*, *Clostridium*, *Eubacterium*, and *Coprococcus* (328), these could be attractive therapeutic strategies to limit inflammation.

Finally, as I observed *sliP* presence was resulting in cellular inflammatory signaling, I investigated if *sliP* contributes to *C. jejuni* induced inflammation *in vivo*. Using the IL-10$^{-/-}$ murine model of campylobacteriosis, wild-type and deletion mutant of *sliP C. jejuni* were shed in the feces at similar rates. Similarly, both strains were able to colonize the colonic and cecal tissue at comparable levels. Yet, when weight changes were observed in these mice, the *sliP* mutant infected and uninfected mice were able to maintain weight gain through the duration of the study, while wild-type infected mice retained their initial weights, indicative of differential inflammation. Furthermore, proinflammatory cytokine production occurred in a *sliP* dependent manner. To confirm *sliP* is performing histone H3 deacetylation *in vivo*, resulting in host inflammation, I used confocal microscopy to demonstrate histone deacetylation within the colonic tissue, there were marked decreases in histone H3 acetylation, specifically where wild-type *C. jejuni* colonized. To correlate this, when we purified leukocytes from the colonic tissue, SliP binds to immune cell histone H3 with decreased acetylation levels. We therefore hypothesize that *sliP* is dispensable for host colonization, but indispensable for inducing inflammation within the murine model of campylobacteriosis. As the *Campylobacter* field has lacked in the understanding

161

of the host immune response due to the absence of a reproducible animal model to human campylobacteriosis, this study provides crucial insight into the murine model of campylobacteriosis.

The work discussed in chapter three of this dissertation identified and characterized a previously unknown protein within *C. jejuni* resulting in unique inflammation. The DUF4917 family proteins have yet to be characterized, therefore, with this study, other groups whose organism encodes a DUF4917 family protein could investigate this further. As other pathogenic bacteria, including *Legionella pneumophila* and *Yersinia enterocolitica*, possess DUF4917 proteins homologous to *C. jejuni* SliP, this family of proteins could have broad inflammatory responses in various infections. Furthermore, while other bacterial pathogens utilize host sirtuins and HDACs to promote their infection (114,115,117), it is intriguing that *C. jejuni* has acquired the ability to bypass the host cell and secrete their own sirtuin. As histones possess numerous cellular functions other than organizing host chromatin, it is a very attractive target for a bacterial effector to manipulate. While histone posttranslational modifications play a key role in NETosis, they also play a key role in chromatin organization. By SliP deacetylating these proteins, it could have tremendous transcriptional repression abilities, along with inducing NETs (329). As such, more research needs to be conducted on how SliP influences the 3D genome structure of neutrophils. Finally, the *Campylobacter* field has hypothesized that the inflammation induced during campylobacteriosis are thought to arise from the unique virulence factors produced by the bacterium (330). With the discovery of SliP, targeted therapeutics against this protein could be of interest within the clinical setting. Specifically, as a *sliP* mutant can colonize a host without inducing potent inflammation, this strain could have promising therapeutic usage to induce protective immunity against other virulent strains of *C. jejuni* (331).

In chapter four of this dissertation, we sought to identify and characterize a protein produced by *C. jejuni* to evade NET antimicrobial killing strategies. To achieve this, I utilized a previously published *C. jejuni* arrayed transposon library

produced by the Johnson lab. In this, I screened individual transposon mutants for nuclease activity both through commercially available DNase agar and a quantitative qPCR approach. After the completion of the primary and secondary nuclease screens, I identified twelve mutants with deficient nuclease activities. Most of these isolates were involved with bacterial metabolism, specifically in iron and phosphate uptake, along with amino acid catabolism. Interestingly, iron and phosphate acquisition systems are necessary for *C. jejuni* chick and human colonization (161,332,333). Yet, the only transposon isolate sensitive to NET antimicrobial activity was a mutant in *mugA*. I was able to generate a non-polar deletion of this mutant and showed a strain lacking *mugA* was sensitive to NET killing activity. As MugA was previously identified by another group as a secreted protein in another *C. jejuni* wild-type strain (encoded as Cj1254 in *C. jejuni* 11168) (334), I sought to determine how MugA assists in *C. jejuni* evasion of NET killing mechanisms. However, more research should be focused on how metabolism of *C. jejuni* leads to the potential production of a nuclease.

To understand how MugA could assist and promote the degradation of NETs, I demonstrated pure MugA can degrade the DNA backbone of NETs, resulting in diminished capabilities to entrap *C. jejuni*. To show MugA is secreted, I demonstrated supernatant of *C. jejuni* under secretion growth conditions resulted in rapid NET hydrolysis in wild-type and *mugA* complement bacterium, but not in the *mugA* deletion mutant strain. Furthermore, when I assayed for intact NETs, the *mugA* mutant strain had higher intact NETs, with comparable neutrophil activation rates. To see if degraded DNA products were seen in wild-type infected cells, I visualized mononucleosomal formation occurring in infected cells, but not in uninfected neutrophils. When this size of DNA was purified, the origin of this DNA was human, demonstrating degraded neutrophil DNA. As such, I hypothesized that MugA is a secreted protein, which promotes the degradation of NETs, allowing *C. jejuni* to evade NET-dependent killing. Notably, while most bacteria induce the formation of NETs, the ability to inhibit NETs or degrade NETs are far less prevalent (335).

As degraded NETs have been highly associated with altering the immune signaling of tissue resident macrophages (336), I investigated if *C. jejuni* induced NETs could further alter the innate immune response during campylobacteriosis. Particularly, as it has been shown that extracellular citrullinated histones can lead to inflammasome activation (140) and that IL-1β, a product of inflammasome activation, is abundant during animal models, I sought to determine if *C. jejuni* induced NETs lead to this response. To determine if NETs play a role in macrophage inflammasome activation, I determined wild-type *C. jejuni* infected neutrophils, known to induce and degrade NETs, was able to activate macrophage inflammasome. However, *mugA* mutant strain infected neutrophils, which are unable to degrade NETs, had significant decreases in IL-1β compared to wild-type infected. Accordingly, neutrophils infected with *C. jejuni sliP* mutant strain, which is unable to induce NETs, IL-1β was additionally decreased compared to wild-type infected neutrophils. As such, I hypothesized that the induction and cleavage of NETs by *C. jejuni* play a significant role in macrophage inflammasome activation and subsequent IL-1β production during campylobacteriosis.

To further understand the molecular mechanism underlying NET induced macrophage inflammasome activation, CRISPR knockouts of numerous inflammasome components were obtained, namely NLRC4 and NAIP. To inhibit the NLRP3 inflammasome pathway, I chemically inhibited this pathway using MCC950. Using PMA induced NETs, I demonstrated MugA degraded NETs resulted in elevated IL-1β production in wild-type macrophages compared to macrophages treated with NETs preincubated with protein eluents from *E. coli* harboring empty vector. Yet, the only inflammasome components with significantly decreased levels of IL-1β was NLRP3. The NLRP3 inflammasome has been investigated during human campylobacteriosis and chick colonization (297,305), therefore, NET degradation could additionally promote IL-1β production during infection. Hence, the NLRP3 inflammasome could be targeted during campylobacteriosis to reduce host inflammation during infection. While degraded NETs lead to macrophage inflammasome activation, neutrophil-macrophage

164

synergy could have tremendous antimicrobial activity during campylobacteriosis. As such, more research needs to be done on how neutrophil-macrophage cooperativity diminishes pathogen burden during *C. jejuni* infection.

Finally, as previously demonstrated in chapter three of this dissertation that NETs play a significant role in campylobacteriosis, I hypothesized the *C. jejuni* *mugA* mutant would have decreased ability to colonize and promote inflammation in the murine model of campylobacteriosis relative to wild-type. I observed a majority of *mugA* mutant infected mice were not colonized at all or to levels of wild-type infected mice. Similar to *sliP* mutant infected mice as seen in chapter three, while wild-type *C. jejuni* infected mice lost weight, the uninfected and *mugA* mutant *C. jejuni* infected mice were able to maintain during the early days of infection and then gain weight during the later stages of infection. Furthermore, I demonstrated *mugA* mutant infected mice harbored significantly less viable bacteria in the colon, ceca, and spleen compared to wild-type infected mice. When bacterial burden in the spleen as an extraintestinal site for bacterial dissemination was observed for colonization, while wild-type bacteria colonized most of the mice, most of the *mugA* infected mice did not harbor viable splenic bacteria. A similar phenotype has been previously demonstrated in nuclease deficient *S. aureus*, whereby *S. aureus* unable to produce a nuclease are able to be cleared by the host more readily than its wild-type strain (282). Finally, I observed inflammatory cytokines often induced during wild-type murine inflammation were lost in *mugA* mutant infected mice. Hence, I hypothesize that NETs play a crucial role in maintaining *C. jejuni* within the colon and that MugA assists *C. jejuni* to evade these antimicrobial structures. In summary, I have identified and determined in this dissertation that *C. jejuni* secretes a sirtuin, SliP, into neutrophil, whereby the neutrophil undergoes NETosis, and that another *C. jejuni* secreted protein, MugA, assists *C. jejuni* to evade NET killing mechanisms while still promoting inflammation.

Future Directions

The work in this dissertation demonstrates the importance of NETs within campylobacteriosis and revealed factors produced by *C. jejuni* that influence the production and functionality of these structures. We determined that *C. jejuni* is a potent activator of primary human neutrophils, causing the upregulation of numerous inflammatory antimicrobial proteins. Work by the Johnson lab has shown that *C. jejuni* can induce neutrophil differentiation, therefore, the field is primed to further investigate neutrophil plasticity during infection (82). As neutrophil differentiation and NETosis are both linked to colorectal cancer, future work should be done on the long-term effects of *C. jejuni*-neutrophil interactions (76,337). Additionally, we demonstrated that *C. jejuni* is a potent inducer of NETs, whereby it requires intracellular bacteria. In the future, it would be of importance to investigate if *C. jejuni* is within a *Campylobacter* containing vacuole (CCV) or survives within the phagosome of neutrophils. This could be achieved by examining *C. jejuni* trafficking in neutrophils through confocal microscopy. Additionally, we determined that ferret neutrophils can become activated and NETose in response to *C. jejuni* and NET-like structures can be found within the colonic tissue of infected animals. As a future direction, it is imperative to perform neutrophil depletions through cyclophosphamide (338) or PAD4 inhibition (339) to determine how neutrophils and NETs shape the course of campylobacteriosis within the ferret model. Through these studies, clinical therapeutics for human campylobacteriosis could start to be developed to diminish host inflammation and tissue pathology.

Furthermore, we demonstrate in this dissertation that a secreted *C. jejuni* effector protein, SliP, is responsible for NETosis and contributes to host inflammation. As preliminary data suggests that *sliP* is operonic with numerous components necessary for flagellar biogenesis and T3SS, including *dnaK* and *grpE*, more research should be done on the molecular mechanism for SliP secretion. SliP belongs to the DUF4917 family proteins and have yet to be characterized. In the present study, we identify numerous bacterial pathogens,

including *Yersinia enterocolitica* and *Legionella pneumophila*, which encode DUF4917 family proteins homologous to SliP. As these pathogens have a repertoire of effector proteins and secretion systems, it would be interesting to investigate the role of their respective DUF4917 protein in their disease model (215,340). Furthermore, we demonstrate that the glycine residue in the twenty sixth position of SliP is crucial for maximal NAD^+ hydrolysis and lysine deacetylation. While preliminary evidence shows that this residue is involved with NAD^+ binding, more research should be conducted on the biochemical and structural role of this glycine residue within the predicted Rossmann fold (341). Specifically, making a single amino acid substitution in the other glycine residue of the Rossmann fold (G24) could have crucial insight into the Rossmann fold of SliP. In this dissertation, we additionally demonstrated that SliP binds to and deacetylates numerous host proteins, including histone H3. As histone H3 epigenetically influence the 3D architecture of chromatin and regulates transcription, future research should seek to investigate how SliP modulates chromatin structure and host transcription (342). This can be performed using Hi-C and ChIP-seq of histone H3K9ac and K3K79ac to determine if this could be a way for the bacteria to suppress host transcription (343). By correlating this data with RNA-seq, the transcriptional repressive activity of SliP on host cells can be thoroughly investigated. Furthermore, with the identification of deacetylated targets in the neutrophil and bacteria, future research should seek to understand how SliP could be influencing other processes. Additionally, as NAD^+ depletion occurs in *C. jejuni* infected neutrophils in a SliP-dependent manner, neutrophils should be analyzed through Seahorse technology to understand how this depletion alters neutrophil metabolic processes.

Additionally, within chapter three of this dissertation, we demonstrate that SliP contributes to inflammation within the murine model of campylobacteriosis. We were able to demonstrate that a *sliP* mutant was able to colonize and be shed in feces at similar rates to wild-type *C. jejuni*, however, inflammation and tissue pathology were all significantly decreased. As we have shown sodium butyrate and

trichostatin A can chemically inhibit SliP-dependent deacetylation, future research should investigate the potential therapeutic effects of these on campylobacteriosis. As the gut microbiota produces sodium butyrate, it would be interesting to investigate if these microbiota members could shape campylobacteriosis inflammation (344). Fascinatingly, *C. jejuni* possesses a butyrate sensing two-component system, termed BumRS (13). Therefore, it would be insightful to investigate this system during campylobacteriosis and potential SliP production. Furthermore, as a *sliP* mutant can colonize, but not induce long term inflammation, future research can investigate the protective properties of this strain to investigate if it modulates wild-type *C. jejuni* infection.

Finally, we identified and characterized a MugA protein in *C. jejuni*, which assists in NET evasion strategies. Interestingly, MugA is annotated as a hypothetical protein, with homology with G:T/U-mismatch repair DNA glycosylase enzymes. MugA degrades NET DNA, allowing it to evade entrapment of the NET. While there is literature demonstrating neutrophil DNA can undergo mismatching upon neutrophil activation-derived hypochlorous acid (345), the mechanism underlying the ability of MugA to break the DNA through cleaving the glycosidic bond remains unknown. Additionally, as we observed mononucleosome formation in *C. jejuni* infected neutrophils, it is crucial to investigate if MugA leads to these inflammatory structures. Furthermore, MugA degraded NETs induce inflammasome activation in neighboring macrophages through an NLRP3-dependent manner. For future work, the role of IL-1R and NLRP3 should be investigated in their role in shaping the inflammation and tissue pathology observed during campylobacteriosis. We additionally demonstrate in this work that a *mugA* mutant had defective colonization in the murine model of campylobacteriosis. Therefore, using neutrophil depleted mice through Ly6G antibody depletion, it would be interesting to see if colonization of a *mugA* mutant could be restored to wild-type levels upon depletion of neutrophils (346). Additionally, using a double mutant of *sliP* and *mugA* should be investigated in the future, as the absence of *sliP* should result in a rescuing in colonization of *C. jejuni*

deficient in *mugA* due to the absence of NETs. With the future research of *C. jejuni*-neutrophil interactions, targeted novel therapeutics can be developed to mitigate inflammation and promote host resolution. With such therapeutics, host inflammation could be prevented, resulting in lowered tissue pathology and potentially reduce risk for post-infectious autoimmune disorder onset.

LIST OF REFERENCES

1. Igwaran, A. & Okoh, A. I. Human campylobacteriosis: A public health concern of global importance. *Heliyon* **5**, e02814 (2019).

2. Janssen, R. *et al.* Host-Pathogen Interactions in *Campylobacter* Infections: the Host Perspective. *Clin Microbiol Rev* **21**, 505–518 (2008).

3. Kaakoush, N. O., Castaño-Rodríguez, N., Mitchell, H. M. & Man, S. M. Global Epidemiology of Campylobacter Infection. *Clin Microbiol Rev* **28**, 687–720 (2015).

4. Damborg, P., Olsen, K. E. P., Møller Nielsen, E. & Guardabassi, L. Occurrence of *Campylobacter jejuni* in Pets Living with Human Patients Infected with *C. jejuni*. *J Clin Microbiol* **42**, 1363–1364 (2004).

5. Tribble, D. R. *et al.* Assessment of the Duration of Protection in *Campylobacter jejuni* Experimental Infection in Humans. *Infect Immun* **78**, 1750–1759 (2010).

6. Stahl, M. & Vallance, B. A. Insights into *Campylobacter jejuni* colonization of the mammalian intestinal tract using a novel mouse model of infection. *Gut Microbes* **6**, 143–148 (2015).

7. Stahl, M. *et al.* The Helical Shape of Campylobacter jejuni Promotes *In Vivo* Pathogenesis by Aiding Transit through Intestinal Mucus and Colonization of Crypts. *Infect Immun* **84**, 3399–3407 (2016).

8. Black, R. E., Levine, M. M., Clements, M. L., Hughes, T. P. & Blaser, M. J. Experimental Campylobacter jejuni Infection in Humans. *Journal of Infectious Diseases* **157**, 472–479 (1988).

9.   McMurry, T. L. *et al.* Duration of Postdiarrheal Enteric Pathogen Carriage in Young Children in Low-resource Settings. *Clinical Infectious Diseases* **72**, e806–e814 (2021).

10.   Du, K. *et al.* Less Pronounced Immunopathological Responses Following Oral Butyrate Treatment of Campylobacter jejuni-Infected Mice. *Microorganisms* **10**, 1953 (2022).

11.   Lozupone, C. A., Stombaugh, J. I., Gordon, J. I., Jansson, J. K. & Knight, R. Diversity, stability and resilience of the human gut microbiota. *Nature* **489**, 220–230 (2012).

12.   Canani, R. B. Potential beneficial effects of butyrate in intestinal and extraintestinal diseases. *WJG* **17**, 1519 (2011).

13.   Goodman, K. N., Powers, M. J., Crofts, A. A., Trent, M. S. & Hendrixson, D. R. *Campylobacter jejuni* BumSR directs a response to butyrate via sensor phosphatase activity to impact transcription and colonization. *Proc. Natl. Acad. Sci. U.S.A.* **117**, 11715–11726 (2020).

14.   Elmi, A., Nasher, F., Dorrell, N., Wren, B. & Gundogdu, O. Revisiting Campylobacter jejuni Virulence and Fitness Factors: Role in Sensing, Adapting, and Competing. *Front. Cell. Infect. Microbiol.* **10**, 607704 (2021).

15.   Nyati, K. K. & Nyati, R. Role of *Campylobacter jejuni* Infection in the Pathogenesis of Guillain-Barré Syndrome: An Update. *BioMed Research International* **2013**, 1–13 (2013).

16. Scallan Walter, E. J., Crim, S. M., Bruce, B. B. & Griffin, P. M. Incidence of *Campylobacter*-Associated Guillain-Barré Syndrome Estimated from Health Insurance Data. *Foodborne Pathogens and Disease* **17**, 23–28 (2020).

17. Buzby, J. C., Allos, B. M. & Roberts, T. The Economic Burden of *Campylobacter-Associated* Guillain-Barré Syndrome. *J INFECT DIS* **176**, S192–S197 (1997).

18. Tam, C. C. & O'Brien, S. J. Economic Cost of Campylobacter, Norovirus and Rotavirus Disease in the United Kingdom. *PLoS ONE* **11**, e0138526 (2016).

19. Nielsen, H. L., Dalager-Pedersen, M. & Nielsen, H. High risk of microscopic colitis after *Campylobacter concisus* infection: population-based cohort study. *Gut* **69**, 1952–1958 (2020).

20. Pope, J. E., Krizova, A., Garg, A. X., Thiessen-Philbrook, H. & Ouimet, J. M. Campylobacter Reactive Arthritis: A Systematic Review. *Seminars in Arthritis and Rheumatism* **37**, 48–55 (2007).

21. Lehman, H. K. Autoimmunity and Immune Dysregulation in Primary Immune Deficiency Disorders. *Curr Allergy Asthma Rep* **15**, 53 (2015).

22. Chang, C. & Miller, J. F. *Campylobacter jejuni* Colonization of Mice with Limited Enteric Flora. *Infect Immun* **74**, 5261–5271 (2006).

23. Teunis, P. F. M., Bonačić Marinović, A., Tribble, D. R., Porter, C. K. & Swart, A. Acute illness from Campylobacter jejuni may require high doses while infection occurs at low doses. *Epidemics* **24**, 1–20 (2018).

24. Mills, D. C. *et al.* Increase in Campylobacter jejuni Invasion of Intestinal Epithelial Cells under Low-Oxygen Coculture Conditions That Reflect the *In Vivo* Environment. *Infect Immun* **80**, 1690–1698 (2012).

25. Reid, A. N., Pandey, R., Palyada, K., Naikare, H. & Stintzi, A. Identification of *Campylobacter jejuni* Genes Involved in the Response to Acidic pH and Stomach Transit. *Appl Environ Microbiol* **74**, 1583–1597 (2008).

26. Yao, R. *et al.* Isolation of motile and non-motile insertional mutants of Campylobacter jejuni: the role of motility in adherence and invasion of eukaryotic cells. *Mol Microbiol* **14**, 883–893 (1994).

27. Konkel, M. E., Talukdar, P. K., Negretti, N. M. & Klappenbach, C. M. Taking Control: Campylobacter jejuni Binding to Fibronectin Sets the Stage for Cellular Adherence and Invasion. *Front. Microbiol.* **11**, 564 (2020).

28. de Zoete, M. R., Keestra, A. M., Roszczenko, P. & van Putten, J. P. M. Activation of Human and Chicken Toll-Like Receptors by *Campylobacter* spp. *Infect Immun* **78**, 1229–1238 (2010).

29. Hu, L. & Hickey, T. E. *Campylobacter jejuni* Induces Secretion of Proinflammatory Chemokines from Human Intestinal Epithelial Cells. *Infect Immun* **73**, 4437–4440 (2005).

30. Cui, J. *et al.* The ALPK1 pathway drives the inflammatory response to Campylobacter jejuni in human intestinal epithelial cells. *PLoS Pathog* **17**, e1009787 (2021).

31. Konkel, M. E. *et al.* Secretion of Virulence Proteins from *Campylobacter jejuni* Is Dependent on a Functional Flagellar Export Apparatus. *J Bacteriol* **186**, 3296–3303 (2004).

32. Grant, C. C., Konkel, M. E., Cieplak, W. & Tompkins, L. S. Role of flagella in adherence, internalization, and translocation of Campylobacter jejuni in nonpolarized and polarized epithelial cell cultures. *Infect Immun* **61**, 1764–1771 (1993).

33. Buelow, D. R., Christensen, J. E., Neal-McKinney, J. M. & Konkel, M. E. Campylobacter jejuni survival within human epithelial cells is enhanced by the secreted protein CiaI: C. jejuni survival within epithelial cells. *Molecular Microbiology* **80**, 1296–1312 (2011).

34. Samuelson, D. R. *et al.* The Campylobacter jejuniCiaD effector protein activates MAP kinase signaling pathways and is required for the development of disease. *Cell Commun Signal* **11**, 79 (2013).

35. Watson, R. O. & Galán, J. E. Campylobacter jejuni Survives within Epithelial Cells by Avoiding Delivery to Lysosomes. *PLoS Pathog* **4**, e14 (2008).

36. Rosales, C., Demaurex, N., Lowell, C. A. & Uribe-Querol, E. Neutrophils: Their Role in Innate and Adaptive Immunity. *Journal of Immunology Research* **2016**, 1–2 (2016).

37. Teng, Y., Luo, H. R. & Kambara, H. Heterogeneity of neutrophil spontaneous death: TENG et al. *Am J Hematol* **92**, E156–E159 (2017).

38. Hong, C.-W. Current Understanding in Neutrophil Differentiation and Heterogeneity. *Immune Netw* **17**, 298 (2017).

39. Evrard, M. *et al.* Developmental Analysis of Bone Marrow Neutrophils Reveals Populations Specialized in Expansion, Trafficking, and Effector Functions. *Immunity* **48**, 364-379.e8 (2018).

40. Martin, C. *et al.* Chemokines Acting via CXCR2 and CXCR4 Control the Release of Neutrophils from the Bone Marrow and Their Return following Senescence. *Immunity* **19**, 583–593 (2003).

41. Petty, J. M., Lenox, C. C., Weiss, D. J., Poynter, M. E. & Suratt, B. T. Crosstalk between CXCR4/Stromal Derived Factor-1 and VLA-4/VCAM-1 Pathways Regulates Neutrophil Retention in the Bone Marrow. *The Journal of Immunology* **182**, 604–612 (2009).

42. Eash, K. J., Greenbaum, A. M., Gopalan, P. K. & Link, D. C. CXCR2 and CXCR4 antagonistically regulate neutrophil trafficking from murine bone marrow. *J. Clin. Invest.* **120**, 2423–2431 (2010).

43. Hidalgo, A., Chilvers, E. R., Summers, C. & Koenderman, L. The Neutrophil Life Cycle. *Trends in Immunology* **40**, 584–597 (2019).

44. Brinkmann, V. *et al.* Neutrophil Extracellular Traps Kill Bacteria. *Science* **303**, 1532–1535 (2004).

45. Lee, W. L., Harrison, R. E. & Grinstein, S. Phagocytosis by neutrophils. *Microbes and Infection* **5**, 1299–1306 (2003).

46. Nguyen, J. A. & Yates, R. M. Better Together: Current Insights Into Phagosome-Lysosome Fusion. *Front. Immunol.* **12**, 636078 (2021).

47. Foote, J. R., Patel, A. A., Yona, S. & Segal, A. W. Variations in the Phagosomal Environment of Human Neutrophils and Mononuclear Phagocyte Subsets. *Front. Immunol.* **10**, 188 (2019).

48. Lacy, P. Mechanisms of Degranulation in Neutrophils. *All Asth Clin Immun* **2**, 98 (2006).

49. Li, Y. *et al.* Nuclear envelope rupture and NET formation is driven by PKCα-mediated lamin B disassembly. *EMBO Rep* **21**, (2020).

50. Thiam, H. R. *et al.* NETosis proceeds by cytoskeleton and endomembrane disassembly and PAD4-mediated chromatin decondensation and nuclear envelope rupture. *Proc. Natl. Acad. Sci. U.S.A.* **117**, 7326–7337 (2020).

51. Yipp, B. G. & Kubes, P. NETosis: how vital is it? *Blood* **122**, 2784–2794 (2013).

52. Poli, V. & Zanoni, I. Neutrophil intrinsic and extrinsic regulation of NETosis in health and disease. *Trends in Microbiology* **31**, 280–293 (2023).

53. Branzk, N. *et al.* Neutrophils sense microbe size and selectively release neutrophil extracellular traps in response to large pathogens. *Nat Immunol* **15**, 1017–1025 (2014).

54. de Bont, C. M., Koopman, W. J. H., Boelens, W. C. & Pruijn, G. J. M. Stimulus-dependent chromatin dynamics, citrullination, calcium signalling

and ROS production during NET formation. *Biochimica et Biophysica Acta (BBA) - Molecular Cell Research* **1865**, 1621–1629 (2018).

55. Kolaczkowska, E. & Kubes, P. Neutrophil recruitment and function in health and inflammation. *Nat Rev Immunol* **13**, 159–175 (2013).

56. Thomas, C. J. & Schroder, K. Pattern recognition receptor function in neutrophils. *Trends in Immunology* **34**, 317–328 (2013).

57. Nemelka, K. W. *et al.* Immune response to and histopathology of Campylobacter jejuni infection in ferrets (Mustela putorius furo). *Comp Med* **59**, 363–371 (2009).

58. Sun, X., Liu, B., Sartor, R. B. & Jobin, C. Phosphatidylinositol 3-Kinase-γ Signaling Promotes *Campylobacter jejuni* –Induced Colitis through Neutrophil Recruitment in Mice. *J.I.* **190**, 357–365 (2013).

59. Shank, J. M. *et al.* The Host Antimicrobial Protein Calgranulin C Participates in the Control of Campylobacter jejuni Growth via Zinc Sequestration. *Infect Immun* **86**, e00234-18 (2018).

60. Negretti, N. M. *et al.* A porcine ligated loop model reveals new insight into the host immune response against *Campylobacter jejuni*. *Gut Microbes* **12**, 1814121 (2020).

61. Huang, Y. *et al.* The clinical significance of neutrophil-to-lymphocyte ratio and monocyte-to-lymphocyte ratio in Guillain–Barré syndrome. *International Journal of Neuroscience* **128**, 729–735 (2018).

62. Murphy, H., Cogan, T. & Humphrey, T. Direction of neutrophil movements by Campylobacter-infected intestinal epithelium. *Microbes and Infection* **13**, 42–48 (2011).

63. Mixter, P. F., Klena, J. D., Flom, G. A., Siegesmund, A. M. & Konkel, M. E. In Vivo Tracking of *Campylobacter jejuni* by Using a Novel Recombinant Expressing Green Fluorescent Protein. *Appl Environ Microbiol* **69**, 2864–2874 (2003).

64. Maunder, C. L. *et al. Campylobacter* Species and Neutrophilic Inflammatory Bowel Disease in Cats. *J Vet Intern Med* **30**, 996–1001 (2016).

65. Kaneda, M. M. *et al.* PI3Kγ is a molecular switch that controls immune suppression. *Nature* **539**, 437–442 (2016).

66. Rickert, P. Leukocytes navigate by compass: roles of PI3Kγ and its lipid products. *Trends in Cell Biology* **10**, 466–473 (2000).

67. Sun, X., Threadgill, D. & Jobin, C. Campylobacter jejuni Induces Colitis Through Activation of Mammalian Target of Rapamycin Signaling. *Gastroenterology* **142**, 86-95.e5 (2012).

68. Walan, A., Dahlgren, C., Kihlström, E., Stendahl, O. & Lock, R. Phagocyte killing of Campylobacter jejuni in relation to oxidative activation. *APMIS* **100**, 424–430 (1992).

69. Carvalho, A. *et al.* S100A12 in Digestive Diseases and Health: A Scoping Review. *Gastroenterology Research and Practice* **2020**, 1–11 (2020).

70. Barry, R. *et al.* Faecal neutrophil elastase-antiprotease balance reflects colitis severity. *Mucosal Immunology* **13**, 322–333 (2020).

71. Chami, B., Martin, N. J. J., Dennis, J. M. & Witting, P. K. Myeloperoxidase in the inflamed colon: A novel target for treating inflammatory bowel disease. *Archives of Biochemistry and Biophysics* **645**, 61–71 (2018).

72. Papayannopoulos, V. Neutrophil extracellular traps in immunity and disease. *Nat Rev Immunol* **18**, 134–147 (2018).

73. Dinallo, V. *et al.* Neutrophil Extracellular Traps Sustain Inflammatory Signals in Ulcerative Colitis. *Journal of Crohn's and Colitis* **13**, 772–784 (2019).

74. Euler, M. & Hoffmann, M. H. The double-edged role of neutrophil extracellular traps in inflammation. *Biochemical Society Transactions* **47**, 1921–1930 (2019).

75. Li, T. *et al.* Neutrophil Extracellular Traps Induce Intestinal Damage and Thrombotic Tendency in Inflammatory Bowel Disease. *Journal of Crohn's and Colitis* **14**, 240–253 (2020).

76. Mizuno, R. *et al.* The Role of Tumor-Associated Neutrophils in Colorectal Cancer. *IJMS* **20**, 529 (2019).

77. Germann, M. *et al.* Neutrophils suppress tumor-infiltrating T cells in colon cancer via matrix metalloproteinase-mediated activation of TGF β. *EMBO Mol Med* **12**, (2020).

78. Gao, Z.-Y. *et al.* Microbe-based management for colorectal cancer. *Chinese Medical Journal* **134**, 2922–2930 (2021).

79. Galeano Niño, J. L. *et al.* Effect of the intratumoral microbiota on spatial and cellular heterogeneity in cancer. *Nature* **611**, 810–817 (2022).

80. Mangifesta, M. *et al.* Mucosal microbiota of intestinal polyps reveals putative biomarkers of colorectal cancer. *Sci Rep* **8**, 13974 (2018).

81. He, Z. *et al. Campylobacter jejuni* promotes colorectal tumorigenesis through the action of cytolethal distending toxin. *Gut* **68**, 289–300 (2019).

82. Dolislager, C. G., Callahan, S. M., Donohoe, D. R. & Johnson, J. G. *Campylobacter jejuni* induces differentiation of human neutrophils to the CD16 [hi] /CD62L [lo] subtype. *J Leukocyte Bio* JLB.4A0322-155RR (2022) doi:10.1002/JLB.4A0322-155RR.

83. Coburn, B., Sekirov, I. & Finlay, B. B. Type III Secretion Systems and Disease. *Clin Microbiol Rev* **20**, 535–549 (2007).

84. Miletic, S. *et al.* Substrate-engaged type III secretion system structures reveal gating mechanism for unfolded protein translocation. *Nat Commun* **12**, 1546 (2021).

85. Notti, R. Q. & Stebbins, C. E. The Structure and Function of Type III Secretion Systems. *Microbiol Spectr* **4**, 4.1.09 (2016).

86. Diepold, A. & Armitage, J. P. Type III secretion systems: the bacterial flagellum and the injectisome. *Phil. Trans. R. Soc. B* **370**, 20150020 (2015).

87. Abby, S. S. & Rocha, E. P. C. The Non-Flagellar Type III Secretion System Evolved from the Bacterial Flagellum and Diversified into Host-Cell Adapted Systems. *PLoS Genet* **8**, e1002983 (2012).

88. Halte, M. & Erhardt, M. Protein Export via the Type III Secretion System of the Bacterial Flagellum. *Biomolecules* **11**, 186 (2021).

89. Erhardt, M., Namba, K. & Hughes, K. T. Bacterial Nanomachines: The Flagellum and Type III Injectisome. *Cold Spring Harbor Perspectives in Biology* **2**, a000299–a000299 (2010).

90. Christensen, J. E., Pacheco, S. A. & Konkel, M. E. Identification of a *Campylobacter jejuni* -secreted protein required for maximal invasion of host cells. *Molecular Microbiology* **73**, 650–662 (2009).

91. Scanlan, E., Yu, L., Maskell, D., Choudhary, J. & Grant, A. A quantitative proteomic screen of the Campylobacter jejuni flagellar-dependent secretome. *Journal of Proteomics* **152**, 181–187 (2017).

92. Burnham, P. M. & Hendrixson, D. R. Campylobacter jejuni: collective components promoting a successful enteric lifestyle. *Nat Rev Microbiol* **16**, 551–565 (2018).

93. Malik-Kale, P., Parker, C. T. & Konkel, M. E. Culture of *Campylobacter jejuni* with Sodium Deoxycholate Induces Virulence Gene Expression. *J Bacteriol* **190**, 2286–2297 (2008).

94. Negretti, N. M., Gourley, C. R., Clair, G., Adkins, J. N. & Konkel, M. E. The food-borne pathogen Campylobacter jejuni responds to the bile salt deoxycholate with countermeasures to reactive oxygen species. *Sci Rep* **7**, 15455 (2017).

95. Funabashi, M. *et al.* A metabolic pathway for bile acid dehydroxylation by the gut microbiome. *Nature* **582**, 566–570 (2020).

96. Stensrud, K. F. *et al.* Deoxycholate Interacts with IpaD of Shigella flexneri in Inducing the Recruitment of IpaB to the Type III Secretion Apparatus Needle Tip. *Journal of Biological Chemistry* **283**, 18646–18654 (2008).

97. Chatterjee, S. *et al.* The crystal structures of the *Salmonella* type III secretion system tip protein SipD in complex with deoxycholate and chenodeoxycholate: Salmonella SipD-Bile Salts Crystal Structures. *Protein Science* **20**, 75–86 (2011).

98. Hermans, D. *et al.* Colonization factors of Campylobacter jejuni in the chicken gut. *Vet Res* **42**, 82 (2011).

99. Christensen, D. G. *et al.* Post-translational Protein Acetylation: An Elegant Mechanism for Bacteria to Dynamically Regulate Metabolic Functions. *Front. Microbiol.* **10**, 1604 (2019).

100. Galdieri, L., Zhang, T., Rogerson, D., Lleshi, R. & Vancura, A. Protein Acetylation and Acetyl Coenzyme A Metabolism in Budding Yeast. *Eukaryot Cell* **13**, 1472–1483 (2014).

101. Shi, L. & Tu, B. P. Acetyl-CoA and the regulation of metabolism: mechanisms and consequences. *Current Opinion in Cell Biology* **33**, 125–131 (2015).

102. McArthur, E. & Capra, J. A. Topologically associating domain boundaries that are stable across diverse cell types are evolutionarily constrained and

enriched for heritability. *The American Journal of Human Genetics* **108**, 269–283 (2021).

103. Nichols, M. H. & Corces, V. G. Principles of 3D compartmentalization of the human genome. *Cell Reports* **35**, 109330 (2021).

104. Reed, K. S. M. *et al.* Temporal analysis suggests a reciprocal relationship between 3D chromatin structure and transcription. *Cell Reports* **41**, 111567 (2022).

105. Sefer, E. Hi–C interaction graph analysis reveals the impact of histone modifications in chromatin shape. *Appl Netw Sci* **6**, 54 (2021).

106. Milon, B. C. *et al.* Role of Histone Deacetylases in Gene Regulation at Nuclear Lamina. *PLoS ONE* **7**, e49692 (2012).

107. Tang, J., Yan, H. & Zhuang, S. Histone deacetylases as targets for treatment of multiple diseases. *Clinical Science* **124**, 651–662 (2013).

108. Makkar, R., Behl, T. & Arora, S. Role of HDAC inhibitors in diabetes mellitus. *Current Research in Translational Medicine* **68**, 45–50 (2020).

109. Yoon, S. & Eom, G. H. HDAC and HDAC Inhibitor: From Cancer to Cardiovascular Diseases. *Chonnam Med J* **52**, 1 (2016).

110. Dietz, K. C. & Casaccia, P. HDAC inhibitors and neurodegeneration: At the edge between protection and damage. *Pharmacological Research* **62**, 11–17 (2010).

111. Grabiec, A. M. & Potempa, J. Epigenetic regulation in bacterial infections: targeting histone deacetylases. *Critical Reviews in Microbiology* **44**, 336–350 (2018).

112. Houtkooper, R. H., Pirinen, E. & Auwerx, J. Sirtuins as regulators of metabolism and healthspan. *Nat Rev Mol Cell Biol* **13**, 225–238 (2012).

113. Vachharajani, V. T. *et al.* Sirtuins Link Inflammation and Metabolism. *Journal of Immunology Research* **2016**, 1–10 (2016).

114. Pereira, J. M. *et al.* Infection Reveals a Modification of SIRT2 Critical for Chromatin Association. *Cell Reports* **23**, 1124–1137 (2018).

115. Gogoi, M. *et al.* Salmonella escapes adaptive immune response via SIRT2 mediated modulation of innate immune response in dendritic cells. *PLoS Pathog* **14**, e1007437 (2018).

116. Wang, M. *et al.* Golgi stress induces SIRT2 to counteract Shigella infection via defatty-acylation. *Nat Commun* **13**, 4494 (2022).

117. Bhaskar, A. *et al.* Host sirtuin 2 as an immunotherapeutic target against tuberculosis. *eLife* **9**, e55415 (2020).

118. Ciarlo, E. *et al.* Sirtuin 2 Deficiency Increases Bacterial Phagocytosis by Macrophages and Protects from Chronic Staphylococcal Infection. *Front. Immunol.* **8**, 1037 (2017).

119. Gallego-Jara, J. *et al.* Bacterial Sirtuins Overview: An Open Niche to Explore. *Front. Microbiol.* **12**, 744416 (2021).

120. Jeter, V. L. & Escalante-Semerena, J. C. Sirtuin-Dependent Reversible Lysine Acetylation Controls the Activity of Acetyl Coenzyme A Synthetase in Campylobacter jejuni. *J Bacteriol* **203**, (2021).

121. Hua, Z., Ouellette, M., Makkay, A. M., Papke, R. T. & Zhaxybayeva, O. Nutrient supplementation experiments with saltern microbial communities implicate utilization of DNA as a source of phosphorus. *ISME J* **15**, 2853–2864 (2021).

122. Pinchuk, G. E. *et al.* Utilization of DNA as a Sole Source of Phosphorus, Carbon, and Energy by *Shewanella* spp.: Ecological and Physiological Implications for Dissimilatory Metal Reduction. *Appl Environ Microbiol* **74**, 1198–1208 (2008).

123. Wasmund, K. *et al.* Genomic insights into diverse bacterial taxa that degrade extracellular DNA in marine sediments. *Nat Microbiol* **6**, 885–898 (2021).

124. Lewenza, S., Johnson, L., Charron-Mazenod, L., Hong, M. & Mulcahy-O'Grady, H. Extracellular DNA controls expression of Pseudomonas aeruginosa genes involved in nutrient utilization, metal homeostasis, acid pH tolerance and virulence. *Journal of Medical Microbiology* **69**, 895–905 (2020).

125. Sugimoto, S. *et al.* Broad impact of extracellular DNA on biofilm formation by clinically isolated Methicillin-resistant and -sensitive strains of Staphylococcus aureus. *Sci Rep* **8**, 2254 (2018).

126. Alhede, M. *et al.* The origin of extracellular DNA in bacterial biofilm infections *in vivo. Pathogens and Disease* **78**, ftaa018 (2020).

127. Pressler, K. *et al.* Characterization of Vibrio cholerae's Extracellular Nuclease Xds. *Front. Microbiol.* **10**, 2057 (2019).

128. Binnenkade, L., Kreienbaum, M. & Thormann, K. M. Characterization of ExeM, an Extracellular Nuclease of Shewanella oneidensis MR-1. *Front. Microbiol.* **9**, 1761 (2018).

129. Kiedrowski, M. R. *et al.* Staphylococcus aureus Nuc2 Is a Functional, Surface-Attached Extracellular Nuclease. *PLoS ONE* **9**, e95574 (2014).

130. Doke, M. *et al.* Nucleases from *Prevotella intermedia* can degrade neutrophil extracellular traps. *Mol oral Microbiol* **32**, 288–300 (2017).

131. Liu, J. *et al.* A Nuclease from Streptococcus mutans Facilitates Biofilm Dispersal and Escape from Killing by Neutrophil Extracellular Traps. *Front. Cell. Infect. Microbiol.* **7**, (2017).

132. Thammavongsa, V., Missiakas, D. M. & Schneewind, O. *Staphylococcus aureus* Degrades Neutrophil Extracellular Traps to Promote Immune Cell Death. *Science* **342**, 863–866 (2013).

133. Seper, A. *et al.* Vibrio cholerae Evades Neutrophil Extracellular Traps by the Activity of Two Extracellular Nucleases. *PLoS Pathog* **9**, e1003614 (2013).

134. Möllerherm, H. *et al. Yersinia enterocolitica* -mediated degradation of neutrophil extracellular traps (NETs). *FEMS Microbiology Letters* **362**, fnv192 (2015).

135. Juneau, R. A., Stevens, J. S., Apicella, M. A. & Criss, A. K. A Thermonuclease of *Neisseria gonorrhoeae* Enhances Bacterial Escape From Killing by Neutrophil Extracellular Traps. *J Infect Dis.* **212**, 316–324 (2015).

136. Monteith, A. J., Miller, J. M., Maxwell, C. N., Chazin, W. J. & Skaar, E. P. Neutrophil extracellular traps enhance macrophage killing of bacterial pathogens. *Sci. Adv.* **7**, eabj2101 (2021).

137. Farrera, C. & Fadeel, B. Macrophage Clearance of Neutrophil Extracellular Traps Is a Silent Process. *The Journal of Immunology* **191**, 2647–2656 (2013).

138. Warnatsch, A., Ioannou, M., Wang, Q. & Papayannopoulos, V. Neutrophil extracellular traps license macrophages for cytokine production in atherosclerosis. *Science* **349**, 316–320 (2015).

139. Martín-Sánchez, F. *et al.* Inflammasome-dependent IL-1β release depends upon membrane permeabilisation. *Cell Death Differ* **23**, 1219–1231 (2016).

140. Tsourouktsoglou, T.-D. *et al.* Histones, DNA, and Citrullination Promote Neutrophil Extracellular Trap Inflammation by Regulating the Localization and Activation of TLR4. *Cell Reports* **31**, 107602 (2020).

141. Beltrán-García, J. *et al.* Extracellular Histones Activate Endothelial NLRP3 Inflammasome and are Associated with a Severe Sepsis Phenotype. *JIR* **Volume 15**, 4217–4238 (2022).

142. Man, S. M. The clinical importance of emerging Campylobacter species. *Nat Rev Gastroenterol Hepatol* **8**, 669–685 (2011).

143. World Health Organization. *WHO estimates of the global burden of foodborne diseases: foodborne disease burden epidemiology reference group 2007-2015*. (World Health Organization, 2015).

144. Backert, S., Boehm, M., Wessler, S. & Tegtmeyer, N. Transmigration route of Campylobacter jejuni across polarized intestinal epithelial cells: paracellular, transcellular or both? *Cell Commun Signal* **11**, 72 (2013).

145. Reti, K. L., Tymensen, L. D., Davis, S. P., Amrein, M. W. & Buret, A. G. Campylobacter jejuni Increases Flagellar Expression and Adhesion of Noninvasive Escherichia coli: Effects on Enterocytic Toll-Like Receptor 4 and CXCL-8 Expression. *Infect Immun* **83**, 4571–4581 (2015).

146. Silva, J. *et al.* Campylobacter spp. as a Foodborne Pathogen: A Review. *Front. Microbio.* **2**, (2011).

147. Young, K. T., Davis, L. M. & DiRita, V. J. Campylobacter jejuni: molecular biology and pathogenesis. *Nat Rev Microbiol* **5**, 665–679 (2007).

148. Dale, D. C., Boxer, L. & Liles, W. C. The phagocytes: neutrophils and monocytes. *Blood* **112**, 935–945 (2008).

149. Copenhaver, A. M. *et al.* Alveolar Macrophages and Neutrophils Are the Primary Reservoirs for Legionella pneumophila and Mediate Cytosolic Surveillance of Type IV Secretion. *Infect Immun* **82**, 4325–4336 (2014).

150. Fukuto, H. S. & Bliska, J. B. Editorial: *Yersinia pestis* survives in neutrophils and sends a PS to macrophages: bon appétit! *Journal of Leukocyte Biology* **95**, 383–385 (2014).

151. Storisteanu, D. M. L. *et al.* Evasion of Neutrophil Extracellular Traps by Respiratory Pathogens. *Am J Respir Cell Mol Biol* **56**, 423–431 (2017).

152. Saffarzadeh, M. *et al.* Neutrophil Extracellular Traps Directly Induce Epithelial and Endothelial Cell Death: A Predominant Role of Histones. *PLoS ONE* **7**, e32366 (2012).

153. Erpenbeck, L. & Schön, M. P. Neutrophil extracellular traps: protagonists of cancer progression? *Oncogene* **36**, 2483–2490 (2017).

154. He, Y., Yang, F.-Y. & Sun, E.-W. Neutrophil Extracellular Traps in Autoimmune Diseases. *Chinese Medical Journal* **131**, 1513–1519 (2018).

155. Kuijf, M. L. *et al.* TLR4-Mediated Sensing of *Campylobacter jejuni* by Dendritic Cells Is Determined by Sialylation. *The Journal of Immunology* **185**, 748–755 (2010).

156. Rathinam, V. A. K., Appledorn, D. M., Hoag, K. A., Amalfitano, A. & Mansfield, L. S. *Campylobacter jejuni* -Induced Activation of Dendritic Cells Involves Cooperative Signaling through Toll-Like Receptor 4 (TLR4)-MyD88 and TLR4-TRIF Axes. *Infect Immun* **77**, 2499–2507 (2009).

157. Tan, Y., Zanoni, I., Cullen, T. W., Goodman, A. L. & Kagan, J. C. Mechanisms of Toll-like Receptor 4 Endocytosis Reveal a Common

Immune-Evasion Strategy Used by Pathogenic and Commensal Bacteria. *Immunity* **43**, 909–922 (2015).

158. Neal-McKinney, J. M. & Konkel, M. E. The Campylobacter jejuni CiaC virulence protein is secreted from the flagellum and delivered to the cytosol of host cells. *Front. Cell. Inf. Microbio.* **2**, (2012).

159. Prokhorenko, I., Zubova, S., Kabanov, D., Voloshina, E. & Grachev, S. Toll-like receptor 4 in phagocytosis of Escherichia coli by endotoxin-activated human neutrophils in whole blood. *Crit Care* **16**, P80, cc11767 (2012).

160. Bachman, M. A., Miller, V. L. & Weiser, J. N. Mucosal Lipocalin 2 Has Pro-Inflammatory and Iron-Sequestering Effects in Response to Bacterial Enterobactin. *PLoS Pathog* **5**, e1000622 (2009).

161. Crofts, A. A. *et al.* Campylobacter jejuni transcriptional and genetic adaptation during human infection. *Nat Microbiol* **3**, 494–502 (2018).

162. Klebanoff, S. J. Myeloperoxidase: friend and foe. *Journal of Leukocyte Biology* **77**, 598–625 (2005).

163. Weinrauch, Y., Drujan, D., Shapiro, S. D., Weiss, J. & Zychlinsky, A. Neutrophil elastase targets virulence factors of enterobacteria. *Nature* **417**, 91–94 (2002).

164. Whitmore, L. C., Weems, M. N. & Allen, L.-A. H. Cutting Edge: *Helicobacter pylori* Induces Nuclear Hypersegmentation and Subtype Differentiation of Human Neutrophils In Vitro. *The Journal of Immunology* **198**, 1793–1797 (2017).

165. Prichard, A., Khuu, L., Whitmore, L. C., Irimia, D. & Allen, L.-A. H. Helicobacter pylori-infected human neutrophils exhibit impaired chemotaxis and a uropod retraction defect. *Front. Immunol.* **13**, 1038349 (2022).

166. Carabeo, R. Bacterial subversion of host actin dynamics at the plasma membrane: Bacterial subversion of host actin dynamics. *Cellular Microbiology* **13**, 1460–1469 (2011).

167. Cullen, T. W. & Trent, M. S. A link between the assembly of flagella and lipooligosaccharide of the Gram-negative bacterium *Campylobacter jejuni*. *Proc. Natl. Acad. Sci. U.S.A.* **107**, 5160–5165 (2010).

168. Gaasbeek, E. J. *et al.* A DNase Encoded by Integrated Element CJIE1 Inhibits Natural Transformation of *Campylobacter jejuni*. *J Bacteriol* **191**, 2296–2306 (2009).

169. Blutt, S. E. & Estes, M. K. Gut Bacterial Bouncers: Keeping Viral Pathogens out of the Epithelium. *Cell Host & Microbe* **26**, 569–570 (2019).

170. Fournier, B. M. & Parkos, C. A. The role of neutrophils during intestinal inflammation. *Mucosal Immunology* **5**, 354–366 (2012).

171. Chassaing, B. *et al.* Fecal Lipocalin 2, a Sensitive and Broadly Dynamic Non-Invasive Biomarker for Intestinal Inflammation. *PLoS ONE* **7**, e44328 (2012).

172. Akhtar, R., Chaudhary, Z. & He, Y. Modified Method for Isolation of Peripheral Blood Neutrophils from Bovines and Humans. *IJAVMS* **4**, 8 (2010).

173. Zharkova, O. *et al.* A Flow Cytometry-Based Assay for High-Throughput Detection and Quantification of Neutrophil Extracellular Traps in Mixed Cell Populations. *Cytometry* **95**, 268–278 (2019).

174. Brinkmann, V., Laube, B., Abu Abed, U., Goosmann, C. & Zychlinsky, A. Neutrophil Extracellular Traps: How to Generate and Visualize Them. *JoVE* 1724 (2010) doi:10.3791/1724.

175. Lebeis, S. L., Powell, K. R., Merlin, D., Sherman, M. A. & Kalman, D. Interleukin-1 Receptor Signaling Protects Mice from Lethal Intestinal Damage Caused by the Attaching and Effacing Pathogen *Citrobacter rodentium. Infect Immun* **77**, 604–614 (2009).

176. Brinkmann, V., Abu Abed, U., Goosmann, C. & Zychlinsky, A. Immunodetection of NETs in Paraffin-Embedded Tissue. *Front. Immunol.* **7**, (2016).

177. Doster, R. S., Sutton, J. A., Rogers, L. M., Aronoff, D. M. & Gaddy, J. A. Streptococcus agalactiae Induces Placental Macrophages To Release Extracellular Traps Loaded with Tissue Remodeling Enzymes via an Oxidative Burst-Dependent Mechanism. *mBio* **9**, e02084-18 (2018).

178. Liu, F., Lee, S. A., Xue, J., Riordan, S. M. & Zhang, L. Global epidemiology of campylobacteriosis and the impact of COVID-19. *Front. Cell. Infect. Microbiol.* **12**, 979055 (2022).

179. Poropatich, K. O., Fischer Walker, C. L. & Black, R. E. Quantifying the Association between *Campylobacter* Infection and Guillain-Barré Syndrome: A Systematic Review. *J Health Popul Nutr* **28**, 545–552 (2010).

180. Berumen, A. *et al.* Characteristics and Risk Factors of Post-Infection Irritable Bowel Syndrome After Campylobacter Enteritis. *Clinical Gastroenterology and Hepatology* **19**, 1855-1863.e1 (2021).

181. Keithlin, J., Sargeant, J., Thomas, M. K. & Fazil, A. Systematic review and meta-analysis of the proportion of Campylobacter cases that develop chronic sequelae. *BMC Public Health* **14**, 1203 (2014).

182. Callahan, S. M., Dolislager, C. G. & Johnson, J. G. The Host Cellular Immune Response to Infection by Campylobacter Spp. and Its Role in Disease. *Infect Immun* **89**, e00116-21 (2021).

183. Sørensen, N. B., Nielsen, H. L., Varming, K. & Nielsen, H. Neutrophil activation by Campylobacter concisus. *Gut Pathog* **5**, 17 (2013).

184. Barneda-Zahonero, B. & Parra, M. Histone deacetylases and cancer. *Molecular Oncology* **6**, 579–589 (2012).

185. Hamminger, P., Rica, R. & Ellmeier, W. Histone deacetylases as targets in autoimmune and autoinflammatory diseases. in *Advances in Immunology* vol. 147 1–59 (Elsevier, 2020).

186. Shakespear, M. R., Halili, M. A., Irvine, K. M., Fairlie, D. P. & Sweet, M. J. Histone deacetylases as regulators of inflammation and immunity. *Trends in Immunology* **32**, 335–343 (2011).

187. Pennini, M. E., Perrinet, S., Dautry-Varsat, A. & Subtil, A. Histone Methylation by NUE, a Novel Nuclear Effector of the Intracellular Pathogen Chlamydia trachomatis. *PLoS Pathog* **6**, e1000995 (2010).

188. Ribet, D. & Cossart, P. Post-translational modifications in host cells during bacterial infection. *FEBS Letters* **584**, 2748–2758 (2010).

189. Ribet, D. & Cossart, P. Pathogen-Mediated Posttranslational Modifications: A Re-emerging Field. *Cell* **143**, 694–702 (2010).

190. Rolando, M. *et al.* Legionella pneumophila Effector RomA Uniquely Modifies Host Chromatin to Repress Gene Expression and Promote Intracellular Bacterial Replication. *Cell Host & Microbe* **13**, 395–405 (2013).

191. Bernal, V. *et al.* Regulation of bacterial physiology by lysine acetylation of proteins. *New Biotechnology* **31**, 586–595 (2014).

192. Luu, J. & Carabetta, V. J. Contribution of N $^{\varepsilon}$-lysine Acetylation towards Regulation of Bacterial Pathogenesis. *mSystems* **6**, e00422-21 (2021).

193. Salomon, D. & Orth, K. What Pathogens Have Taught Us About Posttranslational Modifications. *Cell Host & Microbe* **14**, 269–279 (2013).

194. Mariño-Ramírez, L., Kann, M. G., Shoemaker, B. A. & Landsman, D. Histone structure and nucleosome stability. *Expert Review of Proteomics* **2**, 719–729 (2005).

195. Glozak, M. A. & Seto, E. Histone deacetylases and cancer. *Oncogene* **26**, 5420–5432 (2007).

196. Kurdistani, S. K. & Grunstein, M. Histone acetylation and deacetylation in yeast. *Nat Rev Mol Cell Biol* **4**, 276–284 (2003).

197. Greer, C. B. *et al.* Histone Deacetylases Positively Regulate Transcription through the Elongation Machinery. *Cell Reports* **13**, 1444–1455 (2015).

198. Haberland, M., Montgomery, R. L. & Olson, E. N. The many roles of histone deacetylases in development and physiology: implications for disease and therapy. *Nat Rev Genet* **10**, 32–42 (2009).

199. Nusinzon, I. & Horvath, C. M. Histone Deacetylases as Transcriptional Activators? Role Reversal in Inducible Gene Regulation. *Sci. STKE* **2005**, (2005).

200. Gatla, H. R., Zou, Y., Uddin, M. M. & Vancurova, I. Epigenetic regulation of interleukin-8 expression by class I HDAC and CBP in ovarian cancer cells. *Oncotarget* **8**, 70798–70810 (2017).

201. Marumo, T. *et al.* Histone deacetylase modulates the proinflammatory and -fibrotic changes in tubulointerstitial injury. *American Journal of Physiology-Renal Physiology* **298**, F133–F141 (2010).

202. Zhu, H., Shan, L., Schiller, P. W., Mai, A. & Peng, T. Histone Deacetylase-3 Activation Promotes Tumor Necrosis Factor-α (TNF-α) Expression in Cardiomyocytes during Lipopolysaccharide Stimulation. *Journal of Biological Chemistry* **285**, 9429–9436 (2010).

203. Chen, Z. *et al.* HDAC Inhibitor Attenuated NETs Formation Induced by Activated Platelets In Vitro, Partially Through Downregulating Platelet Secretion. *Shock* **54**, 321–329 (2020).

204. Hamam, H. J. & Palaniyar, N. Histone Deacetylase Inhibitors Dose-Dependently Switch Neutrophil Death from NETosis to Apoptosis. *Biomolecules* **9**, 184 (2019).

205. Poli, V. *et al.* Zinc-dependent histone deacetylases drive neutrophil extracellular trap formation and potentiate local and systemic inflammation. *iScience* **24**, 103256 (2021).

206. Rohrbach, A. S., Slade, D. J., Thompson, P. R. & Mowen, K. A. Activation of PAD4 in NET formation. *Front. Immun.* **3**, (2012).

207. Leshner, M. *et al.* PAD4 mediated histone hypercitrullination induces heterochromatin decondensation and chromatin unfolding to form neutrophil extracellular trap-like structures. *Front. Immun.* **3**, (2012).

208. Silva, Y. P., Bernardi, A. & Frozza, R. L. The Role of Short-Chain Fatty Acids From Gut Microbiota in Gut-Brain Communication. *Front. Endocrinol.* **11**, 25 (2020).

209. Siddiqui, M. T. & Cresci, G. A. The Immunomodulatory Functions of Butyrate. *JIR* **Volume 14**, 6025–6041 (2021).

210. Yin, L., Laevsky, G. & Giardina, C. Butyrate Suppression of Colonocyte NF-κB Activation and Cellular Proteasome Activity. *Journal of Biological Chemistry* **276**, 44641–44646 (2001).

211. Vigushin, D. M. *et al.* Trichostatin A is a histone deacetylase inhibitor with potent antitumor activity against breast cancer in vivo. *Clin Cancer Res* **7**, 971–976 (2001).

212. You, W. & Steegborn, C. Structural Basis of Sirtuin 6 Inhibition by the Hydroxamate Trichostatin A: Implications for Protein Deacylase Drug Development. *J. Med. Chem.* **61**, 10922–10928 (2018).

213. Kankaanranta, H. *et al.* Histone deacetylase inhibitors induce apoptosis in human eosinophils and neutrophils. *J Inflamm* **7**, 9 (2010).

214. Toki, S. *et al.* The histone deacetylase inhibitor trichostatin A suppresses murine innate allergic inflammation by blocking group 2 innate lymphoid cell (ILC2) activation. *Thorax* **71**, 633–645 (2016).

215. Milne-Davies, B. *et al.* Life After Secretion—Yersinia enterocolitica Rapidly Toggles Effector Secretion and Can Resume Cell Division in Response to Changing External Conditions. *Front. Microbiol.* **10**, 2128 (2019).

216. Shames, S. R. *et al.* Multiple *Legionella pneumophila* effector virulence phenotypes revealed through high-throughput analysis of targeted mutant libraries. *Proc. Natl. Acad. Sci. U.S.A.* **114**, (2017).

217. Takaya, A., Tomoyasu, T., Matsui, H. & Yamamoto, T. The DnaK/DnaJ Chaperone Machinery of *Salmonella enterica* Serovar Typhimurium Is Essential for Invasion of Epithelial Cells and Survival within Macrophages, Leading to Systemic Infection. *Infect Immun* **72**, 1364–1373 (2004).

218. Shi, W., Zhou, Y., Wild, J., Adler, J. & Gross, C. A. DnaK, DnaJ, and GrpE are required for flagellum synthesis in Escherichia coli. *J Bacteriol* **174**, 6256–6263 (1992).

219. Kelley, L. A., Mezulis, S., Yates, C. M., Wass, M. N. & Sternberg, M. J. E. The Phyre2 web portal for protein modeling, prediction and analysis. *Nat Protoc* **10**, 845–858 (2015).

220. Roy, A., Kucukural, A. & Zhang, Y. I-TASSER: a unified platform for automated protein structure and function prediction. *Nat Protoc* **5**, 725–738 (2010).

221. Satoh, A., Stein, L. & Imai, S. The Role of Mammalian Sirtuins in the Regulation of Metabolism, Aging, and Longevity. in *Histone Deacetylases: the Biology and Clinical Implication* (eds. Yao, T.-P. & Seto, E.) vol. 206 125–162 (Springer Berlin Heidelberg, 2011).

222. Kelley, B. R. *et al.* Whole-Genome Sequencing and Bioinformatic Analysis of Environmental, Agricultural, and Human Campylobacter jejuni Isolates From East Tennessee. *Front. Microbiol.* **11**, 571064 (2020).

223. Moniot, S., Weyand, M. & Steegborn, C. Structures, Substrates, and Regulators of Mammalian Sirtuins – Opportunities and Challenges for Drug Development. *Front. Pharmacol.* **3**, (2012).

224. Imai, S. & Guarente, L. NAD+ and sirtuins in aging and disease. *Trends in Cell Biology* **24**, 464–471 (2014).

225. Barrero-Tobon, A. M. & Hendrixson, D. R. Flagellar biosynthesis exerts temporal regulation of secretion of specific *C ampylobacter jejuni* colonization and virulence determinants: Flagella-dependent secretion of *C. jejuni* proteins. *Molecular Microbiology* **93**, 957–974 (2014).

226. Chakravarthy, S., Huot, B. & Kvitko, B. H. Effector Translocation: Cya Reporter Assay. in *Bacterial Protein Secretion Systems* (eds. Journet, L. & Cascales, E.) vol. 1615 473–487 (Springer New York, 2017).

227. Johnson, J. G., Gaddy, J. A. & DiRita, V. J. The PAS Domain-Containing Protein HeuR Regulates Heme Uptake in Campylobacter jejuni. *mBio* **7**, e01691-16 (2016).

228. Konkel, M. E., Kim, B. J., Rivera-Amill, V. & Garvis, S. G. Bacterial secreted proteins are required for the internalization of Campylobacter jejuni into cultured mammalian cells. *Mol Microbiol* **32**, 691–701 (1999).

229. Aizawa, S.-I. Bacterial flagella and type III secretion systems. *FEMS Microbiology Letters* **202**, 157–164 (2001).

230. Russo, B. C., Duncan-Lowey, J. K., Chen, P. & Goldberg, M. B. The type 3 secretion system requires actin polymerization to open translocon pores. *PLoS Pathog* **17**, e1009932 (2021).

231. Kenny, E. F. *et al.* Diverse stimuli engage different neutrophil extracellular trap pathways. *eLife* **6**, e24437 (2017).

232. Callahan, S. *et al.* Induction of neutrophil extracellular traps by *Campylobacter jejuni*. *Cellular Microbiology* **22**, (2020).

233. Chen, D. *et al.* Campylobacter Colonization, Environmental Enteric Dysfunction, Stunting, and Associated Risk Factors Among Young Children in Rural Ethiopia: A Cross-Sectional Study From the Campylobacter Genomics and Environmental Enteric Dysfunction (CAGED) Project. *Front. Public Health* **8**, 615793 (2021).

234. Ren, F. *et al.* Insights into the impact of flhF inactivation on Campylobacter jejuni colonization of chick and mice gut. *BMC Microbiol* **18**, 149 (2018).

235. Gupta, A. *et al.* Sodium Butyrate Reduces Salmonella Enteritidis Infection of Chicken Enterocytes and Expression of Inflammatory Host Genes in vitro. *Front. Microbiol.* **11**, 553670 (2020).

236. Rivera-Chávez, F. *et al.* Depletion of Butyrate-Producing Clostridia from the Gut Microbiota Drives an Aerobic Luminal Expansion of Salmonella. *Cell Host & Microbe* **19**, 443–454 (2016).

237. Xiong, H. *et al.* Butyrate upregulates endogenous host defense peptides to enhance disease resistance in piglets via histone deacetylase inhibition. *Sci Rep* **6**, 27070 (2016).

238. Ahmed, I. *et al.* Dietary Interventions Ameliorate Infectious Colitis by Restoring the Microbiome and Promoting Stem Cell Proliferation in Mice. *IJMS* **23**, 339 (2021).

239. Jiminez, J. A., Uwiera, T. C., Abbott, D. W., Uwiera, R. R. E. & Inglis, G. D. Butyrate Supplementation at High Concentrations Alters Enteric Bacterial

Communities and Reduces Intestinal Inflammation in Mice Infected with Citrobacter rodentium. *mSphere* **2**, e00243-17 (2017).

240. Park, J. W. *et al.* Short-chain Fatty Acids Inhibit Staphylococcal Lipoprotein-induced Nitric Oxide Production in Murine Macrophages. *Immune Netw* **19**, e9 (2019).

241. Traisaeng, S., Herr, D. R., Kao, H.-J., Chuang, T.-H. & Huang, C.-M. A Derivative of Butyric Acid, the Fermentation Metabolite of Staphylococcus epidermidis, Inhibits the Growth of a Staphylococcus aureus Strain Isolated from Atopic Dermatitis Patients. *Toxins* **11**, 311 (2019).

242. Bernstein, B. E. *et al.* Methylation of histone H3 Lys 4 in coding regions of active genes. *Proc. Natl. Acad. Sci. U.S.A.* **99**, 8695–8700 (2002).

243. Ryu, H.-Y. & Hochstrasser, M. Histone sumoylation and chromatin dynamics. *Nucleic Acids Research* **49**, 6043–6052 (2021).

244. Zencheck, W. D., Xiao, H. & Weiss, L. M. Lysine post-translational modifications and the cytoskeleton. *Essays in Biochemistry* **52**, 135–145 (2012).

245. Zhang, X. *et al.* H3 ubiquitination by NEDD4 regulates H3 acetylation and tumorigenesis. *Nat Commun* **8**, 14799 (2017).

246. Li, G. *et al.* Microbiota metabolite butyrate constrains neutrophil functions and ameliorates mucosal inflammation in inflammatory bowel disease. *Gut Microbes* **13**, 1968257 (2021).

247. Saha, P. *et al.* PAD4-dependent NETs generation are indispensable for intestinal clearance of Citrobacter rodentium. *Mucosal Immunol* **12**, 761–771 (2019).

248. Gideon, H. P., Phuah, J., Junecko, B. A. & Mattila, J. T. Neutrophils express pro- and anti-inflammatory cytokines in granulomas from Mycobacterium tuberculosis-infected cynomolgus macaques. *Mucosal Immunol* **12**, 1370–1381 (2019).

249. Tecchio, C., Micheletti, A. & Cassatella, M. A. Neutrophil-Derived Cytokines: Facts Beyond Expression. *Front. Immunol.* **5**, (2014).

250. Li, H. *et al.* Neutrophil Extracellular Traps Augmented Alveolar Macrophage Pyroptosis via AIM2 Inflammasome Activation in LPS-Induced ALI/ARDS. *JIR* **Volume 14**, 4839–4858 (2021).

251. Mangold, A. *et al.* Neutrophil extracellular traps and monocyte subsets at the culprit lesion site of myocardial infarction patients. *Sci Rep* **9**, 16304 (2019).

252. Parackova, Z. *et al.* Neutrophil Extracellular Trap Induced Dendritic Cell Activation Leads to Th1 Polarization in Type 1 Diabetes. *Front. Immunol.* **11**, 661 (2020).

253. Aarts, C. E. M. *et al.* Neutrophils as Suppressors of T Cell Proliferation: Does Age Matter? *Front. Immunol.* **10**, 2144 (2019).

254. Dorward, D. A. *et al.* Technical Advance: Autofluorescence-based sorting: rapid and nonperturbing isolation of ultrapure neutrophils to determine cytokine production. *Journal of Leukocyte Biology* **94**, 193–202 (2013).

255. Iwasaki, W. *et al.* Contribution of histone N-terminal tails to the structure and stability of nucleosomes. *FEBS Open Bio* **3**, 363–369 (2013).

256. Jeon, J.-H., Hong, C.-W., Kim, E. Y. & Lee, J. M. Current Understanding on the Metabolism of Neutrophils. *Immune Netw* **20**, e46 (2020).

257. Buzas, E. I. The roles of extracellular vesicles in the immune system. *Nat Rev Immunol* (2022) doi:10.1038/s41577-022-00763-8.

258. Zhou, Y. & Bréchard, S. Neutrophil Extracellular Vesicles: A Delicate Balance between Pro-Inflammatory Responses and Anti-Inflammatory Therapies. *Cells* **11**, 3318 (2022).

259. Immler, R., Simon, S. I. & Sperandio, M. Calcium signalling and related ion channels in neutrophil recruitment and function. *Eur J Clin Invest* **48**, e12964 (2018).

260. Collison, K. S. *et al.* RAGE-mediated neutrophil dysfunction is evoked by advanced glycation end products (AGEs). *J Leukoc Biol* **71**, 433–444 (2002).

261. Durán-Laforet, V. *et al.* Role of TLR4 in Neutrophil Dynamics and Functions: Contribution to Stroke Pathophysiology. *Front. Immunol.* **12**, 757872 (2021).

262. Hendrixson, D. R. & DiRita, V. J. Transcription of σ54-dependent but not σ28-dependent flagellar genes in Campylobacter jejuni is associated with formation of the flagellar secretory apparatus: Flagellar transcriptional cascade in C. jejuni. *Molecular Microbiology* **50**, 687–702 (2003).

263. Kelley, B. R., Callahan, S. M. & Johnson, J. G. Transcription of Cystathionine β-Lyase (MetC) Is Repressed by HeuR in Campylobacter jejuni, and Methionine Biosynthesis Facilitates Colonocyte Invasion. *J Bacteriol* **203**, (2021).

264. Callahan, S. M., Hancock, T. J. & Johnson, J. G. Characterization of *Campylobacter jejuni* –Neutrophil Interactions. *Current Protocols* **1**, (2021).

265. Sory, M.-P. & Cornelis, G. R. Translocation of a hybrid YopE-adenylate cyclase from Yersinia enterocolitica into HeLa cells. *Mol Microbiol* **14**, 583–594 (1994).

266. *Antibodies: a laboratory manual.* (Cold Spring Harbor Laboratory Press, 2014).

267. Wagner, A. S. *et al.* Cek1 regulates ß(1,3)-glucan exposure through calcineurin effectors in Candida albicans. *PLoS Genet* **18**, e1010405 (2022).

268. Price, C. T. D. *et al.* Dot/Icm-Dependent Restriction of Legionella pneumophila within Neutrophils. *mBio* **12**, e01008-21 (2021).

269. Sharma, P., Garg, N., Sharma, A., Capalash, N. & Singh, R. Nucleases of bacterial pathogens as virulence factors, therapeutic targets and diagnostic markers. *International Journal of Medical Microbiology* **309**, 151354 (2019).

270. Beenken, K. E., Spencer, H., Griffin, L. M. & Smeltzer, M. S. Impact of Extracellular Nuclease Production on the Biofilm Phenotype of Staphylococcus aureus under *In Vitro* and *In Vivo* Conditions. *Infect Immun* **80**, 1634–1638 (2012).

271. Forson, A. M., Rosman, C. W. K., van Kooten, T. G., van der Mei, H. C. & Sjollema, J. Micrococcal Nuclease stimulates Staphylococcus aureus Biofilm Formation in a Murine Implant Infection Model. *Front. Cell. Infect. Microbiol.* **11**, 799845 (2022).

272. Baslé, A. *et al.* Crystal structure of NucB, a biofilm-degrading endonuclease. *Nucleic Acids Research* **46**, 473–484 (2018).

273. Jakubovics, N. S., Shields, R. C., Rajarajan, N. & Burgess, J. G. Life after death: the critical role of extracellular DNA in microbial biofilms. *Lett Appl Microbiol* **57**, 467–475 (2013).

274. Finkel, S. E. & Kolter, R. DNA as a Nutrient: Novel Role for Bacterial Competence Gene Homologs. *J Bacteriol* **183**, 6288–6293 (2001).

275. Mell, J. C. & Redfield, R. J. Natural Competence and the Evolution of DNA Uptake Specificity. *J Bacteriol* **196**, 1471–1483 (2014).

276. Huang, L., Zhang, Y., Du, X., An, R. & Liang, X. Escherichia coli Can Eat DNA as an Excellent Nitrogen Source to Grow Quickly. *Front. Microbiol.* **13**, 894849 (2022).

277. Ferrando, M. L. *et al.* Active Human and Porcine Serum Induce Competence for Genetic Transformation in the Emerging Zoonotic Pathogen Streptococcus suis. *Pathogens* **10**, 156 (2021).

278. Cordero, M. *et al.* The induction of natural competence adapts staphylococcal metabolism to infection. *Nat Commun* **13**, 1525 (2022).

279. Dubnau, D. & Blokesch, M. Mechanisms of DNA Uptake by Naturally Competent Bacteria. *Annu. Rev. Genet.* **53**, 217–237 (2019).

280. Mutua, V. & Gershwin, L. J. A Review of Neutrophil Extracellular Traps (NETs) in Disease: Potential Anti-NETs Therapeutics. *Clinic Rev Allerg Immunol* **61**, 194–211 (2021).

281. Riyapa, D. *et al.* Neutrophil Extracellular Traps Exhibit Antibacterial Activity against Burkholderia pseudomallei and Are Influenced by Bacterial and Host Factors. *Infect Immun* **80**, 3921–3929 (2012).

282. Berends, E. T. M. *et al.* Nuclease Expression by Staphylococcus aureus Facilitates Escape from Neutrophil Extracellular Traps. *J Innate Immun* **2**, 576–586 (2010).

283. Callahan, S. M. *et al. Battle for the histones: a secreted bacterial sirtuin from* Campylobacter jejuni *activates neutrophils and induces inflammation during infection.* http://biorxiv.org/lookup/doi/10.1101/2022.07.19.497369 (2022) doi:10.1101/2022.07.19.497369.

284. Smith, C. K. *et al. Campylobacter jejuni* -Induced Cytokine Responses in Avian Cells. *Infect Immun* **73**, 2094–2100 (2005).

285. Al-Banna, N. A., Raghupathy, R. & Albert, M. J. Induction of cytokines in different organs after intranasal inoculation of Campylobacter jejuni in mice. *Gut Pathog* **4**, 23 (2012).

286. Shang, Y. *et al.* Insights into Campylobacter jejuni colonization and enteritis using a novel infant rabbit model. *Sci Rep* **6**, 28737 (2016).

287. Dinarello, C. A. Overview of the IL-1 family in innate inflammation and acquired immunity. *Immunol Rev* **281**, 8–27 (2018).

288. Ren, K. & Torres, R. Role of interleukin-1β during pain and inflammation. *Brain Research Reviews* **60**, 57–64 (2009).

289. Dinarello, C. A. Interleukin-1 in the pathogenesis and treatment of inflammatory diseases. *Blood* **117**, 3720–3732 (2011).

290. Zheng, D., Liwinski, T. & Elinav, E. Inflammasome activation and regulation: toward a better understanding of complex mechanisms. *Cell Discov* **6**, 36 (2020).

291. Broz, P. & Dixit, V. M. Inflammasomes: mechanism of assembly, regulation and signalling. *Nat Rev Immunol* **16**, 407–420 (2016).

292. Vance, R. E. The NAIP/NLRC4 inflammasomes. *Current Opinion in Immunology* **32**, 84–89 (2015).

293. Naseer, N. *et al.* Human NAIP/NLRC4 and NLRP3 inflammasomes detect Salmonella type III secretion system activities to restrict intracellular bacterial replication. *PLoS Pathog* **18**, e1009718 (2022).

294. Yang, Y., Wang, H., Kouadir, M., Song, H. & Shi, F. Recent advances in the mechanisms of NLRP3 inflammasome activation and its inhibitors. *Cell Death Dis* **10**, 128 (2019).

295. Nagar, A., Rahman, T. & Harton, J. A. The ASC Speck and NLRP3 Inflammasome Function Are Spatially and Temporally Distinct. *Front. Immunol.* **12**, 752482 (2021).

296. Fang, R. *et al.* ASC and NLRP3 maintain innate immune homeostasis in the airway through an inflammasome-independent mechanism. *Mucosal Immunol* **12**, 1092–1103 (2019).

297. Bouwman, L. I., de Zoete, M. R., Bleumink-Pluym, N. M. C., Flavell, R. A. & van Putten, J. P. M. Inflammasome Activation by *Campylobacter jejuni. J.I.* **193**, 4548–4557 (2014).

298. Iula, L. *et al.* Autophagy Mediates Interleukin-1β Secretion in Human Neutrophils. *Front. Immunol.* **9**, 269 (2018).

299. Marsman, G., Zeerleder, S. & Luken, B. M. Extracellular histones, cell-free DNA, or nucleosomes: differences in immunostimulation. *Cell Death Dis* **7**, e2518–e2518 (2016).

300. Allam, R., Darisipudi, M. N., Tschopp, J. & Anders, H.-J. Histones trigger sterile inflammation by activating the NLRP3 inflammasome: Innate Immunity. *Eur. J. Immunol.* **43**, 3336–3342 (2013).

301. Huang, H. *et al.* Histones Activate the NLRP3 Inflammasome in Kupffer Cells during Sterile Inflammatory Liver Injury. *J.I.* **191**, 2665–2679 (2013).

302. Callahan, S. M. & Johnson, J. G. Transposon-Based Identification of Factors That Promote *Campylobacter jejuni* Nuclease Activity. *Current Protocols* **1**, (2021).

303. Clark, D. J. Nucleosome Positioning, Nucleosome Spacing and the Nucleosome Code. *Journal of Biomolecular Structure and Dynamics* **27**, 781–793 (2010).

304. Chowdhury, M. N. Campylobacter jejuni enteritis; a review. *Trop Geogr Med* **36**, 215–222 (1984).

305. Karaffová, V. *et al.* Local intestinal immune response including NLRP3 inflammasome in broiler chicken infected with *Campylobacter jejuni* after administration of *Lactobacillus reuteri* B1/1. *Food and Agricultural Immunology* **31**, 954–966 (2020).

306. Lee, M. K. S., Sreejit, G., Nagareddy, P. R. & Murphy, A. J. Attack of the NETs! NETosis primes IL-1β-mediated inflammation in diabetic foot ulcers. *Clinical Science* **134**, 1399–1401 (2020).

307. Shi, C. *et al.* Extracellular Histone H3 Induces Pyroptosis During Sepsis and May Act Through NOD2 and VSIG4/NLRP3 Pathways. *Front. Cell. Infect. Microbiol.* **10**, 196 (2020).

308. Yang, J., Wise, L. & Fukuchi, K. TLR4 Cross-Talk With NLRP3 Inflammasome and Complement Signaling Pathways in Alzheimer's Disease. *Front. Immunol.* **11**, 724 (2020).

309. Qin, Z. *et al.* Toll-like receptor 4 activates the NLRP3 inflammasome pathway and periodontal inflammaging by inhibiting Bmi-1 expression. *Int J Mol Med* **47**, 137–150 (2020).

310. Halverson, T. W. R., Wilton, M., Poon, K. K. H., Petri, B. & Lewenza, S. DNA Is an Antimicrobial Component of Neutrophil Extracellular Traps. *PLoS Pathog* **11**, e1004593 (2015).

311. Song, Y. *et al.* Antimicrobial Microwebs of DNA–Histone Inspired from Neutrophil Extracellular Traps. *Adv. Mater.* **31**, 1807436 (2019).

312. Doolin, T. *et al.* Mammalian histones facilitate antimicrobial synergy by disrupting the bacterial proton gradient and chromosome organization. *Nat Commun* **11**, 3888 (2020).

313. Blevins, H. M., Xu, Y., Biby, S. & Zhang, S. The NLRP3 Inflammasome Pathway: A Review of Mechanisms and Inhibitors for the Treatment of Inflammatory Diseases. *Front. Aging Neurosci.* **14**, 879021 (2022).

314. Kahlenberg, J. M., Carmona-Rivera, C., Smith, C. K. & Kaplan, M. J. Neutrophil Extracellular Trap–Associated Protein Activation of the NLRP3 Inflammasome Is Enhanced in Lupus Macrophages. *The Journal of Immunology* **190**, 1217–1226 (2013).

315. Skjesol, A. *et al.* The TLR4 adaptor TRAM controls the phagocytosis of Gram-negative bacteria by interacting with the Rab11-family interacting protein 2. *PLoS Pathog* **15**, e1007684 (2019).

316. Cazzini, P. *et al.* Proposed grading scheme for inflammatory bowel disease in ferrets and correlation with clinical signs. *J VET Diagn Invest* **32**, 17–24 (2020).

317. Montaldo, E. *et al.* Cellular and transcriptional dynamics of human neutrophils at steady state and upon stress. *Nat Immunol* **23**, 1470–1483 (2022).

318. Kobayashi, S. D., Malachowa, N. & DeLeo, F. R. Neutrophils and Bacterial Immune Evasion. *J Innate Immun* **10**, 432–441 (2018).

319. Ciurkiewicz, M. *et al.* Ferrets are valuable models for SARS-CoV-2 research. *Vet Pathol* **59**, 661–672 (2022).

320. Evans, D. R. *et al.* Systematic detection of horizontal gene transfer across genera among multidrug-resistant bacteria in a single hospital. *eLife* **9**, e53886 (2020).

321. Hanukoglu, I. Proteopedia: Rossmann fold: A beta-alpha-beta fold at dinucleotide binding sites: Rossmann Fold in FAD, NAD and NADP Binding Domains. *Biochem. Mol. Biol. Educ.* **43**, 206–209 (2015).

322. Park, M. J. & Sohrabji, F. The histone deacetylase inhibitor, sodium butyrate, exhibits neuroprotective effects for ischemic stroke in middle-aged female rats. *J Neuroinflammation* **13**, 300 (2016).

323. Kim, M., Park, C., Jung, J. & Yeo, S. G. The histone deacetylase class I, II inhibitor trichostatin A delays peripheral neurodegeneration. *J Mol Hist* **50**, 167–178 (2019).

324. Liu, T. F. & McCall, C. E. Deacetylation by SIRT1 Reprograms Inflammation and Cancer. *Genes & Cancer* **4**, 135–147 (2013).

325. Von Knethen, A. & Brüne, B. Histone Deacetylation Inhibitors as Therapy Concept in Sepsis. *IJMS* **20**, 346 (2019).

326. Denis, H. *et al.* Functional Connection between Deimination and Deacetylation of Histones. *Molecular and Cellular Biology* **29**, 4982–4993 (2009).

327. Hoshikawa, Y., Kwon, H. J., Yoshida, M., Horinouchi, S. & Beppu, T. Trichostatin A Induces Morphological Changes and Gelsolin Expression by Inhibiting Histone Deacetylase in Human Carcinoma Cell Lines. *Experimental Cell Research* **214**, 189–197 (1994).

328. Zhu, L.-B., Zhang, Y.-C., Huang, H.-H. & Lin, J. Prospects for clinical applications of butyrate-producing bacteria. *WJCP* **10**, 84–92 (2021).

329. Gallinari, P., Marco, S. D., Jones, P., Pallaoro, M. & Steinkühler, C. HDACs, histone deacetylation and gene transcription: from molecular biology to cancer therapeutics. *Cell Res* **17**, 195–211 (2007).

330. Lopes, G. V. *et al.* Virulence factors of foodborne pathogen Campylobacter jejuni. *Microbial Pathogenesis* **161**, 105265 (2021).

331. Pfister, S. P. *et al.* Uncoupling of invasive bacterial mucosal immunogenicity from pathogenicity. *Nat Commun* **11**, 1978 (2020).

332. Sinha, R., LeVeque, R. M., Bowlin, M. Q., Gray, M. J. & DiRita, V. J. Phosphate Transporter PstSCAB of Campylobacter jejuni Is a Critical Determinant of Lactate-Dependent Growth and Colonization in Chickens. *J Bacteriol* **202**, (2020).

333. Liu, M. M. *et al.* Investigating the Campylobacter jejuni Transcriptional Response to Host Intestinal Extracts Reveals the Involvement of a Widely Conserved Iron Uptake System. *mBio* **9**, e01347-18 (2018).

334. Pacheco, S. A. IDENTIFICATION OF CAMPYLOBACTER JEJUNI SECRETED PROTEINS. (2010).

335. Schultz, B. M., Acevedo, O. A., Kalergis, A. M. & Bueno, S. M. Role of Extracellular Trap Release During Bacterial and Viral Infection. *Front. Microbiol.* **13**, 798853 (2022).

336. Chen, L. *et al.* Neutrophil extracellular traps promote macrophage pyroptosis in sepsis. *Cell Death Dis* **9**, 597 (2018).

337. Yang, L. *et al.* DNA of neutrophil extracellular traps promotes cancer metastasis via CCDC25. *Nature* **583**, 133–138 (2020).

338. Nickel, K., Bjorner, M., Ladiges, W. & Zhu, L. Neutrophil response to cyclophosphamide predicts resilience to age-related learning impairment. *Aging Pathobiol Ther* **2**, 230–231 (2020).

339. Luo, Y. *et al.* Inhibitors and Inactivators of Protein Arginine Deiminase 4: Functional and Structural Characterization ʹ. *Biochemistry* **45**, 11727–11736 (2006).

340. Du Toit, A. The effector repertoire of Legionella. *Nat Rev Microbiol* **17**, 126–126 (2019).

341. Ferron, F. *et al.* Structural and molecular basis of mismatch correction and ribavirin excision from coronavirus RNA. *Proc. Natl. Acad. Sci. U.S.A.* **115**, (2018).

342. Rowley, M. J. & Corces, V. G. Organizational principles of 3D genome architecture. *Nat Rev Genet* **19**, 789–800 (2018).

343. Lan, X. *et al.* Integration of Hi-C and ChIP-seq data reveals distinct types of chromatin linkages. *Nucleic Acids Research* **40**, 7690–7704 (2012).

344. Amiri, P. *et al.* Role of Butyrate, a Gut Microbiota Derived Metabolite, in Cardiovascular Diseases: A comprehensive narrative review. *Front. Pharmacol.* **12**, 837509 (2022).

345. Theruvathu, J. A., Kim, C. H., Darwanto, A., Neidigh, J. W. & Sowers, L. C. pH-Dependent Configurations of a 5-Chlorouracil-Guanine Base Pair. *Biochemistry* **48**, 11312–11318 (2009).

346. Kleinholz, C. L. *et al.* Ly6G deficiency alters the dynamics of neutrophil recruitment and pathogen capture during Leishmania major skin infection. *Sci Rep* **11**, 15071 (2021).

VITA

Sean M. Callahan was born in Binghamton, NY and grew up in Conklin. After attending University of New Haven in West Haven, CT, he received a double B.S. in Forensic Science and Pre-Medicine. During this time, he worked in a microbiology research lab and teaching assistant for microbiology labs. After doing a summer Research Experience for Undergraduates (REU) in the Department of Microbiology at the University of Tennessee – Knoxville, he decided to pursue a PhD in the Department of Microbiology at the University of Tennessee – Knoxville. Following five years working in the Johnson Lab at the University of Tennessee – Knoxville, he defended in the spring of 2023 before moving to the University of Pennsylvania to pursue postdoctoral training in epigenetics.